Protein post-translational modification mimicry for cargo sorting to extracellular vesicles

Carla Martin Perez

Department of Physiology, Anatomy and Genetics

SOMERVILLE COLLEGE, UNIVERSITY OF OXFORD

Thesis submitted for the degree of

Doctor of Philosophy

Declaration

The work presented in this thesis was undertaken in Professor Matthew Wood's laboratory at the Department of Physiology, Anatomy and Genetics, University of Oxford, between 2018 and 2022. I, Carla Martin Perez, hereby declare that all work presented is my own with the following exceptions. The EV transfer experiments in Results I were done in collaboration with Oana Pelea (DPhil student). The *in vivo* EV transfer experiment in Results III was done in collaboration with Dr. Xiuming Liang (from Samir EL Andaloussi lab at Karolinska institutet). This work has not been submitted for any other degree at this university or any other institute of learning. My thesis includes text excerpts of my first-author article published during my DPhil as listed in **Section 8.1**. Where required, permission from individual journals was obtained to use excerpts of text in this thesis.

Acknowledgements

First of all, I would like to thank Professor Matthew Wood, for giving me the opportunity to work in your laboratory and for your support throughout this project. Secondly, I would also like to thank Dr. Thomas Roberts for his support, time, and patience and for giving me the freedom to develop my own ideas. I would further like to thank Dr. Imre Mäger for his guidance during the first year of my DPhil and for teaching me how to think critically about EV research.

I would also like to express my gratitude to all the members of the Wood lab, especially I would like to thank, Dr. Hans Friedrichsen, Dr. Mariana Conceição, Dr. Britt Hanson, Dr. Yulia Lomonosova and Scott Bonner. In particular, I would like to thank Dr. David Seoane for making me feel at home in the lab. Thank you for selflessly helping me out with my experiments and for always being by my side when I needed it. Antonio, thank you for our insightful discussions about extracellular vesicles and for your sound advice over the years. Ambra, thank you for our shared laughter in those moments of despair trying to fix the NanoFCM. Claire, I am thankful I could share the last part of my DPhil journey with someone as passionate about extracellular vesicles as I am. Dora, although we only crossed paths for a short time, thank you for your positive energy and for your good mood.

To my parents and my brother, thank you for your love, for trusting me, and for supporting me throughout these years. Thank you for those unexpected visits to Oxford in my most difficult moments and for being connected at any time I needed. I couldn't have gotten this far without you. Thanks. Thanks. Thanks.

Alessandro, a thank you is not enough for expressing how grateful I am for accompanying me on this journey that we started together five years ago. Thank you for your love, your understanding, for your patience, for your advice, for the trust you placed in me at times that even I doubted, and for being able to count on you unconditionally.

Lastly, thanks to my cat Keiko, who I adopted the first day I came to Oxford and is now part of my family, thank you for your purrs, your softness, and your ability to cheer me up.

Abstract

Extracellular vesicles (EVs) are cell-derived, membranous nanoparticles released by cells that facilitate the intercellular transfer of proteins and nucleic acids. This intrinsic delivery property of EVs, together with their low immunogenicity and potential for repeat administration, makes them promising delivery vehicles for novel therapeutics.

The loading of cargo molecules into EVs constitutes one of the main challenges limiting clinical translation of EV-based therapies. Post-translational modification (PTM) of proteins with ubiquitin-like protein 3 (UBL3) has been previously implicated in the sorting of specific proteins into EVs. Initially, we assessed the utility of UBL3 as an EV-scaffold to enhance EV-loading of Cas9/sgRNA complexes by fusing Cas9 to UBL3 (to mimic the UBL3 PTM). This approach was shown to be successful in terms of the loading of Cas9 and sgRNA into the EVs, although no functional activity of the complexes was observed in the recipient cells after EV transfer.

PTMs such as myristylation, ubiquitination, and prenylation have also been shown to play a role in EV-protein sorting. We were motivated to identify additional PTMs (and other sequence features) associated with EV loading that may be exploited for therapeutic purposes. To this end, we developed a novel bioinformatics analysis: integrated proteomics and feature annotation analysis (IPFA) that enabled the identification of EV-enriched annotated PTMs, protein motifs, and domains by combining protein feature annotations from UniProt with experimentally-observed EV-enriched proteins observed in proteomics data. This analysis identified several promising features, of which N-glycosylation was selected as the most promising PTM associated with EV protein enrichment. Specifically, the majority of N-glycosylation-annotated transmembrane proteins were EV-enriched, and nearly half of all EV-enriched transmembrane proteins were annotated as being N-glycosylated.

Candidate protein features that were identified with the IPFA analysis were then experimentally assessed for their capacity to mediate functional cargo protein delivery. PTTG1P (Pituitary tumor-transforming gene 1 protein-interacting protein), a single-pass transmembrane protein with two annotated N-glycosyation sites, was selected as a putative EV-sorting scaffold. PTTG1IP was found to be highly enriched in EVs in an N-glycosylation dependent manner. Highly efficient functional delivery of Cre recombinase to reporter cells and mouse xenograft tumors was accomplished using PTTG1IP as an EV scaffold. Indeed, cargo molecules fused to PTTG1IP scaffolds were successfully delivered to recipient cell cultures with improved efficiency relative to the commonly used CD63-based scaffold. The PTTG1IP platform was further utilized for successful Cas9 and Cas9/sgRNA complex delivery to reporter cells. Several PTTG1IP variants with improved properties for therapeutic delivery were also developed (i.e., reduced size, enhanced loading potential, and enhanced intrinsic cleavage for cargo release), demonstrating the potential for further engineering PTTG1IP beyond its native human amino acid sequence. To achieve functional delivery, PTTG1IP-cargo fusion constructs were designed to include self-cleaving sequences (i.e., an intein from *Mycobacterium tuberculosis* or an intrinsic cleavage sequence derived from PTTG1IP itself) to facilitate cargo release from the EV scaffold. Furthermore, co-expression of the fusogenic protein VSVG (vesicular stomatitis virus glycoprotein) was utilized to enhance cellular uptake and promote endosomal escape.

In summary, PTTG1IP was identified as a suitable EV-loading scaffold using IPFA, and its ability to efficiently package and deliver protein and protein/RNA complexes was demonstrated in both cell cultures and *in vivo*. Notably, PTTG1IP EV-sorting was shown to be dependent on its N-glycosylation PTMs, providing a validation of the robustness of the IPFA approach. The PTTG1IP-based platform offers significant advantages over other EV-loading

strategies, (such as favorable membrane topology, the potential for further engineering, and functional delivery capability), which will enable the development of improved EV-based therapeutics.

Table of Contents

List of Figures

List of Tables

List of Abbreviations

APOB	Apolipoprotein B
AREs	AU-rich elements
BBB	Brain blood barrier
Cas9	CRISPR associated protein 9
CFP	Cyan fluorescent protein
CPP	Cell penetrating peptides
Cq	Quantification cycles
CRISPR	Clustered regularly interspaced short palindromic repeat
DG	Density gradient centrifugation
DMEM	Dulbecco's Modified Eagle's Media
DNA	Deoxyribonucleic acid
dUC	Differential ultracentrifugation
ECM	Extracellular matrix
EGFR	Epidermal growth factor receptor
EMNVs	Exosome-mimetic nanovesicles
ESCRT	Endosomal sorting complex required for transport
EVs	Extracellular vesicles
FHV	Flock house nodavirus
GFP	Green fluorescent protein
hnRNPs	Heterogeneous nuclear ribonucleoproteins
HIV	Human immunodeficiency virus
ICH	Immunohistochemistry
ILV	ILVs
IPFA	Integrated proteomics and feature annotation analysis
ISEV	International Society for Extracellular Vesicles
kDa	Kilodaltons
LBPA	Lysobisphosphatidic acid
LC	Liquid chromatography
LDLRs	Low-density lipoprotein receptor

LPS	Lipopolysaccharide
MHC	Major histocompatibility complex
miRNAs	microRNA
MLV	Murine leukemia virus
mRNA	Messenger RNA
MSCs	Mesenchymal stem cells
MVBs	Multivesicular bodies
MWCO	Molecular weight cut-off
nanoFCM	Nano flow-cytometry
NTA	Nanoparticle tracking analysis
PAGE	Polyacrylamide gel electrophoresis
PBS	Phosphate buffer saline
PBF	PTTG1-binding factor
PCR	Polymerase chain reaction
PEI	Polyethylenimine
PTM	Post translational modification
PTTG	Pituitary tumor-transforming gene 1
PVDF	Polyvinylidene fluoride
qPCR	Quantitative PCR
RBDs	RNA-binding domains
RBPs	RNA-binding proteins
RISC	RNA-induced silencing complex
RNA	Ribonucleic acid
RT-qPCR	Reverse transcription quantitative PCR
RVG	Rabies virus glycoprotein
saCas9	Staphylococcus aureus Cas9
SEC	Size exclusion chromatography
sgRNA	single-guide RNA
siRNAs	small interfering RNAs
TAR	Transactivation response element
TFF	Tangential-flow filtration

TFRC	Transferrin receptor gene
tTA	Tetracyclin transactivator
UC	Ultracentrifugation
UUO	Unilateral ureteral obstruction
VLPs	Virus-like particles
VPR	VP64-p65-Rta
VSVG	Vesicular stomatitis virus glycoprotein
WT	Wild-type

1. Introduction

Extracellular vesicles (EVs) are lipid bilayer-enclosed nanoparticles secreted by the majority of cells[1,2] which mediate cell-to-cell communication in both physiological and pathological conditions[3]. EVs contain membrane proteins, soluble proteins, metabolites, mRNA and noncoding RNA species, and are able to transfer their contents to recipient cells in order to induce a physiological response[4]. EVs constitute a heterogeneous population in terms of size, density, function and content[5,6]. EV composition is highly variable, and is dependent on the cell type of origin, specific EV biogenesis pathway and physiological status of the producer cell[5,7].

Findings suggesting the existence of EVs emerged in the 1940s from blood clotting studies. Early observations by Chargaff and West identified a particulate fraction in blood that was separated by sedimentation and was able to induce blood coagulation[8,9]. In 1967, Peter Wolf *et al*. further explored the nature of this particles, which he referred as "platelet dust"[10]. He described their platelet-cell origin, pro-coagulant activity, and phospholipid content. A possible role of vesicles from bone cartilage matrix on calcification was also proposed at around the same time by Anderson and Bonnuci[11,12]. While several studies had identified vesicular structures in biofluids, it was only in 1971 that the term "extracellular vesicle" was used for the first time to describe membranous vesicles released by *Ochromonas danica*, a flagellated alga[13].

In 1974, Nunez *et al*. observed that EVs were released from bat thyroid glands[14]. Importantly, the authors were the first to propose that EVs can be released from the cells by the fusion of multivesicular bodies (MVBs) with the plasma membrane. This notion was supported by the close proximity observed between the MVBs and the apical membrane in thyroid glands. EVs were also identified in non-mammalian organisms such as yeast[15] and bacteria[16]. In the

1980s, two different studies by Stahl *et al*. and Johnstone *et al*. shed light into the mechanism underlying exosome secretion. Transferrin receptor (TFRC) loss during reticulocyte maturation was shown to be the result of its release in vesicular structures[17,18]. Moreover, electron microscopy images demonstrated that the vesicles originated in the MVB lumen and were released to the extracellular space upon fusion of the MVB with the plasma membrane.

The conception of EVs as waste disposal entities arose in 1991 from a study by Johnstone *et al*, in which the authors reported that membrane proteins were released from cells via EVs in response to cellular stress[19]. They speculated that this represented a mechanism to dispose of obsolete membrane proteins. Despite this, new insights into EV biology and function were obtained in the following years. These included the observation that EV secretion was increased in several pathological conditions and the identification of key EV components such as CD9, ARF and Rab4[20,21]. It was not until 1996 that the therapeutic potential of EVs was demonstrated in a study showing that EVs from immune cells were able to release functional antigen presenting vesicles, thus indicating that they could be harnessed as anti-tumor vaccines[22]. This was later shown in a study by Zitvogel *et al*. in which dendritic cell-derived EVs were capable of priming cytotoxic T-cells leading to tumor suppression *in vivo*[23]. A major breakthrough in the EV research was the demonstration in 2006-2007 that EVs were able to transfer RNA and protein cargo to recipient cells, hence establishing their role in cell-to-cell communication[24–26]. These findings led researchers to explore their use as drug delivery vehicles, opening a new avenue for the therapeutic application of EVs.

1.1. EV heterogeneity

EVs are highly heterogeneous in nature both at a physical (e.g., size, density) and biochemical level (e.g., molecular composition, cargoes), and thus should be regarded as a diverse population with distinct properties[5]. EVs can be classified into three main categories depending on their biosynthetic origins: exosomes, microvesicles, and apoptotic bodies. Exosomes have a size range of 50-150 nm in diameter and are generated in the late endosome[27]. They are formed as a result of inward budding of the limiting membrane of MVBs, giving rise to intraluminal vesicles (ILVs). Once these ILVs are released into the extracellular space via the fusion of MVBs with the plasma membrane, they are referred to as exosomes[27]. In contrast, microvesicles are formed by direct outward budding (i.e., blebbing) of the plasma membrane and are typically between 100-1,000 nm in diameter[27]. Apoptotic bodies are vesicles released by dying cells as a product of apoptotic cell blebbing[28]. Despite their differences in biogenesis, it is technically very challenging to distinguish and separate exosomes and microvesicles once they have been secreted into the extracellular space due to their highly similar biophysical properties (i.e., size, density, membrane topology), and often common biochemical composition[29]. The terms “exosome” and “microvesicles” are often used interchangeably to describe heterogeneous mixtures of vesicles, leading to misconception and confusion in the EV-field. To address this issue, the International Society for Extracellular Vesicles (ISEV) recommended the use of the more general term “extracellular vesicles” when the biosynthetic origin of the vesicles has not been established[30].

1.2. Exosome biogenesis

Exosomes derive from endosomal compartments and are formed in multi-step processes involving several sorting machineries. Early endosome maturation is triggered by endocytic vesicle fusion and gradual acidification, leading to the formation of late endosomes. ILVs are then formed by inward budding of the limiting membrane from late endosomes, giving rise to MVBs[4]. MVBs can then be transported to the plasma membrane, where ILVs are released to the extracellular space as exosomes upon the fusion of MVBs with the plasma membrane. Alternatively, MVBs can be degraded by fusing with the lysosomes or the autophagosomes[29].

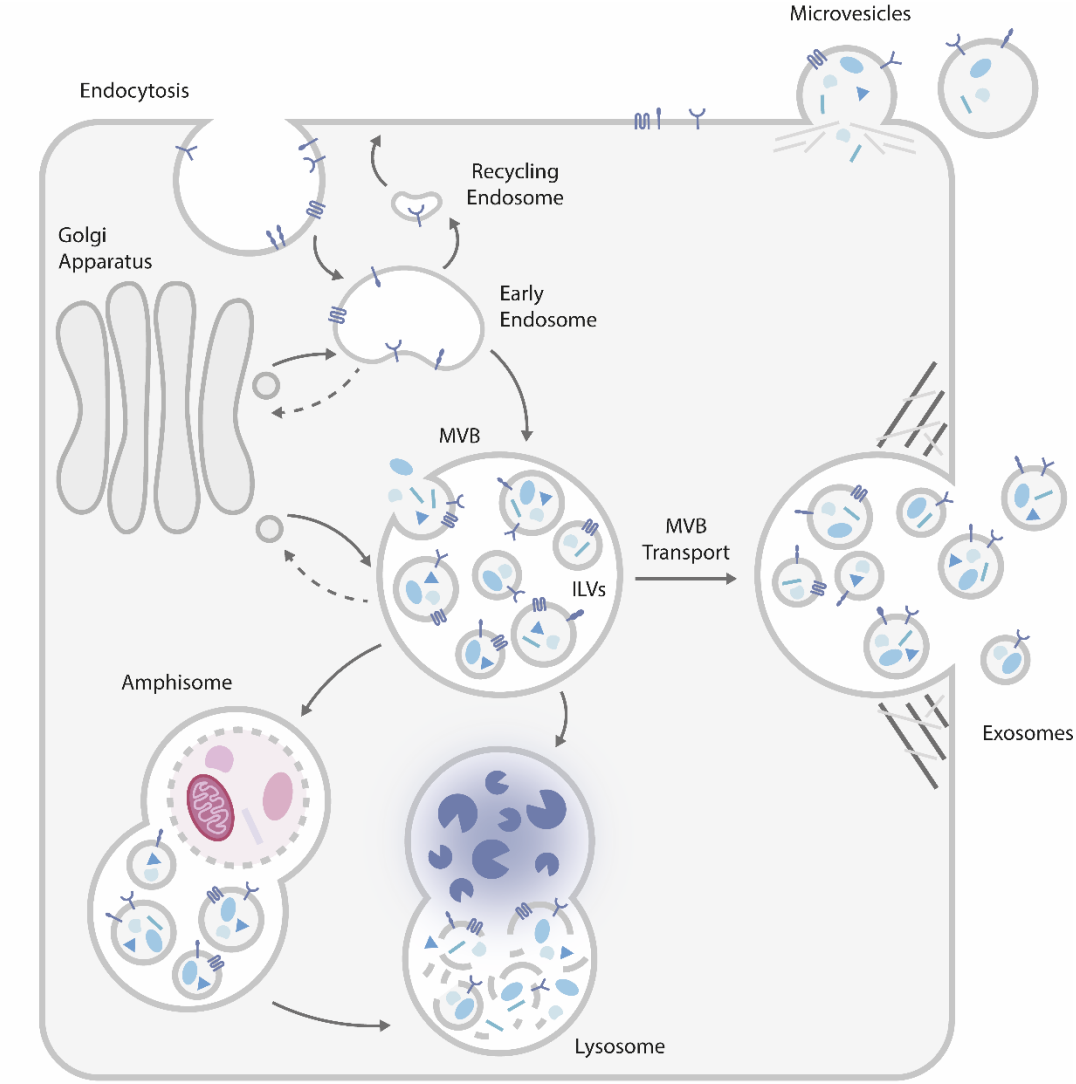

Figure 1.1. Exosome and microvesicle biogenesis.

Microvesicles arise from outward budding of specific plasma membrane microdomains. This process that involves membrane and cytoplasm remodeling mediated by flippases and P2X7 receptors, and small GTPases ARF6 and ARF1, respectively. Exosomes derive from endosomal compartments that originate from endocytosis events in the plasma membrane. These events result in early endosome formation and progressive maturation into late endosomes, which is triggered by fusion with secretory vesicles from the trans-golgi network and gradual acidification. Molecular cargo is then clustered into defined regions of the late endosome membrane by ESCRT-dependent and ESCRT-independent mechanisms that induce membrane curvature and scission. As a result, intraluminal vesicles are formed by inward budding of the limiting membrane from late endosomes, giving rise to multivesicular bodies (MVBs). MVBs can then be transported and fuse with the plasma membrane to release ILVs into the extracellular space as exosomes. Alternatively, MVB contents can be degraded by fusion with autophagosomes with subsequent amphisome formation or to lysosomes.

1.2.1. MVB formation

The ESCRT complexes (endosomal sorting complex required for transport) were the first to be identified as key components promoting membrane remodeling, scission, and subsequent formation of ILVs[31]. In the canonical ESCRT-dependent pathway, ubiquitinated membrane cargoes derived from plasma membrane internalization or the golgi apparatus are clustered into specific microdomains in the endosomal membrane[32]. This is mediated by ESCRT-0, that is recruited to endosomal membranes by phosphatidylinositol 3-phosphate (PtdIns(3)P)[33], and associates with both clathrin and ubiquitinated cargo forming a clathrin lattice[34]. ESCRT-I is then recruited by direct interaction between HRS (Hepatocyte growth factor-regulated tyrosine kinase substrate, ESCRT-0 component) and TSG101 (Tumor susceptibility gene 101 protein, ESCRT-I component)[35], which in turn recruit ESCRT-II to promote membrane budding[36]. This is followed by the further recruitment of ESCRT-III complex via interaction with ESCRT-II, which

triggers fission of the budding microdomains into ILVs[37]. After scission, ESCRT-III is disassembled from the MVB membrane by VPS4 (Vacuolar protein sorting-associated protein 4A)[38].

Alternative mechanisms that only require ESCRT-III have also been described, the most studied of which is the syndecan-syntenin-ALIX pathway. In this pathway, the transmembrane protein syndecan (SDC2) in the endosomal membrane interacts with syntenin (SDCBP2), which in turn binds to ALIX (PDCP6ID), that recruits ESCRT-III promoting membrane invagination and scission[39]. In a different mechanism, ALIX is recruited to endosomal membranes by lysobisphosphatidic acid (LBPA), followed by ESCRT-III recruitment and ILV formation[40].

The finding that MVB formation is not abolished by ESCRT complex depletion indicated the existence of ESCRT-independent mechanisms regulating exosome biogenesis[41]. The hydrolysis of sphingomyelinase into ceramide by neutral sphingomyelinase 2 (nSMAse2) was found to mediate the formation of membrane microdomains and triggers membrane budding[42]. Recently, a ceramide-dependent mechanism to generate epidermal growth factor receptor (EGFR) positive exosomes involving small GTPase RAB31 was uncovered[43]. In this mechanism, RAB31 activation by EGFR promotes RAB31 recruitment to ceramide and cholesterol-rich endosomal membranes via interaction with flotillin, promotes ILV formation, and drives EGFR incorporation into nascent ILVs. Interestingly, other receptor tyrosine kinases were also able to activate RAB31 to trigger their sorting to ILVs[43]. Tetraspanins also play a role in ESCRT-independent mechanisms. The tetraspanin CD63, one of the most well-known EV markers, was found to influence protein sorting and ILV formation in melanocytes[44]. Ablation of the tetraspanin CD9 was also reported to reduce EV secretion in dendritic cells[45]. However, the reports on the effect of CD9 on EV release are contradictory[46,47], possibly due to cell-type

differences. Interestingly, both of the tetraspanins CD9[48] and CD81[49] structures exhibit a reverse cone-like shape, which would be implicated in membrane curvature induction[50].

In summary, several ESCRT-dependent and ESCRT-independent mechanisms exist that regulate exosome biogenesis. The contribution of each mechanism may depend on cell type, physiological state and specific cargoes.

1.2.2. MVB transport to the plasma membrane

The mechanisms determining the fate of ILVs and MVBs once formed are still not well understood. It has been recently reported that some ILVs are able to retrofuse with MVB membrane, a process that co-exists with ILV release as exosomes and ILV degradation by lysosomes[51]. ISGylation (covalent attachment to interferon-stimulating gene 15) has also been shown to influence exosome secretion by promoting lysosomal degradation of MVBs[52]. Moreover, the E3 ubiquitin-protein ligase MGRN1 has been reported to inhibit the fusion of MVBs with lysosomes via TSG101 ubiquitination[53]. Interestingly, anchoring of MVBs to microtubules by the microtubule-binding protein HOOK has been shown to prevent fusion of MVBs with lysosomes and autophagosomes under non-autophagic conditions[54].

Intracellular trafficking of organelles (including late endosomes) requires the coordinated action of the cytoskeleton (i.e., microtubules and actin filaments), molecular motors (i.e., kinesins, dynein and myosins) and small GTPases[55]. MVB transport along microtubular networks is inferred from the finding that polarized secretion of exosomes takes place during immune synapses between T-cells and antigen presenting cells[56]. In addition, viral egression from insect cells via MVBs requires the actin-myosin transport system[57]. The molecular motors driving this process have not yet been established. However, several important players have been

identified. Kinesin-like protein KIFC2 was found to associate with MVB-like structures in neuronal cells[58], suggesting a possible function as a motor for MVB trafficking. Nevertheless, the role of kinesins in other cell types remains to be determined. Several Ras-related proteins have been implicated in regulating MVB transport to the plasma membrane and thus exosome release. Small GTPases RAB27A and RAB27B have been reported to regulate MVB plasma membrane trafficking and docking in various cell types[59,60]. Other Ras-related proteins such as RAB11[61], RAB35[62], RALA[63], and RALB[63] have also been shown to promote MVB motility. However, the effect of specific Ras-related proteins on EV release is cell-type dependent. This is reflected by the distinct outcomes from RAB inhibition when different cell lines are evaluated[64].

1.2.3. MVB fusion with the plasma membrane

In the last step of exosome biogenesis, multivesicular bodies fuse with the plasma membrane, releasing ILVs into the extracellular milieu as exosomes. This process is mediated by SNARE (soluble N-ethylmaleimide-sensitive fusion attachment protein receptor) complexes. The SNARE protein VAMP7 was reported to promote exosome secretion in human leukaemia cell line K562[65], however, VAMP7 inhibition did not prevent exosome release in MDCK cells[66]. Syntaxin-1A (STX1A) was also shown to control exosome release in a variety of cell lines[67]. More recently, SNARE protein SNAP23 (synaptosomal-associated protein 23) was reported to positively regulate exosome secretion in A549 and HeLa cells[68]. Additional SNARE proteins have been reported to play a role in exosome secretion in non-mammalian cells. Synaptobrevin homologue Ykt6[69] and syntaxin 5[63] were shown to be involved in exosome release in *Drosophila* and *C. elegans*, respectively. The diversity of mechanisms regulating both MVB formation and fusion with the plasma membrane reflect the complexity of exosome biogenesis and contribute to extracellular vesicle heterogeneity.

1.3. Microvesicle biogenesis

Microvesicles are formed by outward blebbing of the plasma membrane. The release of microvesicles requires membrane and cytoplasm remodelling events that enable vesicle fission from the plasma membrane[4]. Activation of small GTPases ARF6 and ARF1 has been reported to trigger myosin phosphorylation and actomyosin contraction, leading to vesicle scission and release in cancer cells[70]. Lipid composition of the plasma membrane also has a major influence on membrane budding. Translocation of phosphatidylserine to the outer leaflet of the plasma membrane by flippases has been shown to promote membrane curvature[70,71]. Moreover, ATP-mediated activation of P2X7 receptors leads to the mobilization of acidic sphingomyelinase to the plasma membrane outer leaflet, where it catalyzes the formation of ceramide, altering the membrane structure and promoting microvesicle release[72]. Similarly, loss of tat-5 flippase in *C.elegans* leads to an increase in phosphatidylethanolamine exposure on the outer leaflet of the plasma membrane, triggering microvesicle shedding[73]. Interestingly, microvesicle release required ESCRT-0 and ESCRT-I, but was unaffected by ESCRT-II or ESCRT-III depletion[73]. In further support of the role of ESCRTs in microvesicle biogenesis, the ubiquitin ligase adaptor ARRDC1 was found to recruit ESCRT complex to microvesicle budding sites leading to microvesicle release via an interaction between the PSAP motif on ARRDC1 and ESCRT-I component TSG101[74].

1.4. EV cargo sorting

EV protein cargo sorting and EV biogenesis are closely related processes that usually take place in parallel[4]. Packaging of protein cargo relies on ubiquitination-dependent ESCRT machinery, interaction with lipidic components of the budding membrane sites or association to EV-enriched proteins.

ESCRT proteins have a pivotal role in the sorting of ubiquitinated membrane cargo. ESCRT-0 components contain ubiquitin interacting motifs that cluster ubiquitinated cargo in clathrin-rich membrane microdomains[32]. ESCRT-I and ESCRT-II components also contain ubiquitin binding domains and contribute to ubiquitin-dependent cargo sorting as part of the ILV formation pathway[34]. Notably, soluble protein galectin-3 (LGALS3) was found to be sorted to EVs independently of ubiquitination by direct binding with ESCRT-I component TSG101 via P(S/T)AP motifs on TSG101[75].

The capacity of ALIX to bind polyubiquitin chains (Lysine 63-linked) has been shown to promote MVB sorting of protein cargo[76]. In yeast, the ALIX homologue BRO1 acts as a ubiquitin receptor by sorting and probably clustering ubiquitinated membrane proteins in a manner analogous to that of ESCRT-0[77]. ALIX has also been implicated in EV-loading of tetraspanins and G-protein-coupled receptors[40,78,79]. ALIX has been reported to sort CD63, CD81, and CD9 to EVs by interacting with LBPA in the MVB membrane and subsequently recruiting ESCRT-III[40]. In the case of CD9, this interaction was found to rely on CD9 ubiquitination, although direct binding of ALIX to ubiquitin was not explored. Similarly, ALIX was found to bind to G-protein-coupled receptors P2Y1 and PAR1 (via YPX3L motif interaction) to facilitate their EV packaging[78,79]. An ALIX paralog containing the Bro1 domain, HD-PTP, has also been proposed to influence the sorting of ubiquitinated membrane proteins by binding to ubiquitin and then recruiting ESCRT-III and VPS4[80]. Notably, an overlap exists between EV release and the viral budding. Several viruses have been shown to exploit ESCRT-dependent EV biogenesis for their sorting into EVs, which relies on late domain motifs found on viral proteins that recruit ALIX and ESCRT-I components[81].

CD63, one of the most abundant proteins in EVs, has also been implicated in EV loading. For example, CD63 has been reported to mediate EV packaging of the luminal domain of PMEL transmembrane protein in melanocytes in an ESCRT- and ceramide-independent manner52. Other tetraspanins such as TSPAN6[82], CD9[83], and CD82[84] have also been reported to target protein cargo to the EVs. However, the mechanism behind EV sorting has not yet been described. Moreover, interaction with EV-enriched ubiquitin ligase adaptor NDFIP1 was found to sort NEDD4 family proteins to the EVs[85]. In a similar mechanism, ubiquitin ligase adaptor ARRDC1 was involved in sorting DMT1 (divalent metal ion transporter) to the EVs[86]. Both ubiquitin ligase adaptors contain PPXY motifs that bind to WW-domains present in protein cargoes to be sorted.

Autophagy machinery has recently emerged as an important regulator of extracellular vesicle loading and secretion[87]. In a mechanism closely related to microautophagy, the chaperone HSPA8 was reported to associate with phosphatidylethanolamine in the MVB membrane and to bind to proteins containing KFERQ motif, thus promoting exosomal-loading of soluble cytosolic proteins containing these motifs[88]. Notably, this mechanism relied on TSG101 and ESCRT-III. The MVB membrane has a distinct lipid composition that promotes its interaction with proteins containing lipidic moieties. Protein myristoylation[89], GPI-anchoring[90], farnesylation[91], geranyl-geranylation and palmitoylation[92] have been shown to target proteins to specific membrane microdomains in the MVBs and plasma membrane, hence promoting their EV loading. Notably, ubiquitin-like protein UBL3, which is itself modified with geranyl-geranylation and palmitoylation was found to mediate sorting of several RAS proteins to EVs[92].

Multiple studies have reported that EVs contain various types of RNA[93]. Interestingly, EV RNA profiles differ from those of the parental cells, thus suggesting the existence of active

mechanisms for sorting specific RNAs to the EVs[93]. RNA secondary structure can itself act as a determining factor for EV packaging. Secondary structures such as loop regions and G-quadruplex structures have been found to interact with lipidic components of membranes facilitating their sorting to EVs[93,94]. Alternatively, many studies have reported a pivotal role of RNA binding proteins (RBPs) in sorting RNA cargoes with specific sequence motifs to the EVs. Although several RBPs have been described for mRNAs or lncRNAs, most of the studies have focused on microRNA (miRNAs) sorting mechanisms[95]. Heterogeneous nuclear ribonucleoproteins (hnRNPs), particularly hnRNPA2B1, have emerged as important mediators of RNA EV-sorting[93]. hnRNPA2B1 binds to GGAG/CCCU motifs in miRNAs and lncRNA resulting in their selective EV packaging[96]. Another hnRNP family member, SYNCRIP is also involved in the sorting of miRNAs containing GGCU motif[97]. A role in EV-sorting of mRNAs containing defined motifs was also proposed for the methyltransferase NSUN2 and the RBP YBX1[98]. Many additional RBPs that facilitate RNA sorting into EVs have been described to date (mostly for miRNA sorting), though their recognition motifs have not been identified[95].

Two mechanisms have been proposed for the selective sorting of RNAs by RBPs to EVs. The first mechanism relies on the direct transport of RNAs to the sites of EV biogenesis (MVBs or plasma membrane)[99]. In support to this notion, several RBPs identified in EVs have been shown to interact with CD81 or CD81 binding partners[100]. Another example is the loading of RBPs HNRNPK and SAFB into EVs via interaction with autophagy mediator LC3[101]. The second mechanism is based on the fact that EVs encapsulate cytoplasmic material near EV formation sites and that cell contents are distributed asymmetrically. Thus, it is possible that RBPs located nearby EV biogenesis sites are packaged non-selectively[99]. For example, the presence of RBPs in the cytoplasm of contact sites between the endoplasmic reticulum and the

MVBs was found to facilitate their indirect sorting into exosomes[102]. Nevertheless, a recent study by Jeppesen *et al.* showed that several commonly reported EV RBPs such as hnRNPA2B1, MVP or Lupus La protein were not detected in EVs when density gradient was used to purify EVs instead of conventional ultracentrifugation methods[103]. This study highlights the importance of EV isolation methods to avoid contamination of non-vesicular components in EV preparations.

1.5. EV uptake

EV-mediated intercellular communication typically requires docking at the plasma membrane of recipient cells in order to activate an intracellular signaling pathway, or to promote vesicle internalization (either by endocytosis or through direct fusion with the plasma membrane). Endocytosis pathways including phagocytosis, macropinocytosis, and caveolae, clathrin or lipid-raft dependent endocytosis are the most common EV-uptake mechanisms[29]. Internalized EVs are initially trapped inside newly formed endosomes that are destined to either fuse with the lysosome (leading to EV degradation), be recycled back to the plasma membrane for re-release, or (less frequently) escape from the endosome and release their molecular cargo into the cytosol of the recipient cell[27,104]. Target cell specificity is most likely determined by interactions between molecules expressed at the EV-surface and molecules displayed on the target cell plasma membrane (i.e., membrane-exposed protein receptors, lipids or sugars), which may dictate tropism towards certain tissues or facilitate uptake by specific cell types[105]. With respect to EVs, these protein mediators include tetraspanins, integrins, proteoglycans, and other extracellular matrix components[27,106,107]. For example, breast milk EVs are be taken up by monocyte-derived dendritic cells via interactions with DC-SIGN on the monocytes (Dendritic Cell-Specific Intercellular adhesion molecule-3-Grabbing Non-integrin) and MUC1 on the EVs (Mucin-1),

while EVs originated from other sources lacking MUC1 are not internalized by dendritic cells [108].

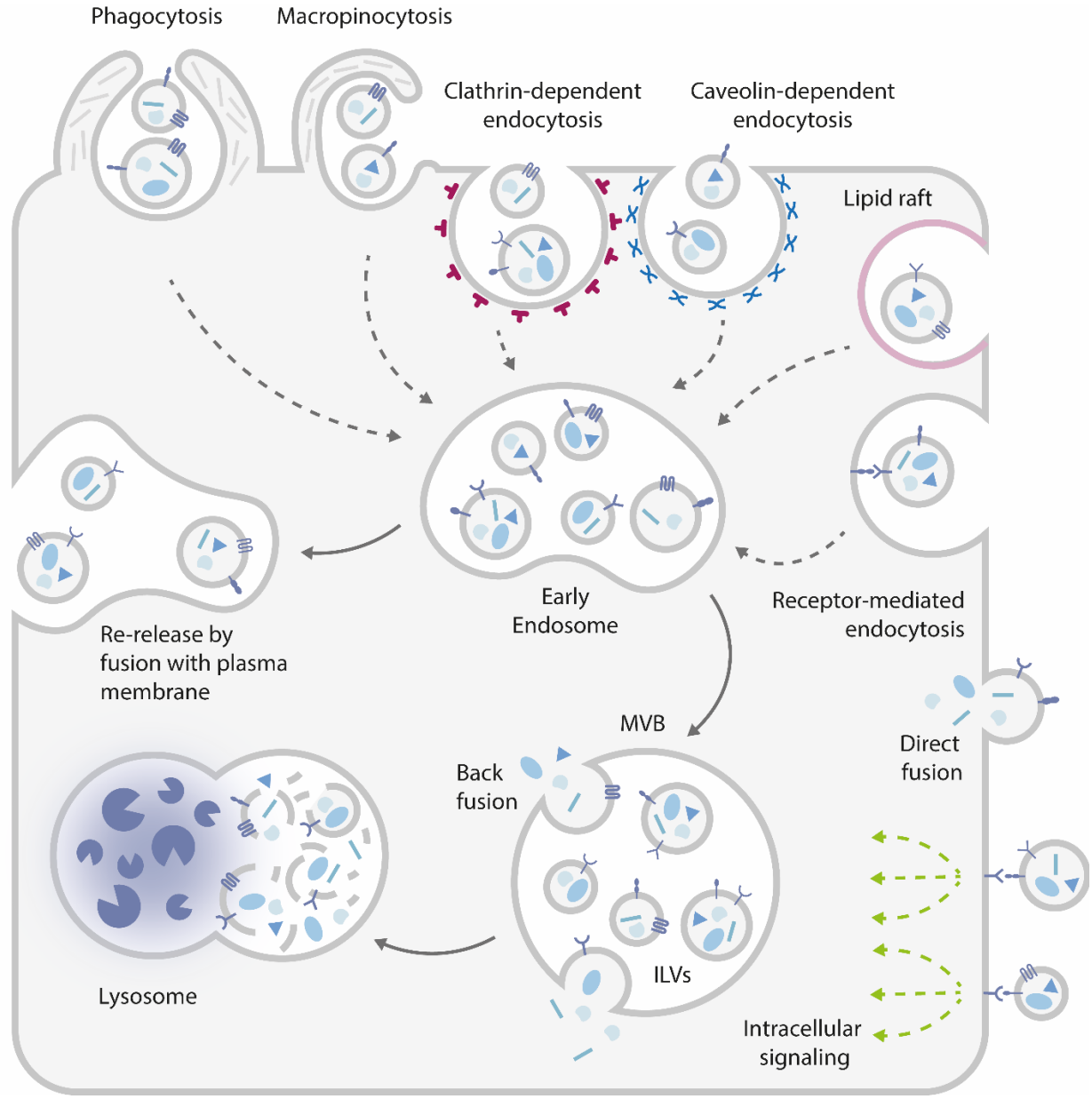

Figure 1.2. Uptake and fate of EVs in recipient cells.
EVs can be internalized by several pathways including phagocytosis, micropinocytosis, clathrin, caveolin or lipid raft-dependent endocytosis or receptor mediated endocytosis. After internalization, EVs will enter the endosomal pathway, through which EVs can either be re-released to the extracellular space or can reach the MVBs. EVs may be degraded by fusion of the MVBs with the lysosome or may release their contents into the cytoplasm by fusing with the limiting membrane of the MVBs. Non-internalized EVs can also release their cargo to the cytosol by directly fusing with the plasma membrane. Alternatively, EVs can remain bound to specific receptors in the cell surface to activate intracellular signalling pathways.

1.6. Biological function of EVs

EVs have been implicated in intracellular communication between neighboring cells as well as distant cells from different tissues or organs. EV-mediated communication may involve the intracellular delivery of EV cargo (particularly miRNAs) or cell-surface interactions to trigger a biological response in the recipient cell.

Under physiological conditions, EVs participate in the regulation of multiple homeostatic processes during cell development[106]. For example, EVs from neural stem cells have been reported to control neuronal stem cell differentiation via miR-9 delivery[109]. A role of EV in cardiovascular protection has also been proposed in numerous studies showing that cardiac-progenitor-cell derived EVs were enriched in cardioprotective miRNAs (e.g., miR-146a-3p) and improved cardiac function after myocardial infarction[110–112]. Moreover, EVs have emerged as major mediators of cell immunity. EVs from antigen-presenting cells have been found to possess MHC (major histocompatibility complex) class-II molecules that are able to induce activation of T cells by directly presenting the peptide antigens in the EV surface[22,113]. The influence of EVs in antigen presentation has been assessed in the context of bacterial infection, where macrophage

derived EVs were reported to trigger antibacterial immune responses by promoting bacterial antigen presentation[114]. Moreover, EVs have been proposed to protect from bacterial toxins by displaying toxin receptors on the EV surface and thus inhibit bacterial toxins binding to target cells[115]. EVs may also help to prevent infection by means of miRNA delivery. EV-mediated delivery of a specific set of miRNAs from trophoblasts to non-placental cells resulted in a reduction of viral replication in the recipient cells by inducing autophagy[116].

Under pathological conditions, EVs are involved in oncogenesis, immune suppression and facilitating viral infection. During oncogenesis, tumor cells release specific EV subpopulation that modulate the tumor microenvironment, alter immune cell activity and promote tumor proliferation (e.g., inducing angiogenesis)[117]. Tumor cells have also been reported to exploit EVs to inactivate T lymphocytes or natural killer cells, and to trigger regulatory T lymphocyte differentiation to suppress immune reactions[118,119]. EV-mediated transmission of miR-212-3p was implicated in tumor immune evasion by down-regulating MHC-II transcription factor RFXAP in dendritic cells. The presence of immunomodulatory molecules such as PD-L1 (programmed cell death ligand 1) or FasL (Fas cell surface death receptor ligand) on the EV surface has also been reported[120]. For example, PD-L1 displayed on melanoma-derived EVs was found to suppress T cell antitumor immunity *in vivo*[121]. In viral infections, viruses exploit the exosome biogenesis machinery to encapsulate into EVs to escape immunity and enhance their infectivity[81]. Furthermore, EVs have been involved in inflammation[106]. For example, EVs secreted by mast cells of asthmatic mice were found to contain immunomodulatory molecules including MHC class II and ICAM-1, which triggered the activation and recruitment of B and T cells, leading to lung inflammation[122].

Within the nervous system, EVs play a dual role both promoting or preventing the aggregation of abnormally folded proteins[123]. Several studies have suggested that misfolded proteins associated with neurodegenerative conditions such as Alzheimer's disease or Parkinson's disease are secreted and delivered via EVs, thus participating in the propagation of abnormal protein aggregates in the brain[124]. Conversely, it has also been reported that EVs can have neuroprotective roles in these diseases, by promoting the clearance of misfolded protein aggregates[123].

Despite the overwhelming number of studies reporting the role of EVs in a myriad of biological processes, caution should be exercised when interpreting EV-mediated biological effects. Most studies do not consider EV stoichiometry and use very high EV concentrations (>10^5 EVs/ cell for *in vitro* settings[125]) that do not reflect physiological conditions to evaluate a given effect, which may lead to misleading results[126]. In addition, EV preparations are often contaminated with protein aggregates or serum components (due to suboptimal EV purification methods) that may at least partially account for the observed biological effects[126]. This was illustrated by Whittaker *et al*., in a study showing that non-vesicular paracrine factors that co-isolated with EVs were responsible for the biological activity that was attributed to mesenchymal stem cell EVs[127]. Moreover, in many studies the effect induced by EVs is attributed to EV-mediated miRNA transmission[106]. However, the typical EV-miRNA concentrations reported in EV studies are usually below the estimated threshold required for achieving functional effects in cells (~100-2,000 copies miRNA/cell[128–130])[126,131]. The notion that functional miRNAs are not transmitted via EVs was further supported in a thorough study that analysed functional miRNA delivery in cell culture, in which no functional delivery of miRNA could be detected[131].

1.7. Intrinsic therapeutic properties of EVs

EVs derived from some cell types have been shown to exhibit an intrinsic capacity to promote tissue regeneration and repair, which may further augment their therapeutic potential as drug delivery vehicles[132]. In particular, much research has focused on mesenchymal stem cell-derived EVs (MSC-EVs) for tissue regeneration applications[133]. MSCs have been reported to elicit their regenerative activity by suppressing pro-inflammatory processes and by reducing oxidative stress and fibrosis[134]. In this manner, the ability of endogenous stem cells to repair injured tissues is enhanced via EV-mediated cell-to-cell communication[135]. The therapeutic effect of human MSC-EVs has been shown extensively in preclinical animal models of numerous pathologies. For example, MSC-EVs have been found to promote regeneration of renal tissue in acute kidney injury models[136], cardiac tissue in myocardial infarction models[133], neural cells in ischemic stroke and traumatic brain injury models[137], and hepatic tissue in models of acute liver injury, hepatic failure and hepatic ischemia[138,139]. EVs possess several advantages over cell-based therapies for regenerative medicine applications, such as lower immunogenicity, longer shelf-life, and there is no possibility of stem cell-induced tumor formation[134]. Indeed, in some cases the beneficial effects of MSC cell therapy have been recapitulated using MSC-EVs alone *in vivo*[134]. To date, two clinical trials involving the use of MSC-EVs derived from bone marrow and umbilical cord have shown promising results for treating graft-versus-host disease[140] and chronic kidney disease[141], respectively. In addition, several clinical trials to determine the safety and efficacy of long-term treatment with human MSC-EVs are ongoing[142]. Specifically, human umbilical cord MSCs EVs and miR-124-loaded MSC-EVs are being assessed to treat macular holes (NCT03437759) and acute ischemic stroke (NCT03384433), respectively.

1.8. Therapeutic application of EVs

EVs are able to deliver cargo to recipient cells, making them attractive candidates for drug delivery[25]. Suitable cargoes include hydrophobic small molecule drugs, or macromolecular therapeutics comprised of nucleic acid or protein-based therapeutics. EVs possess numerous advantages when compared to other delivery systems such as viral delivery or synthetic nanoparticles. Given that EVs are autologous, they exhibit lower toxicity and immunogenicity than virus or cell-based therapies[143]. As compared to the synthetic lipid nanoparticles, EVs can exploit existing biological mechanisms to enhance cargo loading, targeting, and delivery. In addition, EVs confer protection against enzymatic degradation (if the cargo is encapsulated inside EVs) and thereby improve drug stability in the circulation[144]. For instance, several chemotherapeutic drugs have been delivered via EVs in order to improve their solubility, stability, and delivery to target tissues[145,146]. These include curcumin, a hydrophobic drug with low bioavailability[146], paclitaxel[147], and doxorubicin[145]. Moreover, several studies have shown that EVs have the potential to cross tissue and cellular barriers, most notably the blood brain barrier (BBB), that represents one of the most important factors limiting the delivery of drugs to the central nervous system[148–150].

Small interfering RNAs (siRNAs) and miRNAs are short RNA molecules that primarily act as post-transcriptional regulators of mRNA expression[151]. Their therapeutic potential has been widely reported in numerous studies[151–153], although their systemic delivery to extrahepatic target tissues remains a major challenge. siRNAs and miRNAs have been delivered using EVs to a variety of cell types both *in vitro* and *in vivo*[154]. EVs have also successfully delivered multiple types of therapeutic proteins such as Cas9 (CRISPR associated protein 9)[155], enzymes[156], receptor decoys[157], or antigens for vaccination[158].

1.9. EV delivery challenges

EVs hold a great promise as therapeutic vehicles, however, several challenges must be addressed before the potential of EVs as therapeutics can be fully realized: poor efficiency of EV-loading, a lack of efficient EV-targeting to specific cells/tissues, a need to promote endosomal escape once EVs are internalized by the recipient cell, and a lack of standardized methods for EV production and isolation[143].

1.9.1. EV clearance from circulation

In vivo clearance studies revealed that EVs are rapidly cleared after systemic administration. More precisely, the half-life of EVs has been estimated to be around 5 minutes in rodents[159,160] and about 40 minutes in primates[161]. After clearance from the circulation, the main sites of EV accumulation have been shown to be liver and spleen, followed by the lungs[160,162]. Nevertheless, EV biodistribution in mice was shown to depend on the EV producer cell type and the route of administration. For example, tail vein injections led to EV accumulation in the spleen and liver, while intraperitoneal injection promoted accumulation in pancreas and gastrointestinal tract[162]. Interestingly, the presence of EV surface markers such as CD47175, or PEG modification[164], have been reported to reduce EV clearance by immune cells by acting as 'don't eat me' signals. However, PEGylated nanoparticles suffer from an immunogenic response known as the "accelerated blood clearance phenomenon" by which nanoparticles are rapidly cleared from blood upon repeated administration[165]. This phenomenon is due to the induction of IgM antibodies against PEG modification[165].

Importantly, it should be considered that most biodistribution studies are based on a single injection of large quantities of EVs, thus not reflecting the native conditions of EV release

(i.e., continuous release of EVs into circulation). Further research is required to understand the mechanisms behind long-range EV transmission across circulation to optimize EV dosage and route of administration by mimicking the natural process.

1.9.2. EV targeting

A major challenge limiting use of EVs for therapeutic purposes is the delivery of sufficient quantities of EVs to specific target cells, while preventing their accumulation in off-target tissues, where they may induce undesired effects[143]. Although the mechanisms are not well-described, after systemic delivery therapeutic EVs need to be transported across the vascular endothelium via extravasation or transcytosis to reach their target tissue or organ. For example, several studies have reported that tumor-derived EVs are capable of traversing the BBB by transcytosis[166]. EV protein and lipid composition is influenced by the producer cell type, which may explain the variation in biodistribution shown by EVs from different cell sources. Along these lines, a study by Hoshino *et al*. revealed distinct integrin combinations that were responsible for tissue specific uptake and accumulation[167]. In this study, expression of integrins α6β4 and α6β1 were associated with lung metastasis, while integrin αvβ5 was linked to liver metastasis[167]. Tetraspanins have also been implicated EV uptake modulation. EVs containing TSPAN8 and integrin α4 (ITGA4) were shown to preferentially interact with CD54 ligand present on endothelial and pancreatic cells triggering EV uptake[168]. Interestingly, several studies have suggested that EV delivery is accentuated in pathological conditions due to a shift in biodistribution towards inflamed tissues. EV uptake was reported to be increased in tumor tissue as compared to neighboring healthy tissues[162]. In addition, systemic inflammation was shown to increase BBB EV permeability in mice[166].

To modulate the tropism of EVs and promote their uptake by target cells, the EV surface can be modified to display protein or peptides with targeting abilities. One of the most commonly utilized peptides is rabies virus glycoprotein (RVG) peptide, a 29 amino acid peptide which has been used to target EVs to tissues expressing the acetylcholine receptor, and thereby promoting EV transport across the BBB since the endothelial cells present at the BBB express these receptors[169]. The target cells of RVG-modified EVs include neurons, endothelial cells, cardiomyocytes, and kidney cells[162]. A landmark example of EV-mediated delivery of therapeutics across the BBB involved the expression of RVG-LAMP2B fusion peptide in the EV surface[149]. This strategy enabled the delivery of siRNA to neurons, microglia, and oligodendrocytes, with concomitant silencing of BACE1 protein expression in wild-type mouse brain after systemic injection[149]. RVG-LAMP2B constructs have also been investigated for delivery to other acetylcholine receptor-rich organs such as kidney and muscle. Intramuscular injections of RVG-EVs loaded with the anti-fibrotic miRNA mimic miR-29 were able to reduce unilateral ureteral obstruction (UUO)-induced muscle loss and renal fibrosis in a UUO mice model induced by ligation of the left ureter[170].

Moreover, additional peptides have also been used to target various cell types such as tumor cells and cardiomyocytes. CendR peptides contain the (R/K)XX(R/K) motif and exhibit a high binding affinity for neuropilin-1 receptor (NRP1), which is also highly expressed in tumor cells[171]. CendR peptides induce extravasation and tissue penetration, which may compensate for the high interstitial pressure in solid tumours[172]. CendR-modified EVs demonstrated efficient doxorubicin delivery to αv integrin-positive breast cancer cells and to tumor xenografts *in vivo* after intravenous injection, where they inhibited tumor growth with low off-tumor toxicity[171]. GE11 peptide, which targets EGFR-expressing tumor cells, fused to PDGFR in the EV

membrane was also reported to enhance the delivery of synthetic let-7a miRNA mimics to EGFR-expressing breast cancer cells[173]. This strategy resulted in an increase in EV tumor accumulation after an intravenous injection of GE11-modified EVs. To target cardiac muscle, two separate studies used LAMP2 fused to cardiac-targeting peptides identified by phage display[174,175]. Both LAMP2-peptide fusion constructs improved the delivery to cardiomyocytes in cell culture and to mice hearts *in vivo*[174,175]. In one of the studies, decreased cardiomyocyte apoptosis was observed after EVs displaying cardiac-targeting peptides were administered via intramyocardial injection in wild-type C57BL/6 mice[174]. Nanobodies have also been successfully displayed on EV surfaces via association with lipids in the EV membrane. This strategy has been utilized to increase EV uptake by EGFR or HER2 expressing cells for anti-tumor therapy[176–178].

Alternative cloaking strategies have involved the use of click chemistry or the interaction between streptavidin and biotin to anchor specific targeting moieties to EVs. Click chemistry is one of the most common methods to chemically modify EVs and refers to a set of reactions that are simple, stereospecific, high yield, irreversible, bioorthogonal, and can be carried out in physiological buffers[179]. To deliver a chemotherapeutic drug to tumor cells, Lee *et al*. used paclitaxel-loaded EVs decorated with a CGKRK cell-penetrating peptide attached via copper-free click chemistry[180]. CGKRK penetrates tumor cells and tumor endothelium by binding to heparan sulphate, which is highly abundant on the tumor cell surface[181]. Paclitaxel-loaded CGKRK-EVs exhibited increased tumor cell cytotoxicity *in vitro* when compared to non-targeted EVs[180]. Antes *et al*. employed a membrane anchoring strategy based on biotin and streptavidin to decorate EVs with peptides that confer targeting to myoblasts and ischemic heart tissue[182]. This strategy is based on a glycerol-phospholipid-polyethylene glycol-streptavidin conjugate (DMPE-PEG-STVDN) that was added to the isolated EVs. The DMPE-PEG moiety

serves as an anchor by embedding in the EV membrane, while the streptavidin is exposed on the EV surface and available for binding to biotinylated molecules. Membrane intercalating PEG derivatives have also been utilized to anchor targeting moieties within the same EVs to improve targeting. Wang *et al*. used DSPE-PEG (1,2-dioleoyl-sn-glycero-3-phosphoethanolamine-PEG) to attach RGD targeting peptides to EVs. The authors used a double targeting approach involving RGD peptide and folic acid that improved EV delivery to tumor cells. Folic acid is able to bind to the folate receptor, that is highly expressed in cancer cells, and thereby promote receptor-mediated endocytosis[183].

1.9.3. Endosomal escape

Native EVs have been reported to possess an inherent capacity to deliver functional molecules to recipient cells. However, the intrinsic cargo transfer efficiency of EVs appears to be low[131,184]. Albanese *et al*., assessed EV-mediated functional delivery of β-lactamase (actively loaded by CD63 fusion) between 5 different donor and 17 different recipient cell lines[131]. Delivery efficiency was below 1% in all combinations and was lower that 0.1% for most of them. Notably, when endosomal escape was enhanced, functional delivery increased for most cell combinations up to 99%[131]. Several pathways have been proposed to mediate EV cytosolic delivery of cargo, but the mechanisms involved are not well characterized. To achieve efficient cargo delivery, EVs must escape from the endosome and release their contents to the cytoplasm before they are degraded by the lysosome or re-exported from the cell. Most studies have shown that following uptake, EVs accumulate in endo-lysosomal compartments before reaching the lysosome[185,186]. Recently, Joshi *et al*. showed that some EVs are able to fuse with the limiting membrane of endosomes in a process facilitated by acidification, resulting in EV cargo release to the cytoplasm[187]. This was further confirmed by Bonsergent *et al*., who reported that only 4% of the

EVs were taken up after a 20h incubation[184]. Of those EVs that were taken up, 30% were able to release their contents into the cytoplasm in an acidification-dependent manner. Alternatively, gap junctional protein connexin 43 (GJA1) has been involved in mediating direct fusion of EVs with the plasma membrane as well as serving as a channel for transferring low molecular weight cargoes into the cytosol[188]. This property was exploited to promote delivery of EV-loaded RNA to recipient cells by overexpressing a constitutively active connexin 43 mutant (S368A) in the EV surface[189].

Bacteria and viruses have evolved multiple strategies for target cell entry and escape from the endolysosomal pathway, with the potential for exploitation in EV bioengineering applications. These strategies include pore formation in the endosomal membrane, endosomal membrane disruption, fusion with the endosomal membrane, and the proton sponge effect[190,191]. In the latter, acidification of the endosomal lumen leads to protonation of the entrapped molecules, inducing an inflow of H^+, Cl^- and water into the endosomes, which results in endosome bursting[191].

Several viral peptides have been identified that are able to promote endosomal escape, such as TAT peptide (transactivator of transcription), a commonly used cell penetrating peptide (CPP) derived from human immunodeficiency virus 1 (HIV-1) and flock house nodavirus (FHV) arginine-rich peptide[191], which have also been utilized in the context of EV modification[192]. TAT and other arginine-rich peptides have been shown to increase the uptake and cytosolic delivery of various conjugated cargo ranging from small molecules to oligonucleotides and proteins.[193–196] Modification of EVs with arginine-rich peptides has also been used to enhance delivery. Nakase *et al*. used arginine-rich peptides to increase EV uptake efficiency and cytosolic delivery. EV membranes were modified using an amine-to-sulfhydryl crosslinker (Rn-EMCS), that enabled

the conjugation of octaarginine peptide to membrane proteins[197]. Modification with an arginine-rich peptide induced uptake of EVs loaded with saporin (ribosome-inactivating protein) by macropinocytosis and enhanced the cytotoxic anti-tumor effects in CHO cells[198]. Arginine-rich peptides facilitate delivery by promoting electrostatic interactions between positively charged arginine-rich peptides and the plasma membrane, that exhibits a negative charge due to the presence of proteoglycans. In addition, octaarginine peptide improves uptake by inducing clustering of the proteoglycan syndecan-4 at the plasma membrane, resulting in its binding to protein kinase C alpha (PKCα) in the cytoplasm. Both syndecan-4 clustering and PKCα binding triggers a signaling cascade that induces macropinocytosis and cellular uptake of the peptide, suggesting a similar uptake mechanism for octaarginine-modified EVs[199].

Non-cationic peptides which have been reported to promote endosomal escape include GALA peptide, an amphipathic 30 amino acid viral fusion protein mimic that has been reported to promote endosomal escape in HeLa cells[198,200]. Under acidic conditions, GALA peptide converts from a random coil to an amphipathic alpha-helix, exposing negatively charged glutamic acid residues and a hydrophobic region formed by an EALA repeat. This region mediates the interaction with neutral and negatively charged lipid bilayers, which promotes the fusion of the EV and endosome membranes[200].

In addition to peptides, EV pseudotyping has also been used to facilitate EV targeting and endosomal escape. Pseudotyping is a well-known strategy used in virology to modify the tropism of viruses by expressing foreign envelope proteins on their surfaces. Vesicular stomatitis virus glycoprotein (VSVG) protein has been extensively used for EV pseudotyping to promote vesicle endosomal escape due to its fusogenic properties, natural EV-membrane sorting capacity and broad tropism[201–204]. VSVG is a trimeric protein that binds to low-density lipoprotein receptor

(LDLRs) on the cell surface and mediates the fusion between the EVs and the endosomal membrane in response to low pH[205,206]. Baboon endogenous virus envelope (BaEV) protein in combination with VSVG has also been used to enhance cytosolic delivery to T-cells, B-cells, and hematopoietic stem and progenitor cells[207,208]. BaEV binds to human sodium-dependent neutral amino acid transporter type 1 or 2 and thus has a different tropism than VSVG[209]. Notably, envelope proteins dictate the tropism of EVs due to their intrinsic targeting capacities. Thus, this should be taken into account when pseudotyped EVs need to target specific tissues given that the addition of targeting moieties would only serve to broaden the EV tropism, but may not necessarily increase the selectivity. Despite their high efficiency, viral derived proteins are immunogenic, thus limiting their potential therapeutic use. Therefore, the use of endogenous fusogenic proteins has gained interest since they would represent a non-immunogenic alternative to viral proteins. Special consideration should be taken when attempting to replace VSVG, since it not only influences endosomal escape, but also mediates uptake by recipient cells expressing LDLR. Therefore, the uptake efficiency of EVs may as well be compromised in the absence of VSVG. Recently, Segel *et al.* explored the use of mouse syncytins A (*SynA*) and B (*SynB*) (homologous to human syncytins) as an alternative to VSVG to promote endosomal escape[210]. Although syncytin A-pseudotyped EVs were able to deliver cargo to recipient cells, this required the addition of Vectofusin-1, a short histidine-rich amphipathic peptide known to enhance the infectivity of viral vectors, hence limiting the *in vivo* application of syncytins[210].

1.9.4. EV loading

The use of EVs as therapeutic delivery vehicles requires strategies that allow for efficient cargo loading. Two different approaches for EV loading have been developed: exogenous loading, whereby EVs are first isolated and then subsequently loaded with the cargo, and endogenous

loading whereby EV-producer cells are genetically modified to promote loading of the cargo during EV biogenesis.

1.9.4.1. Exogenous loading

Exogenous loading techniques are based on the passive association of hydrophobic molecules with the EV membrane, membrane disruption methods that transiently increase EV membrane permeability, chemical modification of the EV surface, liposome fusion, and strategies that actively promote cargo association with the EV membrane[211]. EV-loading of hydrophobic molecules can be achieved by simple incubation methods that enable moderate loading efficiencies. Most research has focused on loading hydrophobic drugs such as curcumin or paclitaxel to improve their biodistribution and absorption. Saari *et al.* reported that loading of paclitaxel to EVs derived from prostate cancer cells by simple incubation increased paclitaxel cytotoxic effect[147]. Similarly, paclitaxel-loaded MSC-derived EVs were able to elicit a strong anti-tumor activity in in cell culture[212]. In a separate study, curcumin was loaded to the EVs by simple incubation and was delivered to mice models of brain inflammation via intranasal administration. Treatment with EVs was reported to protect from lipopolysaccharide (LPS)-induced brain inflammation, to delay the progression of induced experimental autoimmune encephalomyelitis, and to reduce tumor proliferation in a tumor mode[213]. Amphipathic molecules composed of a lipidic moiety and EV cargo can also be anchored to the EV membrane by simple incubation[214]. This strategy has been used to functionalize EV membranes with targeting peptides or for siRNA loading. RGD targeting peptide was displayed in the EV surface via conjugation with lipidic DSPE-PEG molecule, that spontaneously inserts in the EV membrane[171]. siRNAs have also been passively loaded to EVs via cholesterol conjugation to increase their hydrophobicity and EV membrane interaction. For example, O'Loughlin *et al*. explored the use

of cholesterol-conjugated siRNAs and were able to show dose-dependent silencing of Hu antigen R (HuR), in HEK293T cells after treatment with EVs incubated with the modified siRNAs[215]. Despite the simplicity of passive incubation, this method is only compatible with hydrophobic molecules (or cargo that can be conjugated to hydrophobic compounds), and the efficiency of passive EV loading is usually lower than the expected for active loading[211].

Mechanical methods for permeabilizing the EV membrane have been found to be efficient for encapsulation of both small molecules and macromolecules. The main approaches to induce membrane permeabilization include sonication, electroporation, extrusion and saponin incubation[214]. Sonication applies ultrasound to induce mechanical disruption of the plasma membrane of EVs to enhance membrane permeability[216]. This method has been explored for the loading of hydrophobic drugs such as paclitaxel and doxorubicin, siRNA, and proteins. In a study by Lamichhane *et al*., EVs loaded with siRNA via sonication were able to reduce the expression of HER2 in breast cancer cells[217]. Nevertheless, sonication even at low power has been reported to alter the size, membrane integrity and uptake of EVs by recipient cells[216].

Electroporation is based on applying a transient electric field that generates pores in the membranes inducing their permeabilization and thus facilitating cargo loading into the EV lumen[218]. Numerous studies have used this method to encapsulate nucleic acids such as RNA and DNA, as well as chemotherapeutic drugs into EVs[219]. Usman *et al.* used this technique to load EVs with antisense oligonucleotides targeting miR-125b, or Cas9 mRNA together with single-guide RNA (sgRNA)[220]. RNA delivery was found to inhibit miRNA activity and promote CRISPR-Cas9 genome editing in cell culture and mice[220]. However, electroporation has been observed to promote aggregation of EVs and siRNAs. In a study by Kooijmans *et al.*, electroporation induced siRNA aggregation due to the release of metal ions from the metal

electrodes. Chelation of the metal ions by EDTA prevented siRNA aggregation and co-isolation together with EVs, dropping the loading efficiency from 20% to 0.05%[221]. Consequently, some studies have introduced EDTA during electroporation to prevent cargo aggregation[217]. In addition, Johnsen *et al*. found that electroporation increased EV particle size nearly 5-fold due to EV aggregation[222].

Artificial generation of drug loaded EVs from cell membranes has been achieved by extrusion. In this technique, cells are sequentially extruded together with the drugs to be loaded through a series of micrometer-pore membranes to generate exosome-mimetic nanovesicles (EMNVs) loaded with drugs[223]. This strategy enabled the delivery of EV-encapsulated chemotherapeutic drugs to tumor cells and xenograft mice models which resulted in tumor growth inhibition[223]. Alternatively, EMNVs derived from MSCs have also been produced by ultrasonication[224]. Freeze thaw has also been used alone or in combination with other methods such as sonication to load cargo into the EVs[211]. However, concerns regarding potential deleterious effects on EV contents and membrane integrity have been raised[225].

Membrane permeabilization can also be achieved by non-mechanical approaches using mild surfactants such as saponin that induce pore formation in EV membranes. This technique has been utilized to load gold nanoparticles, porphyrins, and proteins[219]. In a study that explored several physical methods for catalase EV-loading (incubation, saponification, sonication, extrusion and freeze-thaw), saponification showed one of the higher EV-loading efficiencies together with sonication and extrusion[226]. Moreover, EVs loaded with catalase via saponification or sonication elicited a robust neuroprotective effect in Parkinson disease mouse models[226]. Despite these positive results, saponin is difficult to remove from EV preparations and it has only

been assessed in a few studies[225]. Hence, possible effects of saponin on EV integrity and uptake should be assessed in further studies to determine its suitability as an EV-loading method.

Common transfection reagents such as lipofectamine[227,228] and polyethylenimine (PEI)[229] have also been used to enhance EV-loading of nucleic acids. However, the loading efficiency of this method is limited, and it may lead to contamination of EV samples with transfection reagent micelles[211]. Negatively charged cargo such as RNA and DNA, have been loaded into the EVs by generating a pH gradient across luminal and extracellular faces of the EV membrane[230]. This method has been used to enhance EV loading of miRNA, siRNA, and single-stranded DNA at levels comparable to those obtained by sonication or electroporation[230]. Alternative methods to combine liposomes and EVs have been developed to modify the EV membrane composition and luminal cargo. Fusion of drug-loaded liposomes and EVs via freeze-thaw or PEG-mediated fusion enabled the generation of hybrid particles with EV and liposomal properties[231,232]. Hybrid EVs showed improved delivery efficiency of a chemotherapeutic drug as compared to liposome encapsulated drug[232].

The EV membrane can be covalently modified with functional moieties such as targeting peptides or fluorescent molecules using chemical compounds. Amine groups found on proteins exposed in the EV surface or less frequently, amines of phosphatidylethanolamine that are present on the EV surface can be functionalized by click-chemistry[179]. Alternatively, modified lipids containing reactive groups can be integrated in the EV surface by simple incubation[233]. Several simple click-chemistry reactions have been developed to functionalize EVs. These include thiol-malemide chemistry, azide-alkyne cycloaddition chemistry, EDC/NHS chemistry, and amidation chemistry[179]. For example, Di *et al.* used a hydrophobic membrane association strategy to functionalize EVs using maleimide-modified DSPE-PEG lipid[233]. This method

enabled the addition of several thiol-modified moieties to the EVs via maleimide conjugation by click chemistry.

The presence of specific proteins or lipids enriched at the EV surface can be exploited for extraluminal cargo EV loading. Peptides and proteins that associate with EV-enriched components can be directly fused to protein cargo or can be conjugated with nucleic acids to enhance loading efficiency. The C1C2 domain of lactadherin[234], CP05[235], apolipoprotein A-I mimetic peptide 4F[236], and GAPDH G58[192] peptide have been reported to achieve efficient EV cargo loading. C1C2 domain binds to phosphatidylserine that is present in the EV membrane[234] and has been used to display targeting peptides as well as protein antigens for vaccination[229]. In a study by Antes *et al*., EV-producer cells were engineered to express three copies of an ischemic tissue-targeting peptide sequence fused to the C1C2 domain of lactadherin[182]. Using this approach, increased EV uptake levels were observed in ischemic mouse heart tissue. Apolipoprotein A-I mimetic peptide 4F has a high affinity for phospholipids and thus readily associates with the EV lipid bilayer[236]. Ye *et al*. used this peptide to functionalize methotrexate-loaded EVs with therapeutic KLA peptide (KLAKLAKKLAKLAK) and targeting apolipoprotein B (APOB) LDL receptor binding domain (APOB LDLR) peptide to increase glioma targeting and EV-mediated therapeutic effects[237]. KLA peptide is a proapoptotic peptide [238] while APOB-LDLR peptide enables EV transport across the BBB and binding to the LDL receptor[239], that is highly expressed in glioma cells[240]. EVs displaying KLA and APOB-LDLR peptides showed enhanced uptake in a glioma cell line, promoted BBB traversal, and reduced growth of glioma spheroids[237]. In addition, glioma xenograft mice treated with KLA-APOB-LDLR-EVs exhibited increased survival relative to unmodified control EV-treated mice. CP05 peptide binds to CD63 protein on the surface of EVs and can therefore be utilized to modify the

surface of $CD63^+$ EVs. Gao *et al*. used CP05 peptide for both loading and targeting purposes; by conjugating it to a dystrophin splice correcting antisense oligonucleotide (CP05-PMO) and to M12 muscle targeting peptide (CP05-M12) to treat a mouse model of Duchenne muscular dystrophy (the *mdx* mouse)[235]. Systemic injection of EVs displaying both PMO and M12 peptide increased dystrophin protein expression by 18-fold in the muscle of *mdx* mice compared to CP05-PMO alone without apparent toxicity[235]. More recently, CP05 peptide has also been used for peptide display of neuroprotective and anti-angiogenic peptides for optic neuropathy[241] and retinal angiogenesis[242], respectively. In addition, a switchable platform based on CP05 and PEG separated by a labile linker has been described for controlled PEG release from EVs under ultrasound irradiation[243]. G58 peptide from GAPDH is able to associate to the EV surface via phosphatidylserine interaction[192]. To load siRNA on the EV surface and to promote endosomal escape, Dar *et al.* used G58 peptide fused to a dsRNA-binding motif derived from TARBP2 (TAR RNA-binding protein 2) and to FHV (flock house nodavirus) arginine-rich peptides. EVs displaying G58-TARBP2-FHV significantly enhanced siRNA-mediated silencing in cell culture. Moreover, treatment with siRNA-loaded EVs displaying RVG and G58-TARBP2-FHV, induced significant silencing of the *Htt* gene in mouse brain cortex and a significant reduction of p62 inclusion bodies, a molecular feature of Huntington's disease pathology[192]. In addition to peptides and proteins, other molecules have been investigated for EV membrane association. Interaction of DNA aptamers with specific proteins on the EV surface was exploited by Wan *et al*. for EV surface functionalization[244]. Although delivery to recipient cells was not assessed, this method allowed the assembly of DNA nanostructures via a DNA hybridization chain reaction initiated by the aptamer trigger.

Recently, a novel method has been developed that enables the loading of plasmid DNA on the EV surface using highly charged proteins. So-called supercharged proteins contain positively charged amino acid residues on the protein surface that bind to both plasmid DNA cargo and to the negatively charged EV membrane. Modified EVs were able to mediate functional delivery of Cre plasmid to recipient cells. Furthermore, this strategy enabled successful plasmid delivery to mice brains.

1.9.4.2. Endogenous loading

Endogenous loading relies on the cellular machinery of EV producer cells to sort therapeutic cargo to the EVs. Direct cell transfection (e.g., for nucleic acids) or co-incubation (e.g., for membrane-permeable molecules) methods can be utilized to introduce the desired therapeutic molecules into the producer cells before EV sorting[203]. For RNA and protein therapeutics, the cellular machinery can be harnessed not only to sort the cargo into the EVs but also to generate the therapeutic RNAs or proteins by engineering the producer cells. To further enhance loading, several strategies have been developed that promote therapeutic cargo association with molecules that are naturally enriched in the EVs. Proteins that have been used as EV-scaffolds include single-spanning transmembrane proteins (LAMP2A[245], LAMP2B[149,189], PDGFR[173], PTGFRN[246], TFRC[247], VSVG[207,248–250]), tetraspanins (CD63[189,249–253], CD9[254–256], CD81[253,256]), and soluble proteins (BASP1[246]) (**Table 1.1**).

Single spanning transmembrane proteins can be modified on both their extraluminal and intraluminal domains, thus enabling the display of targeting moieties on EV surface as well as the loading of therapeutic cargo in the EV lumen. However, this is not the case for VSVG, since modification of its extracellular domain drastically reduces its fusogenic activity[257]. Notably, several studies have reported lower EV-mediated delivery when using VSVG for both

intraluminal cargo delivery and to promote endosomal escape as compared to combining VSVG with a second EV-sorting molecule[207,250]. Trimer formation followed by a complex conformational change is required for VSVG to promote membrane fusion, a process that may be disrupted due to the C-terminal fusion of VSVG to a cargo protein[249,258]. Despite this, LAMP2 and the transmembrane domains of PDGFR and TFRC have been used to display targeting peptides on the EV surface. Several studies have reported that LAMP2, PDGFR and TFRC EV-loading capacity is notoriously low (no enrichment as compared to passive loading)[246,259]. Conversely, PTGFRN was recently found to be highly enriched in the EVs, and direct fusion to GFP enabled the loading of ~1,000 GFP molecules/EV[246]. Nevertheless, PTGFRN has only been assessed for EV-surface display of signaling proteins and thus its ability to deliver therapeutic cargoes intracellularly has yet to be established. Tetraspanins, particularly CD63, have been extensively used for EV-mediated delivery of RNA and protein cargo due to their high EV-loading capacity[254,256,259]. Members of the tetraspanin family share the same membrane topology, which comprises four membrane-spanning domains, two extracellular loops and intracellular C and N-termini. Although tetraspanins have extracellular domains that could be exploited for cargo loading or peptide display, these are notoriously difficult to engineer without affecting the protein structure or EV-loading capacity[259,260], and therefore their use has been restricted to intraluminal cargo loading.

Recently, BASP1 has been shown to enable EV-loading with remarkably high efficiency, even when compared to tetraspanins. BASP1 contains a myristoylation sequence and a polybasic region that promote its association to membranes and mediate its sorting into EVs. Although several cargoes including Cas9 and ovoalbumin have been successfully loaded via direct fusion to BASP1, functional delivery has only been tested for vaccination purposes[246]. Other proteins

including MARCKSL1, MARCKS[246], and TSPAN14[261] have also been reported to be highly efficient for protein cargo loading. However, their capacity to deliver the EV-sorted cargo has not been tested yet.

The association of lipidic molecules with specific microdomains in the plasma membrane or MVB membrane that will become EVs has been exploited to enhance EV sorting by fusing lipidic tags to the desired protein cargo. GPI-anchor[177], palmitoylation[262], farnesylation[203,263], myristoylation[264,265] and a combination of myristoylation and palmitoylation[207,255] have been successfully used for cargo protein and RNA delivery. GPI-anchors associate with the EV-surface and therefore have been used for extraluminal cargo loading. On the other hand, palmitoylated, farnesylated and myristoylated proteins are embedded in specific sites on the intracellular plasma membrane and on the MVB membrane that will give rise to EVs, thus enabling intraluminal EV sorting. While the EV-sorting capacity of myristoylation, and myristoylation in combination with palmitoylation, was shown to be highly efficient and comparable to tetraspanin sorting in several studies comparing EV-scaffolds[259,264,265], palmitoylation and farnesylation have shown low EV-loading capacities[246,265].

Gag polyprotein is a viral structural protein that multimerizes at the cell membrane triggering the assembly or retroviral particles. Late domain motifs present in Gag sequence recruit ESCRT components that induce the release of virus-like particles (VLPs) to the extracellular space[266]. Several studies have taken advantage of Gag structural properties to package therapeutic cargo into VLPs by associating such cargo with Gag via direct fusion or indirect interaction[207,253,267,268]. Similarly, the Gag-like protein PEG10, derived from an LTR retrotransposon expressed by mammalian cells, has been used for mRNA delivery *in vitro*[210]. PEG10 was found to bind preferentially to its own mRNA, thereby facilitating its secretion in

extracellular vesicles. This ability was harnessed by Segel *et al*., who identified specific sequences in PEG10 mRNA untranslated region to which PEG10 binds to and used them to modify mRNA cargo to promote their selective encapsulation into PEG10 extracellular vesicles. Importantly, this strategy enabled the functional delivery of Cre and Cas9 mRNA to recipient cells[210]. Moreover, PEG10 represents an alternative to Gag proteins that, due to their viral origin, are potentially immunogenic. Two EV-enriched ubiquitin ligase adaptor proteins harboring ESCRT-interacting late domain motifs, ARRDC1 and NDFIP1 have also been explored as EV scaffolds[155,269]. Both proteins are involved in EV sorting of NEDD4 ubiquitin ligase via the interaction between the WW-domain of Nedd4 and PPXY late-domain motifs in ARRDC1 or Ndfip1. Co-expression of cargo proteins fused to WW-domains together with its interacting partners ARRDC1 or Ndfip1 promoted intraluminal EV-packaging of cargo molecules and enabled functional delivery of protein and RNA[155,269]. Interestingly, ARRDC1 expression has been shown to induce budding of ARRDC1 containing microvesicles from the plasma membrane via interaction with ESCRT-I component TSG101[270].

To load therapeutic RNAs into EVs, RNA-binding domains (RBDs) can be fused with EV membrane proteins which can then recruit the cargo RNAs based on their fusion to a specific RBD recognition site. Viral RBPs HIV-1 transactivator of transcription (tat)[155,245] and MS2 RNA bacteriophage coat protein[249,262] have been employed for RNA loading due to their ability to bind to specific stem loop RNA structures. Modification of pre-miRNA and mRNA cargoes with transactivation response element (TAR) enabled their binding to Tat fused to LAMP2B or ARRDC1, respectively, and subsequent encapsulation into EVs[245,262]. However, no functional delivery of RNA was reported for pre-miRNA loaded EVs[245]. On the other hand, MS2 RBP was able to package modified mRNA or miR-21 sponges into EVs, but functional delivery was only

reported for miR-21 sponge EVs[249,262]. This may be explained by the use of different EV-scaffolds to load the RBPs. Similarly, CD63 fusion with archaeal ribosomal protein L7Ae which binds to the C/D box RNA structure has also been used for successful mRNA EV-packaging and delivery[189]. Alternatively, in a study by Li *et al*, human RBP HuR was fused to CD9 to enable EV-loading and functional delivery of miRNA or mRNA molecules containing HuR-binding AU-rich elements (AREs) in their sequence[254]. Cas9/sgRNA complex has also been packaged into the EVs via RBPs. To do so, the sgRNA sequence was modified with an aptamer and the aptamer binding protein was fused to CD63 or VSVG, so that unmodified Cas9 would be indirectly dragged into EVs by binding to the sgRNA[250].

Once EVs are uptaken by the recipient cells, the protein cargo must be released from the EV-scaffold in order to reach the required intracellular location (e.g., the nucleus for Cas9). To achieve this, most studies have employed strategies that rely on either trigger-inducible release systems or reversible protein-protein interactions. The latter include fusion of the EV-scaffold with split GFP, GFP or mCherry and fusion of the protein cargo with the split GFP partner, GFP or mCherry nanobodies, respectively[248,251]. Inducible release systems are based on fusing the EV scaffold and the protein cargo to dimerization partners whose binding is induced under certain conditions. In this manner, the EVs are produced in the presence of blue light or small molecules that promote dimerization and thus facilitate EV-cargo loading. Once the trigger is withdrawn (blue light is stimulus is turned off or the small molecule is washed out in the recipient cells), the cargo will be released from the EV scaffold. Blue light inducible dimer pairs that have been explored for EV-mediated delivery include CIBN2-CRY2[253,255,262,263] and LOVpep-ePDZ[263], while small-molecule induced include FKBP-FRB[207,252,256] and DmrA-DmrC[247,263]. Alternatively, another strategy is the introduction of cleavage sites for HIV or murine leukemia virus (MLV)

proteases between Gag and the therapeutic protein. This has been used to release protein cargo into nascent VLPs produced in cells expressing the viral proteases[267,268].

While the use of release systems to liberate EV cargoes for functional EV-mediated delivery is predominant, the requirement of endosomal escape enhancing strategies is controversial. Some studies have reported successful functional delivery of a variety of cargoes including RNA, protein, and RNA/protein complexes without additional endosomal escape enhancing molecules (**Table 1.1**). Conversely, other studies have found that functional delivery is not detected unless endosomal enhancing compounds or viral fusogenic proteins are used. For example, Heath *et al* showed that functional delivery of Cre loaded into EVs using CD81 as scaffold and blue light release system, required either VSVG co-expression or the addition of endosomal escape enhancing compounds (e.g., chloroquine)[256]. Notably, studies using the same EV-scaffold proteins which should promote loading into the same EV subpopulations have yielded opposite results. Yim *et al.,* reported highly efficient delivery of various proteins to three different recipient cell types (up to 95% functional Cre delivery in neurosphere-derived cells) using CD9 as EV-scaffold and no endosomal escape molecules[253]. However, in two other separate studies assessing Cas9 and Cre EV delivery to HEK293T cells, functional delivery could not be detected[248,255]. These results, however, could be explained by the difference in recipient cell lines used by the studies. Similarly, significant EV-mediated delivery of Cas9/sgRNA complexes was reported by Ye *et al*. in two separate studies in the absence of endosomal escape enhancing compounds when CD63 was used as the EV scaffold[250,251]. Conversely, Albanese *et al.*, reported no significant functional delivery of CD63-fused β-lactamase unless VSVG was co-expressed to promote endosomal escape[131]. Importantly, this study assessed delivery between a wide variety of donor and recipient cells, including HEK293T

to A549 delivery, which was reported by Ye *et al*. Along these lines, functional delivery of farnesylated tetracycline transactivator (tTA) to HEK293T cells by EVs was found to require VSVG co-expression[203] while a separate study showed EV-mediated functional delivery of farnesylated TALE-VP16 (transcription activator-like effector fused to VP16 transactivation domain) to HEK293T cells without additional endosomal escape enhancing compounds[263]. However, a release system was not included in tTA study, which may have influenced functional delivery. Although the requirement for VSVG or other endosomal escape compounds may be dependent on donor-recipient cell types and EV cargoes, conflicting results have been reported by studies using the same EV scaffold, release system, donor-recipient cell lines and cargo protein211,264. It should be noted that direct comparison of different studies can be challenging due to the use of different EV isolation methods, delivery reporters, and EV concentrations, which may at least partially account for the diverging outcomes.

Ultimately, the method for EV loading and the complexity of the system is determined by multiple factors such as the nature of the therapeutic cargo, targeting requirement or the therapeutic purpose of EV treatment. For example, synthetic drugs can only be packaged via exogenous loading methods, while protein and RNA can be loaded either endogenously or exogenously. In the case of EVs used for vaccination or cell signaling purposes, the complexity of the delivery platform could be simplified, since cargo release or endosomal escape would not be required for their functionality. Moreover, if targeting of a specific tissue is required for the therapeutic application, EVs would need to be modified with targeting moieties. To do so, distinct EV scaffolds could be combined for targeting and cargo loading (i.e., LAMP2B for targeting peptide display and CD63 for therapeutic protein loading). However, due to the heterogeneous nature of EVs, special attention should be taken to ensure that the various

moieties are present on the same EV particles. To facilitate this, EV-scaffolds that enable cargo loading on both their extraluminal and intraluminal domains could be employed. Similarly, co-expressing VSVG or other endosomal escape proteins with EV-scaffold proteins does not imply that they will be found on the same vesicles due to vesicle heterogeneity, thereby adding another layer of complexity to the delivery system.

Table 1.1. Overview of EV-scaffolds for EV-mediated delivery.

Protein Scaffold	Fusion proteins	Intraluminal Cargo	EV-surface Cargo	Release	Endosomal Escape	Loading efficiency	In vitro effect	In vivo effect	Ref
LAMP2A	LAMP2A-TAT	pre-miR-199a (fused to TAR RNA)	-	-	-	65-fold enrichment compared to passive loading	No mRNA inhibition was detected in SK-Hep1 or Huh7 cells	-	[245]
LAMP2B	Direct fusion	siRNA (electroporated)	RVG targeting peptide	-	-	-	60% mRNA silencing in Neuro2A cells	50% BACE1 silencing in mice brain at mRNA and protein levels	[149]
	Direct fusion		MPS targeting peptide	-	-	-	40% mRNA silencing in C2C12 cells	No significant change in mRNA expression	[149]
	Direct fusion to RVG peptide*	mRNA (fused to L7Ae-binding C/D box)	RVG targeting peptide	-	Connexin 43 S368A	-	- Significant nLuc mRNA delivery to HEK293T cells expressing CHRNA7. - EV-mediated delivery of catalase mRNA resulted in a reduction of neurotoxicity in CHRNA7 expressing Neuro2A cells.	Reduced neurotoxicity and neuroinflammation in a Parkinson's disease mouse model after EV-mediated delivery of catalase mRNA by subcutaneously injected EV-producer cells	[189]
PTGFRN	Direct fusion	GFP	IL-12, IL-7, CD40L, anti-CD3 antibody fragments	-	-	95% GFP loading	Display of therapeutic molecules on the EV surface resulted in increased (CD40L delivery to B-cells), similar (anti-CD3 delivery to splenocytes, IL-12 delivery to PBMCs), or reduced (IL-7 delivery to T-cells) *in vitro* potency compared to soluble protein using 5×10^{11} EVs/ml	Intratumoral administration of murine IL-12-PTGFRN EVs (3 doses of 100 µg or 200 µg EVs) improved both tumor growth inhibition and survival compared to recombinant IL-12	[246,271]
PDGFR transmembrane domain (pDisplay)	Direct fusion	- siRNA (transfected in EV producer cells) - Let-7a miRNA (EV-loaded by lipofection)	EGF, GE11 (N-terminal fusion to PDGFR TM)	-	-	20% and 15% loading of EGF and GE11 peptides, respectively	20% silencing efficiency in HCC70 cells treated with siRNA-loaded GE11-PDGFR (TM) EVs	Tumor growth supression in mice treated with 4 systemic injections of 1 µg Let-7a-loaded EVs displaying GE11	[173]
Transferrin membrane anchor domain (CherryPicker)	CherryPicker red-DmrA	- Cas9 (C-terminal fusion to Dmrc) - sgRNA	-	Reversible A/C heterodimerizer induced DmrA-DmrC interaction	VSVG	1% EV-loading of CherryPicker red	8% indel efficiency in Cas9 reporter CHME-5 cell line after spinoculation.	-	[247]

Protein Scaffold	Fusion proteins	Intraluminal Cargo	EV-surface Cargo	Release	Endosomal Escape	Loading efficiency	In vitro effect	In vivo effect	Ref
VSVG	VSVG-GFP11	C-terminally fused to GFP1-10: - β-lactamase - Cre - saCas9/sgRNA - AGO2/shRNA	-	-	VSVG	26-fold higher EV-loading of Cre than with passive loading	- 98% delivery of β-lactamase to HeLa cells. - 66.9% Cre delivery to HEK293T reporter cells using 4000 EVs/cell. - Successful knockdown of PINK1 in HEK293T or HeLa cells by EV-loaded AGO2-shRNA or saCas9/sgRNA complexes.	Reduction of PCSK9 expression in mouse liver and decline of serum LDL cholesterol levels after 3 systemic injections with 1×10^9 EVs	[248]
	VSVG-MS2 RBP	mRNA (fused to 3× MS2-binding HAL motifs)	-	-	VSVG	40-fold enrichment compared to passive RNA loading	No functional mRNA delivery to PC-3 cells	-	[272]
	VSVG-FKBP12	Cas9 (N-terminal fusion to FRB)	-	Reversible AP21967 induced FKBP12-FRB (T2098L variant) interaction	VSVG	-	1.5% indel efficiency in HEK293T cells expressing sgRNA targeting DMD1 treated with Cas9-loaded EVs	-	[207]
	VSVG-aptamer binding protein	- saCas9 - sgRNA (fused to the RNA aptamer)	-	-	VSVG	-	2.5% EV-mediated delivery of saCas9 to HEK293T reporter cells	-	[273]
CD81	CD81-FKBP	Fused to FRB: - Cre - Tetracyclin transactivator (tTA)	-	Reversible rapamycin induced FKBP-FRB interaction	VSVG	70-fold Cre enrichment as compared to passive loading	- Significant activation of gene expression in HEK293T cells mediated by EV-loaded tTA (173-fold increase in activation compared to passive loading). - Robust EV-mediated Cre delivery to HEK293T cells.	-	[252]
	CD81-FKBP	Cre (fused to FRB)	-	Reversible rapamycin induced FKBP-FRB interaction	Chloroquine or undisclosed endosomal escape compound	- 34.1 Cre molecules per EV (in presence of rapamycin, active loading) - 8.9 Cre molecules per EV (without rapamycin, passive loading)	30% or 70% Cre delivery to HEK293T cells in presence of chloroquine or undisclosed endosomal enhancing compound, respectively	-	[256]

Protein Scaffold	Fusion proteins	Intraluminal Cargo	EV S. Cargo	Release	Endo. Esc	Loading efficiency	In vitro effect	In vivo effect	Ref
CD63	CD63-L7Ae*	mRNA (fused to L7Ae-binding C/D box)	RVG peptide	-	Connexin 43 S368A	-	- Significant nLuc mRNA delivery to HEK293T cells expressing CHRNA7. - EV-mediated delivery of catalase mRNA resulted in a reduction of neurotoxicity in CHRNA7 expressing Neuro2A cells.	Reduced neurotoxicity and neuroinflammation in a Parkinson's disease mouse model after EV-mediated delivery of catalase mRNA by subcutaneously injected EV-producer cells	189
	CD63-MS2 RBP	mRNA (fused to 3x MS2-binding HAL motifs)	-	-	-	6-fold enrichment compared to passive RNA loading	No functional mRNA delivery to PC-3 cells	-	272
	CD63-GFP	- spCas9 (N-terminal fusion to GFP nanobody) - sgRNA	-	-	-	-	EV-mediated delivery of Cas9/sgRNA to A549 reporter cells	-	250
	aptamer binding protein-CD63-aptamer binding protein	- saCas9 - spCas9 - adenine base editor (ABE) - sgRNA (fused to the RNA aptamer)	-	-	VSVG	2-5 fold Cas9 or ABE enrichment in EVs containing modified sgRNAs as compared to EVs containing unmodified sgRNAs.	- 39.7% or 24.2% base editing rate of ABE/sgRNA-loaded EVs in HEK293T cells or MDA-MB-231 cells, respectively. - Efficient indel induction in various gene targets ranging from 15.7% to 51.4% in HEK293T cells or 14% to 33.8% in MDA-MB-231 treated with spCas9/sgRNA EVs. - DMD Exon 51 deletion in HEK293T cells by EV-mediated delivery of saCas9 and two sgRNAs targeting different sites. - 96kb deletion in HEK293T cells by EV-mediated delivery of saCas9/sgRNA and spCas9/sgRNA targeting two different sites.	0.2% indel efficiency in tibialis anterior muscle of mdx mice after intramuscular injection of Cas9/sgRNA EVs	273
	CD63-mCherry, CD63-GFP	- Cas9 (N-terminally fused to mCherry or GFP nanobodies) - sgRNA	-	-	-	-	- 1% or 0.5% Cas9/sgRNA delivery to reporter A549 cells or HBE cells, respectively, by A549-derived EVs. - 0.5% Cas9/sgRNA delivery by HBE-derived EVs to reporter A549 cells.	- 1% Cas9/sgRNA delivery to mouse liver after 5 intravenous injections with EVs (50 µg EVs per injection). - 1% and 0.5% Cas9/sgRNA delivery to mouse brain and liver, respectively, 24 days after subcutaneous injection with B16 EV producer cells.	251
	CD63-FKBP	Tetracyclin transactivator (tTA) (fused to FRB)	-	Reversible rapamycin induced FKBP-FRB interaction	VSVG	-	Significant activation of gene expression in HEK293T cells mediated by EV-loaded tTA (44-fold increase in activation compared to passive loading).	-	252

Protein Scaffold	Fusion proteins	Intraluminal Cargo	EV-surface Cargo	Release	Endo. Esc	Loading efficiency	In vitro effect	In vivo effect	Ref
CD9	CIBN-GFP-CD9	Fused to CRY2: - Bax - Super-repressor IkB - Cre	-	Blue light induced reversible interaction between CIBN and CRY2	-	40-fold enrichment compared to extrusion-loaded EVs	- Bax-loaded EVs (0.1mg/ml) induced a rapid release of cytochrome *c* from mitochondria in HeLa cells. - Treatment with IκB-loaded EVs (0.1mg/ml) reduced TNF-alpha induced translocation of the p65 subunit of NF-κB in HeLa cells. - Efficient Cre delivery to HeLa, HT1080, primary rat embryonic neurons, and differentiated neurosphere derived cells (95% delivery using 2×10^{10} EVs/ml).	Successful delivery to brain neurons after ventrolateral injection with 50 µl of 10mg/ml EVs.	[253]
	CD9-HuR RBP	- miR-155, - Cas9 mRNA (fused to 3x HuR-binding ARE sequences) - sgRNA - anti-miR-155 (fused to 3x ARE sequences)	-	-	-	7-fold miR-155 enrichment as compared to passive loading	- Significant knockdown of mRNA target after treatment with miR-155 EVs in THP1 cells. - Supression of C/EBP alpha expression in adipogenic stem cells after delivery of EV-loaded Cas9/sgRNA.	- Successful knockdown of mRNA target in liver and spleen after systemic injection of 100 µg miR-155 EVs. - Treatment with EV-loaded Cas9/sgRNA resulted in significant C/EBP alpha suppression in liver after systemic injection. - Reduced liver inflammation and fibrosis in a liver injury mouse model after treatment with 200 µg EVs twice a week for 3 weeks.	[254]
	CIBN-CD9, Cas9-CRY2	- Cas9 - sgRNA	-	Blue light induced reversible interaction between CIBN and CRY2	-	20 Cas9 molecules per EV	- No detection of Cas9 delivery to HEK293T reporter cells after treatment with 5.5×10^{4} EVs/cell.	-	[255]
GFP motif	Direct fusion	Nanobodies	-	-	-	15-25% loading efficiency	2-fold higher uptake by A431 cells under flow conditions as compared to non-targeted EVs.	-	[177]
Palm	Palm tag-CIBN, CRY2-MCP	miR-21 sponge (fused to MCP-binding MS2)	AS1411 aptamer (conjugated to cholesterol)	Blue light induced reversible interaction between CIBN and CRY2	-	14-fold compared to passive RNA loading	Increased expression of miR-21 target protein PTEN tumor suppressor, and apoptosis in K562 cells.	-	[262]

Protein Scaffold	Fusion proteins	Intraluminal Cargo	EV S. Cargo	Release	Endosomal Escape	Loading efficiency	In vitro effect	In vivo effect	Ref
Farnesylation	CAAX motif fused to CIBN, LOVpep or DmrA C-termini	Fused to DmrC, CRY2PHR or ePDZb: - BFP - TALE-VP16 transcriptional activator	-	- Blue light induced reversible interaction between CIBN and CRY2 - Rapamycin induced reversible interaction between DmrA-DmrC	-	Higher packaging of BFP by farnesylated dimerization domains as compared to LAMP1 fusion	Significant HEK293T reporter cell activation upon treatment with EV-loaded TALE-VP16	-	[263]
	Direct fusion	Tetracyclin transactivator (tTA)	-	-	VSVG	-	Highly efficient HEK293T reporter cell activation		[203]
Myr	Direct fusion	- Cas9 - sgRNA	-	-	VSVG, chloroquine and polybrene	-	45.4% Cas9/sgRNA delivery to HEK293T reporter cells after treatment with 3×10^9 Cas9/sgRNA EVs in presence of chloroquine and polybrene	-	[265]
	Myr tag-GFP	- GFP (fused to Myr tag) - Nluc (fused to Myr tag or unnmodified) - Cre (unmodified) - Cas9 (unmodified)	-	Not required since cargo loading only relies on co-expression with Myr tag	-	- 85-fold EV-enrichment of NLuc fused to Myr tag as compared to passive loading. - 50-fold EV-enrichment of NLuc when co-expressing Myr tag-GFP fusion protein as compared to passive loading. - 5-fold EV-enrichment of Cas9 when co-expressing Myr tag-GFP fusion protein as compared to passive loading.	Functional delivery of Cre and Cas9 to HEK293T reporter cells	-	[264]
Myr Palm	Myr Palm tag-FKBP12-GFP	Cas9 (fused to FRB)	-	Reversible AP21967 induced FKBP12-FRB (T2098L variant) interaction	VSVG	-	2.1% indel efficiency in HEK293T cells expressing sgRNA targeting DMD1	-	[207]
	CIBN-Myr Palm	- Cas9 (fused to CRY2) - sgRNA	-	Blue light induced reversible interaction between CIBN and CRY2	-	30 Cas9 molecules per EV	- 42% or 19% Cas9/sgRNA delivery to HEK293T or HepG2 cells, respectively, after treatment with 5.5×10^4 EVs/cell. - 5.8% Cas9 or 4.4% Cas9/sgRNA-mediated gene editing of PCSK9 in HEK293T cells.	-	[255]

Protein Scaffold	Fusion proteins	Intraluminal Cargo	EV S. Cargo	Release	Endosomal Escape	Loading efficiency	In vitro effect	In vivo effect	Ref
BASP1	Direct fusion	- RNA-binding MS2 (MCP) - Ovalbumin - Cas9	-	-	-	97% GFP loading	-	Ovoalbumin delivery to antigen presenting cells via EVs induced local and systemic T cell responses which were significantly higher than with soluble OVA.	[246]
Ubiquitin tag	Direct fusion	C-terminally fused to ubiquitin: - GFP - HER2 (extracellular domain) - Ag85B-ESAT6	-	-	-	10-fold enrichment of Ag85B-ESAT6 as compared to passive loading	-	Induction of antigen-specific cellular immune response against Ag85B and ESAT6 in liver and spleen of mice after three intranasal treatments of EV-loaded Ag85B-ESAT6 (20 µg EVs/mouse) at two week intervals.	[274]
Ndfip1	-	Cre (fused to WW-tag)	-	-	-	-	1% Cre delivery to MEF reporter cells (250 µg EVs/ well of 12-well plate).	Low recombination activity in multiple brain regions of Cre reported mice treated intranasally with Cre-loaded EVs (72 µg/mouse).	[269]
ARRDC1	Direct fusion, ARRDC1-TAT	- GFP (direct fusion) - p53 (direct fusion) - mRNA (fused to TAR) - Cas9 (fused to 2 or 4x WW-tag)/sgRNA	-	-	-	540 molecules of GFP per EV	- Induction of p53-dependent expression of MDM2 and p21 in H1299 cells after EV-mediated delivery of p53 protein or mRNA. - Significant EV-mediated Cas9/sgRNA delivery to HEK293T reporter cells (13.4% or 4.9% GFP knockdown efficiency with 4WW-Cas9 or passively loaded Cas9, respectively).	Rescue of irradiation-induced apoptosis in thymus and spleen of TP53 KO mice after intravenous injection of ARRDC-p53 EVs (6×10^{10} EVs/ mouse).	[155]
PEG10	-	- Cre mRNA (flanked by PEG10 mRNA UTR) - spCas9 mRNA (flanked by PEG10 mRNA UTR)	-	-	VSVG or (SYNA and Vectofusin-1)	-	- 60% Cre N2a reporter cell activation by VSVG-pseudotyped EVs. - 10% Cre delivery to tail-tip fibroblast cells by SYNA-pseudotyped EVs and Vectofusin-1. - 60% or 30% indel efficiency in Cas9 N2a reporter cells expressing or not sgRNA, respectively, treated with VSVG-pseudotyped EVs.	-	[210]

Protein Scaffold	Fusion proteins	Intraluminal Cargo	EV S. Cargo	Release	Endosomal Escape	Loading efficiency	In vitro effect	In vivo effect	Ref
GAG	Direct fusion	- spCas9 (N-terminally fused to Gag-MLV cleavage site) - dCas9-VPR (N-terminally fused to Gag-MLV cleavage site) - sgRNA - DNA donor template (loaded using polybrene)	-	MLV protease cleavage	VSVG and baboon retroviral envelope glycoprotein	-	- Efficient induction of dsDNA breaks in U2OS and human primary fibroblasts. - 77% or 67% indel efficiency in HEK293T cells or human iPSCs, respectively. - 60-65% GFP indel efficiency in GFP reporter bone marrow cells. - 76% FTO indel efficiency in primary bone marrow cells. - 50% MYD88 indel efficiency in human primary hepatocytes and human hematopoietic stem cells. - 50% FLAG gene knock-in efficiency in HEK293T cells treated with EV-packaged Cas9/sgRNA and donor ssDNA template. - 4kb gene knock-in in HEK293T cells treated with EV-packaged Cas9/sgRNA and donor dsDNA template. - 400-fold transcription activation of TTN in MCF-7 cells using EV-loaded dCas9-VPR/sgRNA as compared to control EVs.	- Indel formation in mouse zygotes after injection in the perivitelline space with Cas9/sgRNA EVs. - 7-13% HPD indel efficiency in mouse liver after retro-orbital injection of Cas9/sgRNA EVs.	[208]
	Myr Palm tag-FKBP12-Gag	- spCas9 (N-terminally fused to FRB) - sgRNA synthesized as TAR-Psi-ribozyme-sgRNA-ribozyme mRNA	-	Reversible AP21967 induced FKBP12-FRB (T2098L variant) interaction	VSVG	-	- 15%, 25% or 50% activation of HEK293T, C2C12, or Hu5 reporter cells, respectively. - 22% or 29% indel efficiency in 404C2 (targeting DMD1) or 1383D2 iPSC cells (targeting DMD23), respectively. - 48% CCR5 indel efficiency in Jurkat T-lymphocyte cells. - 50% knockout of GFP expression in U937 monocyte reporter cells. - 36% SAMHD1 indel efficiency in iPSC-derived cortical neurons. - 25-80% indel efficiency of DMD1, DMD23, SAMHD1, CCR5 and EMX1 in HEK293T cells. - 92% DMD exon 45 skipping in DMD iPSC-differentiated skeletal muscle cells and rescue of dystrophin protein expression upon treatment with EVs targeting two different sites of exon 45.	- 7% DMD exon 45 skipping efficiency in the gastrocnemius muscle of reporter mice after intramuscular injection with EVs targeting two different sites of exon 45. - 1.1% DMD exon 23 skipping in tibialis anterior muscle of a DMD mouse model after intramuscular injection with EVs targeting two different sites of exon 45.	[207]

GAG	Direct fusion	- Cas9 (N-terminally fused to Gag-HIV cleavage site) - sgRNA - Donor template DNA (electroporated)	-	HIV protease cleavage	VSVG or HIV envelope protein (for CD4+ T cells only)	-	- 90-95% B2M indel efficiency in Jurkat and A549 cells treated with Cas9/sgRNA-loaded EVs. - 40% knock-in efficency in HEK293T reporter cells after EV-mediated delivery of Cas9/sgRNA and donor DNA template. - Succesful B2M knockout in CD4+ and CD8+ primary human T-cells at levels comparable to electroporation. - Treatment of primary human T cells with separate Cas9/sgRNA-EVs targeting B2M or TRAC resulted in 23.9% CD4+ and 9.55% CD8+ double-knockout cells. - 15% knockout of BM2 in CD4+ T-cells treated with Cas9/sgRNA EVs.	-	[268]
	Gag-FKBP	Tetracyclin transactivator (tTA) (fused to FRB)	-	Reversible rapamycin induced FKBP-FRB interaction	VSVG	-	Significant activation of gene expression in HEK293T cells mediated by EV-loaded tTA (4.4-fold increase in activation compared to passive loading).	-	[252]

* RVG-LAMP2B and CD63-L7Ae were used in combination in the same study.

1.10. Methods for EV isolation

Several techniques for EV concentration and isolation have been developed to date, however, there is no clear consensus on the most appropriate method[275]. Each technique has both advantages and disadvantages in terms of purity, yield, EV integrity, and time-efficiency. In addition, the choice of method will be determined by the use of the isolated EVs. For instance, if the EVs will be used for diagnostic purposes, yield would be prioritized while purity and vesicle integrity preservation would not be essential. Conversely, if the EVs are to be used for functional assays the EV isolation method should preserve EV structure and enable the isolation of highly pure EVs. According to a worldwide survey from 2020[276], ultracentrifugation (UC) remains the most commonly used EV isolation technique. Nevertheless, in the last few years size-exclusion chromatography (SEC) has emerged as an alternative method for EV isolation alone or in combination with ultrafiltration[276].

1.10.1. Ultracentrifugation

The principle of UC is to separate the components of a sample based on their size and density, and that of the media[277]. In differential centrifugation (dUC), successive centrifugation steps enable the removal of dead cells and cell debris, and the subsequent EV enrichment. Briefly, dead cells and cell debris are pelleted at 300*g* for 10 minutes. Next, large EVs are pelleted by centrifugation at 2,000*g*, medium-sized EVs are pelleted by centrifugation at 10,000*g*, and small-EVs are pelleted at 100,000*g*. Pelleted EVs are then washed in PBS and centrifuged again to obtain the final pellet. When the technique was first described, 10,000*g* and 100,000*g* pellets were assigned to microvesicles and exosomes, respectively[278]. Nevertheless, subsequent studies showed that different types of vesicles are co-purified by dUC, thus indicating that this method is not able to separate microvesicles from exosomes[279]. dUC allows for the isolation of EVs with

moderate yields and purity. However, ultracentrifugation procedures can cause vesicle aggregation and co-purification of nucleic acids or protein aggregates[280–282].

To circumvent this, density gradient centrifugation (DG) techniques were developed to minimize potential non-EV contaminants in dUC EV preparations. In DG, EVs are added to a density gradient solution such as iodixanol or sucrose and subsequently separated based on their buoyant density by centrifugation[283]. Although this method increases EV purity, it is time-consuming and generates low yields[276].

1.10.2. Size exclusion chromatography (SEC)

SEC separates sample components based on their molecular size. In SEC, the sample is added to a column containing porous polymer beads (e.g., Sepharose, Sephacryl). As the sample migrates through the column, the smaller particles will enter the porous beads leading to longer elution times while the larger particles will elute faster since they will not get trapped in the pores[277]. When combined with ultrafiltration methods such as tangential flow-filtration (TFF), SEC is able to achieve higher EV purity than UC-based methods due to lower EV aggregation, lower EV damage, and decreased co-purification of non-EV material while sustaining acceptable yields[284,285].

1.10.3. Ultrafiltration

Ultrafiltration is based on the use of polymer membranes with defined molecular weight cut-off (MWCO) filters to concentrate EVs according to their size. The particles larger than the MWCO are unable to cross the membrane and are therefore retained in the filters, while the particles smaller than the MWCO will be eluted along with the permeate[277]. As compared to UC, this method uses low-speed centrifugation and thus is less disruptive[286]. UF can be divided into dead-

end filtration and TFF depending on the flow direction. In dead-end filtration, the liquid flow direction is perpendicular to the filter surface, whereas in TFF the flow direction is parallel to the filter surface. Due to the retained particles rapidly depositing on the filter surface during dead-end filtration, the pores of the membrane get clogged, and the filtration rate is greatly reduced. Therefore, TFF is more appropriate for filtering large volumes of sample[287].

1.10.4. Precipitation

Polymer-based precipitation methods use reagents that bind to water molecules thereby reducing the solubility of EVs and other non-EV components, which tend to sediment and can be isolated using low-speed centrifugation. The most commonly used reagent for polymer-based EV isolation is PEG, although alternatives such as organic solvents or sodium acetate have also been described[288–290]. This method has gained popularity in the recent years given that it is simpler and more time-efficient than the other techniques described above and due to the availability of commercial kits. However, this method is highly non-specific and co-isolates protein aggregates and other non-EV material such as lipoproteins[276].

1.10.5. Immunoaffinity

Immunoaffinity techniques use specific antibodies that bind to surface molecules present in the EVs to selectively capture them. Antibodies for immunoaffinity isolation can be attached to a variety of surfaces such as magnetic beads, chromatography resins, or microfluidic devices[291]. Common EV markers such as tetraspanins CD63, CD81 or CD9 are generally used to isolate EVs[103,291]. Nevertheless, this technique can also isolate specific EV subpopulations by targeting EV-surface proteins that are exclusively expressed in a given EV subpopulation. For example, EVs released from epithelial tumor cells were isolated from other circulating EVs using anti-

EpCAM antibodies[283]. Immunoaffinity methods allow for the isolation of highly pure EVs, although the yields are very low[275]. In addition, this method is unsuitable for isolating EVs that will be used in functional experiments due to the difficulty in separating the EVs from the antibody-coated matrix[292].

1.11. General aims

- To engineer EVs in order to enhance EV loading of protein and protein/RNA cargoes.
- To develop a novel platform based on engineered EVs for functional delivery of protein and protein/RNA cargoes.

2. Materials and methods

2.1. Cell culture

All cell lines were maintained in a humidified incubator at 37°C and 5% CO2 and were tested for mycoplasma contamination on a weekly basis. 1× TrypLE Express Enzyme (Thermo Fisher Scientific, MA, USA) was used to detach cells for passaging or seeding.

2.2. Gibson Assembly

Plasmid backbone was linearised by restriction enzyme digestion, in a 20 µl reaction containing the appropriate 1× NEB Buffer (NEB, Ipswich, Massachusetts, United States). Samples were incubated at 37°C for 1 hour and digestion was assessed by agarose gel electrophoresis. The linearized backbone was then excised from the agarose gel and purified using the QIAquick Gel Extraction Kit (Qiagen, Hilden, Germany). Inserts containing the appropriate overhangs were obtained from IDT as gBlocks or were amplified by PCR. Plasmid assembly was performed with NEBuilder HiFi DNA Assembly (NEB) as per manufacturer's instructions. Briefly, a reaction mixture containing 50 ng of backbone, 2 - 4-fold molar excess of insert (depending on the size) and 1× NEBuilder HiFi DNA Assembly Master Mix was incubated for 30 min at 50°C. Next, 2 µl of the assembly reaction were transformed into competent bacteria and DNA was isolated as described below.

2.3. Transformation and plating

High Efficiency DH5α Competent Cells (NEB) were transformed with ligated plasmids on ice for 30 mins, heat shocked at 42°C for 45 sec, incubated on ice for 2 mins, plated on Luria Broth

(Thermo Fisher Scientific) agar plates containing 1 µg/mL Ampicillin (Sigma-Aldrich, MO, USA) and incubated overnight at 37°C. Colonies were picked and grown in LB containing 1 µg/mL Ampicillin at 37°C overnight on an orbital shaker. Cultures were pelleted at 1,690 *g* for 10 mins at 4°C, and plasmid DNA extracted using QIAprep Spin Miniprep Kit or HiSpeed Plasmid Maxi Kit (Qiagen).

2.4. EV isolation

HEK293T cells were transfected with different constructs as indicated. 24 hours later, the medium was replaced with Opti-MEM (Thermo Fisher Scientific, Waltham, Massachusetts, United States) and 48h later, cell culture supernatant was collected and centrifuged consecutively at 500 *g* and 2,000 *g* to remove cell debris and large particles, respectively. The media was then filtered through a 0.45 µm filter (STARLAB, Hamburg, Germany) and concentrated using a 10 KDa vivaflow TFF membrane (Sartorius, Gottingen, Germany) to 10-15 ml. Then, using 10 KDa Amicon spin filters (Merck Millipore, Burlington, Massachusetts, United States) media was concentrated further to 1-2 ml by centrifugation at 3,500 *g*. Following this, concentrated media was subjected to size exclusion chromatography using HiPrep Sephacryl S-400 HR 16/60 column (GE Healthcare, Chicago, Illinois, United States) connected to the ÄKTA prime system (GE Healthcare) and eluted at 0.5 ml/min flow rate using PBS as the eluent. EV and protein fractions were selected based on 280 nm absorbance. The yield of vesicles was measured using nanoparticle tracking analysis or single-vesicle analysis.

2.5. Nanoparticle tracking analysis

Nanoparticle tracking analysis (NTA) was performed to determine the size distribution and concentration of isolated EVs with the NS500 nanoparticle analyser and NTA 2.5 analytical

software (NanoSight, Malvern, Worchestershire, UK). EV samples were recorded in triplicate for 30 seconds with a 7 second delay between each recording. Camera level was set at 14 and detection threshold was set at 4. The other post-acquisition settings were automated.

3. Results I – Assessment of UBL3 EV scaffold for EV-mediated delivery of RNA and Cas9-VPR complex

3.1. Introduction

Several miRNA-based therapies have shown promising results in preclinical studies[151]. However, the delivery of therapeutic oligonucleotides by conventional methods such as synthetic nanoparticles or viral vectors is hampered by poor delivery efficiencies, limited tissue targeting, and often, toxic side effects[254]. Thus, EVs have been explored as alternative delivery system for efficient and safe miRNA delivery[120,151,254,293]. miRNAs are short ~22nt RNA molecules that act as post-transcriptional regulators in many biological processes. In the cytoplasm, mature miRNAs associate with RNA-induced silencing complex (RISC) components such as AGO2 to form the miRISC complex or become associated with other miRNA binding proteins. Numerous miRNAs have been found in the extracellular space, although the majority are not associated with EVs[294]. The stability of miRNAs released to the extracellular space in physiological conditions vary widely between different miRNAs. Highly stable miRNAs are likely stabilized by extracellular-ribonucleoprotein complexes. However, mechanisms of miRNA secretion and function of these extracellular miRNAs remain elusive[295].

As outlined in detail in the introduction, EV-mediated secretion of miRNAs has been reported to rely on miRNA association with RBPs that are sorted to the EVs. miRNA encapsulation into EVs has been achieved by exogenous methods such as electroporation, sonication, and the use of transfection reagents[211]. However, these methods are prone to artefacts

as exemplified by the formation of siRNA aggregates observed with EV electroporation protocols[211]. Endogenous strategies have also been explored for miRNA loading and delivery to recipient cells. These strategies have relied on the expression of miRNAs modified to harbor specific RNA sequences that bind to RBPs which are fused to EV scaffold molecules[245,254,262].

CRISPR-Cas9 technology holds great promise for the treatment of genetic conditions. However, its potential has been hampered by a lack of efficient and safe delivery methods[296]. Due to their unique properties, such as biocompatibility and ability to cross biological barriers, EVs have recently emerged as novel vehicles for CRISPR/Cas9 delivery. At the time this study was conceived, only three strategies had been reported for EV-mediated delivery of Cas9. In the first study, Cas9/sgRNA complexes were loaded into cancer derived EVs via electroporation and delivered to ovarian cancer tumor xenografts in mice[297]. Delivery of EVs loaded with Cas9/sgRNA targeting PARP-1 (Poly (ADP-ribose) polymerase 1) resulted in significant suppression of PARP-1 expression and apoptosis induction[297]. In the second study, hybrid liposome-EV nanoparticles containing Cas9/sgRNA plasmids were generated by incubation of liposomes, EVs and plasmid DNA[298]. Importantly, treatment with encapsulated Cas9/sgRNA plasmids was able to induce indel formation in MSCs[298]. In the third study, Cas9/sgRNA complexes were loaded into ARMMs (ARRDC1 microvesicles) by fusing Cas9 to WW domains[155]. These domains can interact with ARRDC1, which is highly enriched in microvesicles when overexpressed in EV producer cells[299]. This strategy enabled efficient delivery of EV-loaded Cas9/sgRNA complexes to HEK293T reporter cells (10% reporter cell activation)[155].

More recently, numerous platforms have been described for delivering Cas9/sgRNA complexes via EVs. While Chen *et al.* reported efficient EV-mediated delivery of Cas9/sgRNA

to recipient cells using EVs obtained by simple overexpression of Cas9 and sgRNA in EV producer cells[300], other studies have relied on active loading methods to achieve successful delivery. The association of Cas9 protein to EV-scaffolds such as VSVG[207], CD63[250,251], Gag[207,252,267] or myristoylation and palmitoylation tags[207,255,265] has been reported as an efficient method for EV loading and delivering both Cas9 and sgRNA. Notably, in these studies, a reversible interaction between Cas9 and the EV scaffold was used to promote Cas9/sgRNA release in EVs or recipient cells. Alternatively, an aptamer-modified sgRNA has been actively loaded into EVs through its interaction with an aptamer-binding protein fused to an EV protein scaffold[273]. In this manner, Cas9 protein was indirectly recruited into the EVs via sgRNA binding[273]. Similarly, Cas9 mRNA has been modified to promote its binding to EV-enriched RBPs or to RBPs fused to EV protein scaffolds[210,254]. Segel *et al*. harnessed the ability of the Gag-like protein PEG10 to bind to its own mRNA and to form EV-loaded capsid-like particles to promote Cas9 mRNA sorting to EVs[210]. This was achieved by the addition of a minimal sequence from PEG10 mRNA to Cas9 mRNA. In this study, treatment with EVs loaded with Cas9 mRNA resulted in highly efficient functional delivery to recipient cells[210].

In this chapter, we investigate methods to enhance EV-cargo loading for EV-mediated delivery of small RNAs and Cas9/sgRNA complexes.

3.2. Hypotheses and aims

Hypotheses:

- EVs can be engineered to deliver small RNAs to recipient cells
- EVs can be engineered to deliver dCas9-VPR/ sgRNA complex to recipient cells

Aims:

- Actively load EVs with AGO2 and small RNA (i.e., miRNA or shRNA) cargo
- EV-mediated delivery of small RNA cargos to recipient cells
- Actively load EVs with dCas9-VPR and sgRNA
- EV-mediated delivery of dCas9-VPR/sgRNA complexes to recipient cells

3.3. Materials and methods

3.3.1. Cell culture and transfection

Human embryonic kidney (HEK) 293T cells were cultured at 37°C with 5% CO2 in Dulbecco's Modified Eagle Medium GlutaMAX (DMEM) (Gibco) supplemented with 10% foetal bovine serum (FBS) and 1% Antibiotic-Antimycotic (PSA: Penicillin, Streptomycin and Amphotericin B) (Gibco). Cells were cultured as described in Chapter 2.

HEK293T cells for EV production were seeded 24h before transfection in 150mm plates. Cells were transfected with 43 μg of plasmid DNA using PEI (Sigma-Aldrich) at a 4:1 ratio PEI:DNA in Opti-MEM (Gibco). 24h later media was removed and replaced by fresh Opti-MEM (Gibco). EVs were isolated as described on Chapter 2. For EV-transfer experiments (transfected controls), HEK293T dCas9-VPR reporter cells were seeded at a density of 1×10^5 cells/well in a 24 well plate. Cells were either transfected with 250 ng dCas9-VPR fusion constructs and 250 ng of sgRNA plasmids or with 250 ng of sgRNA plasmids only. 24h later media was removed and replaced by fresh DMEM (10% FBS and 1% PSA) (Gibco). 48h after transfection, cells were harvested and analyzed by Flow Cytometry. HEK293T dCas9-VPR reporter cells were a kind gift from Oana Pelea and were cultured as described above.

3.3.2. Plasmids

pCMV-AGO2-eGFP was made by cloning full length DNA fragment of AGO2 into pEGFP-n1 vector (Clontech, catalogue number 6085-1) between AgeI and BseRI sites. To generate pCMV -AGO2-eGFP-UBL3, pCMV-AGO2-eGFP-CP05 and pCMV-AGO2-eGFP-C1C2, full length DNA fragment of UBL3, CP05 peptide (CRHSQMTVTSRL) or DNA fragment coding for

aminoacids 53 – 387 from lactadherin, respectively, were cloned into pCMV-AGO2-eGFP between BsrGI and NotI sites. pLKO.1-puro Luciferase shRNA Control Plasmid DNA was obtained from Sigma-Aldrich. pCMV-dCas9-VPR-eGFP was made by cloning PCR amplified sp-dCas9-VP64-p65-Rta (VPR) from SP-dCas9-VPR (Addgene plasmid #63798) into pEGFP-n1 vector between AgeI and BseRI sites. pCMV-dCas9-VPR-eGFP-UBL3 was constructed by cloning PCR amplified sp-dCas9-VP64-p65-Rta (VPR) from SP-dCas9-VPR (Addgene plasmid #63798) into pCMV-AGO2-eGFP-UBL3 linearized using forward primer 5′ tcttcgacacatctctgtttggcggttctgggggc 3′ and reverse primer 5′ tacttcttgtccatggtggcgaccggtggatcccgg 3′. U6-P2-sgRNA plasmid and dCas9-VPR-eCFP reporter plasmid were a kind gift from Oana Pelea. Constructs were confirmed by DNA sequencing.

3.3.3. Western Blot

Cells were lysed in 1× RIPA buffer (Thermofisher Scientific) containing 1× cOmplete protease inhibitor cocktail (Merck). Acetone precipitation was used for EV samples, where acetone at -20°C was added 4:1 and incubated for 24h at -20°C for subsequent centrifugation at 5000 *g* 20min. The resulting pellet was resuspended in 1× RIPA buffer (Thermofisher Scientific) containing 1× cOmplete protease inhibitor cocktail (Merck) and 10% NuPage sample reducing agent (Invitrogen). Protein concentration was measured by Bradford assay (Sigma) following manufacturer's instructions. 5 µg of total protein was heated at 70°C for 10min and then resolved on a 4–12% NuPAGE gel (Thermofisher Scientific) by SDS-PAGE. Gels were run at 150 V for 2 h in 1× NuPAGE Tris-Acetate SDS Running Buffer (Thermo Fisher Scientific). Protein was transferred onto a PVDF membrane (Merck) at 60 V for 1 hr 30 min in 1× NuPAGE Transfer Buffer (Thermo Fisher Scientific). Membranes were blocked in Intercept (PBS) Blocking Buffer (Sigma-Aldrich) for 30 mins at room temperature and incubated in Blocking Buffer with primary

antibodies at 4°C overnight. Blots were washed with PBS supplemented with 0.1% Tween-20 (PBS-T) three times and incubated with secondary antibody for 1 hr at room temperature. Antibody information is described in **Table 3.1**. Blots were imaged imaged using a LI-COR Biosciences Odyssey Fc instrument (LI-COR, NE, USA).

Table 3.1 Primary and secondary antibody information

Application	Antibody	Host	ID	Manufacturer	Dilution	Expected Size (kDa)
Primary	Anti-GFP	Rabbit	ab290	Abcam	1:1000	27
Primary	Anti-βActin	Mouse	MA5-15739	ThermoFisher	1:2000	42
Primary	Anti-ALIX	Rabbit	ab186429	Abcam	1:2000	97
Secondary	Anti-Rabbit	Goat	926-32211	LI-COR	1:5000	N/A
Secondary	Anti-Mouse	Goat	926-32210	LI-COR	1:5000	N/A

3.3.4. Quantitative RT-qPCR

Total RNA was isolated using Trizol (Invitrogen) according to the manufacturer's protocol. cel-miR-39 (non-mammalian miRNA added as an exogenous spike control) was added to all samples before extraction for normalization. RNA used for sgRNA analysis was subjected to DNase I (Thermo Fisher Scientific) treatment prior to cDNA synthesis. cDNA was synthesized using High-Capacity RNA-to-cDNA (Applied Biosystems) for mRNA or TaqMan miRNA cDNA Synthesis Kit (Applied Biosystems) for miRNAs per the manufacturer's instructions. 1:10 cDNA was used for each PCR reaction, performed with PowerUp SYBR Green Master Mix (Thermo Scientific) for mRNA or TaqMan Fast Advanced Master Mix (Thermo Scientific) for

miRNAs on a StepOnePlus real time PCR system (Applied Biosystems). Quantification cycles (Cq) were normalized to Cq of *GAPDH* or cel-miR-39, for cell samples and EV samples respectively, and fold enrichments were calculated as compared to the control values. Number of EVs (quantified by NTA was used to normalize EV samples.

3.3.5. EV-treatment of dCas9-VPR reporter cells

HEK293T reporter cells were seeded at a density of 100,000 cells/well in 24 well plates 12h before EV treatment. Cells for $sgRNA^+$ control (cells that expressed sgRNA) were transfected with U6-P2-sgRNA plasmid 24h before EV transfer. Cells in 500 µl Opti-MEM/ well were treated with 250 ml EVs at 1×10^{11} EVs/ml filtered with 0.45 mm PES syringe filters (Sigma Aldrich). To promote endosomal escape of EVs, 25µM chloroquine (Sigma-Aldrich) was added to the cells together with the EVs when indicated. 24h after EV transfer, cells were harvested and analyzed by Flow Cytometry.

3.3.6. Flow-cytometry analysis of dCas9-VPR reporter cells

Complete media was aspirated, cells were washed with PBS followed by 10min incubation with 50 ml trypsin-EDTA. Trypsin was inactivated using 500 ml FACS buffer (PBS containing 10% FBS). Cells were pipetted up and down several times to remove cellular clumps, followed by filtration using Falcon 70 mm White Cell Strainer and transfered to Falcon Round-Bottom Polystyrene Tubes (Stemcell Technologies). Cells were stored on ice prior to sample analysis using the BD LSR Fortessa Analyzer (BD Biosciences).

Data analysis was performed using FlowJo software (BD Biosciences). Live HEK293T reporter cells were identified by plotting SSC-A (side-scattering area) and FSC-A (forward

scattering area) values, while single-cells were identified by plotting SSC-H (side-scattering height) against SSC-A values. Reporter cells that stably integrated the reporter construct are expected to constitutively express eGFP. Therefore, eGFP positive cells were selected by plotting SSC-H parameter against eGFP intensity (measured at 488-530nm). For experiments where cells were transfected with U6-P2-sgRNA, successfully transfected cells were selected according to iBlue expression in addition to eGFP expression. This was carried out by plotting SSC-H parameter against iBlue intensity (measured at 640-670nm). Reporter activation was analysed measuring mScarlet-I intensity (561-610nm).

3.3.7. NanoFCM analysis

NanoFCM is a flow cytometry technique that enables the quantification of EV samples as well as the size and fluorescence assessment of single EVs. To detect $VSVG^+$ EVs, EVs from cells transfected with VSVG were labeled with primary anti-VSVG antibody (ab1874, Abcam) and secondary goat anti-rabbit (BioRad) by incubation at room temperature for 1h. Labeled EVs were then separated from unbound antibodies by size-exclusion liquid chromatography. Labeled EVs and GFP EVs were analyzed and quantified using Flow Nanoanalyzer instrument (nanoFCM). Samples containing vesicles were diluted in phosphate-buffered saline (PBS) for analysis.

3.4. Results

The delivery of therapeutic oligonucleotides such as miRNA to intracellular targets has proven notoriously difficult[153,301]. Native EVs contain very low levels of miRNAs[302], therefore an active loading strategy is required to load miRNAs to EVs. AGO2 is essential for miRNA-induced silencing complex function as it binds to mature miRNAs and is able to cleave the target transcripts directly[303]. Thus, we reasoned that by fusing AGO2 to peptides/proteins that are targeted to, or associate with EVs, we could increase AGO2: miRNA complexes in EVs. For this purpose, we made four constructs where the N-terminus of AGO2 was fused to either eGFP-C1C2, eGFP-CP05, eGFP-UBL3 or eGFP (**Fig 3.1**). The C1C2 domain of lactadherin associates with the outer EV membrane by interaction with phosphatidylserine[304] while CP05 peptide binds to the highly abundant EV transmembrane protein CD63[235]. Hence, we hypothesised that both fusions could redirect soluble AGO2: miRNA complexes to associate with the EV membrane. UBL3 acts as a post-translational modification factor that regulates protein sorting to small EVs[92], thus UBL3 fusion could target AGO2:miRNA complexes into EVs. The eGFP-only construct served as a control for passive EV-loading.

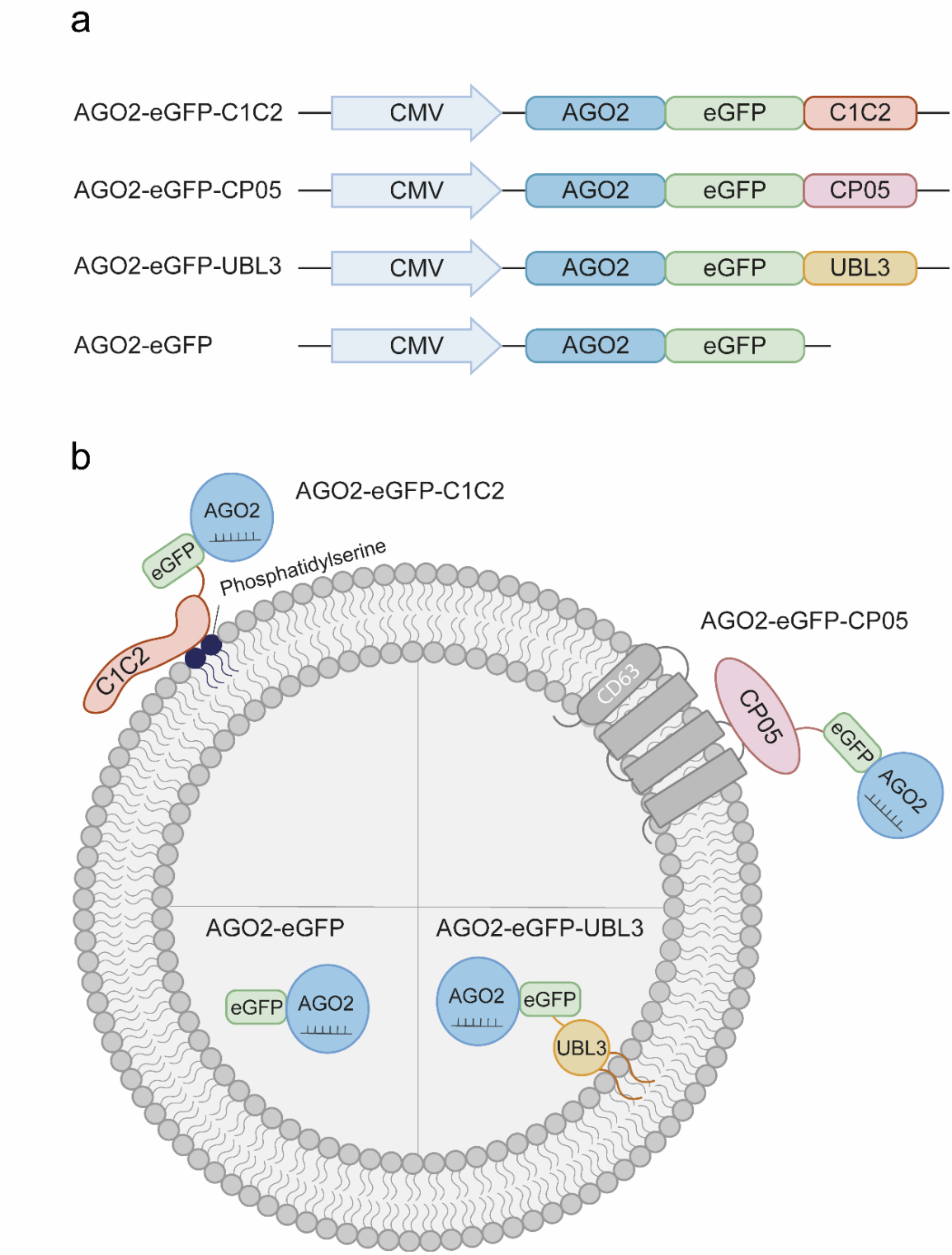
a
AGO2-eGFP-C1C2
CMV
AGO2
eGFP
C1C2
AGO2-eGFP-CP05
CMV
AGO2
eGFP
CP05
AGO2-eGFP-UBL3
CMV
AGO2
eGFP
UBL3
AGO2-eGFP
CMV
AGO2
eGFP
b
AGO2-eGFP-C1C2
AGO2
eGFP
Phosphatidylserine
C1C2
AGO2-eGFP-CP05
CD63
CP05
eGFP
AGO2
AGO2-eGFP
eGFP
AGO2
AGO2-eGFP-UBL3
AGO2
eGFP
UBL3

Figure 3.1 AGO2 EV- loading strategy.

(a) Scheme of constructs tested in this study. **(b)** AGO2 EV-loading methods. Clockwise from top left: AGO2-eGFP-C1C2 fusion, where C1C2 enables the association to the EVs by binding to phosphatidylserine in the EV membrane; AGO2-eGFP-CP05, where CP05 promotes EV-loading via its interaction with CD63 in the EV surface; AGO2-eGFP-UBL3, where UBL3 sorts proteins into the EVs via its two prenylation motifs; AGO2-eGFP, that serves as a stochastic loading control. AGO2, argonaute 2; C1C2, C1C2 domain of lactadherin; UBL3, ubiquitin-like protein 3.

To test the EV-loading ability of AGO2-fusion proteins, we transfected HEK293T cells with the various constructs and then isolated the EVs from conditioned media using tangential flow filtration followed by size exclusion liquid chromatography (LC). EV LC-fraction fluorescence from cells transfected with AGO2-eGFP-UBL3 was notably higher than that of AGO2-eGFP, while a slight increase in fluorescence was observed in cells transfected with AGO2-eGFP-CP05 and AGO2-eGFP-C1C2 as compared to AGO2-eGFP (**Fig 3.2a**). Western blotting of cell lysates and EVs showed that AGO2-eGFP-UBL3 protein levels in EVs were higher than those of AGO2-eGFP while the levels in cells remained similar (**Fig 3.2b**), consistent with the fluorescence data. In AGO2-eGFP-UBL3 EV sample there were additional higher and lower molecular weight bands besides the main band (which had the expected size). Lower molecular weight bands may represent cleavage products while the higher molecular weight bands could represent covalent protein modifications. AGO2-eGFP-CP05 levels were also higher in EVs as compared to AGO2-eGFP, although to a much lesser extent (**Fig 3.2b**). Together these data suggest that AGO2-eGFP-UBL3 and AGO2-eGFP-CP05 are enriched in EVs as compared to untargeted AGO2-eGFP, although AGO2-eGFP-CP05 was enriched to a much lesser extent.

We next assessed endogenous miRNA loading of EVs isolated from HEK293T cells transfected with the AGO2-fusion constructs. The levels of three endogenous miRNAs were

measured: miR-21, miR-100 and miR-106. These miRNAs are present in EVs at low, medium, and high levels, respectively[305]. miR-21 and miR-106 showed a ~5-fold enrichment in EVs from AGO2-eGFP-CP05 and a ~2.5-fold increase in EVs from AGO2-eGFP-UBL3 transfected cells, as compared to AGO2-eGFP EVs (**Fig 3.2c**). miR-100 was enriched ~2.5-fold in EVs from AGO2-eGFP-CP05 and ~5-fold in EVs from AGO2-eGFP-UBL3 cells (**Fig 3.2c**). Despite these data show moderate levels miRNA of enrichment in EVs, we would expect higher level of miRNAs in EVs from AGO2-eGFP-UBL3 cells than in EVs from AGO2-eGFP-CP05 according to the AGO2-fusion protein levels shown in the western blot. This data does not seem to indicate that the enrichment observed in EV miRNAs is linked to the increase of AGO2-fusion-proteins in EVs.

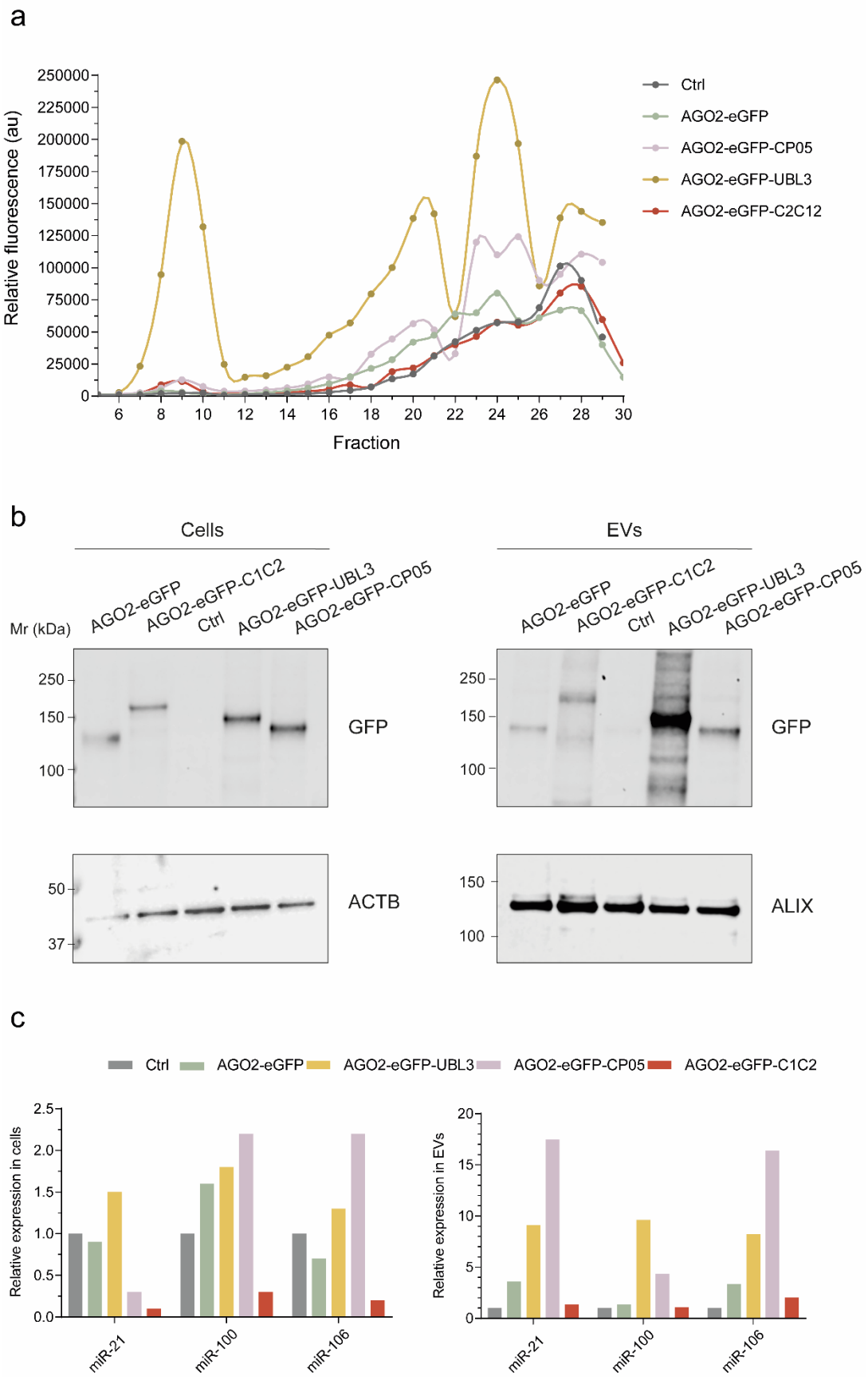
a
Relative fluorescence (au)
250000
225000
200000
175000
150000
125000
100000
75000
50000
25000
0
6
8
10
12
14
16
18
20
22
24
26
28
30
Fraction
Ctrl
AGO2-eGFP
AGO2-eGFP-CP05
AGO2-eGFP-UBL3
AGO2-eGFP-C2C12
b
Cells
EVs
Mr (kDa)
AGO2-eGFP
AGO2-eGFP-C1C2
Ctrl
AGO2-eGFP-UBL3
AGO2-eGFP-CP05
250
150
100
GFP
50
37
ACTB
ALIX
c
Ctrl
AGO2-eGFP
AGO2-eGFP-UBL3
AGO2-eGFP-CP05
AGO2-eGFP-C1C2
Relative expression in cells
Relative expression in EVs
miR-21
miR-100
miR-106

Figure 3.2 Assessment of endogenous miRNA loading to EVs via AGO2-fusion-proteins.
(a) Fluorescence of the fractions derived from size-exclusion liquid chromatography of EV-containing conditioned media from HEK293T cells transfected with AGO2-eGFP, AGO2-eGFP-CP05, AGO2-eGFP-UBL3, AGO2-eGFP-C1C2. Fluorescence relative to 280 nm absorbance values. Untransfected cells were used as control. **(b)** Western blot of native AGO2 and AGO2-fusion-proteins in HEK293T cells and EVs. Cell lysates and isolated EVs were blotted against ACTB and ALIX respectively. Both cell lysates and isolated EVs were blotted against GFP. **(c)** Levels of miR-21, miR-100, miR-106 were measured in EVs and cells by RT-qPCR.

To evaluate if we could increase the miRNA content of EVs using an exogenously expressed shRNA, we tested AGO2-eGFP-UBL3 and AGO2-eGFP-CP05 fusion constructs in HEK293T cells stably expressing shLuc-shRNA. Only AGO2 constructs that were enriched in EVs in previous experiments were assessed. EV-fractions from AGO2-eGFP-UBL3 cells exhibited increased fluorescence, suggesting that this construct is enriched in EVs (**Fig 3.3a**). However, no increase in shRNA levels was observed in EVs (**Fig 3.3b**).

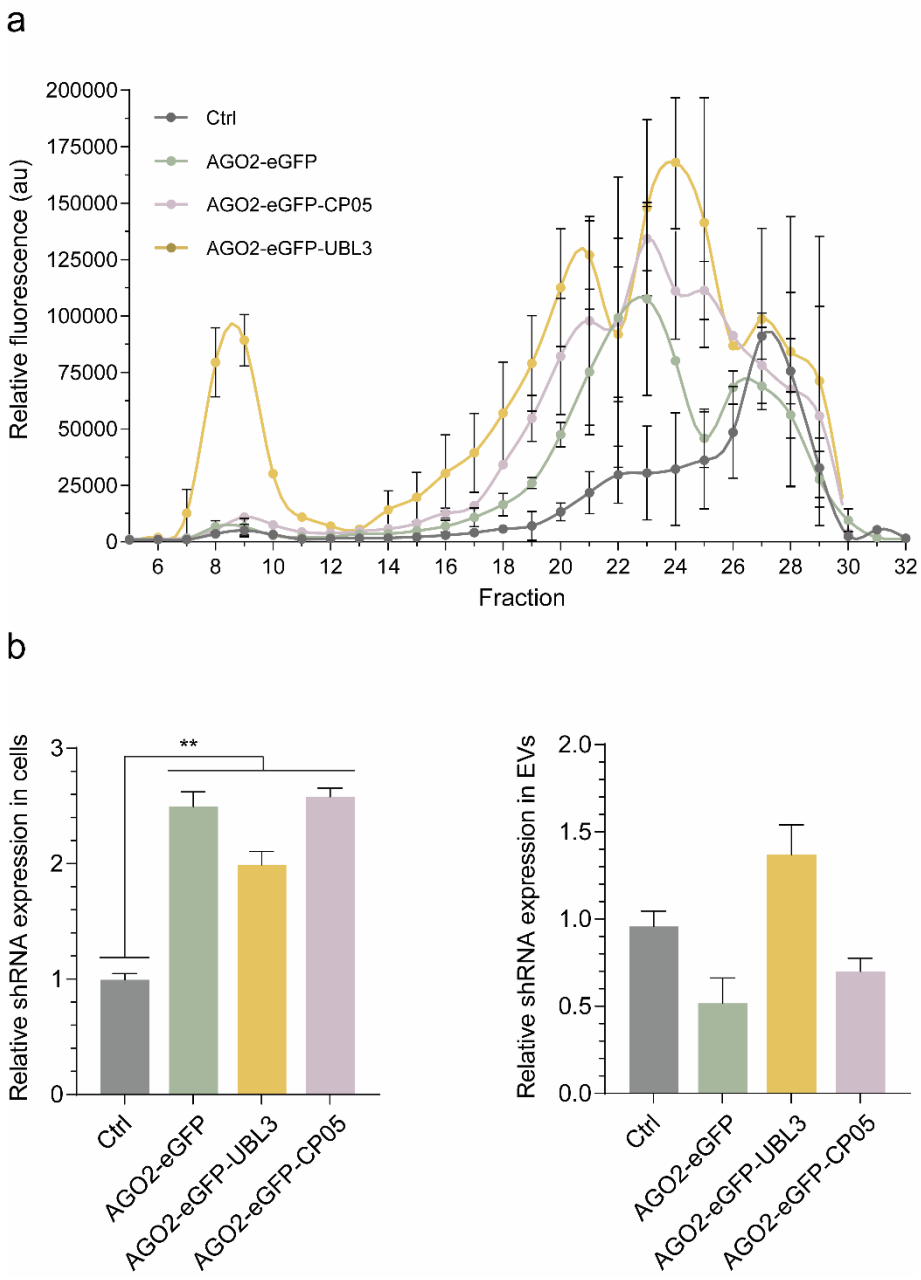

Figure 3.3 shRNA levels are not increased in EVs from cells transfected with AGO2-fusion-proteins despite an increase in EV-protein levels.

(a) Relative fluorescence of the fractions derived from size-exclusion liquid chromatography of EV-containing conditioned media from HEK293T cells stably expressing shLuc transfected with AGO2-eGFP, AGO2-eGFP-CP05, AGO2-eGFP-UBL3. Fluorescence relative to 280 nm absorbance values. Untransfected cells were used as control. **(b)** Levels of shLuc were measured in EVs and HEK293T cells stably expressing shLuc by RT-qPCR. Statistical significance was

tested by one-way ANOVA and Bonferroni *post hoc* test. Data are presented as mean + SEM, n = 3 replicates, ** $P < 0.01$.

Having shown that AGO2 fused to UBL3 was highly enriched in EVs, we decided to focus on the delivery of dCas9-VPR using UBL3 considering the therapeutic relevance of Cas9 delivery. This Cas9 variant is a fusion of nuclease null Cas9 with a tripartite activator (VP64-p65-Rta) that activates transcription[306]. AGO2 and Cas9 have different mechanisms of RNA binding, thus the fact that AGO2 was not able to sort miRNAs to EVs in our experimental conditions did not imply that Cas9 would be sorted to the EVs without its associated sgRNA. We decided to use dCas9-VPR (VP64-p65-Rta) due to the availability of a HEK293T reporter cell line that expresses GFP in response to dCas9VPR transcriptional activation.

As we did for the AGO2 constructs, to assess dCas9-VPR-eGFP-UBL3 loading to EVs we transfected HEK293T cells with sgRNA and dCas9-VPR-eGFP or dCas9-VPR-eGFP-UBL3 and then isolated the EVs from conditioned media using size exclusion LC. EV LC-fractions from cells transfected with dCas9-VPR-eGFP-UBL3 had higher fluorescence values as compared with dCas9-VPR-eGFP (**Fig 3.4a**), indicating that UBL3 promotes dCas9-VPR-eGFP EV-sorting. In the same Western blot of cell lysates and EVs showed that dCas9-VPR-eGFP was only detected in EVs when it was fused to UBL3 (**Fig 3.4b**). We next tested sgRNA sorting to EVs in cells transfected with dCas9-VPR constructs. A ~6-fold increase was observed in dCas9-VPR-eGFP-UBL3 EVs sgRNA levels as compared to those in dCas9-VPR-eGFP EVs, without significant changes in intracellular sgRNA expression (**Fig 3.4c**). We then estimated by RT-qPCR using an sgRNA standard curve that on average 4 out of 100 EVs had a molecule of sgRNA for dCas9-VPR-eGFP EVs and 35 out of 100 EVs had a molecule of sgRNA for dCas9-

VPR-eGFP-UBL3 EVs (**Fig 3.4d**). All together, these data indicate that both dCas9-VPR-eGFP-UBL3 protein and sgRNA are enriched in EVs from cells expressing dCas9-VPR-eGFP-UBL3.

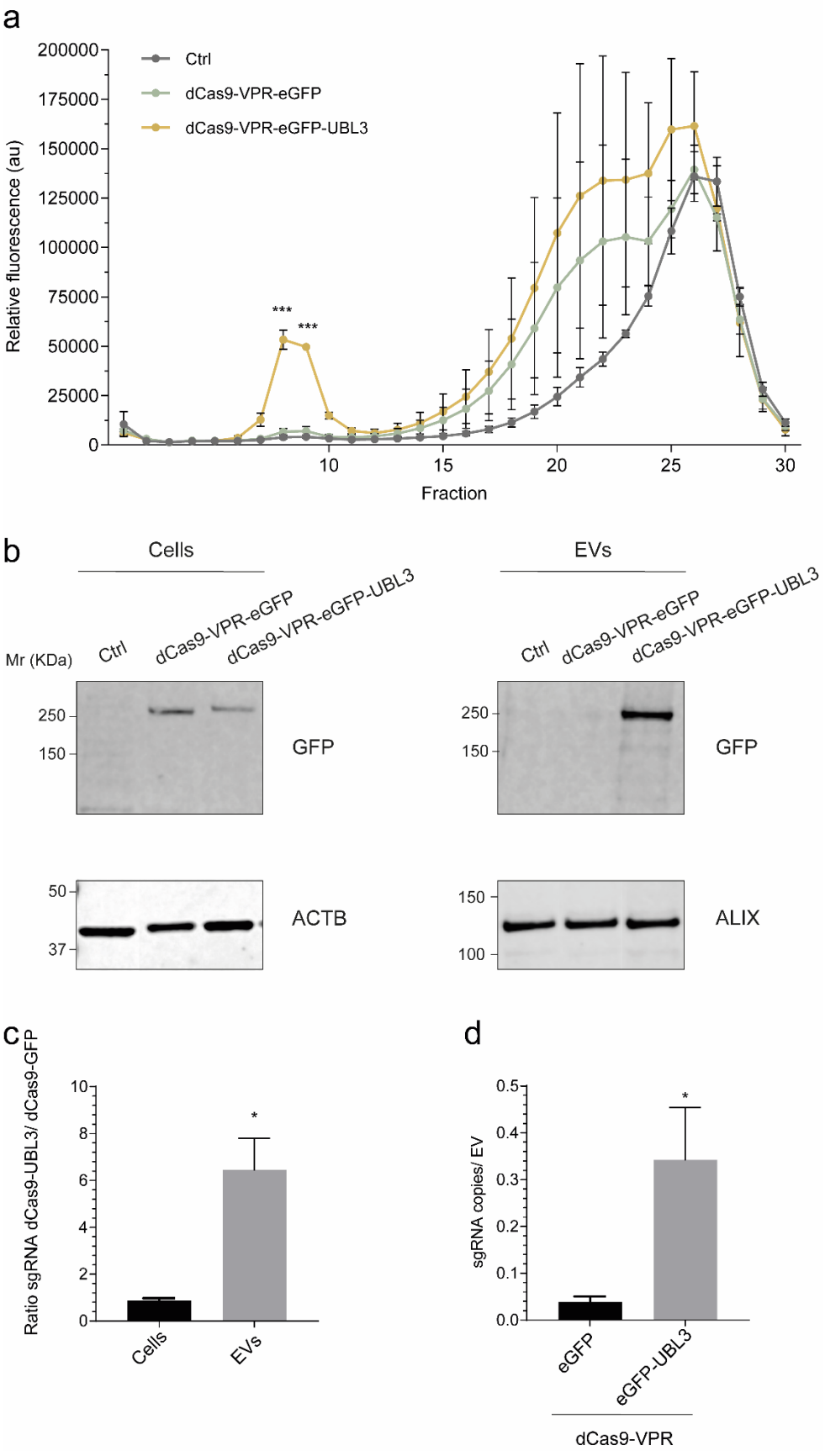
a
Ctrl
dCas9-VPR-eGFP
dCas9-VPR-eGFP-UBL3
Relative fluorescence (au)
Fraction
***
***
b
Cells
EVs
Mr (KDa)
Ctrl
dCas9-VPR-eGFP
dCas9-VPR-eGFP-UBL3
GFP
ACTB
ALIX
c
Ratio sgRNA dCas9-UBL3/ dCas9-GFP
Cells
EVs
d
sgRNA copies/ EV
eGFP
eGFP-UBL3
dCas9-VPR

Figure 3.4 dCas9-VPR fused to UBL3, and sgRNA are enriched in EVs from dCas9-VPR-eGFP-UBL3 transfected cells.

(a) Relative fluorescence of the fractions derived from size-exclusion liquid chromatography of EV-containing conditioned media from HEK293T cells co-transfected with single guide RNA (sgRNA) and dCas9-VPR-eGFP or dCas9-VPR-eGFP-UBL3. Fluorescence relative to 280 nm absorbance values. Untransfected cells were used as control. Data represent three independent replicates and is presented as the mean ± SEM. $*P < 0.05$ **(b)** Western blot of dCas9-VPR-eGFP and dCas9-VPR-UBL3 in HEK293T cells and EVs. Cell lysates and isolated EVs were blotted against ACTB and ALIX respectively. Both cell lysates and isolated EVs were blotted against GFP. **(c)** Level of sgRNAs were measured in EVs and cells by RT-qPCR. **(d)** sgRNA copies per vesicle were measured by absolute quantification RT-qPCR using a known concentration of sgRNA plasmid as standard. Data are presented as mean + SEM, n = 3 independent replicates, $*P < 0.05$, $***P < 0.001$.

We next assessed whether the dCas9-VPR and sgRNA loaded into the EVs could be delivered to recipient cells. To do so, we used HEK293T reporter cells that express mScarlet red fluorescent protein in response to dCas9-VPR transcriptional activation (**Fig 3.5a**). To determine if dCas9-VPR-fusion-proteins retained their function, we measured the transcriptional activation of mScarlet in reporter cells transfected with the construct. dCas9-VPR-eGFP and dCas-VPR-eGFP-UBL3 transcriptional activity were not significantly different to that of dCas9-VPR (**Fig 3.5b**), suggesting that eGFP or eGFP-UBL3 fusion did not alter dCas9-VPR function. To assess dCas9-VPR EV transfer, we incubated reporter cells with EVs from HEK293T cells transfected with dCas9-VPR-eGFP-UBL3 and sgRNA plasmids and performed flow cytometry analysis 48h later. Treatment with dCas9-VPR-eGFP-UBL3 and sgRNA EVs did not lead to a detectable increase in mScarlet expression as compared to dCas9-VPR-eGFP and sgRNA EVs (**Fig 3.5c**). To rule out the possibility that the lack of activity was due to low sgRNA levels in the EVs, we incubated the EVs with reporter cells expressing the sgRNA. To do so, reporter cells were

transfected with sgRNA plasmid 24h before EV transfer. No activity was detected in reporter cells (**Fig 3.5d**). These results indicate that EV-loaded dCas9-VPR-eGFP-UBL3 is not able to activate transcription at detectable levels in our reporter system.

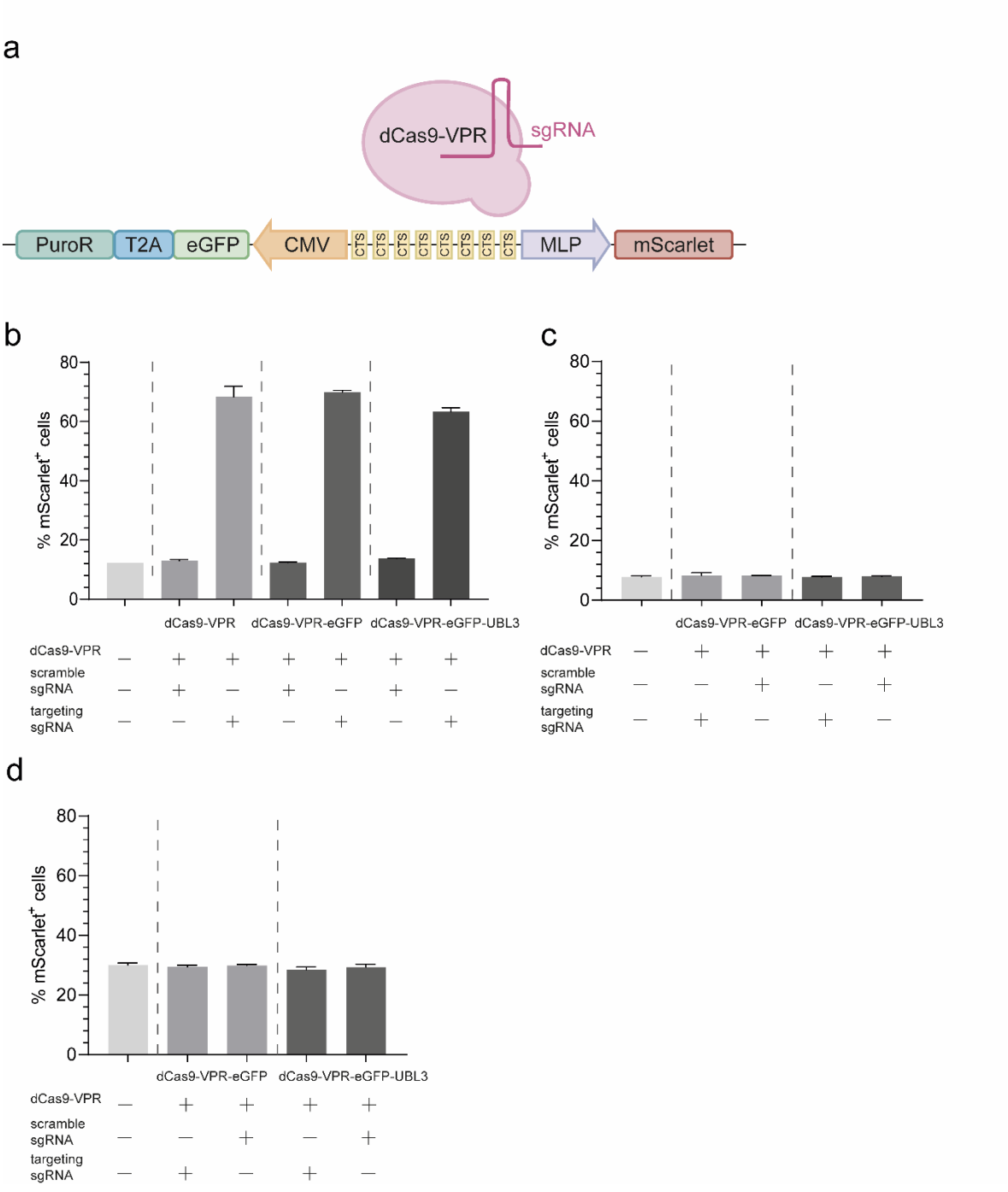

Figure 3.5 Delivery of dCas9-VPR via EVs is not able to activate reporter cell transcription at detectable levels.

(a) Scheme of the HEK293T reporter cell line. dCas9-VPR binds to CTS (CRISPR-Cas9 target sites) guided by its sgRNA and promotes the transcriptional activation of mScarlet. eGFP is constitutively expressed by CMV promoter. **(b)** Flow cytometry data showing reporter cells transfected with dCas9-VPR (positive control), dCas9-VPR-eGFP, dCas9-VPR-eGFP-UBL3 and untransfected cells (negative control). **(c)** Flow cytometry data of reporter cells treated with 1×10^{11} EVs per well (24-well plate). EVs were isolated from cells transfected with; dCas9-VPR-eGFP and scramble sgRNA, dCas9-VPR-eGFP and targeting sgRNA, dCas9-VPR-eGFP-UBL3 and scramble sgRNA, dCas9-VPR-eGFP-UBL3 and targeting sgRNA. **(d)** Flow cytometry data of reporter cells expressing sgRNA treated with 1×10^{11} EVs per well (24-well plate). EVs were isolated from cells transfected with; dCas9-VPR-eGFP and scramble sgRNA, dCas9-VPR-eGFP and targeting sgRNA, dCas9-VPR-eGFP-UBL3 and scramble sgRNA, dCas9-VPR-eGFP-UBL3 and targeting sgRNA. Only single cells that are positive for GFP were plotted. Data represent three independent replicates and is presented as the mean + SEM.

Once EVs have been taken up by recipient cells, the majority enter the endocytic pathway and become entrapped in the endosomes[184]. Thus, EV content must be released to the cytosol before EVs are re-exported to the extracellular space or degraded by lysosomal enzymes. To increase cytosolic delivery of EV cargo, producer cells can be modified to express membrane proteins that integrate in the EV membrane and promote endosomal escape. One of the most commonly used is VSVG, a viral protein that promotes EV uptake by receptor mediated endocytosis and facilitates the fusion of the EV and endosome membranes with the subsequent release of EV contents to the cytoplasm[202].

To enhance functional delivery of dCas9-VPR to recipient cells by EVs, we co-expressed dCas9-VPR-eGFP-UBL3 and sgRNA in HEK293T cells stably expressing VSVG with the aim of producing EVs with both dCas9-VPR and VSVG. To determine whether dCas9-VPR-eGFP-

UBL3 and VSVG were present in the same EVs, we measured the percentage of EVs positive for dCas9-VPR-eGFP-UBL3, VSVG or both by nano flow-cytometry. As observed in **Fig 3.6b, c**, 10.9% of EVs were dCas9-VPR-eGFP-UBL3 positive and these EVs had a median size of ~100 nm. Regarding VSVG, 17.7% of EVs were positive for VSVG and these EVs showed a median size of ~60 nm (**Fig 3.6a, c**). Only 2.5% of EVs were double positive, meaning that only a minor proportion of EVs contained both dCas9-VPR and VSVG (**Fig 3.6c**). The above results suggest that dCas9-VPR-eGFP-UBL3 and VSVG are primarily expressed in mutually exclusive subpopulations of EVs.

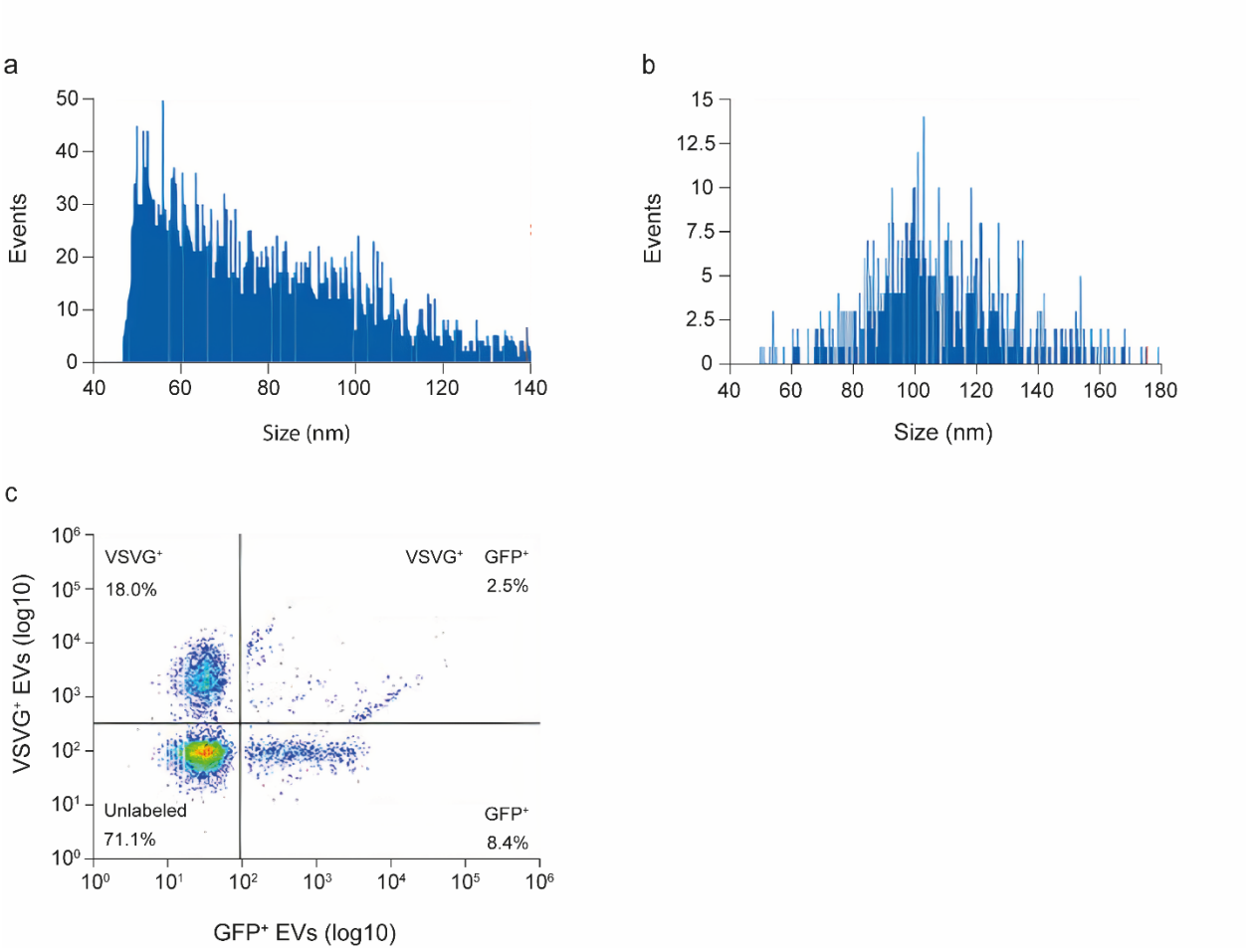

Figure 3.6 dCas9-VPR-eGFP-UBL3 and VSVG protein are present on different EV subpopulations.

Nano flow-cytometry (nano-FCM) analysis of EVs from stable HEK293T cells expressing vesicular stomatitis virus glycoprotein (VSVG) transfected with dCas9-VPR-eGFP-UBL3. **(a)** Size distribution of VSVG positive EVs. VSVG presence in EVs was assessed using fluorescent antibodies against VSVG. **(b)** Size distribution of EVs positive for dCas9-VPR-eGFP-UBL3. Cas9-fusion-protein was detected by GFP fluorescence. **(c)** VSVG positive, dCas9-VPR-eGFP-UBL3 positive and double positive EVs.

To determine if endosomal escape was the factor limiting EV-dCas9-VPR delivery, we assessed the transfer of dCas9-VPR-eGFP or dCas9-VPR-UBL3 loaded EVs in presence of chloroquine.

Chloroquine is a membrane-permeable endosomal escape enhancing molecule that promotes cytosolic release of endosomal content by the proton sponge effect[190]. During endosome maturation, chloroquine becomes protonated, which induces Cl^- and H_2O influx, endosome swelling and ultimately endosome rupture, thereby releasing endosomal cargo to the cytoplasm[191,256].

To this end, we used a reporter plasmid that expresses eCFP in response to dCas9-VPR transcriptional activation (**Fig 3.7a, b**). In this set of experiments, we decided to use an alternative dCas9 reporter cell line given that the reporter cell line used in previous experiments showed a high background signal (**Fig 3.5**). As observed in **Fig 3.7c**, incubation of reporter cells with EVs from dCas9-VPR-eGFP-UBL3 did not lead to a detectable increase in eCFP expression as compared to dCas9-VPR-eGFP or untreated control. Similar results were obtained when we incubated the EVs with reporter cells expressing the sgRNA. No dCas9-VPR activity was detected in reporter cells (**Fig 3.7d**). These results suggest that endosomal escape is not the only factor limiting the functional delivery dCas9-VPR loaded EVs.

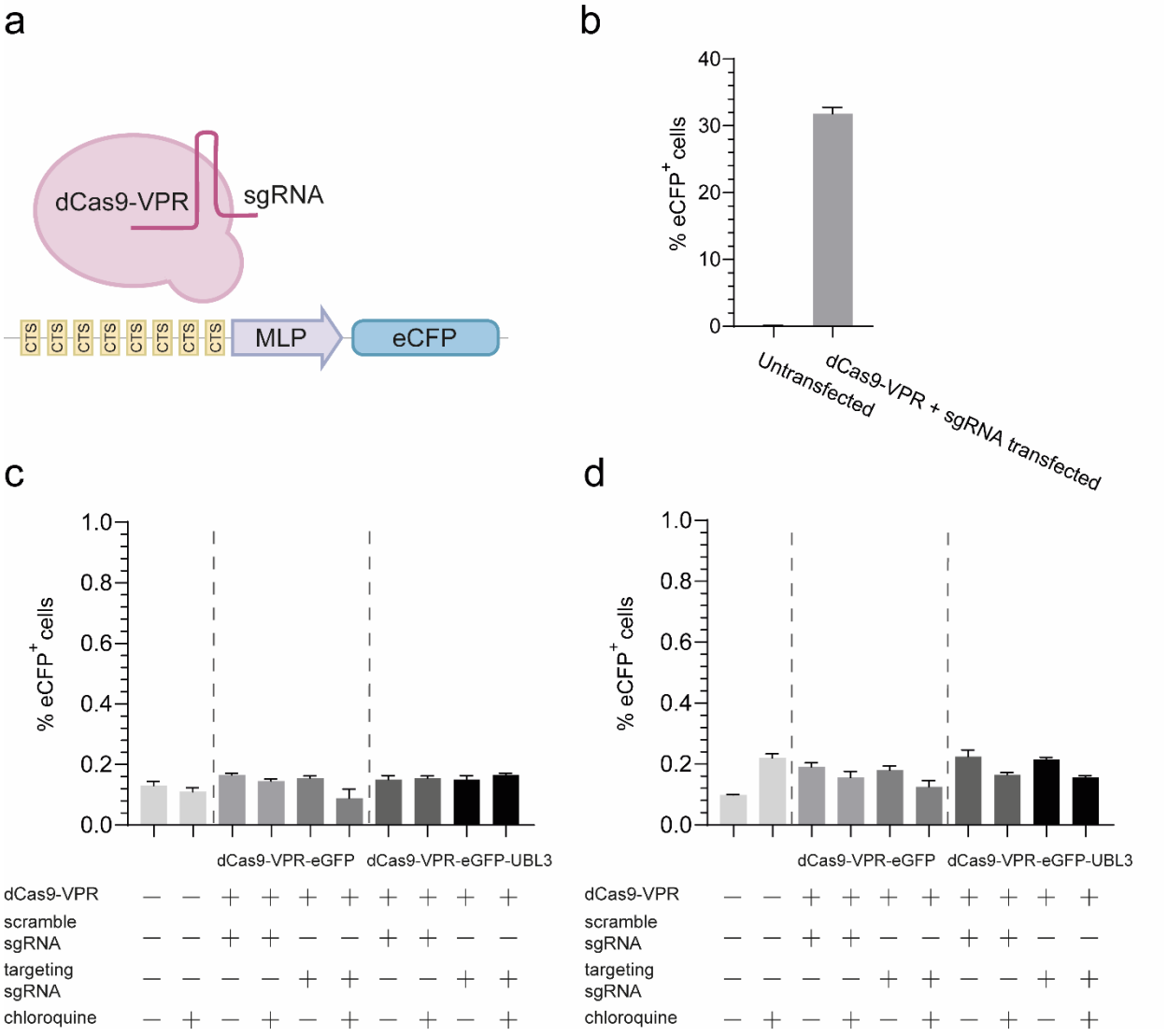

Figure 3.7 Endosomal escape is not the only limiting factor hindering functional EV-delivery of dCas9-VPR.

(a) Scheme of the dCas9-VPR reporter plasmid. dCas9-VPR binds to CTS guided by its sgRNA and promotes the transcriptional activation of eCFP. **(b)** Flow cytometry data showing reporter cells transfected with dCas9-VPR, sgRNA and reporter plasmid (positive control) and untransfected cells (negative control). **(c)** Flow cytometry data of reporter cells treated with 1×10^{11} EVs per well (24-well plate) with or without 25 μM chloroquine. EVs were isolated from cells transfected with; dCas9-VPR-eGFP and scramble sgRNA, dCas9-VPR-eGFP and targeting sgRNA, dCas9-VPR-eGFP-UBL3 and scramble sgRNA, dCas9-VPR-eGFP-UBL3 and targeting

sgRNA. (d) Flow cytometry data of reporter cells expressing sgRNA treated with 1×10^{11} EVs per well (24-well plate) with or without chloroquine. EVs were isolated from cells transfected with; dCas9-VPR-eGFP and scramble sgRNA, dCas9-VPR-eGFP and targeting sgRNA, dCas9-VPR-eGFP-UBL3 and scramble sgRNA, dCas9-VPR-eGFP-UBL3 and targeting sgRNA. Data represent n = 2 and is presented as the mean + SEM.

3.5. Discussion

In this study we sought to develop a strategy to sort dCas9-VPR/sgRNA complexes into EVs and to deliver functional dCas9-VPR/sgRNA complexes to recipient cells via a UBL3 tag. UBL3 is protein that acts as a post-translational modification (similar to ubiquitin) and regulates protein sorting to the EVs[92]. UBL3 itself is modified by palmitoylation and prenylation (geranylgeranylation), which enable its anchoring to membranes[307]. It has been shown that UBL3 fusion is capable of sorting GFP to the EVs, indicating that proteins could be sorted to EVs by UBL3[92].

At first, the aim was to deliver miRNAs or shRNAs to recipient cells via AGO2-UBL3/miRNA complex sorting to EVs. Despite that AGO2-eGFP-UBL3 was highly enriched in EVs (**Fig 2b**), miRNA and shRNAs levels in the EVs were not concomitantly increased (**Fig 2c, Fig 3b**). It may be possible that AGO2 fused to UBL3 is sorted to the EVs before having the opportunity to bind to miRNAs/shRNAs due to time or space constraints. Another possibility could be that AGO2 is not the main protein binding to miRNAs or shRNAs in native EVs.

Nevertheless, considering AGO2 targeting to the EVs was highly enhanced via UBL3 fusion, we decided to investigate delivery of dCas9-VPR/sgRNA complexes using the same UBL3 strategy. The CRISPR-Cas9 system represents a potent tool for gene editing and transcription regulation due to its high efficiency and specificity[308]. However, this potential is hampered by the lack of efficient delivery methods[309]. When fused to UBL3, dCas9-VPR-eGFP and sgRNA were successfully loaded to the EVs (**Fig 4**) and 10.9% of EVs were positive for GFP fluorescence (**Fig 6c**). However, functional activity of dCas9-VPR was not detected when EVs were transferred to recipient reporter cells (**Fig 5**). This could be in part due to the high

background mScarlet levels in reporter cells that may have masked EV dCas9-VPR function signal.

In order to deliver functionally active cargo, dCas9-VPR EVs need to be taken up and their contents released to the cytoplasm, whereby dCas9-VPR can then be transported to the nucleus in order to activate transcription. Having ruled out that the lack of detectable activation was due to low sgRNA levels in EVs by using reporter cells transfected with sgRNA (**Fig 5d**), we decided to tackle the likely possibility that EV cargo was not reaching the cytosol of recipient cells due to endosomal entrapment. For this reason, we decided to produce EVs in stable cells expressing VSVG, a well-known endosomal escape protein expressed in EV membrane that facilitates both uptake and EV-endosome membrane fusion, releasing EV content to the cytoplasm[202]. Although 10.9% and 17.7% of EVs were positive for dCas9-VPR-UBL3 and VSVG respectively, only 2.5% of EVs contained both proteins, suggesting that they are not mostly expressed in the same EV subpopulations. In fact, the two subpopulations differed in median size of EVs (**Fig 6a, b**). To determine if the factor limiting EV delivery of dCas9-VPR was the cytosolic release of cargo from endosomes, we performed the EV transfer experiments in presence of chloroquine, an endosomolytic molecule that has been previously used to enhance functional delivery of cargo proteins via EVs[256]. Efficiency of EV transfer to reporter cells was too low and could not be detected (**Fig 7**). This indicates that endosomal escape might not be the only factor restricting functional delivery of EV cargo. Although some studies indicate EVs are uptaken by recipient cells[185], several studies have reported low EV uptake efficiencies[104,184,202], thus it is possible that EV uptake by reporter cells was too low to promote cell activation at detectable levels. Another possibility that could account for the lack of detectable activity and that was not explored is the association of UBL3 to the EV membrane. UBL3 sorting to the EVs

is related to its ability to associate to membranes[92]. Although UBL3 could potentially detach from the EV membrane[310], it is still possible that EV-delivered dCas9-VPR-eGFP-UBL3 is not functional due to dCas9-VPR being retained at the EV-membrane and unable to reach the nucleus.

Other studies have attempted to load and deliver Cas9/sgRNA complex via EVs with variable degrees of success. Some have relied on centrifugation of EVs together with recipient cells (spinoculation) in order to deliver Cas9/sgRNA cargo[247,311]. However, despite the uptake efficiency of this method being high, it can only be used for *in vitro* delivery. Cas9/sgRNA sorting to EVs has also been achieved by simple overexpression of dCas9-VPR protein and sgRNA[300,312]. Nevertheless, in this and other studies, functional delivery of Cas9 was not detected in EVs unless Cas9 was tagged with an EV-targeting protein[155,207,273]. Several recent studies have successfully delivered Cas9 ribonucleoprotein using Gag viral proteins[207,267], ARRDC1[155] or CD63[250,273] as EV-scaffold proteins. In most of these studies, a release system was required to accomplish functional delivery of Cas9. These were based on aptamer-aptamer binding protein interaction, GFP-GFP nanobody interaction, small molecule induced dimerization or the introduction of a viral protease restriction site. This was not the case for the strategy based on ARMMs (arrestin domain containing protein1-mediated microvesicles), in which ARMMs were capable of packaging and delivering Cas9/sgRNA complex *in vitro* with moderate efficiency when Cas9 was fused to ARRDC1-interacting WW-domains[155]. Another study used a myristoylation tag on Cas9 to successfully deliver Cas9/sgRNA complex to recipient cells *in vitro*[265]. However, chloroquine and polybrene transfection reagent were added during the EV transfer, limiting the therapeutic use of this strategy[265]. As for the requirement of an endosomal escape protein, some studies have also included VSVG[202,203,247,272,300,311] or

BaEVRLess[208] (baboon endogenous virus envelope glycoprotein) at the EV surface to enhance uptake and cytoplasmic delivery.

The majority of the aforementioned studies used nuclease-competent Cas9 and use cells stably expressing GFP as reporter cells for activity detection, while in our study we used transcriptional activating dCas9. Our system is less sensitive than those using nuclease-competent Cas9 due to promoter leakage and the fact that dCas9-VPR must be present at the activation site to trigger the expression of the reporter fluorescent protein, whereas with nuclease-competent Cas9 a single cutting event triggers the expression of the fluorescent reporter. Thus, these differences together with the fact that EV-uptake is cell-type dependent[185] and differing EV-isolation methods might explain the lack of activity detection in our system as compared to other studies. Importantly, these studies normally do not report the concentration of EVs used in the EV-transfer experiments, thus hindering possible comparisons with our study.

3.6. Conclusions

The EV-delivery strategy assessed in this chapter was unsuccessful, nevertheless we were able to identify the key parameters limiting EV-mediated functional delivery. These include the requirement of an EV surface protein that mediates uptake by the recipient cells, an endosomal escape moiety that promotes cytosolic release of the cargo protein and an EV-release system to enable cargo protein transport to its final intracellular location. In addition, our results exposed the importance of single vesicle analysis to ascertain if the various protein components are present in the same vesicles. These findings provided motivation to search more broadly for alternative EV-loading approaches that would meet the aforementioned requirements.

4. Results II – *In silico* identification of novel protein features to enhance cargo loading into the EVs

4.1. Introduction

The enrichment of specific proteins in EVs compared to their parental cell levels is suggestive of the existence of mechanisms for regulating the sorting of protein cargo to EVs[313]. Although these mechanisms are beginning to be deciphered, they still are not fully understood. Interestingly, protein features including post translational modifications (PTMs), protein motifs, and protein domains have been shown to play a major role in EV-protein sorting and EV biogenesis[314].

Motifs can either facilitate binding interactions between specific protein partners or may constitute signals for enzyme-mediated covalent addition of PTMs. For example, late domain motifs in viral Gag proteins can be recognized by the ALIX and ESCRT-I component TSG101, which mediate in their sorting and release in EVs[315,316]. In addition, the CAAX motif found in Rab GTPases promotes their geranylgeranylation, a modification that enables their binding to cellular membranes[317]. Similarly, protein domains can also play a role in protein-protein binding, and promote interactions between proteins and other macromolecules such as carbohydrates or lipids[318]. For example, the C1C2 domain of lactadherin binds to phosphatidylserine, which is enriched in EV membranes and has been implicated in sorting of lactadherin to EVs[234].

PTMs are covalent modifications of proteins that occur after protein biosynthesis. They are able to modulate protein properties such as their activity, subcellular location, and interaction with other molecules. The main classes of PTMs include irreversible amino acid modifications

(e.g., deamidation), proteolysis, and the addition chemical moieties (e.g., phosphorylation, hydroxylation), complex molecules (e.g., lipidation, glycosylation), or other polypeptides (e.g., ubiquitination, sumoylation). Although the majority of post-translational modifications are reversible, the enzymes involved in PTM processing are highly regulated. Ubiquitination has emerged as a key player in protein cargo clustering and sorting to EVs[319]. Several types of ubiquitination have been described depending on the number of ubiquitin molecules added (monoubiquitination or polyubiquitination) and on the amino acid in ubiquitin by which the polyubiquitin chains are linked (i.e., K6, K11, K27, K29, K33, K48, K63, or M1)[320]. While K48-linked polyubiquitin chains have been implicated in the targeting of proteins for proteasomal degradation, K63-linked chains have been shown to be involved in endocytic traffic and ILV formation[321]. The latter is mediated by the recognition of K63 by ubiquitin interacting motifs in ESCRT-0 components[76]. One of the most common PTMs is protein glycosylation[322]. This modification is involved in protein stability, trafficking, and cell surface recognition processes[318]. Interestingly, lectin microarrays have indicated that EVs from various cell sources exhibit a common glycan signature. EVs are enriched in polylactosamine, α2-6 linked sialic acid, high mannose, and complex N-linked glycans[323]. Conversely, blood group A and B-antigens were less abundant on EVs than on the cell surface[323]. These differences between parental and EV membranes have been suggested to derive from the segregation of a specific subset of glycoproteins into the membrane microdomains from which EVs arise. The oligomerization of glycoproteins mediated by lectin recruitment has been reported to regulate endocytosis and intracellular vesicle trafficking[324]. In particular, galectins have been found in EVs[325] and have been reported to be involved in lipid raft organization and endocytosis[326].

Protein lipidation has also been implicated in EV protein sorting. Shen *et al*., showed that the addition of myristoylation or prenylation/palmitoylation tags to TyA, a cytoplasmic protein, promoted TyA sorting into EVs[327]. In addition, UBL3 modification by geranylgeranylation and palmitoylation was reported to be essential for EV-packaging of UBL3[92].

In this chapter, we develop a bioinformatics analysis to identify novel protein features to enhance cargo loading into EVs.

4.2. Hypotheses and aims

Hypothesis:

- There exist novel protein features (domains, post-translational modifications, and/or motifs) that promote protein loading to the EVs.

Aim:

- *In silico* identification of novel protein domains, post-translational modifications, and/or motifs that could be used as scaffolds to sort proteins into the EVs.

4.3. Materials and methods

4.3.1. Bioinformatics analysis

For the bioinformatics analysis, custom scripts were generated in Python (version 3.8) to find statistically significant EV-enriched UniProt[328]-annotated features on proteins using matched EV and producer cell mass spectrometry data (from HEK293T cells, MSCs and adipocytes). This analysis was named integrated proteomics and feature annotation analysis (IPFA). Numpy, seaborn, functools, math, matplotlib, scipy, json, and request Python packages were used. To identify features that were significantly EV-enriched (P value < 0.05), the Kolmogorov-Smirnov test followed by Benjamini-Yekuteli *post hoc* test was applied. This test compared the distributions of "EV vs cell abundance ratio". of proteins with a given feature and that of all proteins in the dataset and determine if the distributions were significantly different. In order to deal with the missing data problem, a value of one was added to every mass spectrometry area measurement (abundance). As such, the mathematical distances between samples were maintained and any zeros effectively removed.

4.3.2. Proteomics data generation (published by Sork et Al.)

Proteomics mass spectrometry data used in this study was previously published[305]. Briefly, EVs were isolated from cell culture supernatants of HEK293T cells (n = 3), MSCs (n = 3), and adipocytes (n = 3) by dUC. Conditioned medium centrifuged at 300 g 5 min, followed by a spin at 1500 g 10 min, and a 0.22 μm filtration step. EVs were pelleted by two consecutive centrifugation steps at 110000 g 90 min. The resulting EV pellet was resuspended in PBS and stored at −80 °C for proteomic analysis. EVs and cells were analysed by LC-MS/MS as

described previously[284]. Protein abundance was calculated from the MS Area of the given protein over the total MS Area of the sample proteome.

4.4. Results

4.4.1. Development of a bioinformatics analysis to identify potential EV-sorting features

As shown previously in Chapter I, PTM-mimicry by UBL3 results in efficient AGO2 and dCas9-VPR protein sorting to EVs. Therefore, we were motivated to develop an *in silico* approach to identify protein features with utility for EV-loading, preferentially features that could be used for sorting proteins in a soluble form. To this end, we integrated proteomics data (from EVs and producer cells) with protein annotation data (i.e. UniProt motifs, domains, and PTMs). Data for HEK293T cells, MSCs and adipocytes was published previously[305].

Custom Python scripts were used to identify EV-enriched protein features using mass spectrometry proteomics data and protein data from UniProt (**Fig 4.1**). The first step of the analysis was the extraction of protein motif, domain, and PTM annotations from the UniProt database. For PTMs and motifs, data were manually curated to remove duplicates and pool together identical features. Additionally, groups of related (e.g. glycosylation) PTMs were pooled and included as additional features. Data from protein features were then integrated with publicly available mass spectrometry proteomics data[305] and features that appeared on less than 5 proteins filtered out for reasons of statistical power. We considered EV-enriched features as those that were significant by Kolmogorov-Smirnov test, and which exhibited an increase in the EV vs cell abundance ratio relative to the median ratio for all proteins. EV-enriched features matching these criteria are shown in **Fig 4.2, 4.3, 4.4**.

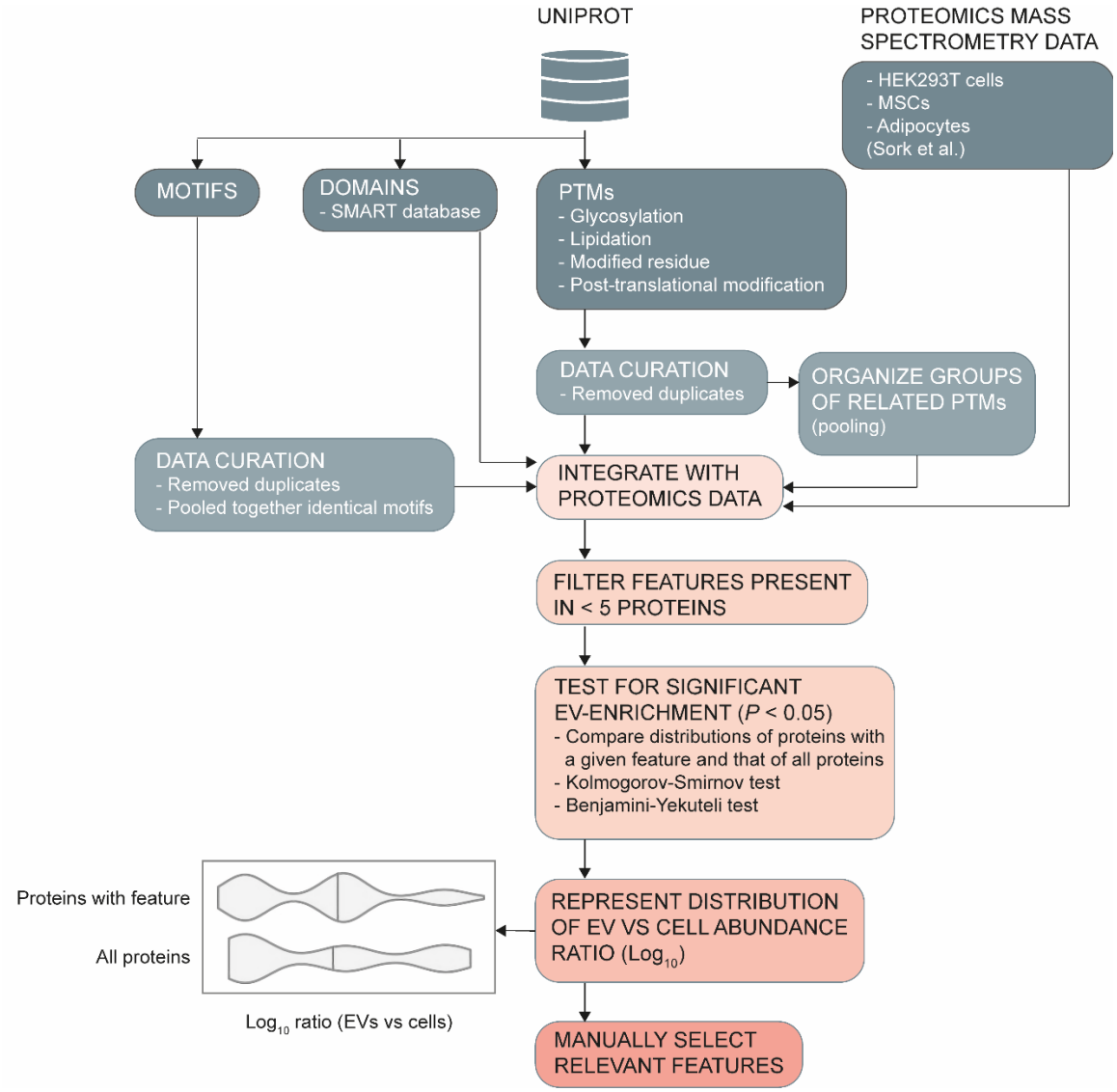
UNIPROT
PROTEOMICS MASS SPECTROMETRY DATA
- HEK293T cells
- MSCs
- Adipocytes
(Sork et al.)
MOTIFS
DOMAINS
- SMART database
PTMs
- Glycosylation
- Lipidation
- Modified residue
- Post-translational modification
DATA CURATION
- Removed duplicates
ORGANIZE GROUPS OF RELATED PTMs
(pooling)
DATA CURATION
- Removed duplicates
- Pooled together identical motifs
INTEGRATE WITH PROTEOMICS DATA
FILTER FEATURES PRESENT IN < 5 PROTEINS
TEST FOR SIGNIFICANT EV-ENRICHMENT (P < 0.05)
- Compare distributions of proteins with a given feature and that of all proteins
- Kolmogorov-Smirnov test
- Benjamini-Yekuteli test
Proteins with feature
All proteins
Log10 ratio (EVs vs cells)
REPRESENT DISTRIBUTION OF EV VS CELL ABUNDANCE RATIO (Log10)
MANUALLY SELECT RELEVANT FEATURES

Figure 4.1 Bioinformatics analysis scheme.

Protein motif, domain (as annotated on SMART database), and post-translational modification (PTM) data were extracted from the UniProt database. Motif and PTM data were then manually curated to remove duplicates and pool together identical features. In the case of PTMs, additional groups of related PTMs were pooled and included in the analysis as separate categories. Protein feature data were integrated with mass spectrometry proteomics data[305] (from HEK293T cells, MSCs, and adipocytes) and only features that appear on at least 5 proteins were included in the analysis because of the difficulty to detect statistically significant changes of feature annotations when data was scant. Distributions of proteins with a given feature and that of all proteins were then compared by Kolmogorov-Smirnov test followed by Benjamini-Yekuteli *post hoc* test to identify features that were significantly EV-enriched ($P < 0.05$). The distribution of EV vs cell abundance ratio ($\log_{10}$) of proteins with significantly EV-enriched features was then represented and relevant features were manually selected.

4.4.2. Protein motif analysis

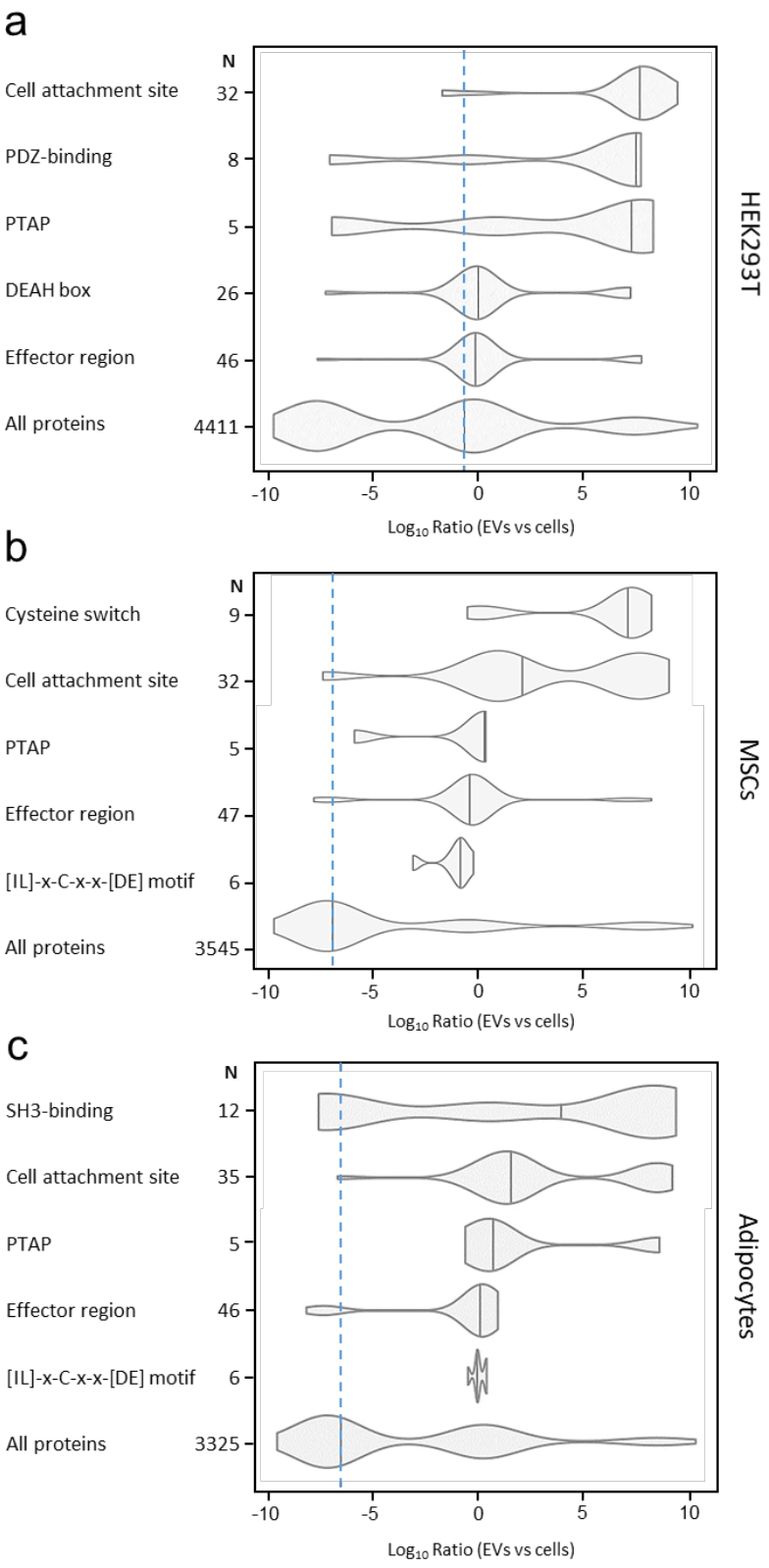

Figure 4.2. *In silico* identified EV-enriched annotated motifs.

Violin plots representing the EV vs cell abundance ratios (log_{10}) of proteins with statistically significant EV-enriched ($P < 0.05$) annotated motifs identified in HEK293T cells **(a)**, MSCs **(b)** and adipocytes **(c)**. The number of proteins with the given motif in the dataset is depicted next to plot. Violin plot of the EV vs cell abundance ratios (log_{10}) of all proteins in the dataset is included as a reference. The median abundance ratio for all proteins in the dataset is represented as a dashed line.

Using the IPFA approach, PTAP, cell attachment site, and effector region motifs were found to be enriched in EVs and common across the 3 cell lines (**Fig 4.2**).

4.4.3. Protein domain analysis

a

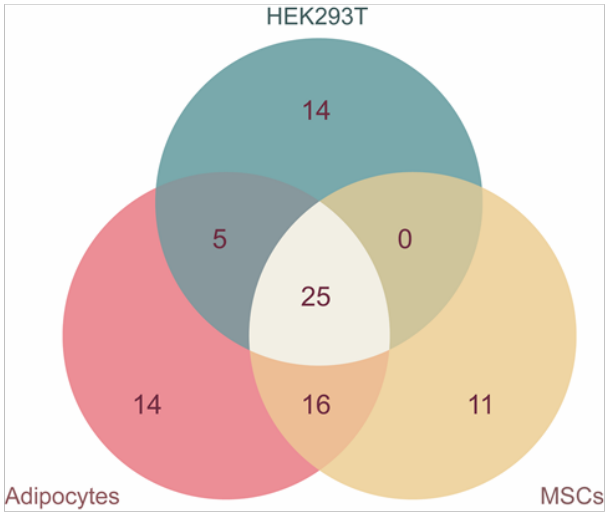

b

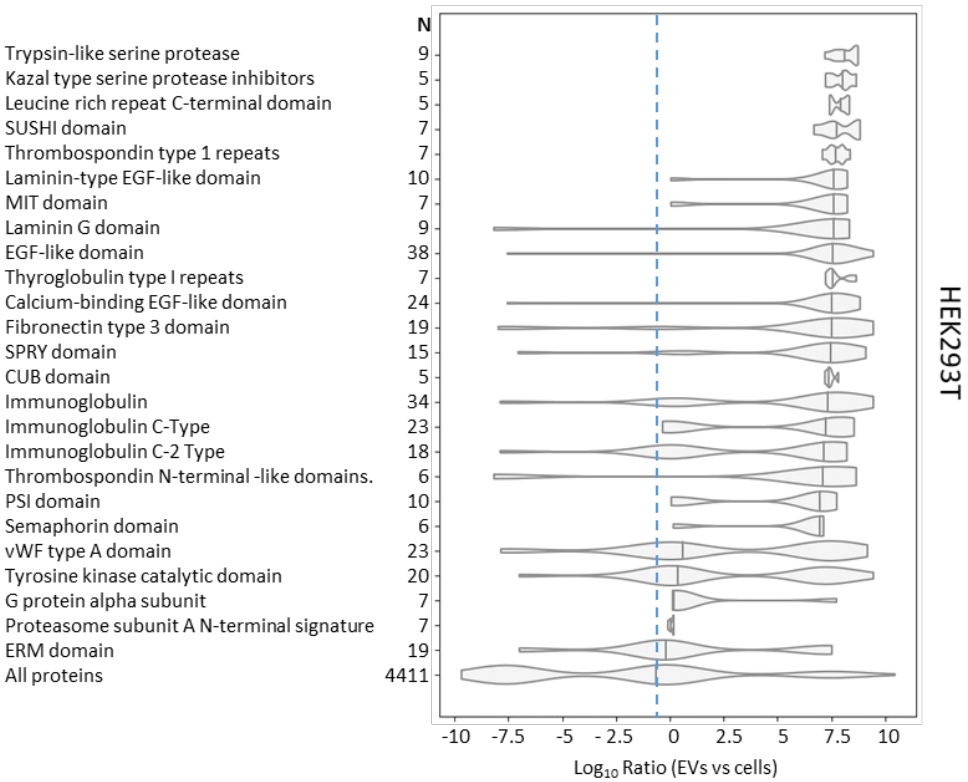

c

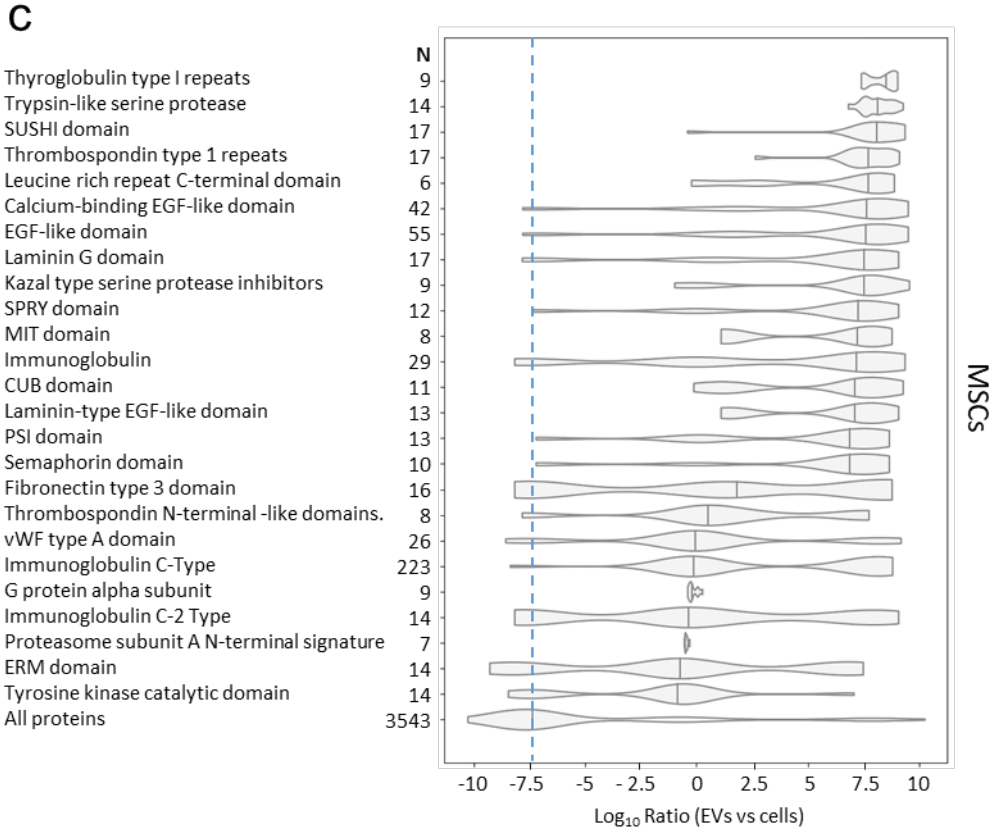
N
Thyroglobulin type I repeats 9
Trypsin-like serine protease 14
SUSHI domain 17
Thrombospondin type 1 repeats 17
Leucine rich repeat C-terminal domain 6
Calcium-binding EGF-like domain 42
EGF-like domain 55
Laminin G domain 17
Kazal type serine protease inhibitors 9
SPRY domain 12
MIT domain 8
Immunoglobulin 29
CUB domain 11
Laminin-type EGF-like domain 13
PSI domain 13
Semaphorin domain 10
Fibronectin type 3 domain 16
Thrombospondin N-terminal -like domains. 8
vWF type A domain 26
Immunoglobulin C-Type 223
G protein alpha subunit 9
Immunoglobulin C-2 Type 14
Proteasome subunit A N-terminal signature 7
ERM domain 14
Tyrosine kinase catalytic domain 14
All proteins 3543
-10 -7.5 -5 -2.5 0 2.5 5 7.5 10
Log10 Ratio (EVs vs cells)
MSCs

d

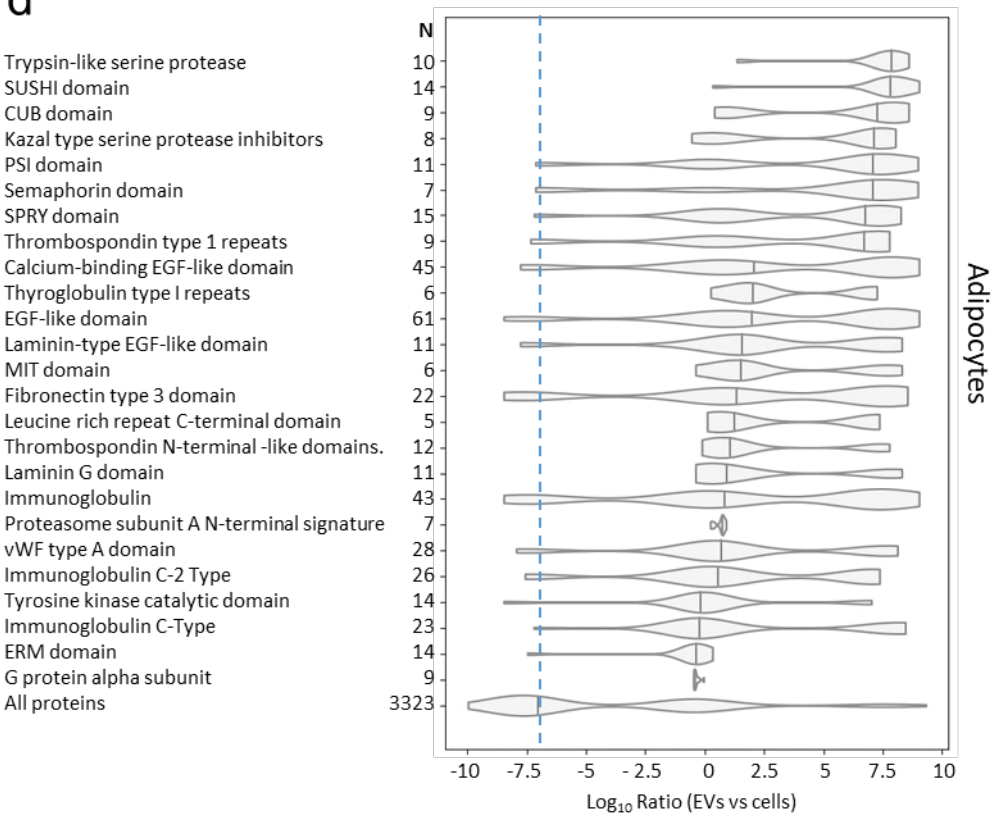
N
Trypsin-like serine protease 10
SUSHI domain 14
CUB domain 9
Kazal type serine protease inhibitors 8
PSI domain 11
Semaphorin domain 7
SPRY domain 15
Thrombospondin type 1 repeats 9
Calcium-binding EGF-like domain 45
Thyroglobulin type I repeats 6
EGF-like domain 61
Laminin-type EGF-like domain 11
MIT domain 6
Fibronectin type 3 domain 22
Leucine rich repeat C-terminal domain 5
Thrombospondin N-terminal -like domains. 12
Laminin G domain 11
Immunoglobulin 43
Proteasome subunit A N-terminal signature 7
vWF type A domain 28
Immunoglobulin C-2 Type 26
Tyrosine kinase catalytic domain 14
Immunoglobulin C-Type 23
ERM domain 14
G protein alpha subunit 9
All proteins 3323
-10 -7.5 -5 -2.5 0 2.5 5 7.5 10
Log10 Ratio (EVs vs cells)
Adipocytes

Figure 4.3. *In silico*-identified EV-enriched domain annotations.

(a) Venn diagram of statistically significant EV-enriched annotated domains ($P < 0.05$) in HEK293T cells, MSCs, and adipocytes. The number of domains identified for each group are shown in the diagram. Violin plots representing the EV vs cell abundance ratios ($\log_{10}$) of proteins with statistically significant EV-enriched domain annotations identified in **(b)**HEK293T cells, **(c)**MSCs, and **(d)** adipocytes. Only EV-enriched annotated domains common across all three cell lines are shown. The number of proteins with the given domain in the dataset is depicted next to plot. Violin plot of the EV vs cell abundance ratios ($\log_{10}$) of all proteins in the dataset is included as a reference. The median abundance ratio for all proteins in the dataset is represented as a blue dashed line.

SMART ID	Name	Description	Domain+ proteins comment
SM00020	Trypsin-like serine protease	Domain containing the active site found in trypsin family members.	Extracellular proteins
SM00280	Kazal-type serine protease domain	Domain similar to the reactive site of serin protease inhibitors involved in protein binding.	Extracellular proteins
SM00032	SUSHI repeat	Domain identified in several proteins of the complement system involved in protein recognition processes.	Extracellular proteins
SM00181	Epidermal growth factor-like domain	Domain found in membrane-bound or secreted proteins involved in lipid and protein binding.	Extracellular proteins
SM00179	Calcium-binding EGF-like domain	EGF-like domain that contains a calcium binding site.	Extracellular proteins
SM00042	CUB domain	Mainly found in developmentally regulated extracellular and membrane proteins.	Extracellular proteins
SM00211	Thyroglobulin type I repeats	Domain that inhibits cysteine proteases and binds heparin.	Extracellular proteins
SM00180	Laminin-type EGF-like domain	Domain found in laminins similar in its N-terminal to EGF-like domain.	ECM proteins
SM00282	Laminin G domain	Heparin-binding and dystroglycan-binding domain found in extracellular proteins.	ECM proteins
SM00209	Thrombospondin type 1 repeats	Domain mainly found in thrombospondins involved in cell- and extracellular matrix-binding.	ECM proteins
SM00210	Thrombospondin N-terminal -like domain	Heparin-binding and cell adhesion domain of thrombospondin.	ECM proteins
SM00082	Leucine rich repeat C-terminal domain	2-45 motifs of 20-30 amino acids that mediate protein-protein interactions.	ECM or membrane proteins
SM00060	Fibronectin type 3 domain	Internal repeat found in fibronectin that is involved in protein-binding.	ECM or membrane proteins
SM00327	von Willebrand factor type A	Domain found in mainly in secreted proteins. Mediates metal ion-dependent adhesion.	ECM or membrane proteins
SM00409	Immunoglobulin	Similar to Ig domain of immunoglobulin. Involved in recognition processes.	Membrane proteins
SM00407	Immunoglobulin C-Type	Ig-like domains similar to the antibody constant domain. Involved in recognition processes.	Membrane proteins
SM00408	Immunoglobulin C-2 Type	Subtype of C-Type immunoglobulin domain.	Membrane proteins
SM00423	PSI domain	Cysteine-rich domain found in the extracellular region of signaling proteins.	Membrane proteins
SM00630	Semaphorin domain	Domain found in semaphorins and plexins. Serves as a receptor/ligand recognition site.	Membrane proteins
SM00219	Tyrosine kinase, catalytic domain	Tyrosine-specific kinase subfamily.	Tyrosine-kinases
SM00275	G protein alpha subunit	Subunit of G proteins that contains the guanine nucleotide binding site.	G proteins
SM00948	Proteasome subunit A N-terminal signature	N-terminal domain conserved in the A subunits of the proteasome complex.	Proteosome components
SM00745	MIT domain	Domain found in vacuolar sorting proteins, spastin, and sorting nexins. May play a role in intracellular trafficking.	Soluble proteins
SM00449	SPRY domain	Protein interaction module involved in several signaling pathways.	Soluble proteins
SM00295	ERM domain	Mediates membrane association by direct binding to the cytoplasmic domain of transmembrane proteins.	Soluble proteins

Table 4.1. List of EV-enriched common domains identified with the IPFA analysis.
Includes SMART database ID, name, description, and comment on proteins containing the domain in our dataset.

The IPFA analysis was applied in this case to identify protein domains that could influence protein EV-sorting. 44, 52, and 60 EV-enriched domain annotations were found on HEK293T cells, MSCs, and adipocytes, respectively (**Fig 4.3a**). Among the identified domains, 25 were common across all 3 cell lines according to our analysis (**Fig 4.3a**, **Table 1**). To select the most relevant domains for our objective, we manually filtered the domains by inspecting the subcellular location and type of proteins that harboured each of the EV-enriched domains. As expected, various domains (11) were present almost exclusively in extracellular matrix (ECM) proteins or in proteins known to be secreted to the extracellular space (**Table 4.1**), and so they are unlikely to have a role in luminal EV-sorting. The tyrosine kinase catalytic domain, the G protein alpha subunit, and the proteasome subunit A N-terminal signature were only present on specific protein families and had a known role unrelated to protein sorting. Among the other 11 domains, five were present mostly on membrane proteins, three on membrane and ECM proteins, and three on soluble proteins (**Table 4.1**). The latter include the SPRY, the MIT and the ERM domain.

4.4.4. Protein PTM analysis

To identify EV-enriched PTMs we performed the IPFA analysis. 53, 39, and 75 EV-enriched domains were found on HEK293T cells, MSCs, and adipocytes, respectively (**Fig 4.4a**). Among the identified PTMs, 25 were common across all 3 cell lines (**Fig 4.4a**). Most of the identified PTMs were either types of glycosylation (**Table 4.2**) or types of lipidation (**Table 4.2**). Notably, N-linked GlcNAc asparagine (N-GlcNAc) was highly enriched and present in ~10% of all proteins in the three datasets (**Fig 4.4b, c, d**). Although to a lesser extent than glycosylation, lipidation was also present on numerous proteins (~5%). Hydroxyproline, pyrrolidone carboxylic acid, and specific kinase phosphorylation were also identified. The other 8 PTMs that were identified (**Table 4.2**) are not suitable for facilitating EV-sorting (eg. ADP-ribosylarginine by cholera toxin).

a

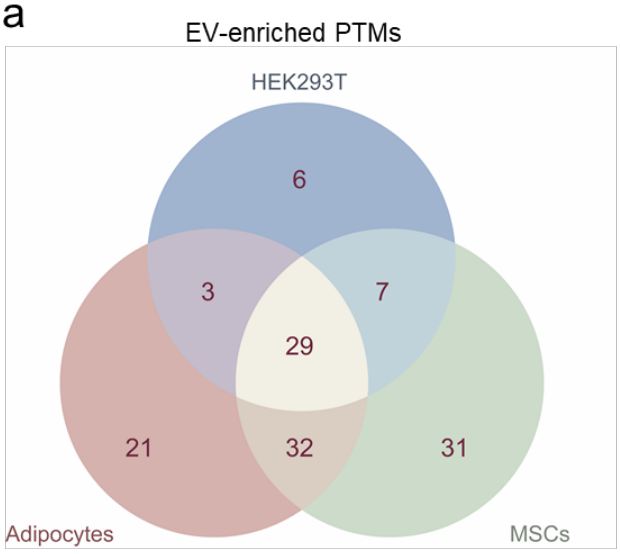
EV-enriched PTMs
HEK293T
6
3
7
29
21
32
31
Adipocytes
MSCs

b

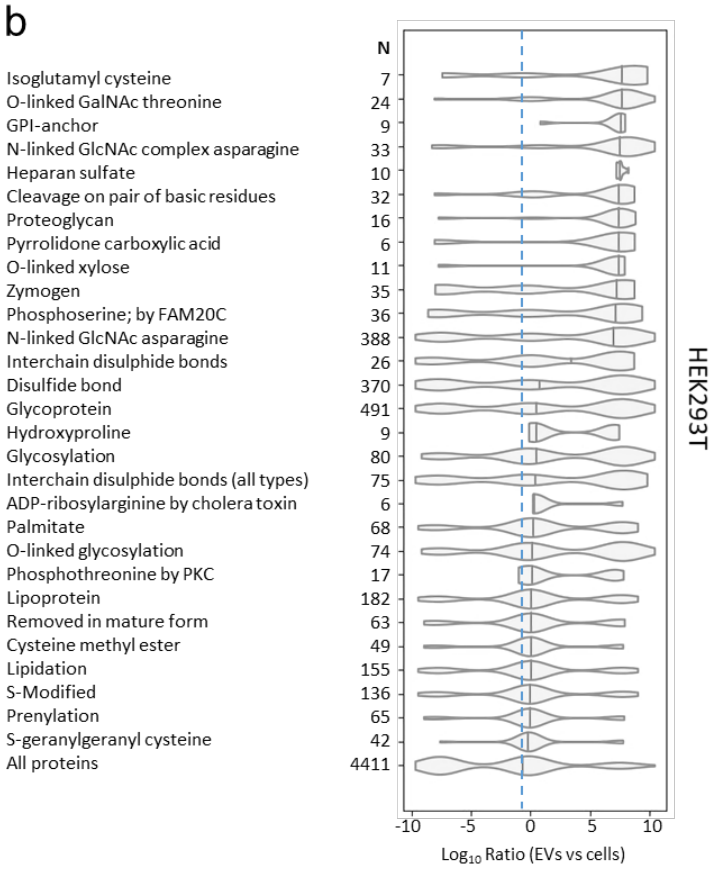
N
Isoglutamyl cysteine 7
O-linked GalNAc threonine 24
GPI-anchor 9
N-linked GlcNAc complex asparagine 33
Heparan sulfate 10
Cleavage on pair of basic residues 32
Proteoglycan 16
Pyrrolidone carboxylic acid 6
O-linked xylose 11
Zymogen 35
Phosphoserine; by FAM20C 36
N-linked GlcNAc asparagine 388
Interchain disulphide bonds 26
Disulfide bond 370
Glycoprotein 491
Hydroxyproline 9
Glycosylation 80
Interchain disulphide bonds (all types) 75
ADP-ribosylarginine by cholera toxin 6
Palmitate 68
O-linked glycosylation 74
Phosphothreonine by PKC 17
Lipoprotein 182
Removed in mature form 63
Cysteine methyl ester 49
Lipidation 155
S-Modified 136
Prenylation 65
S-geranylgeranyl cysteine 42
All proteins 4411
-10
-5
0
5
10
Log10 Ratio (EVs vs cells)
HEK293T

c

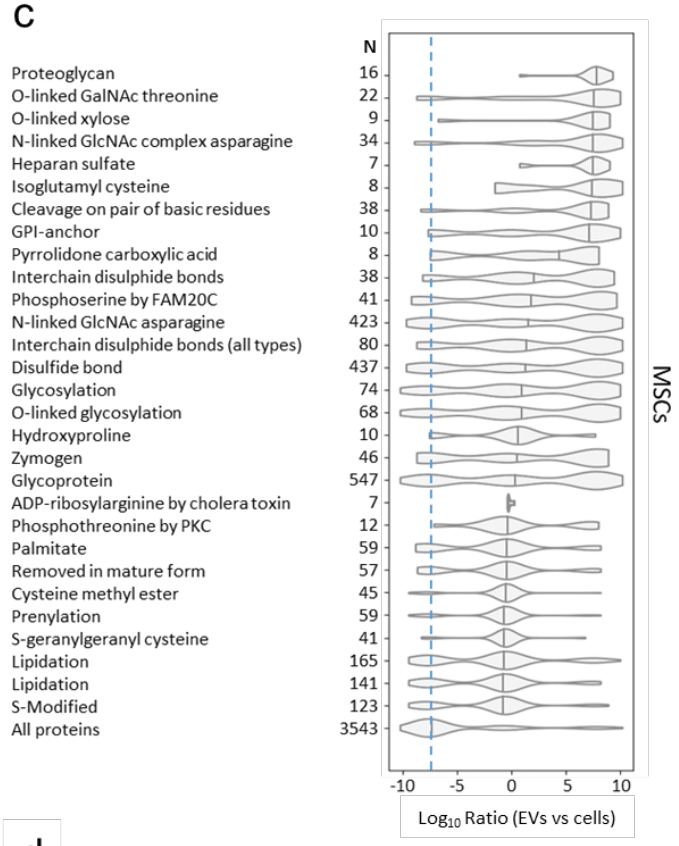
N
Proteoglycan 16
O-linked GalNAc threonine 22
O-linked xylose 9
N-linked GlcNAc complex asparagine 34
Heparan sulfate 7
Isoglutamyl cysteine 8
Cleavage on pair of basic residues 38
GPI-anchor 10
Pyrrolidone carboxylic acid 8
Interchain disulphide bonds 38
Phosphoserine by FAM20C 41
N-linked GlcNAc asparagine 423
Interchain disulphide bonds (all types) 80
Disulfide bond 437
Glycosylation 74
O-linked glycosylation 68
Hydroxyproline 10
Zymogen 46
Glycoprotein 547
ADP-ribosylarginine by cholera toxin 7
Phosphothreonine by PKC 12
Palmitate 59
Removed in mature form 57
Cysteine methyl ester 45
Prenylation 59
S-geranylgeranyl cysteine 41
Lipidation 165
Lipidation 141
S-Modified 123
All proteins 3543
-10 -5 0 5 10
Log10 Ratio (EVs vs cells)
MSCs

d

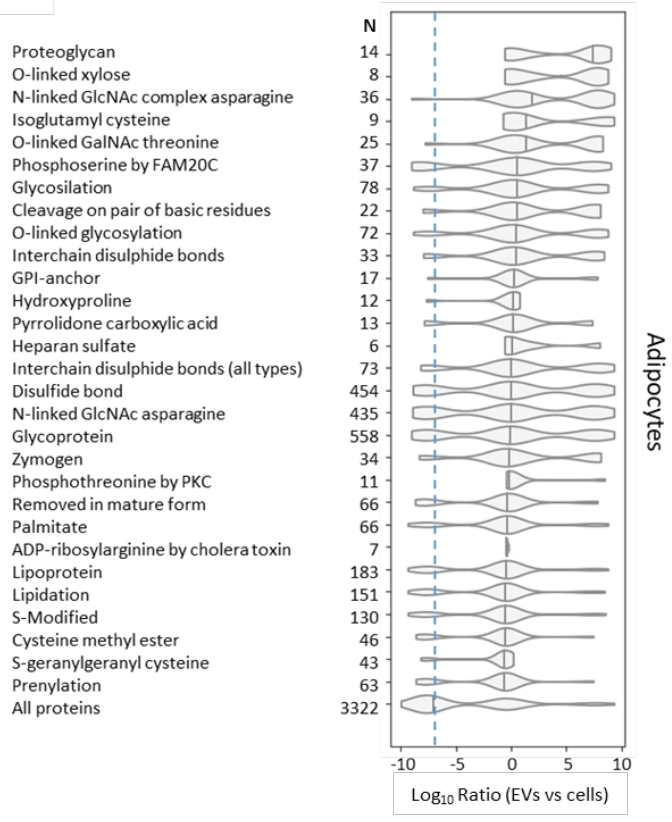
N
Proteoglycan 14
O-linked xylose 8
N-linked GlcNAc complex asparagine 36
Isoglutamyl cysteine 9
O-linked GalNAc threonine 25
Phosphoserine by FAM20C 37
Glycosilation 78
Cleavage on pair of basic residues 22
O-linked glycosylation 72
Interchain disulphide bonds 33
GPI-anchor 17
Hydroxyproline 12
Pyrrolidone carboxylic acid 13
Heparan sulfate 6
Interchain disulphide bonds (all types) 73
Disulfide bond 454
N-linked GlcNAc asparagine 435
Glycoprotein 558
Zymogen 34
Phosphothreonine by PKC 11
Removed in mature form 66
Palmitate 66
ADP-ribosylarginine by cholera toxin 7
Lipoprotein 183
Lipidation 151
S-Modified 130
Cysteine methyl ester 46
S-geranylgeranyl cysteine 43
Prenylation 63
All proteins 3322
-10 -5 0 5 10
Log10 Ratio (EVs vs cells)
Adipocytes

Figure 4.4. *In silico* identified EV-enriched annotated PTMs.

(a) Venn diagram of statistically significant EV-enriched PTM annotations ($P < 0.05$) in HEK293T cells, MSCs, and adipocytes. Number of PTMs identified for each group are shown in the diagram. Violin plots representing the EV vs cell abundance ratios ($\log_{10}$) of proteins with statistically significant EV-enriched PTM annotations identified in **(b)** HEK293T cells, (c) MSCs, and (d) adipocytes. Only EV-enriched PTM annotations common across all three cell lines are shown. The number of proteins with the given PTM in the dataset is depicted next to plot. Violin plot of the EV vs cell abundance ratios ($\log_{10}$) of all proteins in the dataset is also shown. Median value of all proteins in the dataset is represented as a blue dashed line. *$P < 0.05$.

PTM	Type	Comments
O-linked GalNAc threonine	Glycosylation	-
N-linked GlcNAc complex asparagine	Glycosylation	-
Heparan sulfate	Glycosylation	-
Proteoglycan	Glycosylation	Includes glycoprotein and heparan sulphate
O-linked xylose	Glycosylation	-
N-linked GlcNAc asparagine	Glycosylation	-
Glycoprotein	Glycosylation	Includes N and O-linked glycosylation
O-linked glycosylation	Glycosylation	Includes O-linked fucose. galactose, GalNAc GlcNAc, xylose, hexose, HexNAc, mannose-6-phosphate
GPI-anchor	Lipidation	-
Palmitate	Lipidation	-
Lipoprotein	Lipidation	Includes GPI-anchor, prenylation, palmitoylation and myristoylation
Lipidation	Lipidation	Includes prenylation, palmitoylation and myristoylation
S-Modified	Lipidation	Includes prenylation and S-palmitoylation
Prenylation	Lipidation	Includes farnesylation and geranylgeranylation
S-geranylgeranyl cysteine	Lipidation	-
Cysteine methyl ester	Aminoacid modification	Derived from prenylation
Pyrrolidone carboxylic acid	Aminoacid modification	-
Hydroxyproline	Aminoacid modification	-
Interchain disulphide bonds	Disulfide bond	Not applicable for protein loading
Disulfide bond	Disulfide bond	Not applicable for protein loading
Interchain disulphide bonds (all types)	Disulfide bond	Not applicable for protein loading
Phosphoserine; by FAM20C	Phosphorylation	-
Phosphothreonine by PKC	Phosphorylation	-
Cleavage on pair of basic residues	Cleavage	Not applicable for protein loading
Removed in mature form	Cleavage	Not applicable for protein loading
Zymogen	Precursor protein	Not applicable for protein loading
Isoglutamyl cysteine	Crosslink	Not applicable for protein loading
ADP-ribosylarginine by cholera toxin	ADP-ribosylation	Not applicable for protein loading

Table 4.2. EV-enriched PTMs identified with our bioinformatics analysis.

NGlcNAc+ Proteins	HEK293T	MSC	Adipocytes
Total NGlcNAc+	388	528	435
Transmembrane	218 (56%)	261 (49%)	212 (47%)
Secreted	136 (35%)	219 (41%)	164 (38%)
Transmembrane or secreted	334 (86%)	448 (84%)	350 (80%)

Table 4.3. Number and percentage of transmembrane, secreted, and transmembrane or secreted N-glycosylation annotated proteins in HEK293T cells, MSC and adipocyte datasets.

$NGlcNAc^+$ corresponds to proteins with N-glycosylation.

It has been previously reported that N-glycosylation is primarily found on membrane-bound and secreted proteins[318]. Thus, we assessed the nature of N-glycosylation annotated proteins in the dataset to determine if that was also the case. As expected, most N-glycosylated proteins were transmembrane or secreted proteins (86% HEK293T cells, 87% MSCs, 80% adipocytes) (**Table 3**). To assess the effect of N-glycosylation on EV-enrichment, we compared the EV vs cell abundance distribution of transmembrane and secreted proteins with or without N-glycosylation (**Fig 4.5**). Both secreted and transmembrane N-glycosylation annotated proteins were EV-enriched as compared to all proteins. However, while secreted proteins were EV-enriched regardless of N-glycosylation, only N-glycosylation annotated transmembrane proteins were EV-enriched. (**Fig 4.5**). Notably, ~70% of N-glycosylation annotated transmembrane proteins were EV-enriched and most of the EV-enriched transmembrane proteins were annotated as N-glycosylated (63% HEK293T cells, 47% MSCs, 49% adipocytes) (**Table 4.4**).

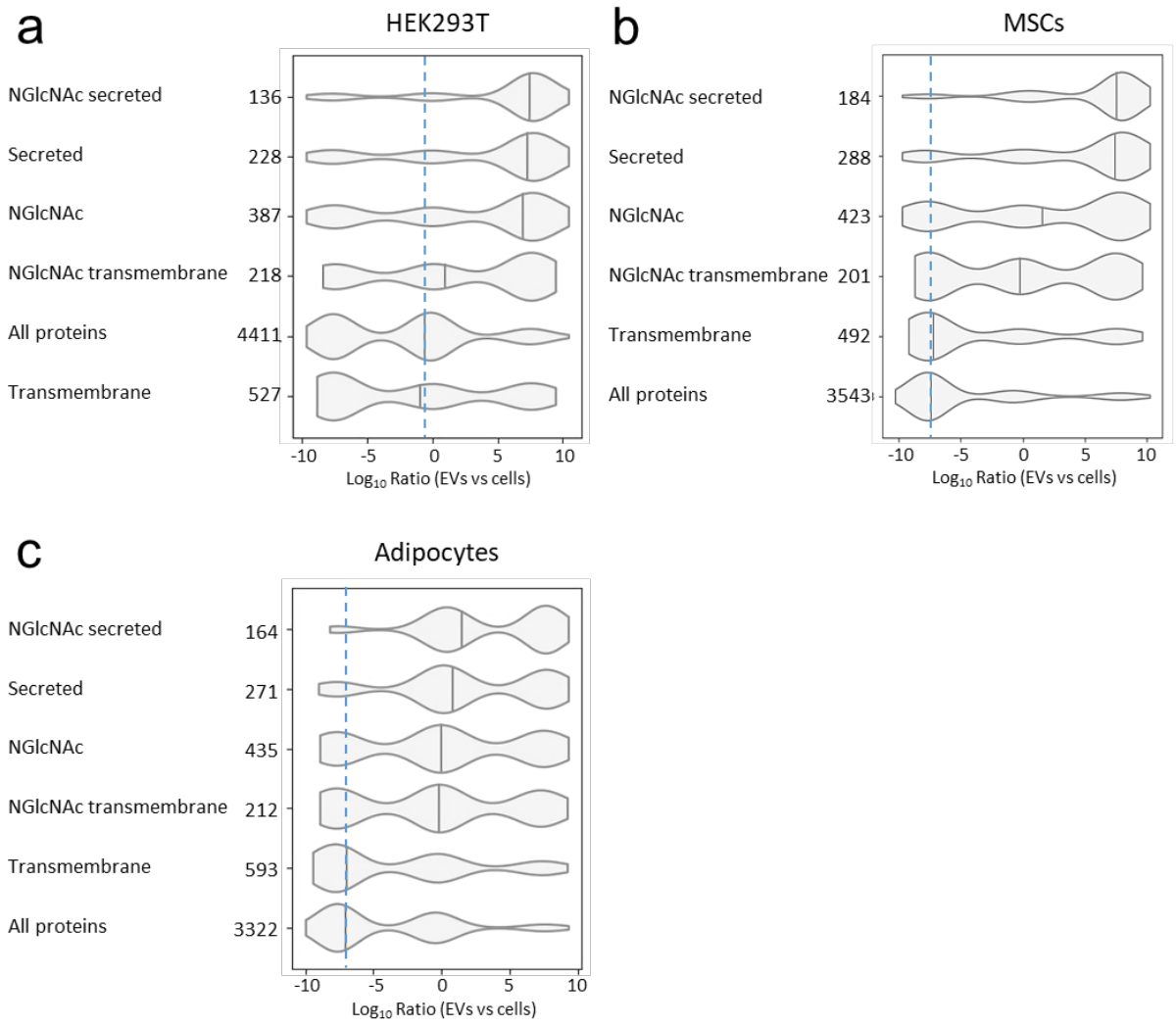

Figure 4.5. N-glycosylation annotation is predominantly found on secreted and transmembrane proteins.

Violin plots representing the EV *vs* cell abundance ratios (log_{10}) of transmembrane, secreted, NGlcNAc transmembrane, NGlcNAc secreted, and NGlcNAc proteins in **(a)** HEK293T *cells*, **(b)** MSCs, and **(c)** adipocytes. The number of proteins for each group are shown. Violin plot of the EV vs cell abundance ratios (log_{10}) of all proteins in the dataset is also shown. Median value of all proteins in the dataset is represented as a blue dashed line. Difference in log10 Ratio (EVs vs cells) distribution between transmembrane and NGlcNAc transmembrane is statistically significant in the three cell types analysed ($P < 0.05$).

	Transmembrane proteins		NGlcNAc⁺ Transmembrane proteins		% NGlcNAc⁺ EV-enriched	% EV-enriched NGlcNAc⁺
	Total	EV-enriched	Total	EV-enriched		
HEK293T	527	254	218	159	73%	63%
MSC	683	415	261	196	74%	47%
Adipocytes	593	302	212	148	70%	49%

Table 4.4. N-glycosylation annotated transmembrane proteins are EV-enriched and constitute almost half of total EV-enriched transmembrane proteins.

Number of total and EV-enriched transmembrane proteins with or without N-glycosylation annotation in HEK293T cells, MSC, and adipocyte datasets are shown in the first and second columns. Percentage of N-glycosylated transmembrane proteins that are EV-enriched and percentage of EV-enriched transmembrane proteins with N-glycosylation are shown in columns 3 and 4. $NGlcNAc^+$ corresponds to proteins with N-glycosylation.

4.5. Discussion

In this chapter, the main objective was to identify novel EV-loading motifs, domains and PTMs that could be used to generate scaffolds for protein EV-sorting. Ideally, we would select EV-loading features that could be used to target proteins inside the EVs and that are found on soluble proteins. In this way, protein EV-cargoes would be protected from the extraluminal environment and would not be retained in the membrane. Numerous studies have investigated the involvement of specific motifs, domains and PTMs in protein EV-sorting *in vitro*[269,320]. However, to our knowledge no other study has attempted to identify EV-sorting features *in silico.* This approach would enable a fast and cost-efficient analysis of large volumes of protein feature data. To do so, we used custom python scripts to analyze mass spectrometry proteomics data from HEK293T cells, MSCs, and adipocytes combined with UniProt protein feature annotations.

Despite the previously mentioned advantages of the IPFA analysis, it presented several limitations. The main assumption of our approach was that EV-enrichment was indicative of EV-sorting functionality. Even though this assumption is supported by the identification of well-known EV-sorting features, this analysis might have identified features where this is not the case. Given that the mass spectrometry data[305] were generated using ultracentrifugation isolated EVs, protein components from the ECM may have co-precipitated with the EVs during the ultracentrifugation procedure. Thus, protein features identified in the EV samples were expected to not be only those found inside or outside the EVs, but also those associated with contaminating extracellular proteins[329,330]. Common features from proteins that belong to a same EV-enriched protein family would be detected in the analysis regardless of their potential EV-sorting role (e.g., if the GTPase protein family is EV enriched due to prenylation, other GTPase common features such as the effector region will also be detected by our analysis). Thus, if

several EV-enriched features tend to appear together, the analysis would not distinguish between the potential EV-sorting feature from the other EV-enriched features. Regarding the PTM analysis, UniProt-annotated PTMs include predicted, and experimentally validated PTMs. For predicted PTMs, the presence of the feature annotation does not mean that the PTM exists in the experimental samples. In the case of validated PTMs, these may or may not be present on the protein depending on the physiological context. In future studies, IPFA analysis could be performed using mass spectrometry data from SEC purified EVs to avoid the interference of extracellular protein contaminants in the analysis. Moreover, a deeper proteomics analysis could be performed to detect additional proteins that the present proteomics analysis may have missed.

4.5.1. Protein motif analysis

The PTAP, cell attachment site, and effector region motifs were identified as potential EV-enriched motifs using the IPFA analysis (**Fig 4.2**). The PTAP motif is a viral late domain motif found in many enveloped viruses that promotes viral budding by interacting with the ESCRT machinery via TSG101 (tumor suppressor gene 101) binding[316]. This motif has also been shown to promote galectin 3 (LGALS3) recruitment to the EVs[75]. Cell attachment site refers to the RGD motif (Arg-Gly-Asp), a well-known cell adhesion motif found in several ECM components including fibronectin and laminin[331]. Integrins on the cell surface recognize and bind this motif, thus establishing a physical connection between the cells and the ECM[331]. Proteins containing this motif were mainly ECM proteins, suggesting that RGD motif was not enriched in the EVs but in proteins secreted to the extracellular milieu that may co-precipitate with EVs during ultracentrifugation. Effector region refers to the G2 motif found in small GTPases that acts as a binding site for effector and GTPase-activating proteins[332]. However, most proteins in the GTPase family harbor a CAAX motif in their C-terminus, which mediates EV-membrane

association by isoprenylation[333]. Thus, the EV-enrichment observed in the analysis is most likely caused by the CAAX motif rather than the effector region. Out of the three candidate motifs identified, we decided to select PTAP for further assessment given that it could be easily fused as a tag on proteins and that it was found on soluble proteins.

4.5.2. Protein domain analysis

We identified 25 EV-enriched annotated domains that were common in the three cell lines analyzed (**Fig 4.3**). Of those, we focused on the 3 domains that are not associated to the ECM and occur in soluble proteins (**Table 4.1**). These were the MIT, SPRY, and ERM domains. The first is found in vacuolar sorting proteins, spastin, and sorting nexins, and mediates the binding with MIT-interacting motifs found on ESCRT-III proteins[334]. The SPRY domain is a protein interaction domain involved in several signaling pathways, although its binding partners have not been identified[335]. ERM domains mediate membrane association by binding to the cytoplasmic domain of transmembrane proteins. However, to detach from transmembrane proteins ERM domain must bind an inactivating domain through a complex conformational change, which rules it out as an EV-sorting domain[336]. Thus, MIT and SPRY domains were selected for further analysis.

4.5.3. Protein PTM analysis

PTMs increase protein complexity by regulating their activity, stability, subcellular localization, and molecular interactions. A wide variety of PTMs have been identified in EVs, some of which play important roles in EV biogenesis and cargo sorting[320,337]. We identified 29 EV-enriched annotated PTMs that were common across the three cell lines analyzed (**Fig 4.4**). 7 of the PTMs identified were types of lipidation, more specifically, palmitoylation, prenylation,

and GPI-anchors (**Table 4.2**). Lipidation is involved in regulating many aspects of protein function, such as protein association with membranes, protein-protein interactions, and protein stability[338]. Prenylation is the addition of polyisoprenyl groups to cysteine residues at the protein C-termini. There are two types of prenylation: farnesylation (three isoprene molecules) and geranylgeranylation (four isoprene molecules). Palmitoylation is the addition of a palmitoyl molecule via thioester bonds on protein cysteine residues and regulates protein stability[310]. GPI-anchors are added onto the C-termini of proteins and consist of a phosphatidylinositol group linked through a glycan moiety. These three modifications have been previously shown to mediate EV-sorting by promoting protein association with membranes and have been used to load protein cargo to the EVs[92,177,246,339,340] . These results support the bioinformatics approach used in this study given that it is able to identify previously described EV-sorting features. Notably, the ubiquitination PTM was not identified although it is one of the most well-described EV-sorting PTMs. This may be because the ubiquitination type is not specified in UniProt and there are many types of ubiquitination of which only some promote EV-sorting[320].

Protein glycosylation was also identified in the analysis as an EV-enriched feature, more specifically: N-linked glycosylation, O-linked glycosylation and heparan sulphate modification (**Fig 4.4**). The most prevalent modification was N-linked glycosylated asparagine, that was found to be annotated in ~10% of all proteins in the dataset and was highly EV-enriched (**Fig 4.4**). Most of the annotated N-glycosylated proteins were either secreted or transmembrane proteins (**Table 4.3**). Secreted proteins are not expected to reside in EVs and there is a high possibility that they appear as EV-enriched due to co-precipitation with EVs during UC isolation, so we focused on transmembrane N-glycosylation annotated proteins. Interestingly, 70% of N-glycosylation annotated transmembrane proteins were EV-enriched and nearly half of all EV-

enriched transmembrane proteins were annotated as N-glycosylated in the three cell lines analyzed (**Table 4.4**). Thus, we decided to select transmembrane protein N-glycosylation for further assessment given that it was the most frequent EV-sorting feature identified in our analysis. To apply N-glycosylation (of transmembrane proteins) for EV-sorting, an N-glycosylation signal could be added on the desired EV-protein cargo. However, this strategy could only be used for transmembrane therapeutic cargoes. Thus, a more robust approach would be to fuse the therapeutic protein to the smallest transmembrane protein with N-glycosylation in our dataset. In addition, to avoid membrane retention, a release system could be introduced between the N-glycosylated transmembrane EV-scaffold and the protein cargo.

Glycosylation plays a critical role in the secretory pathway by controlling intracellular trafficking and proper folding of newly synthesized proteins in the ER[318,324]. These sugars can also influence protein-protein interactions by promoting or inhibiting protein binding (eg. protecting lysosomal proteins from enzymatic degradation)[341]. N-glycosylation has been reported to influence the sorting of several transmembrane proteins to the EVs, however, the extent of this effect is currently unknown. Mutation of IGSF8 (Immunoglobulin superfamily member 8) complex N-glycosylation sites was shown to be detrimental for its recruitment into EVs[342]. In a similar manner, TACSTD2 (Tumor-associated calcium signal transducer 2) N-glycosylation mutants showed impaired EV-loading and increased surface expression[343]. Blockage of different steps of the N-glycosylation pathway has also been used to study protein sorting to EVs. N-glycosylation inhibition by tunicamycin prevented EV-sorting of endoglin[344]. Complex N-glycosylation blockage by swainsonine significantly reduced CD133 secretion and resulted in its accumulation in early endosomes[345]. Interestingly, N-glycosylation modulated CD133 (Prominin-1) secretion by reducing its mono-ubiquitination and inhibiting the interaction

between CD133 and TSG101[345]. Moreover, blockage of N-glycosylation by 2-deoxyglucose (glycolysis inhibitor) or STT3A silencing (gene that mediates N-glycosylation modification) resulted in a reduction of EV secretion[346]. In the same study, treatment with 2-deoxyglucose also inhibited hepatocyte growth factor receptor, ADAM10 and LAMP1 sorting to the EVs. Nevertheless, it should be considered that studying the effect of N-glycosylation on single proteins by blocking the entire N-glycosylation pathway may lead to confounding results given that the effect seen on EV-sorting may not be due to the N-glycosylation presence on the studied protein but on other proteins that may also affected by N-glycosylation in different manners (e.g., protein folding).

Our data suggests that N-glycosylation may have a widespread effect on transmembrane protein sorting to the EVs. EV biogenesis and protein cargo sorting relies on the formation of specific membrane domains where budding and excision events take place. This together with the fact that membrane protein organization and microdomain formation is dependent on N-glycosylation[347–351] may suggest a mechanism by which N-glycosylated transmembrane proteins are specifically sorted to the EVs. However, EV-sorting of some N-glycosylated proteins such as CD63 has been reported to be independent of its N-glycosylation status[346], and not all N-glycosylated proteins are enriched in the EVs (**Table 4.4**), indicating that the potential mechanism may not apply to all proteins. This is to be expected given that protein trafficking is a complex process that is regulated by many factors of which N-glycosylation is only one.

4.6. Conclusion

We developed a bioinformatics approach that enabled the identification of EV-enriched annotated protein motifs, domains and PTMs that could potentially be used for cargo protein loading to the EVs. The PTAP motif, the MIT and SPRY domains, and N-glycosylation of transmembrane proteins were selected for further *in vitro* analysis in the next chapter. Additionally, we showed that the majority of N-glycosylation annotated transmembrane proteins were EV-enriched, and that N-glycosylation annotation is present in nearly half of EV-enriched transmembrane proteins, which suggests a possible role of N-glycosylation in transmembrane protein sorting to the EVs. These findings are supported by the identification of features that have been successfully used to sort cargo proteins to EVs in other studies.

5. Results III – Development of a novel platform for functional cargo delivery based on PTTG1IP EV scaffold

5.1. Introduction

EVs have the potential to overcome the limitations associated with current therapeutic delivery systems, and to become a new generation of drug delivery vehicles. However, this potential is hampered by a lack of efficient EV engineering strategies to enhance EV loading and functional delivery of therapeutic cargo[224]. Exogenous EV loading methods such as chemical modification are usually time consuming and require additional purification methods to remove unbound moieties. We were therefore motivated to explore methods for endogenous EV-loading.

To enhance endogenous EV loading, EVs have been engineered by fusing the therapeutic cargo to membrane interacting moieties (e.g., palmitoylation, myristoylation or prenylation) or to EV-enriched proteins (e.g., tetraspanins, LAMP2, ARRDC1, PTGFRN, and Gag protein). Nevertheless, some of these EV-scaffolds exhibit low EV-loading efficiencies and most of them are not amenable to further EV engineering for the display of functional moieties on the extraluminal surface of the EVs due to their topology[246,255,259,261].

Once EVs reach their recipient cells, their protein cargos must be released from the EV-scaffold in order to reach the required intracellular location. As outlined in the introduction, trigger-inducible release systems or reversible protein-protein interactions between the EV scaffold and the cargo protein have been investigated for this purpose[248,251]. In inducible release systems, the EV scaffold and the protein cargo are fused to dimerization partners whose binding

is induced under certain conditions (such as illumination with blue light or the presence of a specific small molecule drug). Alternatively, cleavage sites for viral proteases have been introduced between Gag protein and the therapeutic cargo for VLP loading and release (e.g., Cas9)[267,268]. This strategy also requires the expression of the viral protease in the EV producer cells. However, existing EV-release strategies have several disadvantages. Reversible dimerization systems and blue light release systems that have been assessed to date for EV-delivery are based on non-human proteins and are therefore potentially immunogenic. In addition, viral proteases and small molecules used in inducible release systems may be packaged into the EVs and co-delivered to recipient cells, where they may cause undesired effects and constitute non-self antigens.

For functional delivery, EV-loaded cargo molecules must escape from the endosome into the cytoplasm before EVs are degraded by endosomal acidification and fusion with the lysosome or re-exported via exocytosis[352]. EV endosomal escape has been reported to be a highly inefficient process and thus represents one of the main bottlenecks for efficient delivery of EV therapeutic cargo[131,184]. To circumvent this, fusogenic peptides, endosomolytic compounds such as chloroquine, and fusogenic proteins have been exploited to enhance endosomal escape of EVs.

In this Chapter, we assess the EV-sorting capacity of the EV-scaffold candidates identified with the IPFA analysis in Chapter II and we develop a novel EV-delivery platform based on the most efficient scaffold. Importantly, we show that our system has a higher efficiency than commonly used CD63-based platforms for functional delivery of both protein and protein/RNA complexes. Furthermore, we describe engineered variants of our EV scaffold that could overcome some of the limitations of current therapeutic EV-loading platforms.

5.2. Hypotheses and aims

Hypotheses:

- Candidate features identified with the IPFA analysis can be utilized for EV-loading of cargo proteins
- Novel EV-loading scaffolds can be used for functional delivery to recipient cells
- N-glycosylation has a role on EV-loading of transmembrane proteins

Aims:

- To achieve active loading of EVs using the protein features identified *in silico*
- Assessment of the effect of N-glycosylation in PTTG1IP EV-sorting
- Development of an EV-based platform for functional protein delivery

5.3. Materials and methods

5.3.1. Plasmids

Plasmid name	Insert	Backbone	Restriction sites	Cloning method
pCMV-GG-mEGFP-cMyc	GG-mEGFP-cMyc	pEGFP-N1	BmtI NotI	Gibson cloning
pCMV-mEGFP-GG-cMyc	mEGFP-GG-cMyc	pEGFP-N1	BmtI NotI	Gibson cloning
pCMV-PTTG1IP-GFP-cMyc	PTTG1IP	GG-mEGFP-cMyc	BbsI	Golden gate cloning
pCMV-SPRY7-GFP-cMyc	SPRY7	GG-mEGFP-cMyc	BbsI	Golden gate cloning
pCMV-GFP-SPRY7-cMyc	SPRY7	mEGFP-GG-cMyc	BbsI	Golden gate cloning
pCMV-MIT-GFP-cMyc	MITD1	GG-mEGFP-cMyc	BbsI	Golden gate cloning
pCMV-GFP-PTAP-cMyc	PTAP motif	mEGFP-GG-cMyc	BbsI	Golden gate cloning
pCMV-PTTG1IP-N45Q-GFP-cMyc	PTTG1IP-N45Q	pCMV-PTTG1IP-GFP-cMyc	SacII BsmBI	Gibson cloning
pCMV-PTTG1IP-N54Q-GFP-cMyc	PTTG1IP-N54Q	pCMV-PTTG1IP-GFP-cMyc	SacII BsmBI	Gibson cloning
pCMV-PTTG1IP-2NQ-GFP-cMyc	PTTG1IP-2NQ	pCMV-PTTG1IP-GFP-cMyc	SacII BsmBI	Gibson cloning
pCMV-PTTG1IP-130-164Del-GFP-cMyc	PTTG1IP-130-164Del	pCMV-PTTG1IP-GFP-cMyc	PstI and AgeI	Gibson cloning
pCMV-PTTG1IP-2YA-GFP-cMyc	PTTG1IP-2YA (Y165A) (Y174A)	pCMV-PTTG1IP-GFP-cMyc	BbsI AgeI	Gibson cloning
pCMV- GG-Cre-cMyc	GG-Cre-cMyc	pEGFP-N1	BmtI NotI	Gibson cloning
pCMV-PTTG1IP-Cre-cMyc	PTTG1IP-Cre	GG-Cre-cMyc	BbsI	Golden gate cloning
pCMV-PTTG1IP-intein-Cre-cMyc	PTTG1IP-intein-Cre	GG-Cre-cMyc	BbsI	Golden gate cloning
pCMV-PTTG1IP-SC-Cre-cMyc	PTTG1IP-SC	GG-Cre-cMyc	BbsI	Golden gate cloning
pCMV-PTTG1IP-130-164Del-intein-Cre-cMyc	PTTG1IP-130-164Del	pCMV-PTTG1IP-intein-Cre-cMyc	SacI AgeI	Gibson cloning
pCMV-PTTG1IP-130-180aa-Cre-cMyc	PTTG1IP-130-180aa	pCMV-PTTG1IP-Cre-cMyc	AgeI	Gibson cloning
pCMV-PTTG1IP-intein-Cas9-cMyc	PCR-amplified spCas9 from pSpCas9-2A-Puro (PX459)	pCMV-PTTG1IP-Cre-cMyc	BamHI NotI	Gibson cloning

pU6-spCas9sgRNA	sgRNA sequence previously described by De Jong *et al*.[353]	pU6-Neo_BbsI-spCas9sgRNA	BbsI	Golden gate cloning

Table 5.1. Plasmids generated in this study.

Cloning method, insert, backbone and restriction sites on the backbone are specified on the table. Construct sequences are described on Appendix 8.2.

Plasmid name	Source
pEGFP-N1	Addgene #6085-1
pCAG-CD63-intein-Cre	Samir EL Andaloussi (Karolinska Institutet, Sweden).
pCAG-CD63-intein-Cas9	Samir EL Andaloussi (Karolinska Institutet, Sweden).
pCMV-VSVG plasmid (pMD2.G)	Addgene #12259
pU6-Neo_BbsI-spCas9sgRNA	Previously generated in the Wood lab

Table 5.2. Plasmids not generated in this study and their source.

The intein sequence from *Mycobacterium tuberculosis* was communicated by Samir EL Andaloussi. Oligonucleotides were synthesized by Integrated DNA Technologies. All constructs were confirmed by DNA sequencing.

5.3.2. Cell culture

Human embryonic kidney (HEK) 293T cells, T47D Cre reporter cells, HeLa Cre reporter cells, B16 Cre reporter cells, and HEK293T CRISPR/Cas9 reporter cells were cultured at 37 °C with 5% CO_2 in Dulbecco's Modified Eagle Medium GlutaMAX (DMEM, Gibco) supplemented with 10% foetal bovine serum (FBS) and 1% Antibiotic-Antimycotic (PSA: Penicillin, Streptomycin and Amphotericin B) (Thermo Fisher Scientific, Waltham, MA, United States). Cells were cultured as described in Chapter 2.

For single vesicle analysis, HEK293T cells were seeded on 12-well plates (100,000 cells per well) 24h before transfection. Cells were transfected with 700 ng of plasmid DNA/well using PEI

(Sigma-Aldrich) at a 4:1 ratio PEI:DNA in Opti-MEM (Thermo Fisher Scientific). The next day, media was replaced with Opti-MEM and 48h later conditioned media was collected.

5.3.3. EV production

For cell culture experiments, at least four 150 mm plates of HEK293T cells per condition were transfected with 35 µg DNA/plate using PEI (Sigma-Aldrich, Missouri, United States) at a 4:1 ratio PEI:DNA in Opti-MEM (Thermo Fisher Scientific). 24h later, media was replaced with Opti-MEM (Thermo Fisher Scientific) and 48h later, cell culture supernatant was collected for subsequent EV isolation (performed as described on Chapter 2).

For the *in vivo* experiment, 60 150 mm plates of HEK293T cells per condition were transfected with 35 µg DNA/plate. 24h later, media was replaced with Opti-MEM (Thermo Fisher Scientific) and 48h later, cell culture supernatant was collected for subsequent EV isolation.

5.3.4. EV transfer to Cre reporter cells

T47D, HeLa, and B16 traffic light Cre reporter cells (30,000 cells per well) were seeded onto 96-well plates with complete culture medium (DMEM + 10% FBS + 1% PSA). The next day, cells were treated with EVs in 65 µl of Opti-MEM (Thermo Fisher Scientific). 24h later, the media was changed to culture medium (DMEM + 10% FBS + 1% PSA) and cell activation was analyzed after 24h.

5.3.5. EV transfer to Cas9 reporter cells

HEK293T stoplight light Cas9 reporter cells[353] (30,000 cells per well) were seeded onto 96-well plates with complete medium and incubated at 37 °C under 5% CO_2. The experiments were performed in two different ways. In one set of experiments, the sgRNA was transfected to

reporter cells 24h prior to the EV transfer. Reporter cells were transfected with 45 ng of sgRNA encoding plasmid /well using PEI (Sigma-Aldrich) at a 4:1 PEI:DNA ratio in complete media. 24h later media was removed, and cells were treated with EVs from donor cells transfected with Cas9 constructs in 65 µl of Opti-MEM (Thermo Fisher Scientific). In the other set of experiments, the sgRNA was transfected to EV-producer cells together with Cas9 cells so it could be packaged into the EVs. In this case, reporter cells were treated 24h after seeding with EVs in 65 µl of Opti-MEM (Thermo Fisher Scientific). In both cases, media was changed to complete medium 24h later and cells were analyzed 48h after EV transfer.

5.3.6. Flow cytometry

Cells were washed with PBS followed by 15 min incubation with 50 µl TrypLE Express (Thermo Fisher Scientific). Trypsin was inactivated using 100 µl FACS buffer (PBS containing 10% FBS) and cells were kept on ice until analysis. Cells were analyzed on CytoFLEX LX flow cytometer (Beckman Coulter) and data analysis was performed using FlowJo software (BD Biosciences, Heidelberg, Germany). Activated reporter cells were identified by GFP expression 48h after EV-transfer (measured at 488-525nm). At least 10.000 cells were counted for each sample.

5.3.7. Single vesicle analysis

Single vesicle analysis is a nano flow-cytometry technique to detect, measure and quantify nanoparticles based on their side scatter and fluorescence. Before single-vesicle analysis, conditioned media was centrifuged first at 500 *g* to remove cells and subsequently at 2,000 *g* to remove large particles. After 0.22 µM filtering (STARLAB), conditioned media was analyzed on a NanoAnalyzer N30 instrument (nanoFCM INC, Xiamen, China). 2,000—12,000 single particle

events were counted for 1 min using light scattering and 488/24 nm blue laser set to 10 mW and 10% SS decay, at a sampling pressure of 1.0 kPa. Data were analyzed using NanoFCM Professional Suite v1.8 software (nanoFCM INC). EV size and concentration were determined by interpolation from a standard curve. Non-transfected HEK293T cells conditioned media was used as a fluorescence negative control to set the threshold for GFP positivity.

5.3.8. N-glycosylation assays

PNGase F and Endonuclease H treatments were performed to assess the N-glycosylation status of PTTG1IP. PNGase F cleaves all types of N-linked glycosylation while Endo H cleaves only high mannose and hybrid types of N-linked glycosylation. Recombinant PNGase F, and Endo H kits (NEB) were used according to manufacturers instructions.

Briefly, for both treatments 20 µg protein lysate from HEK293T cells transfected with the appropriate experimental plasmid constructs was denatured for 10 min at 100°C with 10× Glycoprotein Denaturing Buffer (NEB). For PNGase F, this was followed by incubation with 1 µl PNGase F (NEB), 2 µl 10% NP-40 (NEB) and 2 µl 10× GlycoBuffer 2 (NEB, MA, United States) buffer at 37 °C 1h. For Endonuclease H treatment, after denaturation, samples were incubated with 1.5 µl EndoH and 2 µl 10× GlycoBuffer 3 (all NEB) buffer at 37 °C 1h. Glycosylation status was determined as a shift in protein size by western blot.

5.3.9. Immunofluorescence microscopy

100,000 HEK293T cells were seeded on 12-well plates coated with Matrigel. The next day, cells were transfected with 700 ng PTTG1IP variant plasmids using PEI (4:1 PEI DNA ratio). 24h later, cells were fixed with PFA 4% (Thermo Fisher Scientific) for 10min, washed 3 times with PBS, and permeabilized with 0.1% triton X-100 (Sigma Aldrich) for 15min. After incubating the

cells for 1h in blocking buffer (1× PBS, 5% BSA, 0.1% triton X-100), cells were incubated overnight in primary antibody. The next day, after 3 washes with PBS, cells were incubated with secondary antibody for 2h. Plates were stored at 4°C until acquisition. Three images per well were acquired using a 40× objective on an EVOS m5000 microscope.

Application	Antibody	Host	ID	Manufacturer	Dilution
Primary	Anti-EEA1	Rabbit	3288	Cell Signalling	1:200
Primary	Anti-Rab5a	Mouse	46449	Cell Signalling	1:200
Primary	Anti-Rab7	Rabbit	9367	Cell Signalling	1:200
Primary	Anti-Rab11	Rabbit	5589	Cell Signalling	1:200
Secondary	Anti-Rabbit (Alexa 555)	Goat	ab150078	Abcam	1:500
Secondary	Anti-Mouse (Alexa 555)	Goat	Abcam	ab150114	1:500

Table 5.3. Primary and secondary antibody information for immunofluorescence.

5.3.10. Galectin inhibition

For galectin inhibition experiments, 15 mM N-acetyl-lactosamine (Carbosynth, Newbury, United Kingdom) was added to HEK293T EV-producer cells 4h after transfection with PTTG1IP-GFP and was maintained throughout EV production.

5.3.11. Conditioned media transfer to reporter cells

Approximately 100,000 HEK293T cells/well were seeded on 12-well plates 24h before transfection. The next day, cells were transfected in opti-MEM (Thermo Fisher Scientific). 24h later, media was changed to fresh opti-MEM, and after 48h conditioned media was collected and subjected to 10 min 500g centrifugation to remove cell debris and 10 min 2000 *g* centrifugation

to remove large particles. After 0.45 μM filtration (STARLAB), conditioned media was directly added to Cre reporter cells seeded on 96-well plates 24h before (seeding density 30,000 cells/well). The next day media was changed to complete media (DMEM + 10% FBS + 1% PSA) and 24h after, reporter cell activation (GFP expression) was assessed by microscopy. Three images per well were acquired using a 10× objective on an EVOS m5000 microscope.

5.3.12. Western Blot

Cells were lysed in 1× RIPA buffer (Thermo Fisher Scientific) containing 1× cOmplete protease inhibitor cocktail (Merck, Darmstadt, Germany). Acetone precipitation was used for EV samples, whereby cold (-20°C) acetone was added at a 4:1 ratio and incubated for 24h at -20°C. Protein was pelleted by centrifugation at 5,000 *g* 20min. The resulting pellet was resuspended in 1× RIPA buffer (Thermo Fisher Scientific) containing 1× cOmplete protease inhibitor cocktail (Merck) and 10% NuPage sample reducing agent (Invitrogen). Protein concentration was determined by Bradford assay (Sigma-Aldrich) according to manufacturer's instructions. 5-10 ug of total protein was heated at 70 °C for 10 min and then resolved on a 4–12% NuPAGE gel (Thermo Fisher Scientific) by Sodium dodecyl-sulfate polyacrylamide gel electrophoresis (SDS-PAGE). Gels were run at 150 V for 2h in 1× NuPAGE Tris-Acetate SDS Running Buffer (Thermo Fisher Scientific). Protein was transferred onto a polyvinylidene fluoride (PVDF) membrane (Merck) at 60 V for 1 hr 30 min in 1× NuPAGE Transfer Buffer (Thermo Fisher Scientific). Membranes were blocked in Intercept (PBS) Blocking Buffer (Sigma-Aldrich) for 30 mins at room temperature and incubated in Blocking Buffer with primary antibodies at 4 °C overnight. Blots were washed with PBS supplemented with 0.1% Tween-20 (PBS-T) three times and incubated with secondary antibody for 1 hr at room temperature. Antibody information is

described in Table 1). Blots were imaged using a LI-COR Biosciences Odyssey Fc instrument (LI-COR, NE, USA).

Application	Antibody	Host	ID	Manufacturer	Dilution
Primary	Anti-GFP	Rabbit	ab290/ 338001	Abcam/Biolegend	1:1,000
Primary	Anti-cMyc	Mouse	626801	Biolegend	1:1,000
Primary	Anti-Cre	Rabbit	ab216262	Abcam	1:500
Primary	Anti-bActin	Mouse	MA5-15739	ThermoFisher	1:2,000
Primary	Anti-ALIX	Rabbit	ab186429	Abcam	1:2,000
Secondary	Anti-Rabbit	Goat	926-32211	LI-COR	1:5,000
Secondary	Anti-Mouse	Goat	926-32210	LI-COR	1:5,000

Table 5.4 Primary and secondary antibody information for western blot

5.3.13. *In vivo* EV-transfer

Mice were injected with 500,000 B16F10 Cre reporter cells/mouse 10 days before EV treatment. On day 10, isolated EVs were injected to recipient mice by intra-tumoral injection (1×10^{10} EVs/mouse, tumor size ~10mm). 4 days later, tumors were harvested and Cre activity was analyzed by immunohistochemistry (ICH) and PCR. For ICH, half of the tumor tissues were fixed with PFA for making slides. For PCR, the other half of tumor tissues were lysed using lysis buffer (0.1% TritonX-100) and TissueLyser homogenizer (Qiagen). DNA for PCR was isolated from 50 µL of tissue lysate using the Maxwell RSC tissue DNA Kit (Promega).

5.3.14. Cre loxP site recombination analysis

To amplify the loxP-Cre recombination site in B16 Cre reporter cells, forward primer 5′ CGCAAATGGGCGGTAGGCGTG 3′ and reverse primer 5′ GTGGTGCAGATGAACTTCAGGGT 3′ were used. The forward primer was located in the CMV promoter, before the first loxP site, while the reverse primer located after the second loxP site at the 5′ of GFP. PCR was performed using genomic DNA isolated from tumors as the template with HotStarTaq Plus Master Mix Kit (Qiagen) according to the manufacturer's protocol. PCR products were analyzed on a 1% agarose gel using VersaDoc 3000 Gel Imaging System (Bio-Rad). The intensity of the bands was quantified by densitometric analysis using ImageJ 1.53k software (NIH).

5.3.15. Immunohistochemistry of tumor xenografts

The tumor xenograft tissue slides were fixed at 65°C for 1 hour. Deparaffininization and rehydration were performed by incubating the slides in several solvents as follows: xylene 20 min, 100% ethanol 3 min twice, 95% ethanol 3 min, 70% ethanol 3 min, and 50% ethanol 3 min. Next, slides were rinsed with running cold tap water for 5 min followed by antigen retrieval using citrate buffer at pH 6.0 (Sigma Aldrich). Afterwards, slides were washed 3 times with PBS (5 min each), and then slides were blocked using blocking buffer for 30 min at 37°C. Slides were then incubated overnight with anti-GFP antibody (1:200 dilution, Abcam, ab290). The next day, after 3 washes in PBS, slides were incubated with secondary antibody Goat Anti Rabbit IgG H&L (Alexa Fluor® 488) (1:500 dilution, Abcam, ab150077) for 30 min at 37°C. After 3 washes with PBS, slides were mounted using ProLong™ Diamond Antifade Mountant with DAPI (Thermo Scientific) and images were taken using a confocal microscope (Nikon, Japan).

5.3.16. Statistics

GraphPad Prism software (GraphPad, San Diego, California) was used to generate graphs and calculate standard error of the mean (SEM). Student's *t* test was performed to assess statistical differences between two groups. One-way ANOVA followed by Bonferroni *post hoc* test was performed when analyzing more than 2 groups. Results were considered significant at a confidence of 95%, indicated on graphs with asterisks (* $P < 0.05$).

5.4. Results

5.4.1. PTTG1IP enables highly efficient EV-loading in a N-glycosylation dependent manner

Selected candidate features identified with the IPFA analysis (PTAP motif, SPYR domain, MIT domain and N-linked glycosylation) were assessed for EV-loading by fusing them to GFP and analyzing their sorting to EVs by western Blot and single vesicle analysis (**Fig 5.1**). In the case of the MIT domain and N-linked glycosylation of transmembrane proteins, we decided to test the smallest protein containing the feature that could be found in our dataset to avoid altering protein conformations that may be important for domain or PTM functionality. MIT domain-containing protein 1 (*MITD1*) and PTTG1 Interacting Protein (*PTTG1IP*) were selected for MIT domain and N-glycosylation features, respectively. Importantly, PTTG1IP also has a PSI domain which was also identified to be EV-enriched in the IPFA bioinformatics analysis (**Results II Fig 4.3**). For the PTAP motif and SPRY domain, these protein features were fused directly to GFP.

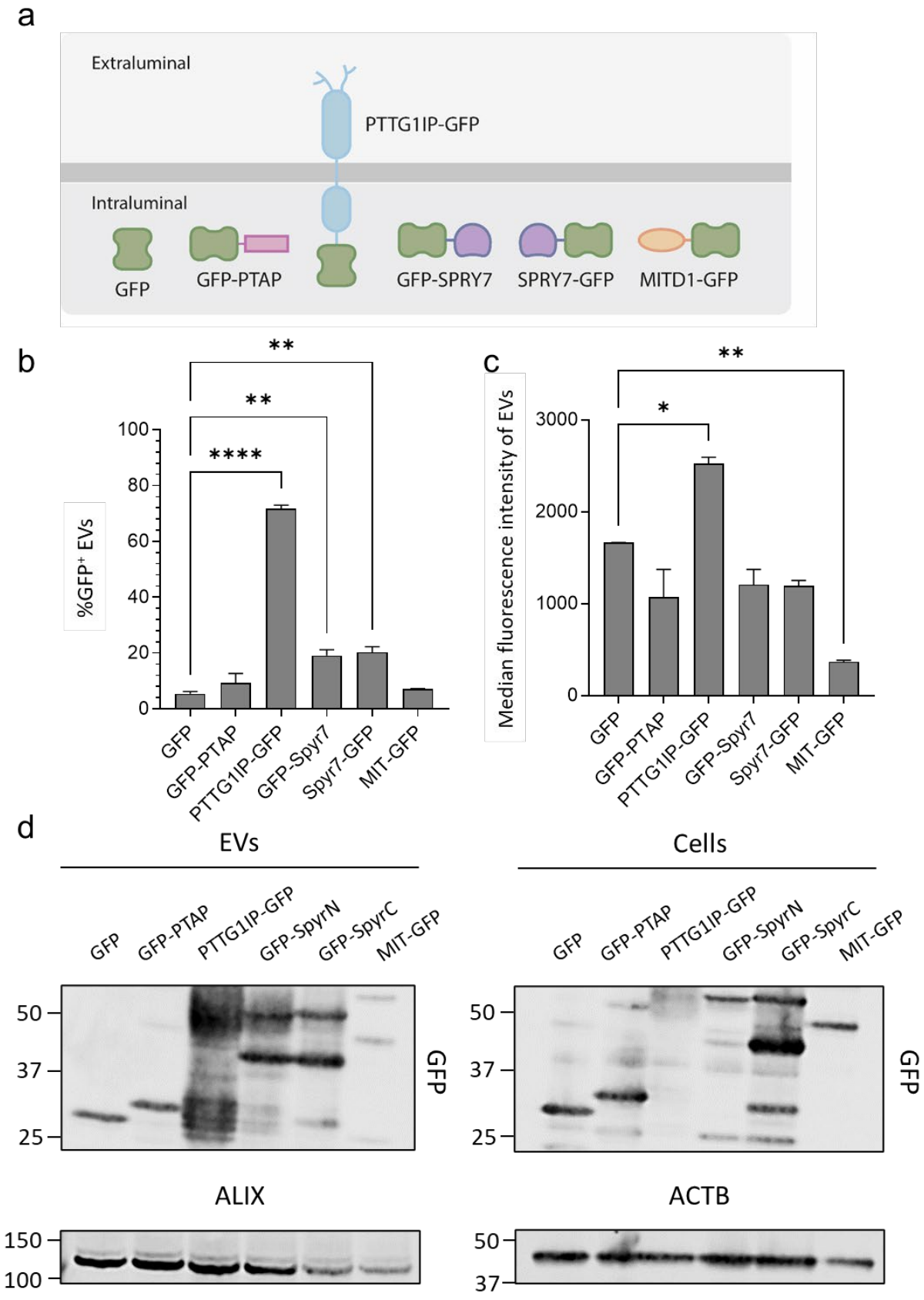
a
Extraluminal
PTTG1IP-GFP
Intraluminal
GFP
GFP-PTAP
GFP-SPRY7
SPRY7-GFP
MITD1-GFP
b
%GFP⁺ EVs
**
**
****
GFP
GFP-PTAP
PTTG1IP-GFP
GFP-Spyr7
Spyr7-GFP
MIT-GFP
c
Median fluorescence intensity of EVs
**
*
d
EVs
Cells
GFP
GFP-PTAP
PTTG1IP-GFP
GFP-SpyrN
GFP-SpyrC
MIT-GFP
ALIX
ACTB

Figure 5.1 Assessment of EV-loading features from bioinformatics analysis.
(a) Scheme of the GFP-fusion constructs that were assessed. **(b)** Percentage of GFP^+ EVs quantified by single-vesicle analysis of conditioned media from HEK293T cells transfected with GFP-fusion constructs. **(c)** Median fluorescence intensity of GFP^+ EVs. **(d)** Western blot of GFP-fusion constructs in HEK293T cells and EVs. Cell lysates and isolated EVs were blotted against ACTB and ALIX respectively. Both cell lysates and isolated EVs were blotted against GFP. Statistical significance was tested by one-way ANOVA and Bonferroni *post hoc* test. Data are presented as mean + SEM, n = 3 replicates, * $P < 0.05$, ** $P < 0.01$, **** $P < 0.0001$.

GFP signal was observed to be highly enriched in the EVs when fused to PTTG1IP (~75% of GFP^+ vesicles) as compared to GFP alone (no scaffold) (~3% of GFP^+ vesicles) (**Fig 5.1 b,d**). In addition, the median fluorescence intensity of PTTG1IP-GFP vesicles was significantly higher (~58%) that that of GFP, indicating a higher amount of GFP loading per vesicle (**Fig 5.1c**). GFP fusion to SPRY domain also increased GFP EV-loading, although to a much lesser extent (~23% of GFP^+ vesicles). Of note, the number of secreted EVs were similar in all conditions (data not shown).

PTTG1IP, also known as PTTG1-binding factor (PBF), is a 180 amino acid single-pass type I transmembrane protein. According to UniProt, PTTG1IP has two putative N-glycosylation sites at residues N45 and N54. N-glycosylation sites annotated in UniProt may not be experimentally validated and N-glycosylation status can depend on the biological context. Thus, to confirm PTTG1IP N-glycosylation status, we mutated residues N45 (N45Q), N54 (N54Q) or N45 and N54 (2NQ) to glutamine to remove potential N-glycosylation sites and subjected HEK293T lysates from cells transfected with PTTG1IP mutants to PNGase F and Endonuclease H (EndoH) treatment (**Fig 5.2a**). PNGase F cleaves all N-glycosylation sites and EndoH cleaves only those of high mannose or hybrid types. N-glycosylation removal can be observed by western blot as a shift in protein mobility (N-glycosylated proteins have a higher molecular weight). Treatment with PNGase F resulted in a shift of protein size from ~55 kDa to ~48 kDa, indicating that PTTG1IP is glycosylated (**Fig 5.2b**). Single N-glycosylation mutants also showed a higher molecular weight than 2NQ mutant (**Fig 5.2b**). Altogether, the shifts in molecular weight of the three mutants as compared to the WT suggest that both sites are N-glycosylated. To further explore the nature of the N-glycosylation sites, PTTG1IP mutants were treated with EndoH. As shown in **Fig 5.2b**, a band shift is only observed for PTTG1IP N45Q, suggesting that N54 N-glycosylation is of high mannose or hybrid type while N45 is of complex type.

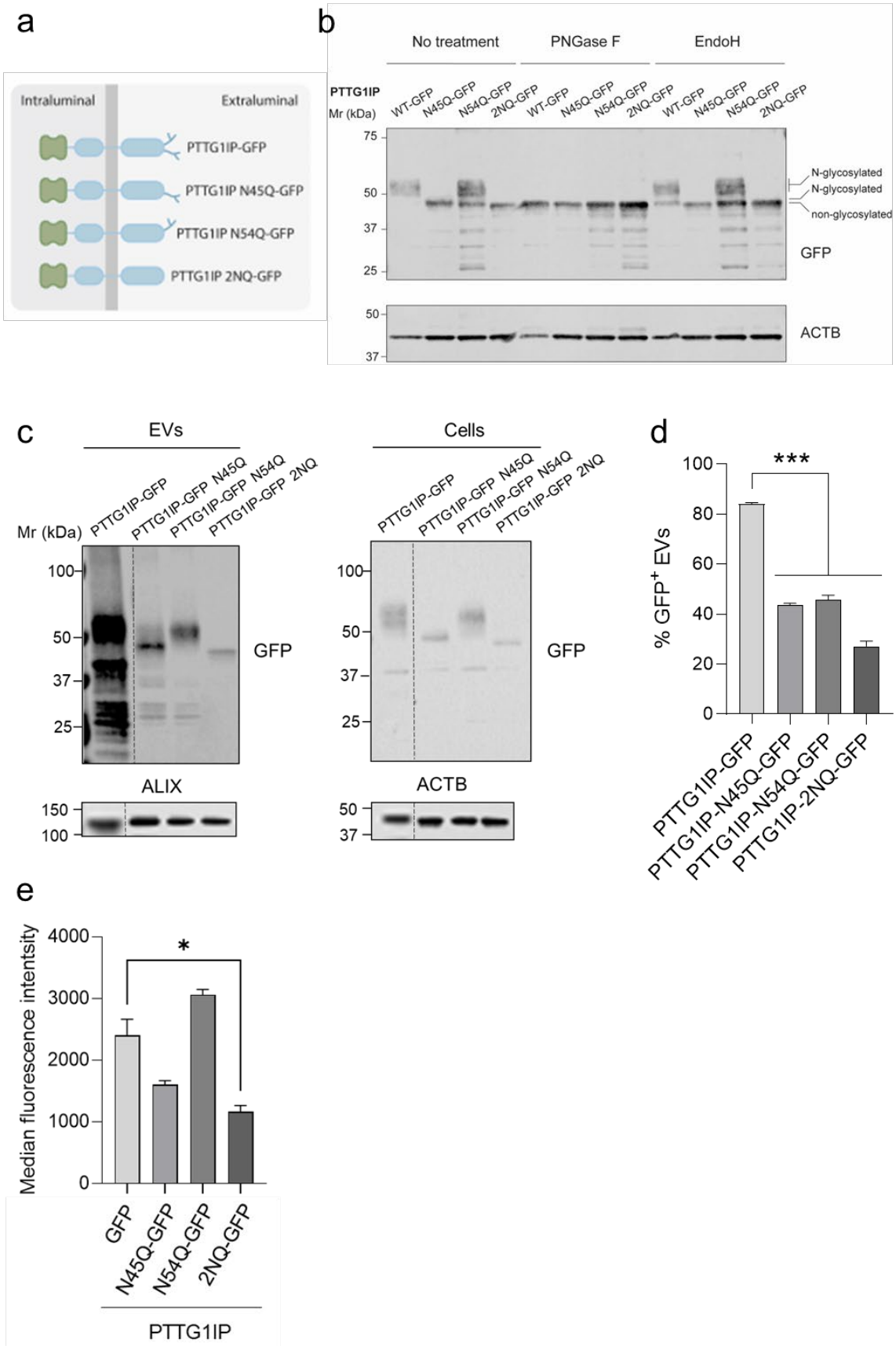
a
Intraluminal
Extraluminal
PTTG1IP-GFP
PTTG1IP N45Q-GFP
PTTG1IP N54Q-GFP
PTTG1IP 2NQ-GFP
b
No treatment
PNGase F
EndoH
PTTG1IP
Mr (kDa)
WT-GFP
N45Q-GFP
N54Q-GFP
2NQ-GFP
75
50
37
25
N-glycosylated
N-glycosylated
non-glycosylated
GFP
ACTB
c
EVs
Cells
Mr (kDa)
PTTG1IP-GFP
PTTG1IP-GFP N45Q
PTTG1IP-GFP N54Q
PTTG1IP-GFP 2NQ
100
50
37
25
GFP
ALIX
150
ACTB
d
% GFP+ EVs
***
PTTG1IP-GFP
PTTG1IP-N45Q-GFP
PTTG1IP-N54Q-GFP
PTTG1IP-2NQ-GFP
e
Median fluorescence intentsity
*
GFP
N45Q-GFP
N54Q-GFP
2NQ-GFP
PTTG1IP

Figure 5.2. N-glycosylation promotes PTTG1IP EV-sorting.

(a) Scheme of PTTG1IP N-glycosylation mutants fused to GFP. **(b)** Western blot of WT PTTG1IP and NGlcNAc mutants fused to GFP in HEK293T cells. Cell lysates were treated with PNGase F to remove all N-glycosylation or with Endonuclease H (EndoH) to remove high-mannose and hybrid N-glycosylations. Lysates were blotted against ACTB and GFP. Molecular weight of N54Q and N45Q mutants was higher or slightly higher, respectively, than that of 2NQ mutant. **(c)** Western blot of WT PTTG1IP and NGlcNAc mutants fused to GFP in HEK293T EVs and cells. Cell lysates and isolated EVs were blotted against ACTB and ALIX respectively. Both cell lysates and isolated EVs were blotted against GFP. **(d)** Percentage of GFP^+ EVs quantified by single-vesicle analysis of conditioned media from HEK293T cells transfected with GFP-fusion constructs. **(e)** Median fluorescence intensity of GFP^+ EVs. Statistical significance was tested by one-way ANOVA and Bonferroni *post hoc* test. Data are presented as mean + SEM, n = 3 replicates, * $P < 0.05$, ** $P < 0.01$, *** $P < 0.001$.

To determine if PTTG1IP EV-sorting was influenced by its N-glycosylation, we assessed EV-loading of PTTG1IP-GFP N-glycosylation mutants in HEK293T by western Blot and single vesicle analysis. PTTG1IP 2NQ-GFP EV-loading (~80% GFP^+ vesicles) was markedly reduced as compared to WT (~25% of GFP^+ vesicles) (**Fig 5.2c,d,e)**. Median fluorescence intensity of 2NQ mutant was also half of that of WT (**Fig 5.2e**), which indicates that 2NQ GFP^+ vesicles have half the amount of GFP per vesicle. The N45Q and N54Q mutants also showed reduced loading (~45% of GFP^+ vesicles) as compared to WT PTTG1IP. Importantly, the expression level of PTTG1IP mutants in cells were similar to that of WT PTTG1P, indicating that the lower sorting to EVs is not due to a lower expression by cells (**Fig 5.2c**). Moreover, both WT PTTG1IP and N-glycosylation mutants were localized in the endosomal compartment, suggesting that PTTG1IP processing and endosomal trafficking were not influenced by the N-glycosylation status (**Fig 5.3a,b**). Direct comparison of WT PTTG1IP and double glycosylation mutant by co-

expression could not be performed since PTTG1IP has been shown to homodimerize, which would alter the intracellular localization results.

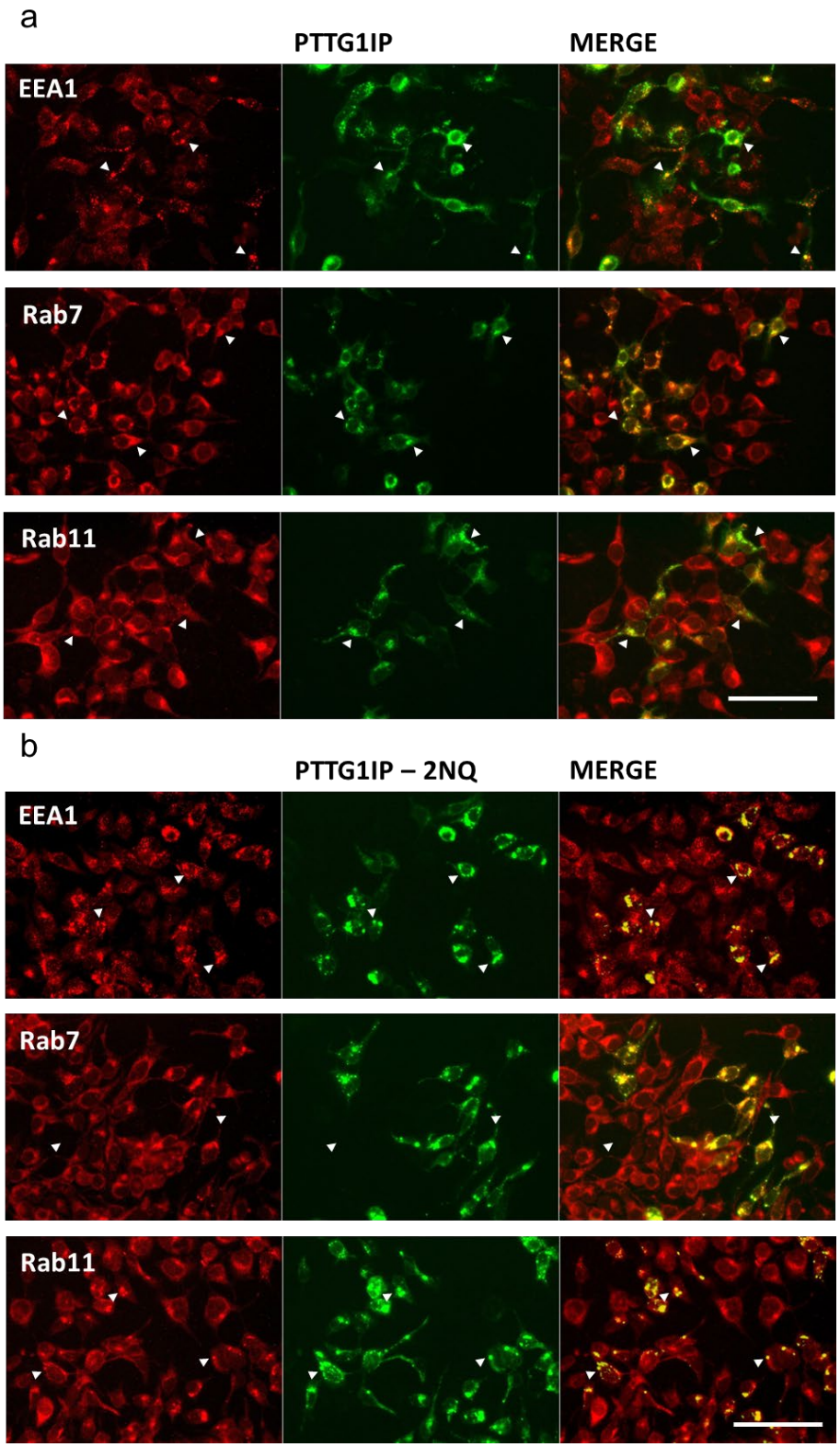

Figure 5.3. Localization of PTTG1IP and PTTG1IP double glycosylation mutant with endosomal markers.

(a) Immunofluorescence microscopy of WT PTTG1IP-GFP (green), and EEA1, RAB7, and RAB11 markers (red) in HEK293T cells. **(b)** Immunofluorescence microscopy of PTTG1IP-GFP double glycosylation (2NQ) mutant (green) and EEA1, Rab7, and Rab11 markers (red) in HEK293T cells. Endosomal markers were detected using Alexa-555 tagged antibodies. EEA1, RAB7, and RAB11 label early, late, and recycling endosomes, respectively. Arrowheads indicate examples of co-localization. Images were taken at 40x magnification, and scale bars indicate 100 μm.

N-glycosylation dependent trafficking of glycoproteins is mediated by carbohydrate-binding proteins (lectins)[318,324]. Notably, members of the galectin protein family have been shown to bind N-glycosylated proteins and have been identified in EVs[75]. To determine if the effect of N-glycosylation on PTTG1IP EV-sorting was mediated by galectins, we evaluated PTTG1IP-GFP packaging when EV-producer cells were treated with galectin inhibitor N-acetyl-lactosamine (LacNAc) (**Fig 5.4**). No significant variation in GFP EV-loading was observed in EVs from treated cells as compared to non-treated (**Fig 5.4**).

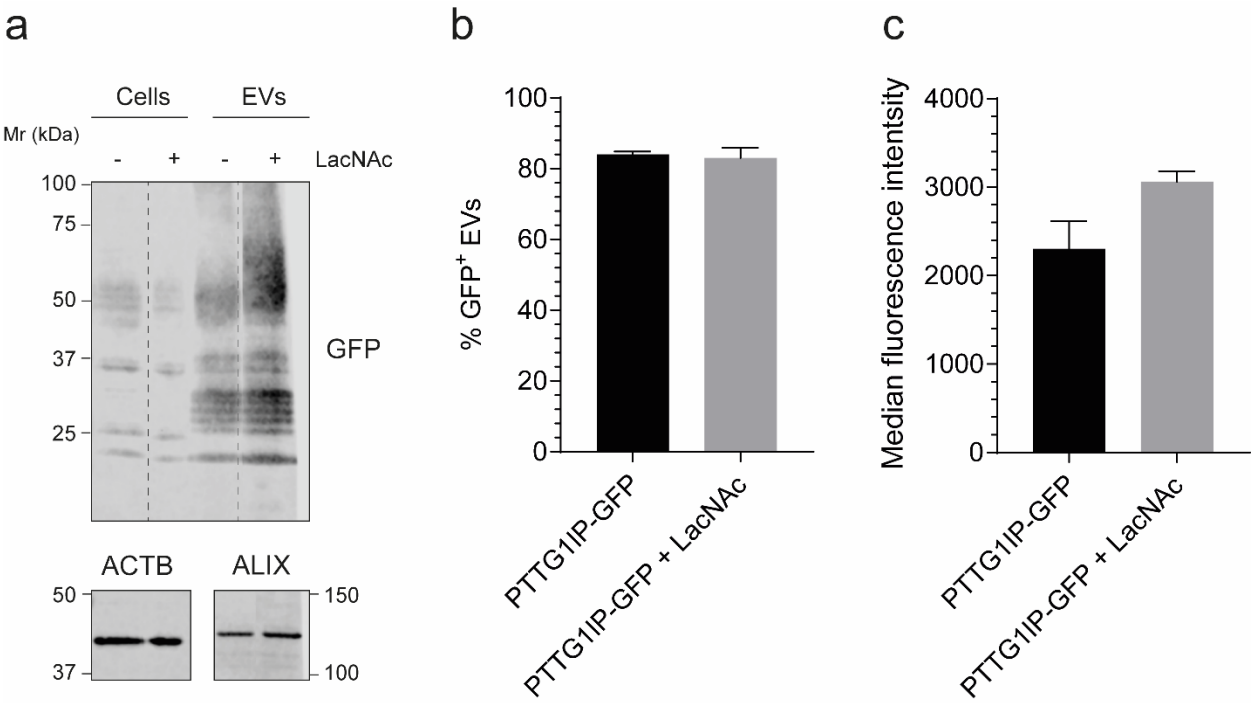

Figure 5.4. Galectin inhibition does not alter EV-secretion of PTTG1IP.

HEK293T EVs from cells treated with galectin inhibitor were assessed by western blot and single vesicle analysis. **(a)** Western blot of HEK293T cells and EVs transfected with PTTG1IP-GFP and treated or not with 15 mM N-acetyl-lactosamine. Cell lysates and isolated EVs were blotted against ACTB and ALIX respectively. Both cell lysates and isolated EVs were blotted against GFP. **(b)** Percentage of GFP^+ EVs quantified by single-vesicle analysis of conditioned media. **(c)** Median fluorescence intensity of GFP^+ EVs quantified by single-vesicle analysis. Data are presented as mean + SEM, n = 2 replicates.

5.4.2. PTTG1IP has a higher EV-loading capacity than CD63

CD63 is a well-described EV-enriched membrane protein of the tetraspanin family that is commonly used as a scaffold for EV-loading of therapeutic cargo[189,250,272,354,355]. To compare the EV-loading capacity of PTTG1IP to that of CD63, we analyzed GFP loading of CD63-GFP and PTTG1IP-GFP fusion proteins by single-vesicle analysis (**Fig 5.5a,b**) and western blot (**Fig 5.5c**). Of note, on EV samples from cells expressing PTTG1IP-GFP, multiple lower bands (~20-37 kDa) were detected in addition to the expected band corresponding to the full construct (~50 kDa) (**Fig 5.1d**, **5.2c**, **Fig 5.4a**). These bands may represent cleavage products of the full construct or unspecific bands; however, this was not further tested. The percentage of GFP positive vesicles was ~30% higher when GFP was fused to PTTG1IP as compared to CD63, while there was no difference in the median fluorescence intensity (**Fig 5.5 a,b**). This indicates that PTTG1IP is able to load a higher percentage of vesicles with GFP although the number of GFP molecules per vesicle was similar with both scaffolds. Altogether, these results show that PTTG1IP-based scaffolds have a higher EV-packaging capacity than CD63.

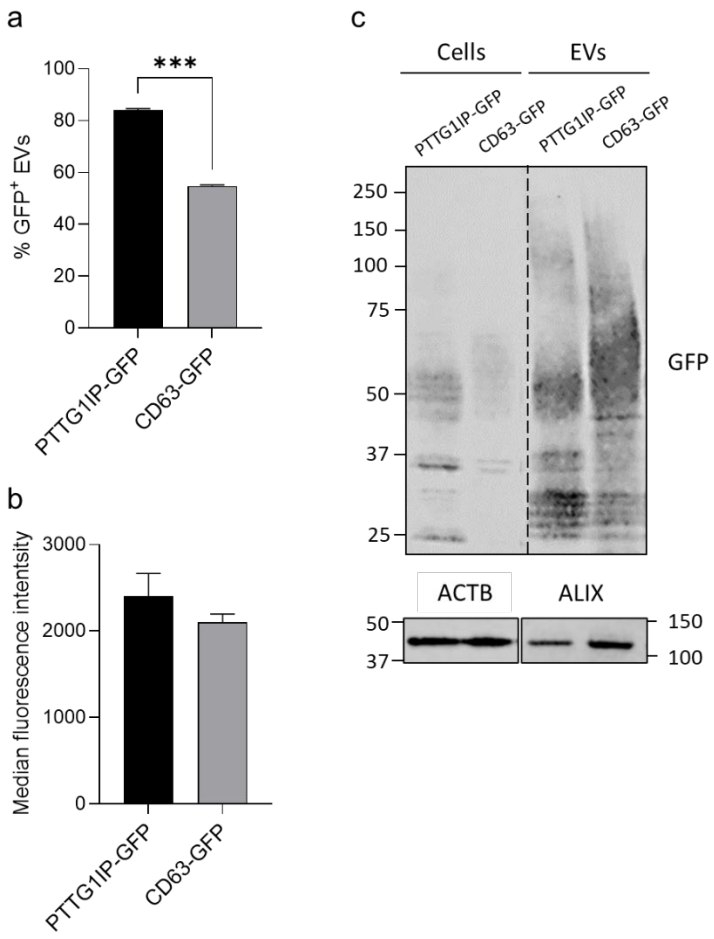

Figure 5.5. PTTG1IP has a higher EV-loading capacity than CD63.

PTTGIP and CD63 EV-loading was compared by single vesicle analysis and WB. **(a)** Percentage of GFP^+ EVs quantified by single-vesicle analysis of conditioned media from HEK293T cells transfected with PTTG1IP-GFP or CD63-GFP. **(b)** Median fluorescence intensity of GFP^+ EVs quantified by single-vesicle analysis. **(c)** Western blot of GFP-fusion constructs in HEK293T donor cells and EVs. Cell lysates and isolated EVs were blotted against ACTB and ALIX respectively. Both cell lysates and isolated EVs were blotted against GFP. Statistical significance was tested by Student's t-test. Data are presented as mean + SEM, $n = 3$ replicates, *** $P < 0.001$.

5.4.3. PTTG1IP can be further engineered to improve its applicability as an EV-scaffold

PTTG1IP is composed by a signal peptide and a PSI domain harboring two N-glycosylation sites in its extracellular N-terminus, a transmembrane domain and an intracellular C-terminus consisting of an unstructured domain followed by a coiled coil region and two endocytosis signals (**Fig 5.6a**). To improve the suitability of PTTG1IP as a scaffold for cargo loading to the EVs, we engineered two different PTTG1IP variants.

In the first variant, PTTG1IP-2YA, the two endocytosis signals of PTTG1IP (YXXL) at the C-terminus were mutated to YXXA (**Fig 5.6b**). It has been previously shown that disrupting the endocytosis signal (YXXΦ motif, where Φ is a hydrophobic residue L, I, M, F, V) of CD63 re-directs the protein towards the microvesicle pathway rather than to the MVB-associated exosome pathway[12]. In the second variant, the coiled coil region of PTTG1IP (130 to 164 amino acids) was deleted, as its intracellular domain has been reported to interact with p53 and alter its activity[356] (**Fig 5.6b**). To determine the EV-loading capacity of the variants, we transfected HEK293T with WT PTTG1IP-GFP, PTTG1IP-2YA-GFP and PTTG1IP-130-164Del-GFP and assessed their loading to EVs by single vesicle analysis. Both variants result in a similar percentage of GFP+ particles (~80%) (**Fig 5.6c**). Nevertheless, the EV-median fluorescence value for the PTTG1IP-2YA mutant was approximately twice the value of WT PTTG1IP, indicating that PTTG1IP-2YA was capable of loading double the amount of GFP per vesicle (**Fig 5.6d**)

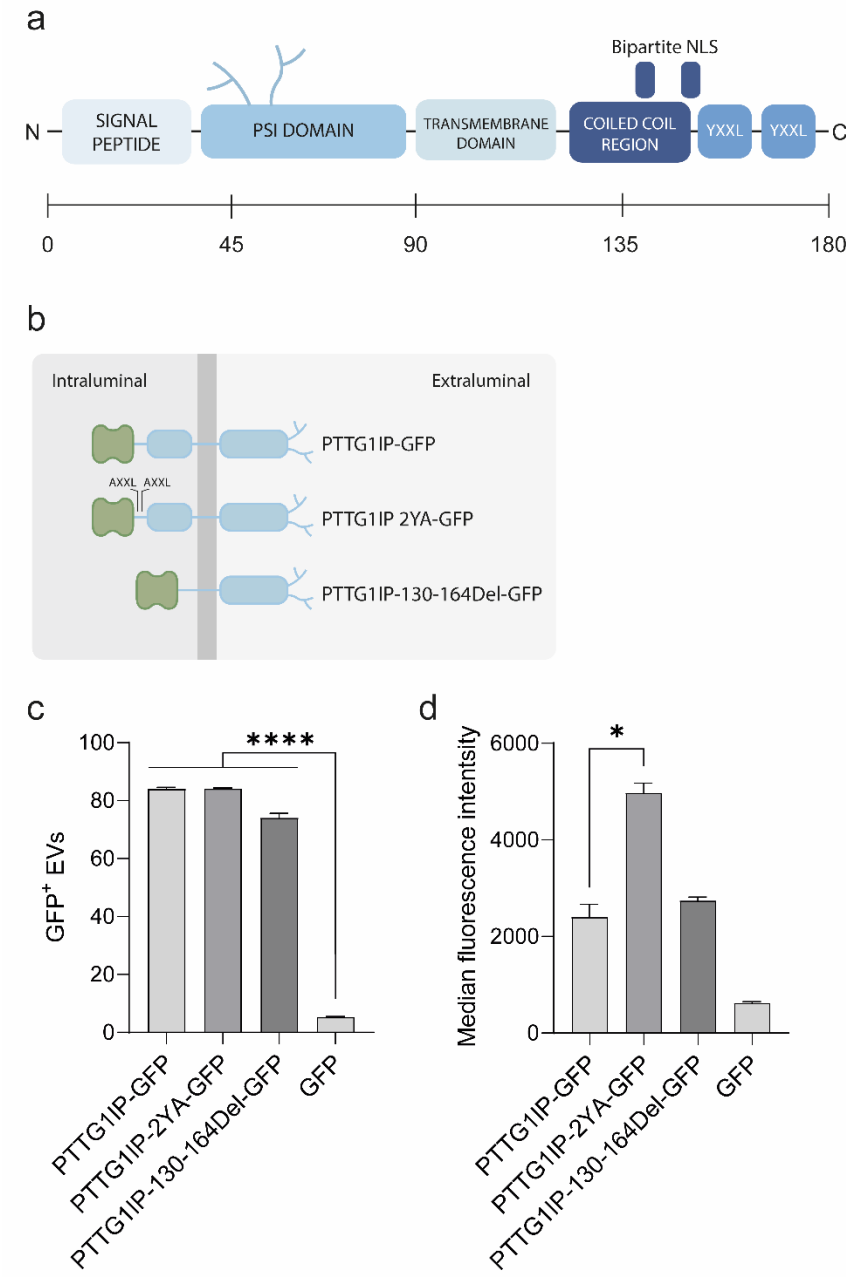

Figure 5.6. EV-loading assessment of PTTG1IP-engineered variants.

(a) Schematic showing PTTG1IP protein domain structure and length**. (b)** Scheme of PTTG1IP variants fused to GFP. PTTG1IP-2YA has its two YXXL endocytosis motifs mutated to AXXL and PTTG1IP-130-164Del has a deletion from amino acid 130 to164. **(c)** Percentage of GFP^+ EVs quantified by single-vesicle analysis of conditioned media from HEK293T cells transfected with GFP-fusion constructs. **(d)** Median fluorescence intensity of GFP^+ EVs. Statistical

significance was tested by one-way ANOVA and Bonferroni *post hoc* test. Data are presented as mean + SEM, $n = 3$ replicates, $*P < 0.05$.

5.4.4. Assessment of Cre recombinase delivery to reporter cells

To assess the ability of PTTG1IP to functionally deliver protein cargo to recipient cells, we investigated the delivery of Cre recombinase to reporter cells using a variety of fusion constructs using PTTG1IP as loading scaffold (**Fig 5.7a**). To achieve functional delivery in recipient cells, several steps need to be accomplished. Firstly, the EVs need to be loaded with sufficient protein cargo in the producer cells. Secondly, when the protein cargo is loaded by fusing it to membrane proteins, such as PTTG1IP or CD63, this cargo needs to be released so that it is able to reach its intracellular location in the target cell. Lastly, once taken up by the recipient cells (in most cases through the endocytic pathway), the EVs must escape endosomes before they are either re-exported to the extracellular space or degraded by the lysosomes. To overcome the cargo-release limitation, we introduced two different self-cleaving sequences from *Mycobacterium tuberculosis*[357] or *Shewanella oneidensis*[358] (**Fig 5.7a**). Ideally, these sequences should self-cleave at lower pH so that this only takes place once the cargo is in the EVs. To promote endosomal escape, we used VSVG, a viral protein that mediates fusion of the EV and endosome membranes at lower pH therefore promoting endosomal escape[202]. Importantly, VSVG and the cargo protein must be on the same EVs to achieve functional delivery. This will depend on the protein scaffold used for cargo loading and on whether VSVG and the scaffold protein are found on the same vesicle subpopulations.

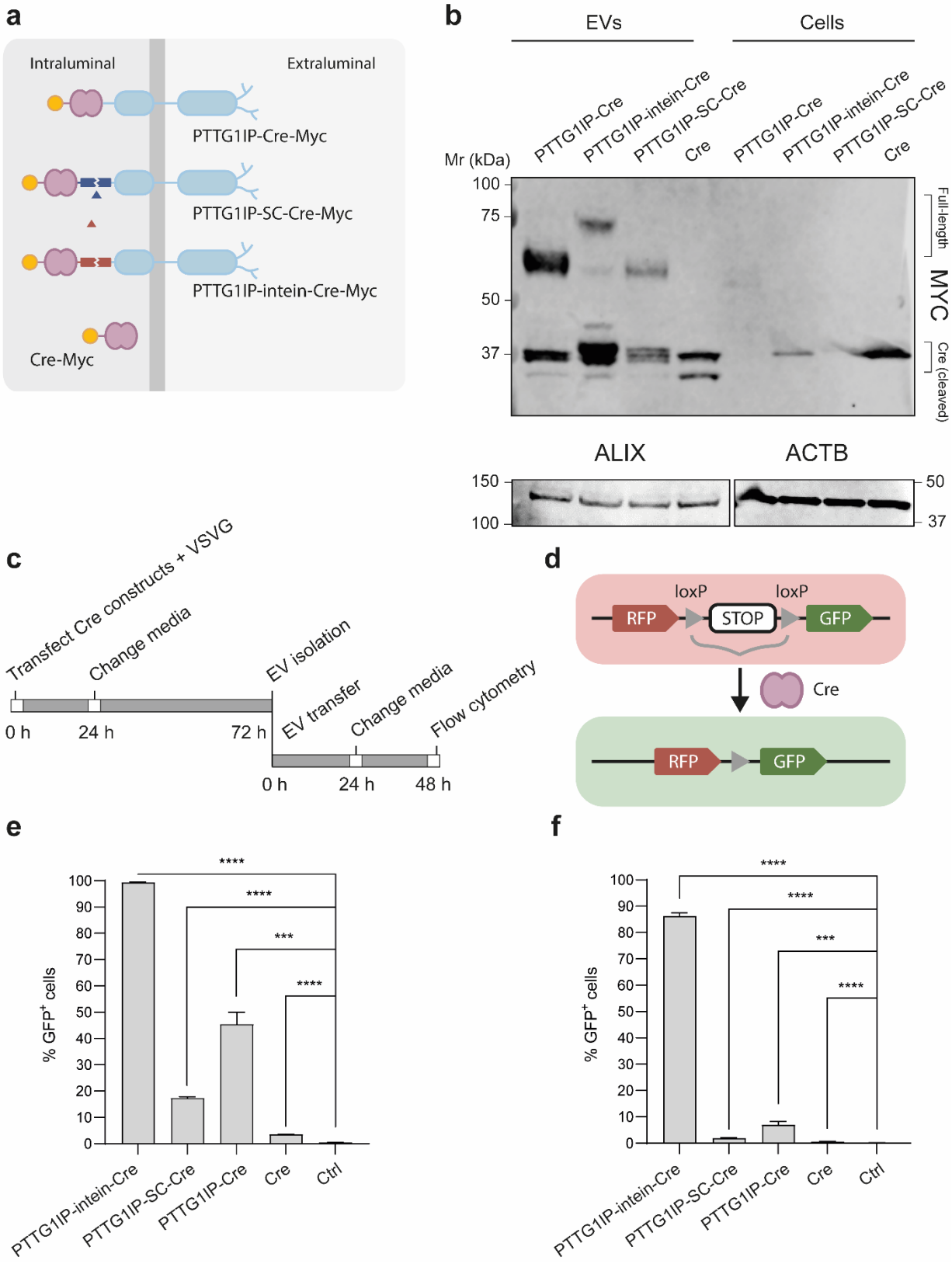
a
Intraluminal
Extraluminal
PTTG1IP-Cre-Myc
PTTG1IP-SC-Cre-Myc
PTTG1IP-intein-Cre-Myc
Cre-Myc
b
EVs
Cells
PTTG1IP-Cre
PTTG1IP-intein-Cre
PTTG1IP-SC-Cre
Cre
Mr (kDa)
100
75
50
37
Full-length
MYC
Cre (cleaved)
ALIX
ACTB
150
100
50
37
c
Transfect Cre constructs + VSVG
Change media
EV isolation
EV transfer
Change media
Flow cytometry
0 h
24 h
72 h
0 h
24 h
48 h
d
loxP
loxP
RFP
STOP
GFP
Cre
RFP
GFP
e
% GFP+ cells
****
****
***
****
PTTG1IP-intein-Cre
PTTG1IP-SC-Cre
PTTG1IP-Cre
Cre
Ctrl
f
% GFP+ cells
****
****
***
****
PTTG1IP-intein-Cre
PTTG1IP-SC-Cre
PTTG1IP-Cre
Cre
Ctrl

Figure 5.7. EV-mediated delivery of Cre to reporter cells by PTTG1IP-based constructs. HEK293T cells were transfected with various PTTG1IP constructs and the capacity to transfer Cre protein was tested in reporter cells. **(a)** Scheme of tested Cre fusion constructs. SC is a self-cleaving endopeptidase from Shewanella oneidensis. The intein is a self-cleaving sequence from Mycobacterium tuberculosis. **(b)** Western blot of Cre-fusion constructs in HEK293T EVs and cells. Both cell lysates and isolated EVs were blotted against MYC. Cell lysates and isolated EVs were blotted against ACTB and ALIX respectively. Bands corresponding to full-length construct, and Cre (double band) are indicated. **(c)** Timeline of EV-transfer experiment to Cre reporter cells. 24h after donor cell transfection with Cre constructs and VSVG, media is replaced with fresh Opti-MEM and EVs are isolated 48h later by SEC. Isolated EVs are then transferred to recipient cells in 96-well plates (5×10^9 EVs/ml). 24h later media is replaced with DMEM 10% FBS and after 24h cells are analysed for GFP expression by flow cytometry. **(d)** Scheme of the Cre reporter cells. RFP is constitutively expressed by reporter cells while GFP is only expressed when the floxed stop cassette is excised by Cre. **(e)** GFP positive cells quantified by flow cytometry 48h after EV-transfer to T47D cells. **(f)** GFP positive cells quantified by flow cytometry 48h after EV-transfer to HeLa cells. Statistical significance was tested by one-way ANOVA and Bonferroni *post hoc* test. Data are presented as mean + SEM, n = 3 replicates, ***$P < 0.001$, ****$P < 0.0001$.

To test delivery of Cre to recipient cells, we first transfected several Cre constructs (**Fig 5.7a,b**) together with VSVG to HEK293T donor cells and the resulting EVs were transferred to Cre reporter cells (**Fig 5.7c**). These reporter cells constitutively express RFP and contain a floxed stop signal followed by GFP. Upon Cre delivery, loxP sites recombine to excise the stop signal and GFP is expressed (**Fig 5.7d**). T47D or HeLa reporter cells were treated with 5×10^9 EVs/ml and reporter activation was assessed 48h after by flow cytometry. PTTG1IP-intein-Cre showed the highest activation (~98% in T47D and ~85% in HeLa cells) while PTTG1IP-Cre induced activation of ~40% in T47D and ~10% in HeLa cells (**Fig 5.7e,f**). Conversely, for Cre alone (no scaffold), activation was ~3% in T47D and ~1% in HeLa cells (**Fig 5.7e,f**). Notably, Cre was

released in the EVs from PTTG1IP-Cre fusion protein without the need of a self-cleaving protein as observed from the ~38 kDa band that corresponds to the expected size of Cre (**Fig 5.7b**). Nevertheless, when the intein is placed between PTTG1IP and Cre there was an increase of released Cre in the EVs (**Fig 5.7b**). This was not the case for the other self-cleaving sequence from *Shewanella oneidensis*. Importantly, while treatment with conditioned media from cells transfected with PTTG1IP-intein-Cre and VSVG resulted in reporter cell activation, no Cre activity was detected in the absence of VSVG (**Fig 5.8**).

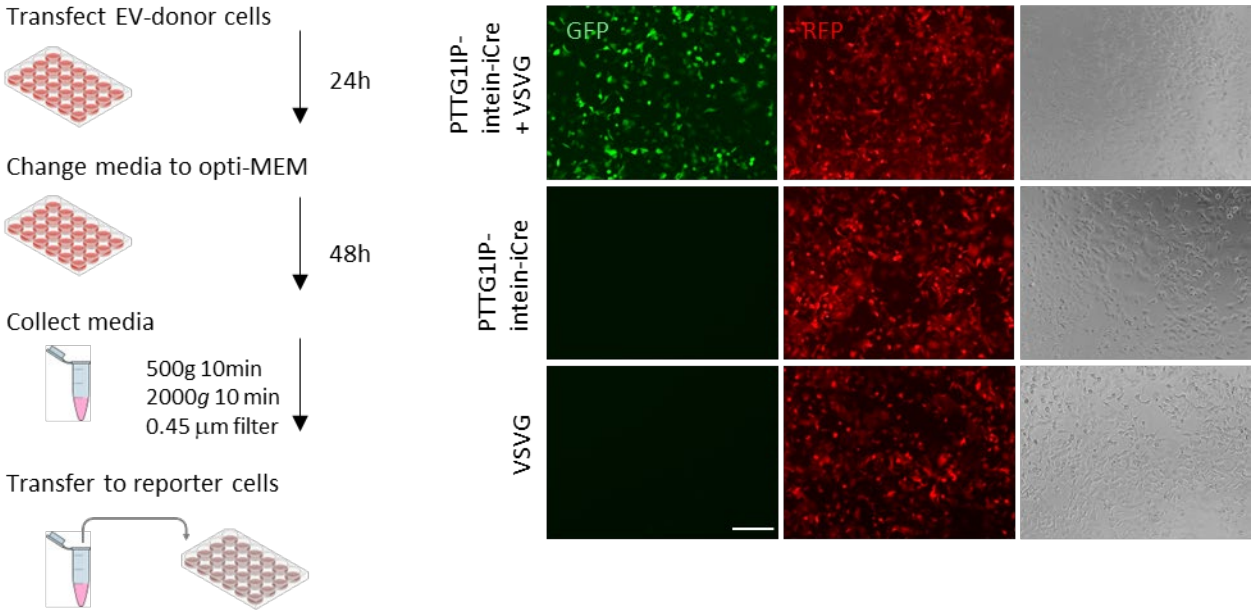

Figure 5.8. Conditioned media transfer to Cre reporter cells.

(a) Scheme of conditioned media preparation and transfer to reporter cells. **(b)** Fluorescence microscopy of T47D cells treated with conditioned media from PTTG1IP-intein-Cre + VSVG, PTTG1IP-intein-Cre, or VSVG transfected HEK293T donor cells. Images were taken at 20x magnification, and scale bars indicate 100 µm.

To take advantage of the natural cleavage of PTTG1IP, we generated a mutant whereby the 130-180 sequence was duplicated at the C-terminus to further promote Cre release (**Fig 5.9a**). Inspection of the Cre WB in **Fig 5.7a**, showed that free Cre and Cre released from PTTG1IP fusion protein were of similar sizes. We therefore reasoned that the site of intrinsic PTTG1IP cleavage was located near to the fusion site (i.e. the C-terminus).

To compare the efficiency of the various PTTG1IP variants (**Fig 5.9a,b)**, we performed an EV dose response of CD63-intein-Cre, PTTG1IP-intein-Cre, PTTG1IP-130-180aa-Cre and PTTG1IP130-164Del-intein-Cre in B16 and T47D reporter cells. CD63-intein-Cre was included as a control scaffold. PTTG1IP-intein-Cre and PTTG1IP130-164Del-intein-Cre showed the highest potency followed by PTTG1IP-130-180aa-Cre (**Fig 5.9c,d**), while CD63-intein-Cre showed the lowest potency, especially in B16 cells (**Fig 5.9c,d**). Notably, PTTG1IP-intein-Cre was almost two log units more potent than CD63-intein-Cre in T47D cells, and at least one log unit more potent in B16 cells (**Table 5.5**). PTTG1IP-130-180aa-Cre efficiency was double of that of PTTG1IP-Cre at the same EV concentration (~40% vs ~99% in T47D cells), suggesting that Cre release was improved (**Fig 5.7e, Fig 5.9c,d**). Notably, cleavage of PTTG1IP-130-180aa-Cre only occurred in the EVs, whereas only fully cleaved PTTG1IP-intein-Cre was detected in cells (**Fig 5.9b**).

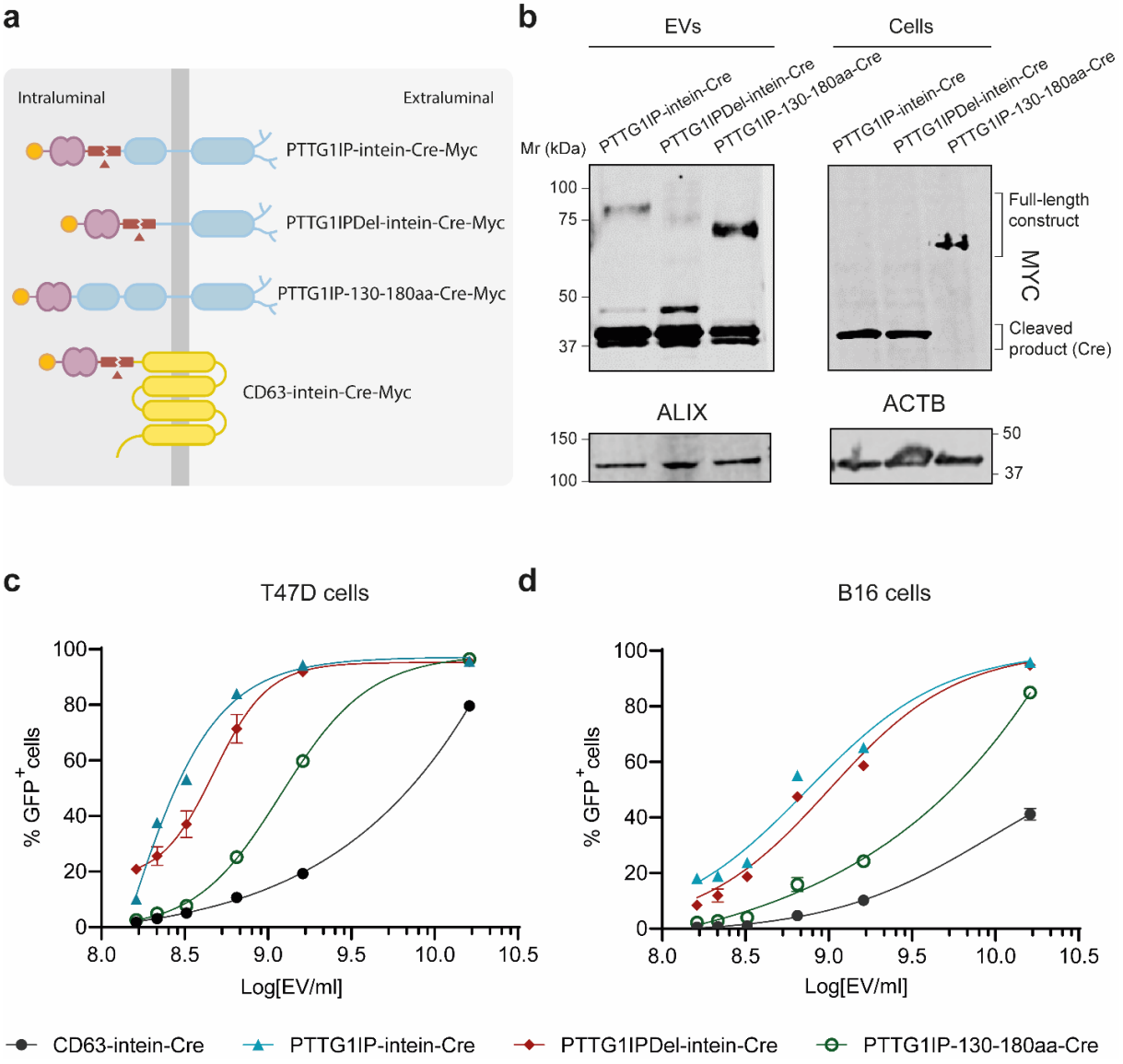

Figure 5.9. EV-mediated delivery of Cre to reporter cells by PTTG1IP-engineered variants. HEK293T cells were transfected with various PTTG1IP and CD63 constructs and the capacity to transfer Cre protein in a dose-dependent manner was tested in reporter cells. **(a)** Scheme of tested Cre fusion constructs. The intein is a self-cleaving sequence from Mycobacterium tuberculosis. PTTG1IPDel has a deletion from amino acid 130 to 164. PTTG1IP-130-180aa has amino acids 130-180 duplicated on PTTG1IP C-terminus. **(b)** Western blot of Cre-fusion constructs in HEK293T cells and EVs. Both cell lysates and isolated EVs were blotted against MYC. Cell lysates and isolated EVs were blotted against ACTB and ALIX respectively. **(c)** EV-transfer dose response in T47D cells. **(d)** EV-transfer dose response in B16 cells. Dose curves were generated using the variable slope model. Data are presented as mean + SEM, n = 3 replicates.

	logEC50		EC50 (EVs/ml)	
	T47D	B16	T47D	B16
PTTG1IP-intein-Cre	8.2	8.9	1.6×10^{8}	8×10^{8}
PTTG1IPDel-intein-Cre	8.7	9	5×10^{8}	1×10^{9}
PTTG1IP-130-180aa-Cre	9.1	9.6	1.3×10^{9}	$\sim4\times10^{9}$
CD63-intein-Cre	~10	>10.1	$\sim1\times10^{10}$	$>1.3\times10^{10}$

Table 5.5. LogEC50 and EC50 (EVs/ml) values of Cre fusion constructs on Fig 5.9.

We next assessed if PTTG1IP 130-180 sequence could be used as an EV-cleavage sequence in a protein context distinct to that of PTTG1IP. We compared the cleavage activity of the intein with the activity of three EV-cleavage sequences from PTTG1IP when fused to CD63 (CD63-intein-Cre vs CD63-3xPTTG1IP130-180aa-Cre, **Fig 5.10**). Cre cleavage in the EVs was observed with both PTTG1IP130-180aa and intein sequences, although a higher cleavage was observed with the intein (**Fig 5.10**). This indicates that PTTG1IP 130-180 sequence can be used to promote cleavage in the EVs in a distinct protein context.

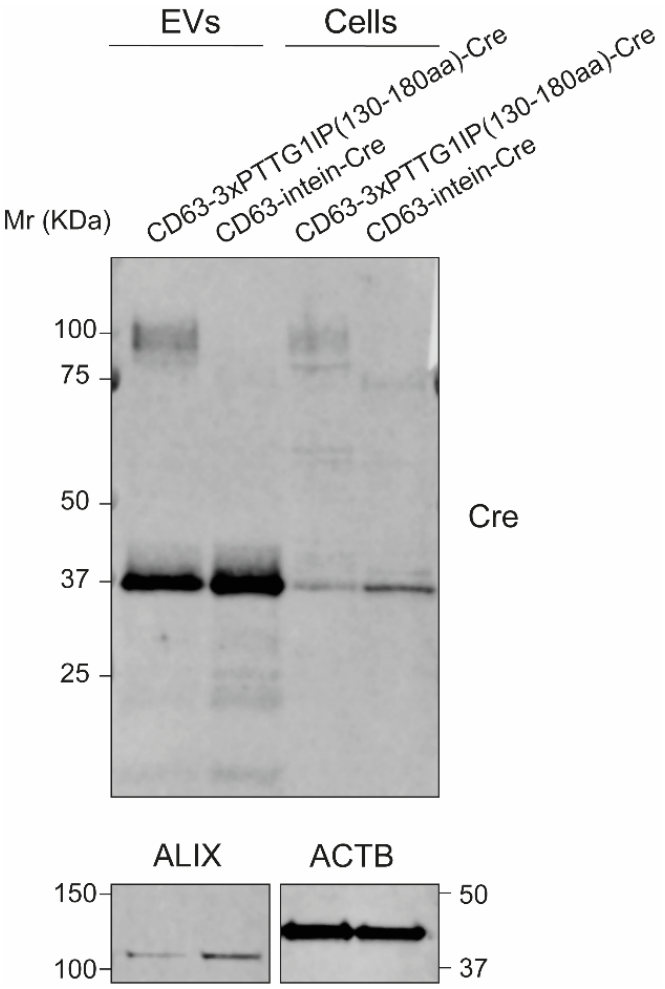

Figure 5.10. Amino acids 130-180 of PTTG1IP are able to induce cleavage in EVs when fused to CD63.

HEK293T cells were transfected with CD63-intein-Cre or CD63-3xPTTG1IP(130-180aa)-Cre, and Cre cleavage in the EVs was analyzed. Western blot of CD63-intein-Cre and CD63-3xPTTG1IP(130-180aa)-Cre in HEK293T cells and EVs. Cell lysates and isolated EVs were blotted against Cre, ALIX and ACTB.

5.4.5. Assessment of Cre recombinase delivery to mice tumor xenografts

Building on positive initial results in cell culture, we assessed EV-mediated Cre delivery *in vivo* using mice harboring cell tumors from B16 Cre reporter cells (**Fig 5.11a**).

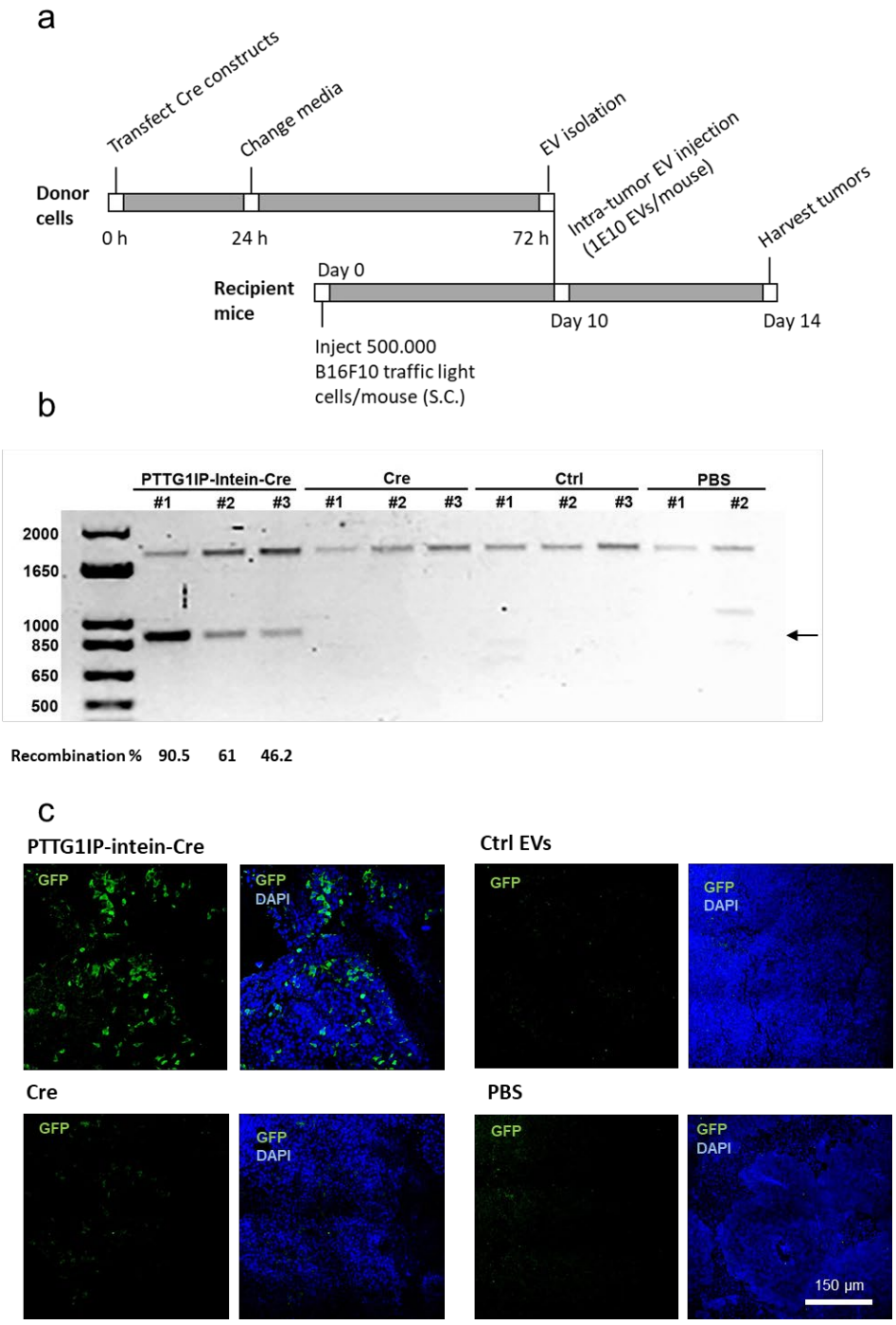

Figure 5.11. EV-mediated delivery of Cre to reporter mice.

(a) Timeline of EV-transfer experiment to Cre reporter mice. 24h after donor cell transfection with Cre constructs and VSVG, media was replaced with fresh Opti-MEM and EVs were isolated 48h later by SEC. 10 days before EV transfer, mice were injected with 5×10^5 B16 Cre reporter cells/mouse. On day 10, isolated EVs were injected to recipient mice by intra-tumoral injection (1×10^{10} EVs/mice). 4 days later, tumors were harvested and Cre activity was analyzed. **(b)** Cre recombination activity in mice tumors treated with PTTG1IP-intein-Cre + VSVG, Cre + VSVG or VSVG only (control EVs). Cre recombination site was amplified by PCR and the products resolved by agarose gel electrophoresis. Cre recombination is indicated by a shorter 900 bp product (arrow) while non-recombined site is observed as a 1,700 bp product. Recombination percentages are indicated for recombined samples **(c)** GFP expression in mice tumors injected via the intratumoral route with PTTG1IP-intein-Cre + VSVG EVs, Cre + VSVG EVs or PBS examined by ICH. n = 3 mice. Scale bar indicates 150 μm.

EVs were isolated from HEK293T cells transfected with PTTG1IP-intein-Cre + VSVG, Cre + VSVG, or VSVG alone. After intratumoral injection of 1×10^{10} EVs/mice, Cre activity was analyzed by PCR and immunohistochemistry. PCR was perfomed using primers which span the reporter cassette and produce a 1,700 bp amplicon. Successful Cre recombination (indicated by a shorter 900 bp product (arrow) (**Fig 5.11b**)) was detected in tumors harvested from the three PTTG1IP-intein-Cre treated mice with recombination efficiencies ranging from 46-90%, while no recombination was detected in control treatment mice (i.e., mice treated with control EVs containing non-fused Cre, EVs containing VSVG alone, or mice injected with PBS) (**Fig 5.11b**). Similarly, GFP signal was only detected in tumors from mice injected with PTTG1IP-intein-Cre (**Fig 5.11c**). Together, these data suggest that PTTG1IP can be used as a scaffold for EV-mediated protein delivery *in vivo*.

5.4.6. Assessment of Cas9 and Cas9/sgRNA complex delivery to reporter cells

Having shown that PTTG1IP can be used for loading and delivering cargo protein via EVs, we next assessed the ability of PTTG1IP in delivering more complex macromolecules, such as the CRISPR-Cas9 system. The CRISPR-Cas9 system represents a potent tool for gene editing and transcription regulation due to its high efficiency and specificity[308]. However, this potential is hampered by the lack of efficient delivery methods[296]. Thus, we explored the use of PTTG1IP to deliver Cas9 and Cas9/sgRNA complexes to recipient cells. To assess Cas9 delivery, we used HEK293T stoplight reporter cells[353]. These cells constitutively express RFP and express GFP upon Cas9 cleavage and indel formation (in 2 out of 3 of the events) (**Fig 5.12a, Fig 5.13**).

To test Cas9 delivery, HEK293T cells were transfected with Cas9 or PTTG1IP-Cas9 together with VSVG and EVs were isolated 72h later (**Fig 5.12b**). 24h prior to EV transfer reporter cells were transfected with sgRNA and 48h later Cas9 activity was assessed by flow cytometry (**Fig 5.12b**). ~3% of reporter cells were GFP^+ after Cas9 EV-transfer while ~10% of the cells were GFP^+ after PTTG1IP-intein-Cas9 transfer (**Figure 5.12c**).

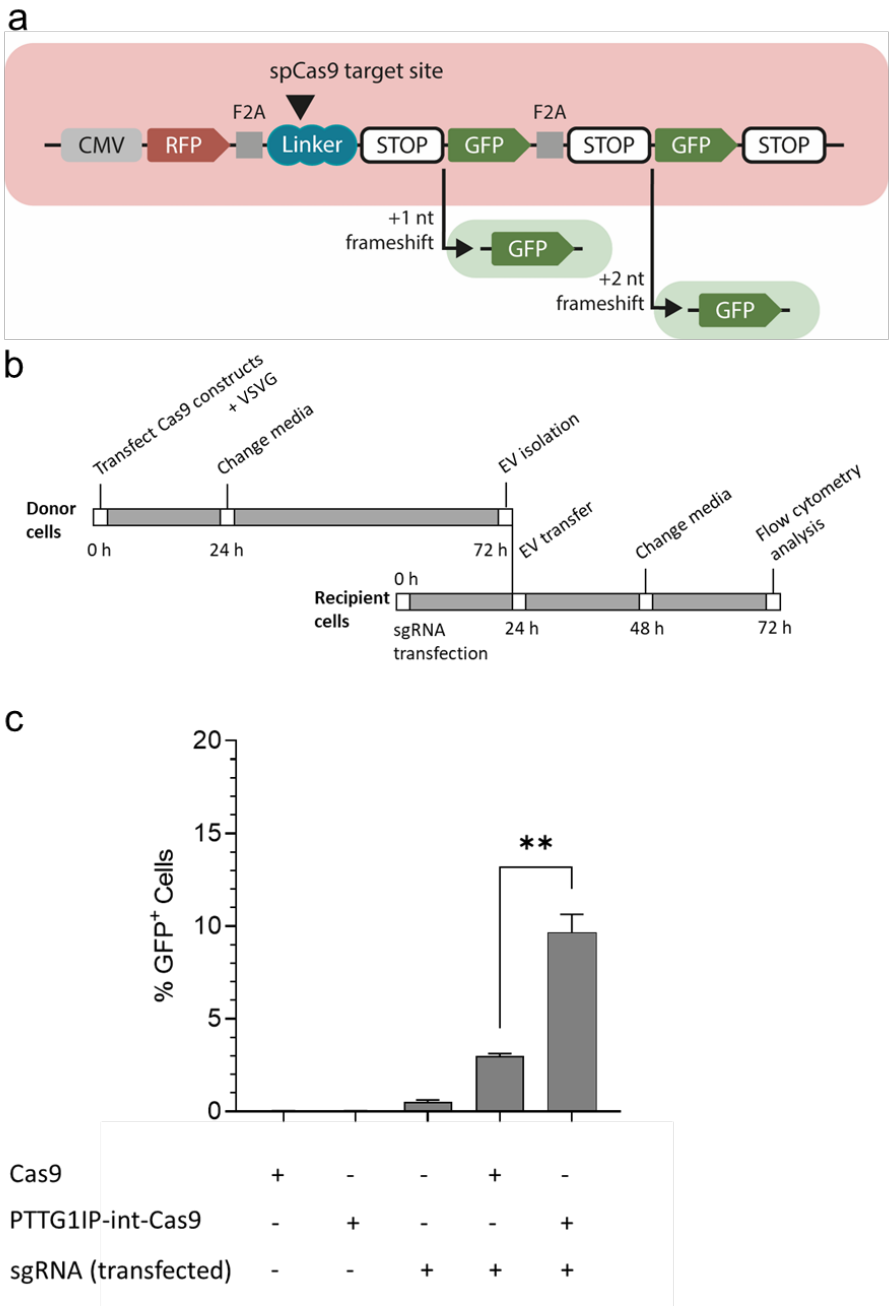

Figure 5.12. EV-mediated delivery of Cas9 to reporter cells.

(a) Scheme of the Cas9 stoplight reporter construct. mCherry is constitutively expressed under a CMV promoter, followed by an F2A self-cleaving peptide sequence, a Cas9-binding linker region and a stop codon. Two GFP open reading frames that are frameshifted by one or two nucleotides are placed after the stop codon, separated by a F2A sequence. Upon Cas9 cleavage and indel formation, the translation reading frame will be shifted and GFP will be expressed

together with mCherry (in 2/3 of the editing events). **(b)** Timeline of EV-transfer experiment. 24h after donor cell transfection with Cas9 constructs and VSVG, media is replaced with fresh Opti-MEM and EVs are isolated 48h later by SEC. Isolated EVs are then transferred to recipient cells (that were transfected with sgRNA 24h before) in 96-well plates (3×10^9 EVs/ml). 24h later media is replaced with DMEM 10% FBS and after 24h cells are analyzed for GFP expression by flow cytometry. **(c)** GFP positive cells quantified by flow cytometry 48h after EV-transfer to sgRNA-transfected reporter cells. **(d)** Timeline of EV-transfer experiment to reporter cells. In this case, reporter cells did not express sgRNA. **(e)** GFP positive cells quantified by flow cytometry 48h after EV-transfer to reporter cells. Statistical significance was tested by one-way ANOVA and Bonferroni *post hoc* test. Data are presented as mean + SEM, n = 3 replicates, $^{**}P < 0.01$.

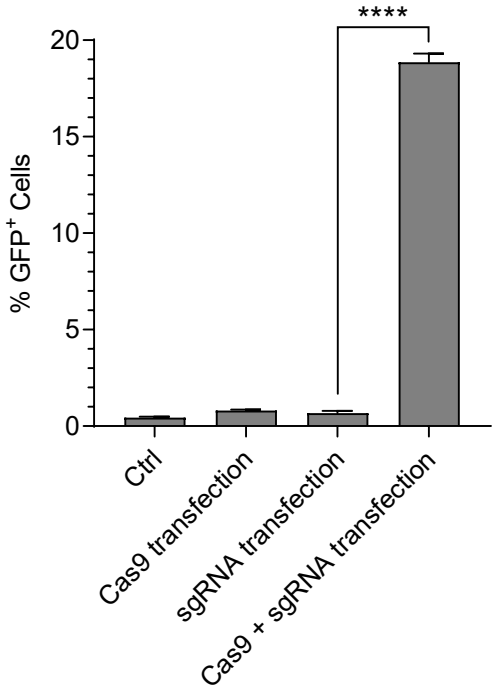

Figure 5.13. Assessment of Cas9 reporter cell activation after Cas9 and sgRNA transfection. GFP positive cells quantified by flow cytometry 48h after Cas9, sgRNA or Cas9 and sgRNA transfection to HEK293T stoplight reporter cells. Statistical significance was tested by one-way ANOVA and Bonferroni *post hoc* test. Data are presented as mean + SEM, n = 3 replicates, ****P < 0.0001.

Notably, Cas9 delivery was twice as efficient with PTTG1IP-intein-Cas9 than with CD63-intein-Cas9 (**Fig 5.14**).

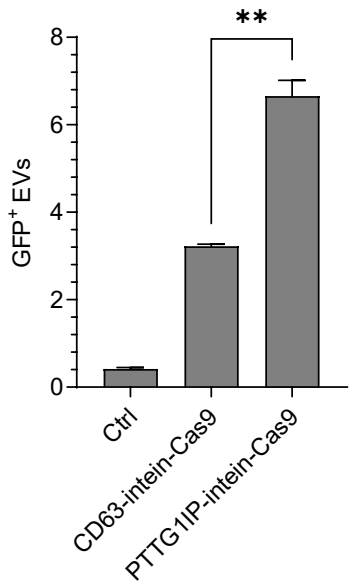

Figure 5.14. Comparison of PTTG1IP and CD63 for EV-mediated delivery of Cas9.
GFP positive cells quantified by flow cytometry 48h after PTTG1IP-intein-Cas9 or CD63-intein-Cas9 EV-transfer to sgRNA transfected HEK293T stoplight reporter cells. Isolated EVs were transferred to recipient cells in 96-well plates (2×10^9 EVs/ml). Statistical significance was tested by Student's t-test. Data are presented as mean + SEM, n = 2, $^{**}P < 0.01$.

To assess Cas9-sgRNA complex delivery, reporter cells were treated with EVs from HEK293T cells transfected with Cas9 or PTTG1IP-Cas9, together with VSVG and sgRNA (**Fig 5.15a**). Efficiency in this case was 0.5% for Cas9 and 3% for PTTG1IP-intein-Cas9 (**Fig 5.15b**). These results suggest that PTTG1IP is a suitable scaffold for delivery of more complex macromolecular cargoes.

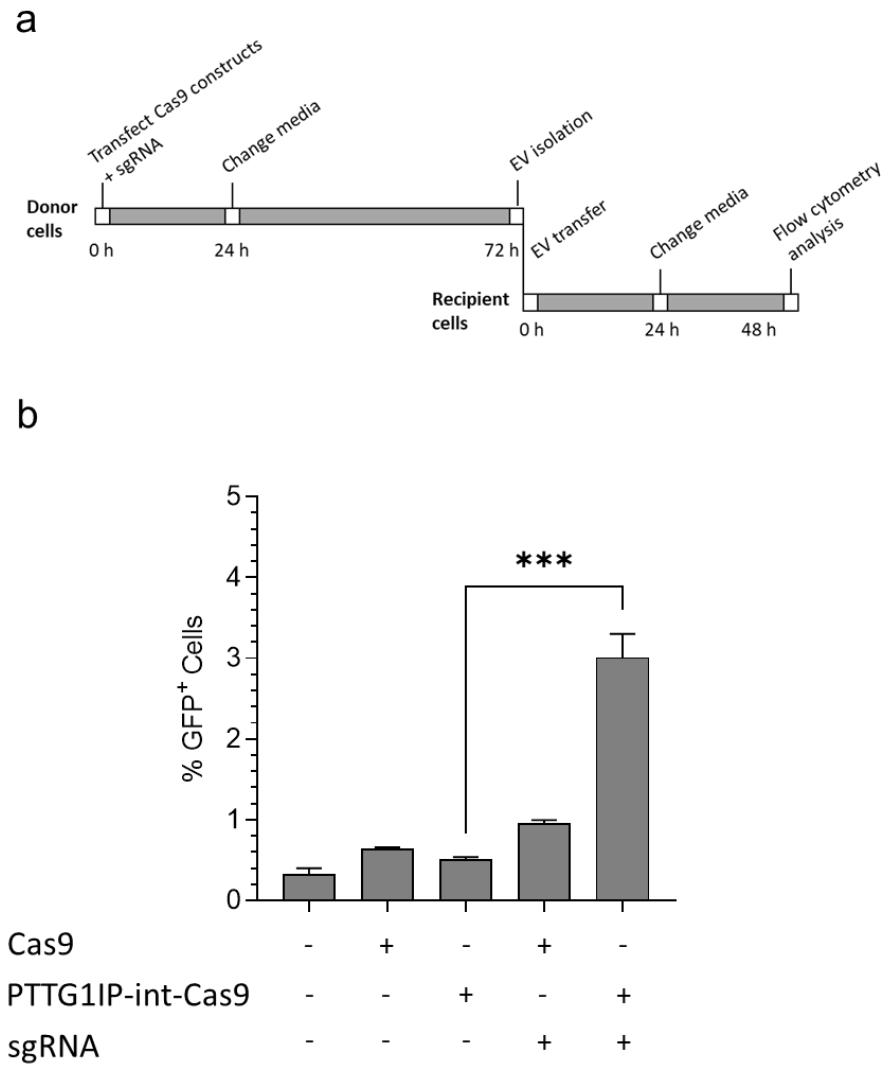

Figure 5.15. **EV-mediated delivery of Cas9/sgRNA complexes to reporter cells.**

(a) Timeline of EV-transfer experiment to reporter cells. 24h after donor cell transfection with Cas9 constructs, sgRNA, and VSVG plasmids, media was replaced with fresh Opti-MEM and EVs were isolated 48h later by SEC. Isolated EVs were then transferred to recipient cells in 96-well plates (3×10^9 EVs/ml). 24h later media was replaced with DMEM 10% FBS and after 24h cells were analyzed for GFP expression by flow cytometry. **(b)** GFP positive cells were quantified by flow cytometry 48h after EV-transfer to reporter cells. Statistical significance was tested by one-way ANOVA and Bonferroni *post hoc* test. Data are presented as mean + SEM, n = 3 replicates, ***$P < 0.001$.

5.5. Discussion

A major challenge in developing EV-based therapies is the loading of therapeutic cargo into the vesicles. Current methods for endogenous EV-protein loading often rely on tetraspanins[252–254], lipidic tags[177,264,327], or viral proteins[267,359] (e.g., Gag), that despite showing a high loading capacity are not suitable for further engineering on the extracellular side (i.e., addition of targeting or endosomal escape peptides). Lipidic tags and viral scaffolds target proteins to the lumen of the EVs, and engineering tetraspanins to display proteins or peptides on their extracellular loops while maintaining their EV-sorting capacity has been proven to be challenging[259,260]. To accomplish EV-loading and targeting, several strategies based on multimodular EV-engineering have been developed[189,235], where different scaffold proteins are used to load the therapeutic cargo, and to display the targeting moiety. However, due to EV heterogeneity, there is a risk that the different modules (i.e., therapeutic cargo, targeting moiety, and endosomal escape moiety) are present in mutually exclusive EV subpopulations, thus reducing the therapeutic efficiency of the EVs. There is therefore a need for more suitable EV scaffold proteins that allow for highly efficient intracellular EV-loading and that are amenable to EV surface modification. Here, we investigate the use of PTTG1IP scaffold for functional protein delivery. We show that PTTG1IP EV-loading is dependent on its N-glycosylation status, and we demonstrate that PTTG1IP is able to efficiently deliver Cre protein *in vivo*, and SpCas9/sgRNA complexes in cell culture. Furthermore, we present various PTTG1IP variants with improved properties for its therapeutic application.

5.5.1. Analysis of putative EV-sorting features

Candidate features identified with the IPFA analysis (PTAP motif, SPYR domain, MIT domain and transmembrane protein N- glycosylation) were assessed for EV-loading by fusing them to

GFP. To assess N-glycosylation EV-loading, we used PTTG1IP, the smallest protein with annotated N-glycosylation PTMs in our dataset. The PTTG1IP EV-scaffold showed the highest EV-loading capacity of the constructs tested (~80% GFP^+ vesicles) (**Fig 5.1**). The SPRY domain also resulted in significant EV-enrichment, although to a lesser extent (~20% GFP^+ vesicles) (**Fig 5.1**). This is perhaps not surprising, since soluble proteins tend to be less effective at loading protein cargo to the EVs[259]. Conversely, MIT domain and PTAP motif did not promote GFP EV-enrichment. ESCRT-III interacts with several proteins involved in EV-membrane fission via the MIT-interacting domains[334], thus it is possible that by overexpressing the MIT domain we are interfering with EV-biogenesis. Banfer *et al*. reported that PTAP motif was required for galectin-3 EV-sorting in MDCK cells[75]. However, in our experimental conditions we were not able to detect increased EV-sorting using the PTAP motif. It is also possible that some of the tested features require the overexpression of additional proteins that mediate their EV-loading (e.g., PTAP motif may require overexpression of its binding partner ALIX).

PTTG1IP was shown to harbor two N-glycosylation sites at N54 (high mannose or hybrid N-glycosylation) and N45 (complex N-glycosylation), and its sorting to the EVs was highly dependent on N-glycosylation modification, with double glycosylation mutant showing less EV-loading than the single mutants (**Fig 5.2**). To determine that N-glycosylation impact on EV-sorting was not influenced by other factors such as protein folding or degradation, we assessed the intracellular location of WT PTTG1IP and PTTG1IP double mutant (2NQ). Given that PTTG1IP is mainly found on intracellular vesicular structures and that it is enriched in the EVs, we explored its co-localization with endosomal markers. Both WT and double N-glycosylation mutant were found in early, late and recycling endosomes, suggesting that the absence of N-glycosylation does not alter PTTG1IP localization. In addition, the cell expression levels of N-

glycosylation mutants were similar to the western blot (**Fig 5.2b, c**), suggesting that protein stability was not altered. These results suggest that the IPFA analysis that we developed, which indicated that N-glycosylation has a role in EV-sorting, can be useful to identify EV-enrichment associated PTMs. Glycan-dependent sorting of glycoproteins to specific cell locations is mediated by carbohydrate-binding proteins (i.e., lectins)[324]. Interestingly, members of the galectin protein family have been shown to bind β-galactoside sugars and regulate membrane glycoprotein organization and endocytosis[326,360,361], processes that are closely related to EV protein sorting.

However, PTTG1IP EV-sorting was not affected by N-acetyl-lactosamine (LacNAc) galectin inhibition (**Fig 5.4**). This result does not rule out a possible role of galectins in EV protein sorting since the affinity towards different types of glycosylation is variable among members of the galectin family[362], and not all galectins may influence protein trafficking in the same manner (i.e., different galectins may have opposite effects). Thus, it is possible that by inhibiting galectins non-specifically we are not able to observe the EV-sorting effect. A more precise approach could be knocking down specific galectins to assess their contribution to EV-loading individually.

Our results suggest that PTTG1IP trafficking to the endosomes is not affected by N-glycosylation (**Fig 5.3**). A possible hypothesis could be that N-glycosylation targets PTTG1IP towards EV-generating MVB whereas non-glycosylated PTTG1IP is directed towards non-productive endosomes. Alternatively, N-glycosylation may sort PTTG1IP to specific membrane microdomains in MVBs or plasma membrane that would eventually become intraluminal vesicles. In a similar way, N-glycosylation ablation of transmembrane protein CD133 (Prominin-1) did not affect its endosomal location despite showing reduced EV-loading[345].

5.5.2. EV-loading of PTTG1IP variants

PTTG1IP is a transmembrane protein ubiquitously expressed in normal human tissues[363]. PTTG1IP is conserved across a wide variety of animal species and does not share significant homology with other human proteins[364]. Initial studies on PTTG1IP function suggested a role in trafficking pituitary tumor-transforming gene 1 (PTTG) to the nucleus, where it induces tumorigenesis via different mechanisms including transcription activation and p53 destabilization[363,365]. However, subsequent studies have shown that PTTG1IP is primarily located on intracellular vesicles structures and not in the nucleus[364,366]. Both PTTG and PTTG1IP are upregulated in several types of cancer[367,368]. However, it has been shown that PTTG1IP has an independent transforming ability by inducing p53 degradation[369]. Nevertheless, PTTG1IP downregulation has been reported in lung cancer tissues[370] and has been associated with a higher risk of breast cancer death[371]. In addition, PTTG1IP overexpression was shown to inhibit proliferation in lung cancer cells[370].

To minimize the possible pro-oncogenic effects of PTTG1IP, we deleted the coiled coil region on PTTG1IP C-terminus (amino acids 130 – 164). This region contains the NLS bipartite signal that is required for its interaction with PTTG[363] as well as the potential p53 binding site[365]. We showed that PTTG1IP 130-164 deletion retained the EV-sorting capacity, suggesting that the deleted region is not important for EV-sorting (**Fig 5.6c,d**). Furthermore, PTTG1IP deletion variant was almost as potent as WT PTTG1IP scaffold when assessed for Cre delivery (**Fig 5.9 d,e**). Thus, indicating that it could be potentially used as a safer alternative to WT PTTG1IP for therapeutic application.

Mathieu *et al*. reported CD63 endocytosis signal (YXXφ) mutant was more abundantly released in the EVs than WT CD63[372]. This increase was due to a re-direction of CD63 from

being released in exosomes via MVB to being released in microvesicles originating from the plasma membrane. Thus, we mutated the two endocytosis signals on PTTG1IP (2YA mutant) to determine if EV-loading could be improved. In line with the previous study, PTTG1IP 2YA mutant was able to load two times more GFP per vesicle than WT PTTG1IP (**Fig 5.6c, d**). It is possible that the mechanism by which CD63 loading is increased also applies to PTTG1IP, although this hypothesis was not further explored.

5.5.3. EV-mediated delivery of PTTG1IP-Cre

To determine if PTTG1IP scaffolds could be used to functionally deliver EV-protein cargo, we assessed Cre packaging and delivery to reporter cells. To promote Cre release in the EVs, we used two different self-cleaving sequences from *Mycobacterium tuberculosis*[357] (intein sequence) and *Shewanella oneidensis*[358] (SC sequence) that have been reported to cleave at low pH conditions similar to those in the endosomal compartment. To mediate endosomal escape, we co-expressed VSVG in the EV-producing cells. We showed that PTTG1IP promoted EV-packaging of Cre and that cleavage by the intein sequence was much more efficient than with the SC sequence (**Fig. 5.7b**). Importantly, PTTG1IP was able to deliver Cre to a variety of reporter cell lines with high efficiency when intein was used as the release sequence (~85-99%) (**Fig 5.7e,f**, **Fig 5.9d,e**). PTTG1IP-intein-Cre, PTTG1IPDel-intein-Cre (deletion variant) and PTTG1IP-130-180aa-Cre variant (double cleavage sequence) were much more potent than CD63-intein-Cre in the two reporter cell lines tested, particularly PTTG1IP-intein-Cre and PTTG1IPDel-intein-Cre (**Table 5.5**, **Fig 5.9d, e**). The difference in potency between PTTG1IP and CD63 scaffolds may be partially explained by the higher EV-loading capacity of PTTG1IP as compared to CD63 (~30%) (**Fig 5.5**). However, a ~30% loading increase does not seem to enough to fully explain such a variation in potency. It is possible that PTTG1IP has a higher co-localization with VSVG

or that it somehow enhances EV uptake or endosomal escape. In line with previous studies[248,252,256], we did not detect Cre delivery in the absence of VSVG (**Fig 5.8**), thus indicating that endosomal escape is a key step limiting EV delivery. Moreover, efficient Cre delivery suggests that PTTG1IP and VSVG are found at overlapping EV subpopulations. However, this hypothesis should be assessed by single vesicle analysis or high-resolution microscopy techniques. Further studies should evaluate PTTG1IP-2YA variant functional delivery to determine if the higher EV-loading translates into a higher efficiency.

Notably, some degree of Cre cleavage was detected in the EVs from PTTG1IP-Cre fusion protein when no self-cleavage domain was present (**Fig 5.7b**). Although not as efficiently as PTTG1IP-intein-Cre, PTTG1IP-Cre also resulted in reporter cell activation (**Fig 5.7e, f**). This difference was most likely due to the lower cleavage rate when the intein was not present. Given that the size difference between Cre and Cre released from PTTG1IP construct, we speculated that the potential cleaving sequence resided between amino acids 130 – 180. Duplication of the potential cleaving sequence resulted in a two-fold Cre delivery improvement (**Fig 5.7e**, **Fig 5.9c**), suggesting that a cleavage site exists between amino acids 130-180 of PTTG1IP. Importantly, we also showed that the sequence could be applied to induce EV-cleavage in different protein contexts such as CD63 (**Fig 5.10**). We suspect that this sequence contains a cleavage site for an enzyme that cleaves predominantly in the EVs due to its intracellular location or pH requirements. Enzyme cleavage sites are usually >8 residues long, thus, further studies could focus on determining the minimal cleaving sequence in 130-180 PTTG1IP. Once identified, several repeats of the minimal site could be used to improve the cleavage activity. Similarly, potential harmful interactions with PTTG and p53 could be avoided by deletions of non-essential sequences at the PTTG1IP C terminus, since the binding sites have been reported locate at

PTTG1IP C-terminus[363]. PTTG1IP intrinsic cleavage sequence presents several advantages for future construct engineering. Firstly, as opposed to the intein sequence, which is derived from *Mycobacterium tuberculosis*, PTTG1IP cleavage sequence is human and thus most likely non-immunogenic. This may avoid B-cell response when EVs are generated externally by producer cells given that the sequence will be hidden inside the EVs, however if the EVs are to be produced endogenously *in situ* as previously shown[189,373], the expression of a bacterial peptide would most likely trigger an immune response towards the producer cells and its subsequent elimination, hampering its therapeutic application. *In situ* EV delivery consists in the production of therapeutic EVs by endogenous or implanted cells in the patient. This approach is particularly interesting for protein replacement therapies and for overcoming some of the main challenges of EV-based therapies such as the limited half-life of exosomes in circulation and the difficulty to reach the target tissues[143]. Secondly, PTTG1IP-Cre cleavage was only detected in the EVs while intein cleavage was detected in the cells. This is feature may also be valuable to prevent the protein cargo from having an effect on the EV-producer cells. Previous studies have relied on blue-light-/ small molecule-induced dimerization[253,256], or on the introduction of viral cleavable linkers from MLV[208] or HIV-1[267] to release protein cargo from the EV-loading scaffolds. However, these strategies present several issues. Conditional dimerization strategies are based on the production of EVs under blue light or the presence of a small molecule that promotes dimerization of the loading scaffold and the protein cargo. Hence, these strategies could not be applied to *in situ* EV therapies. Moreover, small molecules used to induce dimerization will also be delivered to recipient cells. Viral cleavable sequences require the expression of viral proteases in the donor cells, which besides being immunogenic may be packaged into EVs and delivered to

recipient cells. Hence, once optimized, PTTG1IP cleavage sequence would constitute a safer and more convenient alternative for EV-based therapies.

Assessment of EV-delivery is often a time-consuming process that involves generating large amounts of DNA and complex EV-isolation procedures. Unlike CD63-based scaffolds, the PTTG1IP-intein-Cre construct was potent enough to activate Cre reporter cells using conditioned media only (without the need to purify and concentrate EVs by SEC, **Fig 5.8**). This property could be exploited for optimizing EV-delivery conditions such as endosomal escape proteins/peptides, cargo release systems and additional PTTG1IP variants in a high throughput screening setting.

In vivo Cre delivery was demonstrated using EVs expressing PTTG1IP-intein-Cre and VSVG in mice harboring B16 reporter cell tumor xenografts (**Fig 5.10**). Recombination efficiency ranged from 40% to 90%, conversely, no activation was detected in mice treated with Cre and VSVG EVs, suggesting that active loading is required for Cre delivery. Notably, the high efficiency recombination levels detected by PCR were less apparent when assessed by immunohistochemistry since not all cells in the tumor xenograft express the reporter. Once injected, B16 cells proliferate during 10 days without selection pressure to form the tumors and therefore, some will lose the reporter expression.

Other studies have attempted Cre delivery with variable levels of success. The WW domain of E3 ubiquitin-protein ligase NEDD4 binds NDFIP1 (Nedd4 Family Interacting Protein 1) promoting its monoubiquitination and subsequent sorting into EVs[269]. Sterzenbach *et al*., exploited this mechanism to enhance EV-loading by fusing Cre to a WW domain and overexpressing NDFIP1 in the EV producer cells. Although this strategy resulted in reporter cell activation, efficiency was low (1%)[269]. In a separate study, co-expression of the myristylation

sequence derived from CHMP6 protein was used for Cre EV-loading and delivery to reporter cells *in vitro*[264]. Notably, in this case no endosomal escape fusion protein or membrane release system were required to achieve Cre activity since Cre was not fused to the myristoylation tag (the myristoylation tag fused to GFP was co-expressed with unmodified Cre). This differs from another study where a release system as well as VSVG were needed for delivery of protein cargo loaded by myristoylation[207]. Tetraspanins have also been assessed as EV scaffolds for Cre delivery. CD9 in combination with CIBN-CRY2 blue-light dimerization system was used for efficient *in vitro* and *in vivo* Cre delivery without the need of endosomal escape proteins[253]. Conversely, a different study using a CD9 and GFP-based dimerization platform showed minimal Cre delivery (2.9%) without VSVG[255]. Cre delivery was also achieved using CD81 and rapamycin induced dimerization release system. In the two studies where this strategy was tested, endosomolytic compounds[256] or fusion-competent VSVG were essential for functional EV-delivery[252]. VSVG has also been used directly as a scaffold for highly efficient *in vitro* Cre delivery using a split GFP complementation strategy[248].

5.5.4. EV-mediated delivery of Cas9 to reporter cells

We further explored the utility of PTTG1IP to deliver more complex macromolecules such as the CRISPR-Cas9 system. Due to its high efficiency and specificity, CRISPR-Cas9 has emerged as a powerful genome editing tool. However, its therapeutic potential is hampered by the lack of efficient delivery systems[296]. Given the complexity of CRISPR-Cas9 delivery, we first assessed EV-mediated delivery of Cas9 protein by expressing sgRNA in the recipient cells. To deliver Cas9, PTTG1IP was used as the EV-scaffold and the intein for protein release in the EVs. This strategy enabled the activation of ~10% of Cas9 reporter cells, while conventional transfection

of Cas9 and sgRNA resulted in ~20% activation (**Fig 5.12**). In line with Cre delivery results, PTTG1IP was two times more efficient in delivering Cas9 as compared to CD63 scaffold (Fig **5.14**). However, the difference in efficiency between PTTG1IP and CD63 was much more pronounced with Cre delivery. PTTG1IP-intein strategy was also able to deliver Cas9/sgRNA ribonucleoprotein complex to reporter cells, although the delivery efficiency was reduced as compared to Cas9 protein transfer alone.

Both Cas9 and Cas9/sgRNA delivery are complex processes involving two different components and thus a low delivery efficiency was expected. In addition, the sensitivity of the reporter cells was low, as observed by the activation levels after Cas9 and sgRNA transfection (**Fig 5.13**). Cas9 delivery requires binding of Cas9 to the sgRNA in the nucleus after the Cas9 is delivered into the cytosol, while for Cas9/sgRNA delivery the sgRNA must be exported from the nucleus to bind Cas9 in the cytoplasm before it is sorted to the EVs. sgRNA transport to the cytoplasm is likely to be very inefficient, since sgRNA lacks nuclear export signals. Hence, in order to optimize Cas9/sgRNA EV-delivery, further studies should focus on promoting sgRNA export from the nucleus. Moreover, efficiency of sgRNA sequence could be enhanced by extending the sgRNA duplex by 5 bp and mutating the TTTT stretch in the scaffold region to prevent premature transcription termination[374].

The CRISPR/Cas9 system can be delivered as DNA, mRNA, or as Cas9/sgRNA ribonucleoprotein complexes. Delivery of Cas9/sgRNA complex presents several advantages over DNA and mRNA delivery. Cas9/sgRNA complex delivery reduces off-target effects while maintaining high efficiency given that the functional complex is immediately available in the cell and is quickly degraded[268,375]. Recently, several studies have developed Cas9/sgRNA complex delivery platforms based on EVs. Initial studies required centrifugation of EVs (spinoculation)

and recipient cells to obtain functional delivery, which is not applicable for *in vivo* settings[254,311]. Several studies have developed platforms based on VLPs that resulted in high Cas9/sgRNA delivery efficiencies[207,267,268]. However, these methods rely on highly immunogenic proteins that limit their therapeutic use. The three VLP strategies utilized Gag as the scaffold protein and viral envelope proteins to induce endosomal escape. Viral proteases to promote Cas9 release from Gag (MLV[267] and HIV proteases[268]), and Tat protein[207] for active sgRNA loading were also used in some of the VLP studies. Wang *et al*., exploited the interaction between EV-enriched ARRDC1 (Arrestin Domain Containing 1) and WW domains for EV-loading. In that study, Cas9 was fused to WW domains to recruit Cas9/sgRNA complexes to the EVs via ARRDC1 interaction[155]. CD63 has also been used as a scaffold in combination with Cas9 release systems. CD63 was fused to GFP[250] or FP1[251] proteins, which bound to GFP or FP1 nanobodies fused to Cas9, respectively. Conversely, a different study fused the sgRNA to an aptamer and CD63 to an aptamer-binding protein to recruit Cas9 to the EVs via sgRNA binding[273]. Notably, in line with our study, efficiency was higher when CD63-scaffold was combined with VSVG. Other approaches were based on the addition of a myristoylation tag to Cas9. One of the studies utilizing myristoylation required VSVG, chloroquine, and polybrene reagent to achieve Cas9/sgRNA activation of reporter cells[265]. Conversely, the other myristoylation study by Fan *et al*., reported Cas9 delivery complex without the need of endosomal escape compounds or Cas9 release systems[264]. In another study, Zhang, *et al*. used VSVG as a scaffold in combination with a split GFP complementation system to successfully deliver Cas9/sgRNA complexes[248]. More recently, Cas9 myristoylation together with palmitoylation and blue-light induced CIBN-CRY2 dimerization was utilized by Osteikoetxea *et al*. to deliver Cas9/sgRNA complexes in cell culture with high efficiency without VSVG[255]. Notably, in this study the delivery efficiency was reduced

from ~40% to ~4% when LC-purified vesicles were used instead of UC-purified vesicles, exposing the importance of the EV isolation method on EV delivery. Intriguingly, myristoylation and palmitoylation was suggested by the authors to enhance endosomal escape, since using CD9 as the scaffold instead of the lipid tag resulted in no reporter activation despite similar Cas9 EV-loading levels[255]. Direct comparison of our study with other EV-based Cas9/sgRNA delivery studies is difficult given that the EV concentration and gene editing efficiency were not reported in most of the studies. Moreover, efficiency of EV delivery may depend on the EV isolation method, donor-recipient cell line combinations and reporter system.

The PTTG1IP-based platform offers several advantages over existing protein scaffolds for EV-delivery. We have demonstrated PTTG1IP is able to efficiently deliver protein cargo in cell culture and *in vivo.* EV-scaffolds based on tetraspanins, lipidic tags, VSVG, Gag, or ARRDC1 are not amenable for further engineering to display targeting or endosomal escape peptides on the EV surface. Hence a second scaffold that co-localizes with the first should be used for extracellular cargo loading, which would be notoriously difficult to accomplish due to vesicle heterogeneity. Unlike VSVG and Gag viral scaffolds, PTTG1IP would presumably be less immunogenic given that it is an endogenous protein. In addition, as compared to most single spanning proteins such as LAMP2B, PDGFR, or IGFS8 that have a lower EV-loading capacity than CD63[259,261], PTTG1IP is able to package protein cargoes with high efficiency. Recently, Dooley *et al*., identified single spanning protein PTFGRN as a highly EV-enriched protein that enables highly efficient protein surface display[246]. Although PTFGRN could potentially be used for delivery of intraluminal cargoes, this has not been proven yet. In contrast to scaffolds that rely on EV-surface association (i.e., CP05[235], C1C2[234], GPI-anchor[177] and GAPDH[192]), cargo molecules fused to PTTG1IP C-terminus are protected from degradation. The majority of studies,

including the present one, have evaluated EV-loading scaffolds in EVs derived from HEK293T cells. Thus, it would be important to determine how EV-scaffolds perform on EVs from different cell sources, especially for therapeutically relevant cell lines.

Nevertheless, the PTTG1IP-based platform presents several elements that would require further optimization to fully harness its potential. Most importantly, our system requires VSVG for functional delivery, thus future studies should evaluate human-derived fusogenic proteins to replace VSVG. The suitability of PTTG1IP to display targeting moieties on the EV surface should also be assessed in cell uptake experiments. Moreover, PTTG1IP cleavage sequence should be further developed to achieve cleavage levels similar to those of the intein.

5.6. Conclusions

We demonstrated that PTTG1IP EV-enrichment is dependent on its N-glycosylation status, validating our IPFA analysis (Results II). We have shown that PTTG1IP can be used as a scaffold to efficiently package protein cargoes. Importantly, we demonstrated highly efficient EV-mediated functional delivery of Cre protein to recipient cells and mice xenografts, as well as Cas9 and Cas9/sgRNA complex functional delivery to reporter cells. Moreover, we developed various PTTG1IP variants with improved properties for its therapeutic application. Thus, demonstrating that PTTG1IP is amenable to further engineering. Our findings also indicate that additional EV-modifications for membrane cargo release and endosomal escape (i.e. co-expression of VSVG) have a major impact on functional protein delivery. This chapter provides a proof-of-principle demonstration of the utility of PTTG1IP scaffold as a versatile platform for loading and delivering macromolecular cargoes.

6. Discussion and conclusions

6.1.1. Summary of main findings

The work presented in this thesis has explored novel strategies for EV-mediated functional delivery of protein and protein/RNA complexes with the potential for therapeutic applications.

In Chapter 3, we aimed to deliver dCas9-VPR/sgRNA complexes via EVs using UBL3 as an EV-sorting scaffold. UBL3 was previously found to be enriched in the EVs and was therefore a promising candidate for protein EV-loading[92]. We observed a large increase in dCas9-VPR and sgRNA sorting to the EVs when UBL3 was fused to dCas9-VPR as compared to passive loading. To avoid endosomal entrapment of the EV cargo and promote functional delivery, we co-expressed the fusogenic protein VSVG and assessed EV-delivery in the presence of an endosomal escape enhancing compound. However, we were not able to detect functional dCas9-VPR or dCas9-VPR/sgRNA complex delivery to reporter cells. In addition, single-vesicle analysis indicated that UBL3 and VSVG were predominantly found on mutually exclusive EV subpopulations, thus limiting the use of VSVG for enhancing EV uptake and endosomal escape of UBL3 EV-loaded cargo. We speculated that the lack of functional delivery was either due to inefficient EV uptake, or due to the inability of UBL3-fused dCas9-VPR to release from the EV membrane and reach the nucleus after EV uptake. Nevertheless, these findings led us to identify the main requirements for functional EV delivery and provided the motivation to search for alternative EV-sorting strategies that would enable efficient EV-loading, cargo release, and VSVG co-expression on the cargo-carrying vesicles.

UBL3 sorting into EVs is dependent on its association with the EV membrane via geranylgeranylation and palmitoylation PTMs. Therefore, we hypothesized that other protein features such as protein domains, motifs, or PTMs may exist that also promote EV-sorting. In Chapter 4, we developed a bioinformatics approach (i.e., IPFA analysis) to identify UniProt-annotated domains, motifs, and PTMs that were enriched in EVs in order to generate novel scaffolds for protein sorting into EVs. IPFA analysis enabled the identification of several EV-enriched annotated features. Notably, N-glycosylation was found to be the most prevalent EV-enriched annotation feature. This modification was primarily present on EV-enriched transmembrane proteins, suggesting a possible role of N-glycosylation in transmembrane protein sorting to EVs. Moreover, IPFA analysis identified various other PTMs that had been previously reported for EV-loading of therapeutic cargoes into the EVs, which further supports the validity this bioinformatics approach. The following features were selected for further analysis due to their applicability as EV-scaffolds; PTAP motif, SPRY domain, MIT domain, and N-glycosylation of transmembrane proteins.

In Chapter 5, we developed a novel platform for functional EV delivery based on the most efficient EV-loading scaffold identified with the IPFA analysis. Firstly, we assessed the capacity of the candidate features identified with the IPFA analysis to sort protein cargo to the EVs. In order to apply N-glycosylation for EV-loading of non-transmembrane protein cargoes, we used PTTG1IP, the smallest protein in our dataset with an N-glycosylation-annotated modification. The same strategy was applied for the MIT domain, while the PTAP motif and SPRY domains were directly used as EV-scaffolds. We observed that PTTG1IP had the highest EV loading capacity among all the tested features. In addition, EV-sorting efficiency of PTTG1IP was found to be higher than that of CD63, a tetraspanin commonly used for EV-sorting[225]. The IPFA

analysis has identified a wealth of potential features that could translate into EV-loading candidates with improved properties for therapeutic delivery. Our results also showed that N-glycosylation of PTTG1IP was essential for its packaging into EVs, further confirming the utility of IPFA analysis for the identification of EV-loading scaffolds. Interestingly, the ablation of PTTG1IP N-glycosylation did not affect protein stability or intracellular location, which was predominantly endosomal. Follow-up studies will address the mechanistic basis of PTTG1IP-mediated EV loading. Proximity labelling combined with mass spectrometry [352] could be used to identify possible protein mediators by comparing native PTTG1IP, and non-glycosylated PTTG1IP mutant binding partners. In addition, electron microscopy of MVBs from cells expressing non-glycosylated PTTG1IP mutant might be used to determine if N-glycosylation has an effect on PTTG1IP sorting to ILVs. Importantly, we demonstrated that PTTG1IP, in combination with a cargo release system and VSVG co-expression, could be used for highly efficient functional delivery of Cre protein to various cell lines *in vitro*, and *in vivo* to mouse tumor xenografts. We further demonstrated the utility of this platform by delivering more complex macromolecules such as Cas9/sgRNA to reporter cells. In addition, we also developed two PTTG1IP variants with improved EV-loading or diminished capacity to interact with p53, which showed that the PTTG1IP sequence is highly amenable to further protein engineering. Unexpectedly, PTTG1IP showed a certain degree of intrinsic cleavage activity which enabled protein cargo release only in the EVs. We took advantage of this property and generated a PTTG1IP variant in with this intrinsic cleavage activity was increased by including tandem repeats containing the putative cleavage site. We also demonstrated that the PTTG1IP intrinsic cleavage site could be applied in other protein contexts (i.e. CD63) for protein cargo release. PTTG1IP intrinsic cleavage sequence or a bacteria-derived intein (a self-cleaving sequence from

Mycobacterium tuberculosis) were successfully used as release systems for functional experiments, although the intein sequence showed a higher cleavage efficiency. The self-cleaving intein used in this study and other previously described cargo release systems are based on non-human sequences that may activate the immune system. Thus, the PTTG1IP cleavage sequence represents a potentially safer alternative for EV cargo release. Nevertheless, the requirement for VSVG co-expression poses a problem for the repeat dosing of EVs. It would be important to identify novel fusogenic proteins or peptides of human origin to replace VSVG and avoid compromising the low immunogenicity of EVs.

Notably, PTTG1IP-based scaffolds were found to be much more potent than CD63 for functional delivery of EV-loaded proteins. Recently, PTGFRN, BASP1, and myristoylation and palmitoylation tags have been reported to possess a higher EV-loading capacity than CD63[246,255]. Hence, efforts to further develop PTTG1IP-based scaffolds for therapeutic applications must necessarily be compared with other state-of-the-art approaches. Future studies should also investigate the ability of PTTG1IP variants to induce efficient *in vivo* delivery, since this was only demonstrated for native PTTG1IP using the intein as a cargo release system.

One of the main advantages of the utility of PTTG1IP as an EV-scaffold is that its extracellular domain could potentially be used for EV surface display (e.g., functional targeting moieties, fusogenic peptides or signaling proteins). Furthermore, PTTG1IP could be further engineered to optimize its utility for EV delivery. For example, future studies could test the effect of introducing additional N-glycosylation moieties on PTTG1IP to increase EV-loading efficiency.

In this study we demonstrated the utility of PTTG1IP for efficient functional EV-delivery. Nevertheless, transfer of EVs was tested in a limited number of recipient cell lines using EVs

derived from only a single producer cell line (HEK293T cells). Currently, MSCs are the preferred cell source for the production of EVs for therapeutic applications due to their safety profile and (in many cases) intrinsic anti-inflammatory properties[140]. Therefore, follow up studies should assess PTTG1IP EV-delivery efficiency using EVs from different cell sources, especially cell lines that are being used for therapeutic EV production such as MSCs. Along these lines, additional future work should also include the assessment of PTTG1IP-based platform for the delivery of disease relevant cargoes for therapeutic purposes.

In summary, we show that protein PTMs can be exploited to enhance functional cargo loading into EVs. The studies reported here underline the importance of EV uptake, EV cargo release, and endosomal escape enhancement for functional delivery and describe a highly versatile novel platform for EV-mediated delivery of protein and protein/sgRNA complexes based on PTTG1IP EV-scaffold.

6.2. Future prospects for EV-based therapeutics

The EV research field has seen remarkable growth over the past 20 years since the first studies reporting functional delivery of proteins and nucleic acids. The unique properties of EVs as delivery vehicles, such as their biocompatibility, cargo versatility, and capacity for engineering makes them attractive candidates for therapeutic applications. However, several key challenges remain in the effort to unlock their full potential.

As compared to synthetic nanocarriers, EV-based carriers contain a wide variety of molecules besides the therapeutic drug due to their natural complexity. Thus, a full characterization of the isolated EVs will be required to define their functional activity and effective dosage, and to avoid pleiotropic effects. In addition, EV heterogeneity will need to be taken into account when producing therapeutic EVs. Vesicle composition may vary according to the cell source and method of EV isolation, which may result in variable levels of functional EV subpopulations and may hinder the regulation of EV-based products.

In order to optimize EVs as therapeutic vehicles, it will be essential to understand the mechanisms by which specific EV subpopulations achieve efficient functional delivery and to identify the molecules responsible. This will include the study of (i) how EVs can traverse biological barriers, (ii) the tropism of specific EV subpopulations for different target tissues, and (iii) the mechanisms of EV uptake and endosomal escape for specific cell combinations where functional delivery is observed.

A vital step in the translation of EV therapeutics is the standardization of EV research. To this purpose, the International Society for Extracellular Vesicles (ISEV) has published guidelines for EV isolation and characterization methods[275]. Furthermore, the EV-TRACK database has

recently emerged to encourage the centralization of EV-related experiments in an effort to increase reproducibility and standardization of EV research[376]. Similarly, the development of standardized assays for determining EV efficiency will allow for the comparison between the various EV-delivery platforms in terms of potency.

Another major consideration is the selection of a cell source that is well characterized, produces EVs with a good safety profile, and allows for scalable EV production. Allogenic EVs derived from some MSC lines possess immunomodulatory properties and have been found to be safe in numerous clinical trials making them the preferred cell source for therapeutic EVs[377]. Alternatively, EVs can also be produced in an autologous manner by isolating the appropriate cells from patients and culturing them *ex vivo* for EV production. However, the time required for EV manufacturing and the associated costs are exceedingly high for most applications. An exception is the use of plasma derived EVs, which can be readily obtained from patient plasma and exogenously loaded with therapeutic cargo[378].

Although the capacity of native EVs to transfer nucleic acids and proteins has been demonstrated in many studies[25,379], the efficiency of functional EV delivery may not be as high as initially reported due to limited uptake by recipient cells and inefficient cytosolic release of EV contents[131,184,353]. Hence, the application of EVs as drug delivery vehicles may require additional optimization with regards to biodistribution, cargo loading, cytosolic delivery, and clearance by immune cells. Along these lines, in this study we have identified a novel EV scaffold that allows for highly efficient EV loading, cargo release and functional delivery in cell culture and *in vivo* which is based on PTTG1P.

The major advantages that differentiate EVs from other delivery vehicles such as synthetic nanoparticles and viral vectors are their low toxicity and immunogenicity. It is

therefore of utmost importance that the strategies applied for EV engineering do not alter the low immunogenicity of EVs, which would hamper repeat dosing. For example, with the use of non-human EV-loading scaffolds or cargo release systems, or with the co-expression of viral fusogenic proteins (e.g., VSVG). The EV scaffolds based on PTTG1IP as well as the intrinsic cleavage sequence for cargo release identified in this study have a human origin and therefore represent a safer alternative to viral based EV scaffolds or non-human cargo release systems. In addition, the expression of VSVG in cells has been reported to induce cytotoxicity, which may pose additional challenges to EV manufacturing[380]. Therefore, future studies should investigate alternative non-cytotoxic fusogenic proteins from human origin that enable the development of fully human EV delivery platforms.

Clinical translation of EVs will require scale-up of producer cell cultures and reliable EV-isolation methods that enable the production of sufficient quantities of EVs[381]. EV isolation methods that are typically employed in research lab settings, such as ultracentrifugation, are not suitable for processing large volumes of cell culture supernatant and often result in co-isolation of non-vesicular components. Methods based on tangential flow filtration and size-exclusion chromatography show promise in enabling the isolation of EVs from large volumes of culture media with reasonable purity and yield[275]. However, for the isolation of specific EV subpopulations or highly pure EV preparations, orthogonal methods based on affinity may be required at the expense of yield.

A promising therapeutic alternative approach is the *in situ* production of EVs, which would mimic native vesicle production and delivery. In this manner, EVs would be continuously secreted by the producer cells and would therefore avoid the need to manufacture large amounts of vesicles. This strategy was demonstrated by Kojima *et al*, who implanted EV producer cells

subcutaneously in Matrigel to successfully deliver EV-loaded mRNA to the brain[189]. Patient cells could also be harnessed as EV biofactories to expand the delivery of endogenously loaded EV-therapeutics. To achieve this, patient cells could be modified using conventional methods (e.g., AAV delivery) to produce engineered EVs that would deliver the therapeutic protein to cells in the surrounding tissue due to the generation of high local EV-concentrations. For example, this approach could be used to enhance the delivery of gene editing tools (e.g., CRISPR-Cas9, base editors, prime editors) to tissues with low transduction efficiencies.

Numerous clinical trials are currently underway for EV therapeutics[382], although no EV product has been approved by regulatory agencies yet. Nevertheless, clinical trials using non-engineered native EVs from different cell sources have shown that EVs are well tolerated and have a favorable safety profile[132]. Over the last few years, EV research has sparked interest from the pharmaceutical industry, which has resulted in a surge of companies focused on the development of EV therapeutics.

Companies including Aegle therapeutics, Capricor, Direct biologics and ExoPharm are currently conducting clinical trials for EV therapies based on unmodified naïve EVs. On the other hand, Codiak Biosciences has been the first to start clinical trials to investigate the use of engineered EV-based therapeutics. Their exoSTING platform is being evaluated in a phase I/II clinical trial (NCT04592484) for the treatment of solid tumors and preliminary findings have indicated tolerability and tumor shrinkage. exoSTING consists of EVs expressing PTGFRN on the EV surface which have been exogenously loaded with cyclic dinucleotide agonists of the STING (stimulator of interferon genes) pathway in the EV lumen[383]. The PTGFRN transmembrane protein has been shown to promote uptake by antigen presenting cells in the tumor microenvironment while STING agonists are able to induce an anti-tumor response[383].

Codiak has also initiated a phase I clinical trial for exoIL-12 which uses PTGFRN EV-scaffold to display pro-inflammatory IL-12 on the EV surface for the treatment of cutaneous T-cell lymphoma (NCT05156229)[271].

Recently, Codiak launched a phase I clinical trial for their third clinical candidate, exoASO-STAT6 for the treatment of patients with advanced hepatocellular carcinoma and patients with liver metastases (NCT05375604). This platform is based on PTGFRN expressing EVs exogenously loaded with lipid-modified antisense oligonucleotides targeting STAT6 on the EV surface[384]. STAT6 induces the repolarization of immunosuppressive tumor associated M2 macrophages towards immune stimulatory M1-like macrophages thus resulting in an anti-tumor effect[384]. Similar to the exoSTING platform, PTGFRN at the EV surface enhances uptake by macrophages[384].

ILIAS Biologics has also received approval from the Human Research Ethics Committee in Australia to initiate a Phase I clinical trial on ILB-202, an engineered exosome loaded with anti-inflammatory protein super-repressor lκB (srlκB) for the treatment of cardiac surgery-associated acute kidney injury (AKI). ILIAS has developed a platform for inducible cargo loading into the EVs based on CD9 protein scaffold fused to CIBN-CRY2 blue-light inducible dimerization system[253].

Likewise, other companies are on the verge of initiating clinical trials and are currently at late stages of preclinical development. EVOX therapeutics has a proprietary technology based on CD63 and a self-cleaving intein for cargo release (which has been used in the studies presented here). Their main focus is the development of EV-based enzyme replacement therapies for urea cycle disorders. In addition, they are engineering EVs to enhance siRNA delivery to the central nervous system for the treatment of neurodegenerative diseases. Another interesting approach

that is being explored by PureTech is the use of milk-derived EVs for oral administration of a variety of macromolecular cargoes including nucleic acids, peptides, and AAVs.

Despite the challenges ahead, preliminary data from clinical trials supports the suitability of EVs as delivery vehicles[382]. Issues such as in-depth EV characterization techniques, large-scale EV production and isolation, standardization of EV research, and EV engineering for enhanced delivery are currently being addressed. Through this collective effort it is likely that the clinical translation of EV therapeutics will become a reality in the near future.

7. References

1. Johnstone, R. M., Adam, M., Hammond, J. R., Orr, L. & Turbide, C. Vesicle formation during reticulocyte maturation. Association of plasma membrane activities with released vesicles (exosomes). *Journal of Biological Chemistry* **262**, 9412–9420 (1987).

2. Deatheragea, B. L. & Cooksona, B. T. Membrane vesicle release in bacteria, eukaryotes, and archaea: A conserved yet underappreciated aspect of microbial life. *Infection and Immunity* vol. 80 1948–1957 Preprint at https://doi.org/10.1128/IAI.06014-11 (2012).

3. Kalluri, R. & LeBleu, V. S. The biology, function, and biomedical applications of exosomes. *Science (1979)* **367**, (2020).

4. Colombo, M., Raposo, G. & Théry, C. Biogenesis, secretion, and intercellular interactions of exosomes and other extracellular vesicles. *Annu Rev Cell Dev Biol* **30**, 255–289 (2014).

5. Willms, E. *et al.* Cells release subpopulations of exosomes with distinct molecular and biological properties. *Sci Rep* **6**, 1–12 (2016).

6. Huang, G., Lin, G., Zhu, Y., Duan, W. & Jin, D. Emerging technologies for profiling extracellular vesicle heterogeneity. *Lab Chip* **20**, 2423–2437 (2020).

7. Ontoria-Oviedo, I. *et al.* Extracellular Vesicles Secreted by Hypoxic AC10 Cardiomyocytes Modulate Fibroblast Cell Motility. *Front Cardiovasc Med* **5**, 152 (2018).

8. Chargaff, E. Cell structure and the problem of blood coagulation. *Journal of Biological Chemistry* **160**, 351–359 (1945).

9. Chargaff, E. & West, R. The biological significance of the thromboplastic protein of blood. *Journal of Biological Chemistry* **166**, 189–197 (1946).

10. Wolf, P. The nature and significance of platelet products in human plasma. *Br J Haematol* **13**, 269–288 (1967).

11. Bonucci, E. Fine structure of early cartilage calcification. *J Ultrastruct Res* **20**, 33–50 (1967).

12. Anderson, H. C. Vesicles associated with calcification in the matrix of epiphyseal cartilage. *J Cell Biol* **41**, 59–72 (1969).

13. Aaronson, S., Behrens, U., Orner, R. & Haines, T. H. Ultrastructure of intracellular and extracellular vesicles, membranes, and myelin figures produced by Ochromonas danica. *J Ultrastruct Res* **35**, 418–430 (1971).

14. Nunez, E. A., Wallis, J. & Gershon, M. D. Secretory processes in follicular cells of the bat thyroid. 3. The occurrence of extracellular vesicles and colloid droplets during arousal from hibernation. *Am J Anat* **141**, 179–201 (1974).

15. Chigaleichik, A. G., Belova, L. A., Grishchenko, V. M. & Rylkin, S. S. Several properties of the extracellular vesicles of Candida tropicalis yeasts grown on n-alkanes. *Mikrobiologiia* **46**, 467–471 (1977).

16. Kappeli, O. & Finnerty, W. R. Partition of alkane by an extracellular vesicle derived from hexadecane-grown Acinetobacter. *J Bacteriol* **140**, 707–712 (1979).

17. Pan, B. T. & Johnstone, R. M. Fate of the transferrin receptor during maturation of sheep reticulocytes in vitro: selective externalization of the receptor. *Cell* **33**, 967–978 (1983).

18. Harding, C., Heuser, J. & Stahl, P. Receptor-mediated endocytosis of transferrin and recycling of the transferrin receptor in rat reticulocytes. *J Cell Biol* **97**, 329–339 (1983).

19. Johnstone, R. M., Mathew, A., Mason, A. B. & Teng, K. Exosome formation during maturation of mammalian and avian reticulocytes: evidence that exosome release is a major route for externalization of obsolete membrane proteins. *J Cell Physiol* **147**, 27–36 (1991).

20. Kagawa, H. *et al.* Expression of prothrombinase activity and CD9 antigen on the surface of small vesicles from stimulated human endothelial cells. *Thromb Res* **80**, 451–460 (1995).

21. Vidal, M. J. & Stahl, P. D. The small GTP-binding proteins Rab4 and ARF are associated with released exosomes during reticulocyte maturation. *Eur J Cell Biol* **60**, 261–267 (1993).

22. Raposo, G. *et al.* B lymphocytes secrete antigen-presenting vesicles. *J Exp Med* **183**, 1161–1172 (1996).

23. Zitvogel, L. *et al.* Eradication of established murine tumors using a novel cell-free vaccine: dendritic cell-derived exosomes. *Nat Med* **4**, 594–600 (1998).

24. Ratajczak, J. *et al.* Embryonic stem cell-derived microvesicles reprogram hematopoietic progenitors: evidence for horizontal transfer of mRNA and protein delivery. *Leukemia* **20**, 847–856 (2006).

25. Valadi, H. *et al.* Exosome-mediated transfer of mRNAs and microRNAs is a novel mechanism of genetic exchange between cells. *Nature Cell Biology 2007 9:6* **9**, 654–659 (2007).

26. Skog, J. *et al.* Glioblastoma microvesicles transport RNA and proteins that promote tumour growth and provide diagnostic biomarkers. *Nature Cell Biology 2008 10:12* **10**, 1470–1476 (2008).

27. Mathieu, M., Martin-Jaular, L., Lavieu, G. & Théry, C. Specificities of secretion and uptake of exosomes and other extracellular vesicles for cell-to-cell communication. *Nat Cell Biol* **21**, 9–17 (2019).

28. Caruso, S. & Poon, I. K. H. Apoptotic cell-derived extracellular vesicles: More than just debris. *Frontiers in Immunology* vol. 9 1486 Preprint at https://doi.org/10.3389/fimmu.2018.01486 (2018).

29. van Niel, G., D'Angelo, G. & Raposo, G. Shedding light on the cell biology of extracellular vesicles. *Nat Rev Mol Cell Biol* **19**, 213–228 (2018).

30. Witwer, K. W. & Théry, C. Extracellular vesicles or exosomes? On primacy, precision, and popularity influencing a choice of nomenclature. *J Extracell Vesicles* **8**, (2019).

31. Hurley, J. ESCRTs are everywhere. *Embo J* **34**, 2398–2407 (2015).

32. Banjade, S., Zhu, L., Jorgensen, J. R., Suzuki, S. W. & Emr, S. D. Recruitment and organization of ESCRT-0 and ubiquitinated cargo via condensation. *Sci Adv* **8**, 5149 (2022).

33. Marat, A. L. & Haucke, V. Phosphatidylinositol 3-phosphates—at the interface between cell signalling and membrane traffic. *EMBO J* **35**, 561 (2016).

34. Wenzel, E. M. *et al.* Concerted ESCRT and clathrin recruitment waves define the timing and morphology of intraluminal vesicle formation. *Nat Commun* **9**, (2018).

35. Lu, Q., Hope, L. W., Brasch, M., Reinhard, C. & Cohen, S. N. TSG101 interaction with HRS mediates endosomal trafficking and receptor down-regulation. *Proc Natl Acad Sci U S A* **100**, 7626–7631 (2003).

36. Boura, E. *et al.* Solution Structure of the ESCRT-I and -II Supercomplex: Implications for Membrane Budding and Scission. *Structure* **20**, 874 (2012).

37. Wollert, T., Wunder, C., Lippincott-Schwartz, J. & Hurley, J. H. Membrane scission by the ESCRT-III complex. *Nature* **458**, 172–177 (2009).

38. Saksena, S., Wahlman, J., Teis, D., Johnson, A. E. & Emr, S. D. Functional reconstitution of ESCRT-III assembly and disassembly. *Cell* **136**, 97–109 (2009).

39. Baietti, M. F. *et al.* Syndecan-syntenin-ALIX regulates the biogenesis of exosomes. *Nat Cell Biol* **14**, 677–685 (2012).

40. Larios, J., Mercier, V., Roux, A. & Gruenberg, J. ALIX- And ESCRT-III-dependent sorting of tetraspanins to exosomes. *Journal of Cell Biology* **219**, (2020).

41. Stuffers, S., Sem Wegner, C., Stenmark, H. & Brech, A. Multivesicular endosome biogenesis in the absence of ESCRTs. *Traffic* **10**, 925–937 (2009).

42. Trajkovic, K. *et al.* Ceramide triggers budding of exosome vesicles into multivesicular endosomes. *Science (1979)* **319**, 1244–1247 (2008).

43. Wei, D. *et al.* RAB31 marks and controls an ESCRT-independent exosome pathway. *Cell Research 2020 31:2* **31**, 157–177 (2020).

44. van Niel, G. *et al.* The tetraspanin CD63 regulates ESCRT-independent and -dependent endosomal sorting during melanogenesis. *Dev Cell* **21**, 708–721 (2011).

45. Chairoungdua, A., Smith, D. L., Pochard, P., Hull, M. & Caplan, M. J. Exosome release of β-catenin: a novel mechanism that antagonizes Wnt signaling. *J Cell Biol* **190**, 1079–1091 (2010).

46. Böker, K. O. *et al.* The Impact of the CD9 Tetraspanin on Lentivirus Infectivity and Exosome Secretion. *Molecular Therapy* **26**, 634–647 (2018).

47. Suárez, H. *et al.* CD9 inhibition reveals a functional connection of extracellular vesicle secretion with mitophagy in melanoma cells. *J Extracell Vesicles* **10**, (2021).

48. Umeda, R. *et al.* Structural insights into tetraspanin CD9 function. *Nature Communications 2020 11:1* **11**, 1–11 (2020).

49. Frolikova, M. *et al.* CD9 and CD81 Interactions and Their Structural Modelling in Sperm Prior to Fertilization. *Int J Mol Sci* **19**, (2018).

50. Toribio, V. & Yáñez-Mó, M. Tetraspanins interweave EV secretion, endosomal network dynamics and cellular metabolism. *Eur J Cell Biol* **101**, 151229 (2022).

51. Perrin, P. *et al.* Retrofusion of intralumenal MVB membranes parallels viral infection and coexists with exosome release. *Current Biology* **31**, 3884-3893.e4 (2021).

52. Villarroya-Beltri, C. *et al.* ISGylation controls exosome secretion by promoting lysosomal degradation of MVB proteins. *Nat Commun* **7**, (2016).

53. Majumder, P. & Chakrabarti, O. Mahogunin regulates fusion between amphisomes/MVBs and lysosomes via ubiquitination of TSG101. *Cell Death Dis* **6**, (2015).

54. Szatmári, Z. *et al.* Rab11 facilitates cross-talk between autophagy and endosomal pathway through regulation of Hook localization. *Mol Biol Cell* **25**, 522–531 (2014).

55. Bonifacino, J. S. & Neefjes, J. Moving and positioning the endolysosomal system. *Curr Opin Cell Biol* **47**, 1–8 (2017).

56. Mittelbrunn, M. *et al.* Unidirectional transfer of microRNA-loaded exosomes from T cells to antigen-presenting cells. *Nat Commun* **2**, (2011).

57. Wei, T., Hibino, H. & Omura, T. Release of Rice dwarf virus from insect vector cells involves secretory exosomes derived from multivesicular bodies. *Commun Integr Biol* **2**, 324–326 (2009).

58. Saito, N. *et al.* KIFC2 is a novel neuron-specific C-terminal type kinesin superfamily motor for dendritic transport of multivesicular body-like organelles. *Neuron* **18**, 425–438 (1997).

59. Ostrowski, M. *et al.* Rab27a and Rab27b control different steps of the exosome secretion pathway. *Nature Cell Biology 2010 12:1* **12**, 19–30 (2009).

60. Hoshino, D. *et al.* Exosome secretion is enhanced by invadopodia and drives invasive behavior. *Cell Rep* **5**, 1159–1168 (2013).

61. Savina, A., Fader, C. M., Damiani, M. T. & Colombo, M. I. Rab11 promotes docking and fusion of multivesicular bodies in a calcium-dependent manner. *Traffic* **6**, 131–143 (2005).

62. Hsu, C. *et al.* Regulation of exosome secretion by Rab35 and its GTPase-activating proteins TBC1D10A–C. *J Cell Biol* **189**, 223 (2010).

63. Hyenne, V. *et al.* RAL-1 controls multivesicular body biogenesis and exosome secretion. *J Cell Biol* **211**, 27–37 (2015).

64. Kowal, J., Tkach, M. & Théry, C. Biogenesis and secretion of exosomes. *Curr Opin Cell Biol* **29**, 116–125 (2014).

65. Fader, C. M., Sánchez, D. G., Mestre, M. B. & Colombo, M. I. TI-VAMP/VAMP7 and VAMP3/cellubrevin: two v-SNARE proteins involved in specific steps of the autophagy/multivesicular body pathways. *Biochim Biophys Acta* **1793**, 1901–1916 (2009).

66. Proux-Gillardeaux, V., Raposo, G., Irinopoulou, T. & Galli, T. Expression of the Longin domain of TI-VAMP impairs lysosomal secretion and epithelial cell migration. *Biol Cell* **99**, 261–271 (2007).

67. Koles, K. *et al.* Mechanism of evenness interrupted (Evi)-exosome release at synaptic boutons. *J Biol Chem* **287**, 16820–16834 (2012).

68. Wei, Y. *et al.* Pyruvate kinase type M2 promotes tumour cell exosome release via phosphorylating synaptosome-associated protein 23. *Nat Commun* **8**, (2017).

69. Gross, J. C., Chaudhary, V., Bartscherer, K. & Boutros, M. Active Wnt proteins are secreted on exosomes. *Nat Cell Biol* **14**, 1036–1045 (2012).

70. Muralidharan-Chari, V. *et al.* ARF6-regulated shedding of tumor-cell derived plasma membrane microvesicles. *Curr Biol* **19**, 1875 (2009).

71. Xu, P., Baldridge, R. D., Chi, R. J., Burd, C. G. & Graham, T. R. Phosphatidylserine flipping enhances membrane curvature and negative charge required for vesicular transport. *J Cell Biol* **202**, 875 (2013).

72. Thomas, L. M. & Salter, R. D. Activation of macrophages by P2X7-induced microvesicles from myeloid cells is mediated by phospholipids and is partially dependent on TLR4. *J Immunol* **185**, 3740–3749 (2010).

73. Wehman, A. M., Poggioli, C., Schweinsberg, P., Grant, B. D. & Nance, J. The P4-ATPase TAT-5 inhibits the budding of extracellular vesicles in C. elegans embryos. *Curr Biol* **21**, 1951–1959 (2011).

74. Nabhan, J. F., Hu, R., Oh, R. S., Cohen, S. N. & Lu, Q. Formation and release of arrestin domain-containing protein 1-mediated microvesicles (ARMMs) at plasma membrane by recruitment of TSG101 protein. *Proc Natl Acad Sci U S A* **109**, 4146–4151 (2012).

75. Bänfer, S. *et al.* Molecular mechanism to recruit galectin-3 into multivesicular bodies for polarized exosomal secretion. *Proc Natl Acad Sci U S A* **115**, E4396–E4405 (2018).

76. Erpapazoglou, Z. *et al.* A dual role for K63-linked ubiquitin chains in multivesicular body biogenesis and cargo sorting. *Mol Biol Cell* **23**, 2170 (2012).

77. Pashkova, N. *et al.* The Yeast Alix Homolog Bro1 Functions as a Ubiquitin Receptor for Protein Sorting into Multivesicular Endosomes. *Dev Cell* **25**, 520–533 (2013).

78. Dores, M. R., Grimsey, N. J., Mendez, F. & Trejo, J. A. ALIX Regulates the Ubiquitin-Independent Lysosomal Sorting of the P2Y1 Purinergic Receptor via a YPX3L Motif. *PLoS One* **11**, (2016).

79. Dores, M. R. *et al.* ALIX binds a YPX(3)L motif of the GPCR PAR1 and mediates ubiquitin-independent ESCRT-III/MVB sorting. *J Cell Biol* **197**, 407–419 (2012).

80. Doyotte, A., Mironov, A., McKenzie, E. & Woodman, P. The Bro1-related protein HD-PTP/PTPN23 is required for endosomal cargo sorting and multivesicular body morphogenesis. *Proc Natl Acad Sci U S A* **105**, 6308–6313 (2008).

81. Altan-Bonnet, N. Extracellular vesicles are the Trojan horses of viral infection. *Curr Opin Microbiol* **32**, 77–81 (2016).

82. Guix, F. X. *et al.* Tetraspanin 6: a pivotal protein of the multiple vesicular body determining exosome release and lysosomal degradation of amyloid precursor protein fragments. *Mol Neurodegener* **12**, (2017).

83. Buschow, S. I. *et al.* MHC II in dendritic cells is targeted to lysosomes or T cell-induced exosomes via distinct multivesicular body pathways. *Traffic* **10**, 1528–1542 (2009).

84. Odintsova, E. *et al.* Metastasis suppressor tetraspanin CD82/KAI1 regulates ubiquitylation of epidermal growth factor receptor. *J Biol Chem* **288**, 26323–26334 (2013).

85. Putz, U. *et al.* Nedd4 Family-interacting Protein 1 (Ndfip1) Is Required for the Exosomal Secretion of Nedd4 Family Proteins. *Journal of Biological Chemistry* **283**, 32621–32627 (2008).

86. Mackenzie, K. D. *et al.* Regulation of the divalent metal ion transporter via membrane budding. *Cell Discovery 2016 2:1* **2**, 1–14 (2016).

87. Leidal, A. M. & Debnath, J. Emerging roles for the autophagy machinery in extracellular vesicle biogenesis and secretion. *FASEB Bioadv* **3**, 377–386 (2021).

88. Sahu, R. *et al.* Microautophagy of Cytosolic Proteins by Late Endosomes. *Dev Cell* **20**, 131–139 (2011).

89. Babst, M., Katzmann, D. J., Estepa-Sabal, E. J., Meerloo, T. & Emr, S. D. Escrt-III: an endosome-associated heterooligomeric protein complex required for mvb sorting. *Dev Cell* **3**, 271–282 (2002).

90. Vidal, M. Exosomes and GPI-anchored proteins: Judicious pairs for investigating biomarkers from body fluids. *Adv Drug Deliv Rev* **161–162**, 110–123 (2020).

91. Luhtala, N., Aslanian, A., Yates, J. R. & Hunter, T. Secreted Glioblastoma Nanovesicles Contain Intracellular Signaling Proteins and Active Ras Incorporated in a Farnesylation-dependent Manner. *J Biol Chem* **292**, 611–628 (2017).

92. Nakamura, K., Kosaka, N., Nakatani, M., Uezumi, A. & Ide, T. UBL3 modification influences protein sorting to small extracellular vesicles. *Nat Commun* 1–3 (2018) doi:10.1038/s41467-018-06197-y.

93. Fabbiano, F. *et al.* RNA packaging into extracellular vesicles: An orchestra of RNA-binding proteins? *J Extracell Vesicles* **10**, e12043 (2020).

94. Janas, T., Janas, P., Sapoń, K. & Janas, T. Binding of RNA Aptamers to Membrane Lipid Rafts: Implications for Exosomal miRNAs Transfer from Cancer to Immune Cells. *International Journal of Molecular Sciences 2020, Vol. 21, Page 8503* **21**, 8503 (2020).

95. Dellar, E. R., Hill, C., Melling, G. E., Carter, D. R. F. & Baena-Lopez, L. A. Unpacking extracellular vesicles: RNA cargo loading and function. *Journal of Extracellular Biology* **1**, e40 (2022).

96. Villarroya-Beltri, C. *et al.* Sumoylated hnRNPA2B1 controls the sorting of miRNAs into exosomes through binding to specific motifs. *Nat Commun* **4**, 1–10 (2013).

97. Santangelo, L. *et al.* The RNA-Binding Protein SYNCRIP Is a Component of the Hepatocyte Exosomal Machinery Controlling MicroRNA Sorting. *Cell Rep* **17**, 799–808 (2016).

98. Kossinova, O. A. *et al.* Cytosolic YB-1 and NSUN2 are the only proteins recognizing specific motifs present in mRNAs enriched in exosomes. *Biochim Biophys Acta Proteins Proteom* **1865**, 664–673 (2017).

99. Tosar, J. P., Witwer, K. & Cayota, A. Revisiting extracellular RNA release, processing, and function. *Trends Biochem Sci* **46**, 438 (2021).

100. Perez-Hernandez, D. *et al.* The intracellular interactome of tetraspanin-enriched microdomains reveals their function as sorting machineries toward exosomes. *J Biol Chem* **288**, 11649–11661 (2013).

101. Leidal, A. M. & Debnath, J. LC3-dependent extracellular vesicle loading and secretion (LDELS). *Autophagy* **16**, 1162–1163 (2020).

102. Barman, B. *et al.* VAP-A and its binding partner CERT drive biogenesis of RNA-containing extracellular vesicles at ER membrane contact sites. *Dev Cell* **57**, 974-994.e8 (2022).

103. Jeppesen, D. K. *et al.* Reassessment of Exosome Composition. *Cell* **177**, 428-445.e18 (2019).

104. O'Brien, K., Ughetto, S., Mahjoum, S., Nair, A. v. & Breakefield, X. O. Uptake, functionality, and re-release of extracellular vesicle-encapsulated cargo. *Cell Rep* **39**, 110651 (2022).

105. Mulcahy, L. A., Pink, R. C. & Carter, D. R. F. Routes and mechanisms of extracellular vesicle uptake. *Journal of Extracellular Vesicles* vol. 3 Preprint at https://doi.org/10.3402/jev.v3.24641 (2014).

106. Kalluri, R. & LeBleu, V. S. The biology , function , and biomedical applications of exosomes. *Science* **367**, (2020).

107. Charrin, S., Jouannet, S., Boucheix, C. & Rubinstein, E. Tetraspanins at a glance. *J Cell Sci* **127**, 3641–3648 (2014).

108. Näslund, T. I. *et al.* Exosomes from breast milk inhibit HIV-1 infection of dendritic cells and subsequent viral transfer to CD4+ T cells. *AIDS* **28**, 171–180 (2014).

109. Yuan, P. *et al.* Neural Stem Cell-Derived Exosomes Regulate Neural Stem Cell Differentiation Through miR-9-Hes1 Axis. *Front Cell Dev Biol* **9**, 1181 (2021).

110. Barile, L. *et al.* Extracellular vesicles from human cardiac progenitor cells inhibit cardiomyocyte apoptosis and improve cardiac function after myocardial infarction. *Cardiovasc Res* **103**, 530–541 (2014).

111. Barile, L., Moccetti, T., Marbán, E. & Vassalli, G. Roles of exosomes in cardioprotection. *Eur Heart J* **38**, 1372–1379 (2017).

112. Gray, W. D. *et al.* Identification of therapeutic covariant microRNA clusters in hypoxia-treated cardiac progenitor cell exosomes using systems biology. *Circ Res* **116**, 255–263 (2015).

113. Montecalvo, A. *et al.* Exosomes As a Short-Range Mechanism to Spread Alloantigen between Dendritic Cells during T Cell Allorecognition. *The Journal of Immunology* **180**, 3081–3090 (2008).

114. Cheng, Y. & Schorey, J. S. Exosomes carrying mycobacterial antigens can protect mice against Mycobacterium tuberculosis infection. *Eur J Immunol* **43**, 3279–3290 (2013).

115. Keller, M. D. *et al.* Decoy exosomes provide protection against bacterial toxins. *Nature 2020 579:7798* **579**, 260–264 (2020).

116. Delorme-Axford, E. *et al.* Human placental trophoblasts confer viral resistance to recipient cells. *Proc Natl Acad Sci U S A* **110**, 12048–12053 (2013).

117. Dai, J. *et al.* Exosomes: key players in cancer and potential therapeutic strategy. *Signal Transduction and Targeted Therapy 2020 5:1* **5**, 1–10 (2020).

118. Clayton, A., Al-Taei, S., Webber, J., Mason, M. D. & Tabi, Z. Cancer Exosomes Express CD39 and CD73, Which Suppress T Cells through Adenosine Production. *The Journal of Immunology* **187**, 676–683 (2011).

119. Abusamra, A. J. *et al.* Tumor exosomes expressing Fas ligand mediate CD8+ T-cell apoptosis. *Blood Cells Mol Dis* **35**, 169–173 (2005).

120. Ding, G. *et al.* Pancreatic cancer-derived exosomes transfer miRNAs to dendritic cells and inhibit RFXAP expression via miR-212-3p. *Oncotarget* **6**, 29877–29888 (2015).

121. Chen, G. *et al.* Exosomal PD-L1 contributes to immunosuppression and is associated with anti-PD-1 response. *Nature* **560**, 382–386 (2018).

122. Lundy, S. K., Taitano, S. H. & van der Vlugt, L. E. P. M. Characterization and Activation of Fas Ligand-Producing Mouse B Cells and Their Killer Exosomes. *Methods Mol Biol* **2270**, 149–178 (2021).

123. Takeuchi, T. Pathogenic and protective roles of extracellular vesicles in neurodegenerative diseases. *J Biochem* **169**, 181–186 (2021).

124. Yu, H. *et al.* Potential Roles of Exosomes in Parkinson's Disease: From Pathogenesis, Diagnosis, and Treatment to Prognosis. *Front Cell Dev Biol* **8**, (2020).

125. Sverdlov, E. D. Amedeo Avogadro's cry: What is 1 μg of exosomes? *BioEssays* **34**, 873–875 (2012).

126. Piffoux, M., Volatron, J., Silva, A. K. A. & Gazeau, F. Thinking Quantitatively of RNA-Based Information Transfer via Extracellular Vesicles: Lessons to Learn for the Design of RNA-Loaded EVs. *Pharmaceutics 2021, Vol. 13, Page 1931* **13**, 1931 (2021).

127. Whittaker, T. E., Nagelkerke, A., Nele, V., Kauscher, U. & Stevens, M. M. Experimental artefacts can lead to misattribution of bioactivity from soluble mesenchymal stem cell paracrine factors to extracellular vesicles. *J Extracell Vesicles* **9**, (2020).

128. Wittrup, A. *et al.* Visualizing lipid-formulated siRNA release from endosomes and target gene knockdown. *Nat Biotechnol* **33**, 870–876 (2015).

129. Gilleron, J. *et al.* Image-based analysis of lipid nanoparticle–mediated siRNA delivery, intracellular trafficking and endosomal escape. *Nature Biotechnology 2013 31:7* **31**, 638–646 (2013).

130. Brown, B. D. *et al.* Endogenous microRNA can be broadly exploited to regulate transgene expression according to tissue, lineage and differentiation state. *Nature Biotechnology 2007 25:12* **25**, 1457–1467 (2007).

131. Albanese, M. *et al.* MicroRNAs are minor constituents of extracellular vesicles that are rarely delivered to target cells. *PLoS Genet* **17**, (2021).

132. Wiklander, O. P. B., Brennan, M., Lötvall, J., Breakefield, X. O. & Andaloussi, S. E. L. Advances in therapeutic applications of extracellular vesicles. *Sci Transl Med* **11**, (2019).

133. Lai, R. C. *et al.* Exosome secreted by MSC reduces myocardial ischemia/reperfusion injury. *Stem Cell Res* **4**, 214–222 (2010).

134. Mendt, M., Rezvani, K. & Shpall, E. Mesenchymal stem cell-derived exosomes for clinical use. *Bone Marrow Transplantation* vol. 54 789–792 Preprint at https://doi.org/10.1038/s41409-019-0616-z (2019).

135. Yin, K., Wang, S. & Zhao, R. C. Exosomes from mesenchymal stem/stromal cells: A new therapeutic paradigm. *Biomarker Research* vol. 7 8 Preprint at https://doi.org/10.1186/s40364-019-0159-x (2019).

136. Nargesi, A. A., Lerman, L. O. & Eirin, A. Mesenchymal Stem Cell-derived Extracellular Vesicles for Renal Repair. *Curr Gene Ther* **17**, 29 (2017).

137. Bang, O. Y. & Kim, E. H. Mesenchymal Stem Cell-Derived Extracellular Vesicle Therapy for Stroke: Challenges and Progress. *Front Neurol* **10**, 211 (2019).

138. Tan, C. Y. *et al.* Mesenchymal stem cell-derived exosomes promote hepatic regeneration in drug-induced liver injury models. *Stem Cell Res Ther* **5**, (2014).

139. Lou, G., Chen, Z., Zheng, M. & Liu, Y. Mesenchymal stem cell-derived exosomes as a new therapeutic strategy for liver diseases. *Experimental and Molecular Medicine* vol. 49 Preprint at https://doi.org/10.1038/emm.2017.63 (2017).

140. Kordelas, L. *et al.* MSC-derived exosomes: A novel tool to treat therapy-refractory graft-versus-host disease. *Leukemia* vol. 28 970–973 Preprint at https://doi.org/10.1038/leu.2014.41 (2014).

141. Nassar, W. *et al.* Umbilical cord mesenchymal stem cells derived extracellular vesicles can safely ameliorate the progression of chronic kidney diseases. *Biomater Res* **20**, (2016).

142. Gowen, A., Shahjin, F., Chand, S., Odegaard, K. E. & Yelamanchili, S. v. Mesenchymal Stem Cell-Derived Extracellular Vesicles: Challenges in Clinical Applications. *Frontiers in Cell and Developmental Biology* vol. 8 149 Preprint at https://doi.org/10.3389/fcell.2020.00149 (2020).

143. Melling, G. E., Carollo, E., Conlon, R., Simpson, J. C. & Carter, D. R. F. The Challenges and Possibilities of Extracellular Vesicles as Therapeutic Vehicles. *European Journal of Pharmaceutics and Biopharmaceutics* **144**, 50–56 (2019).

144. Vader, P., Mol, E. A., Pasterkamp, G. & Schiffelers, R. M. Extracellular vesicles for drug delivery. *Adv Drug Deliv Rev* **106**, 148–156 (2016).

145. Tian, Y. *et al.* A doxorubicin delivery platform using engineered natural membrane vesicle exosomes for targeted tumor therapy. *Biomaterials* **35**, 2383–2390 (2014).

146. Sun, D. *et al.* A novel nanoparticle drug delivery system: The anti-inflammatory activity of curcumin is enhanced when encapsulated in exosomes. *Molecular Therapy* **18**, 1606–1614 (2010).

147. Saari, H. *et al.* Microvesicle- and exosome-mediated drug delivery enhances the cytotoxicity of Paclitaxel in autologous prostate cancer cells. *Journal of Controlled Release* **220**, 727–737 (2015).

148. Mulvihill, J. J. *et al.* Drug delivery across the blood-brain barrier: Recent advances in the use of nanocarriers. *Nanomedicine* **15**, 205–214 (2020).

149. Alvarez-Erviti, L. *et al.* Delivery of siRNA to the mouse brain by systemic injection of targeted exosomes. *Nat Biotechnol* **29**, 341–345 (2011).

150. Yang, T. *et al.* Exosome delivered anticancer drugs across the blood-brain barrier for brain cancer therapy in Danio Rerio. *Pharm Res* **32**, 2003–2014 (2015).

151. Chakraborty, C., Sharma, A. R., Sharma, G., Doss, C. G. P. & Lee, S. S. Therapeutic miRNA and siRNA: Moving from Bench to Clinic as Next Generation Medicine. *Molecular Therapy - Nucleic Acids* vol. 8 132–143 Preprint at https://doi.org/10.1016/j.omtn.2017.06.005 (2017).

152. Hu, B. *et al.* Therapeutic siRNA: state of the art. *Signal Transduction and Targeted Therapy* vol. 5 1–25 Preprint at https://doi.org/10.1038/s41392-020-0207-x (2020).

153. Roberts, T. C., Langer, R. & Wood, M. J. A. Advances in oligonucleotide drug delivery. *Nature Reviews Drug Discovery* 1–22 Preprint at https://doi.org/10.1038/s41573-020-0075-7 (2020).

154. Jiang, L., Vader, P. & Schiffelers, R. M. Extracellular vesicles for nucleic acid delivery: Progress and prospects for safe RNA-based gene therapy. *Gene Ther* **24**, 157–166 (2017).

155. Wang, Q. *et al.* ARMMs as a versatile platform for intracellular delivery of macromolecules. *Nat Commun* 1–7 doi:10.1038/s41467-018-03390-x.

156. Erkan, E. P. *et al.* Extracellular vesicle-mediated suicide mRNA/protein delivery inhibits glioblastoma tumor growth in vivo. *Cancer Gene Ther* **24**, 38–44 (2017).

157. Conceição, M. *et al.* Engineered extracellular vesicle decoy receptor-mediated modulation of the IL6 trans-signalling pathway in muscle. *Biomaterials* **266**, 120435 (2021).

158. Kuate, S., Cinatl, J., Doerr, H. W. & Überla, K. Exosomal vaccines containing the S protein of the SARS coronavirus induce high levels of neutralizing antibodies. *Virology* **362**, 26–37 (2007).

159. Lai, C. P. *et al.* Dynamic biodistribution of extracellular vesicles in vivo using a multimodal imaging reporter. *ACS Nano* **8**, 483–494 (2014).

160. Gupta, D. *et al.* Quantification of extracellular vesicles in vitro and in vivo using sensitive bioluminescence imaging. *J Extracell Vesicles* **9**, (2020).

161. Driedonks, T. *et al.* Pharmacokinetics and biodistribution of extracellular vesicles administered intravenously and intranasally to Macaca nemestrina. *bioRxiv* 2021.07.28.454192 (2021) doi:10.1101/2021.07.28.454192.

162. Wiklander, O. P. B. *et al.* Extracellular vesicle in vivo biodistribution is determined by cell source, route of administration and targeting. *J Extracell Vesicles* **4**, 1–13 (2015).

163. Kamerkar, S. *et al.* Exosomes facilitate therapeutic targeting of oncogenic KRAS in pancreatic cancer. *Nature* **546**, 498–503 (2017).

164. Kooijmans, S. A. A. *et al.* PEGylated and targeted extracellular vesicles display enhanced cell specificity and circulation time. *Journal of Controlled Release* **224**, 77–85 (2016).

165. Mima, Y., Hashimoto, Y., Shimizu, T., Kiwada, H. & Ishida, T. Anti-PEG IgM Is a Major Contributor to the Accelerated Blood Clearance of Polyethylene Glycol-Conjugated Protein. *Mol Pharm* **12**, 2429–2435 (2015).

166. Matsumoto, J. *et al.* Transmission of α-synuclein-containing erythrocyte-derived extracellular vesicles across the blood-brain barrier via adsorptive mediated transcytosis: another mechanism for initiation and progression of Parkinson's disease? *Acta Neuropathol Commun* **5**, 71 (2017).

167. Hoshino, A. *et al.* Tumour exosome integrins determine organotropic metastasis. *Nature* **527**, 329–335 (2015).

168. Rana, S., Yue, S., Stadel, D. & Zöller, M. Toward tailored exosomes: The exosomal tetraspanin web contributes to target cell selection. *International Journal of Biochemistry and Cell Biology* **44**, 1574–1584 (2012).

169. Kumar, P. *et al.* Transvascular delivery of small interfering RNA to the central nervous system. *Nature* **448**, 39–43 (2007).

170. Wang, H. *et al.* Exosome-Mediated miR-29 Transfer Reduces Muscle Atrophy and Kidney Fibrosis in Mice. *Molecular Therapy* **27**, 571–583 (2019).

171. Sugahara, K. N. *et al.* Tissue-Penetrating Delivery of Compounds and Nanoparticles into Tumors. *Cancer Cell* **16**, 510–520 (2009).

172. Teesalu, T., Sugahara, K. N., Kotamraju, V. R. & Ruoslahti, E. C-end rule peptides mediate neuropilin-1-dependent cell, vascular, and tissue penetration. *Proc Natl Acad Sci U S A* **106**, 16157–16162 (2009).

173. Ohno, S. I. *et al.* Systemically injected exosomes targeted to EGFR deliver antitumor microrna to breast cancer cells. *Molecular Therapy* **21**, 185–191 (2013).

174. Mentkowski, K. I. & Lang, J. K. Exosomes Engineered to Express a Cardiomyocyte Binding Peptide Demonstrate Improved Cardiac Retention in Vivo. *Sci Rep* **9**, 1–13 (2019).

175. Kim, H. *et al.* Cardiac-specific delivery by cardiac tissue-targeting peptide-expressing exosomes. *Biochem Biophys Res Commun* **499**, 803–808 (2018).

176. Kooijmans, S. A. A., Gitz-Francois, J. J. J. M., Schiffelers, R. M. & Vader, P. Recombinant phosphatidylserine-binding nanobodies for targeting of extracellular vesicles to tumor cells: A plug-and-play approach. *Nanoscale* **10**, 2413–2426 (2018).

177. Kooijmans, S. A. A. *et al.* Display of GPI-anchored anti-EGFR nanobodies on extracellular vesicles promotes tumour cell targeting. *J Extracell Vesicles* **5**, (2016).

178. Wang, J. H. *et al.* Anti-HER2 scFv-directed extracellular vesicle-mediated mRNA-based gene delivery inhibits growth of HER2-positive human breast tumor xenografts by prodrug activation. *Mol Cancer Ther* **17**, 1133 (2018).

179. Smyth, T. *et al.* Surface functionalization of exosomes using click chemistry. *Bioconjug Chem* **25**, 1777–1784 (2014).

180. Lee, J. *et al.* Cellular Engineering with Membrane Fusogenic Liposomes to Produce Functionalized Extracellular Vesicles. *ACS Appl Mater Interfaces* **8**, 6790–6795 (2016).

181. Hoffman, J. A. *et al.* Progressive vascular changes in a transgenic mouse model of squamous cell carcinoma. *Cancer Cell* **4**, 383–391 (2003).

182. Antes, T. J. *et al.* Targeting extracellular vesicles to injured tissue using membrane cloaking and surface display. *J Nanobiotechnology* **16**, 61 (2018).

183. Fernández, M., Javaid, F. & Chudasama, V. Advances in targeting the folate receptor in the treatment/imaging of cancers. *Chemical Science* vol. 9 790–810 Preprint at https://doi.org/10.1039/c7sc04004k (2018).

184. Bonsergent, E. *et al.* Quantitative characterization of extracellular vesicle uptake and content delivery within mammalian cells. *Nature Communications 2021 12:1* **12**, 1–11 (2021).

185. Heusermann, W. *et al.* Exosomes surf on filopodia to enter cells at endocytic hot spots, traffic within endosomes, and are targeted to the ER. *Journal of Cell Biology* **213**, 173–184 (2016).

186. Hyenne, V. *et al.* Studying the Fate of Tumor Extracellular Vesicles at High Spatiotemporal Resolution Using the Zebrafish Embryo. *Dev Cell* **48**, 554-572.e7 (2019).

187. Joshi, B. S., de Beer, M. A., Giepmans, B. N. G. & Zuhorn, I. S. Endocytosis of Extracellular Vesicles and Release of Their Cargo from Endosomes. *ACS Nano* **14**, 4444–4455 (2020).

188. Soares, A. R. *et al.* Gap junctional protein Cx43 is involved in the communication between extracellular vesicles and mammalian cells. *Scientific Reports 2015 5:1* **5**, 1–14 (2015).

189. Kojima, R. *et al.* Designer exosomes produced by implanted cells intracerebrally deliver therapeutic cargo for Parkinson's disease treatment. *Nat Commun* **9**, 1–10 (2018).

190. Smith, S. A., Selby, L. I., Johnston, A. P. R. & Such, G. K. The Endosomal Escape of Nanoparticles: Toward More Efficient Cellular Delivery. *Bioconjug Chem* **30**, 263–272 (2019).

191. Varkouhi, A. K., Scholte, M., Storm, G. & Haisma, H. J. Endosomal escape pathways for delivery of biologicals. *Journal of Controlled Release* **151**, 220–228 (2011).

192. Dar, G. H. *et al.* GAPDH controls extracellular vesicle biogenesis and enhances therapeutic potential of EVs in silencing the Huntingtin gene in mice via siRNA delivery. *bioRxiv* 2020.01.09.899880 (2020) doi:10.1101/2020.01.09.899880.

193. Futaki, S. *et al.* Arginine-rich peptides. An abundant source of membrane-permeable peptides having potential as carriers for intracellular protein delivery. *Journal of Biological Chemistry* **276**, 5836–5840 (2001).

194. Nakase, I. *et al.* Cellular uptake of arginine-rich peptides: Roles for macropinocytosis and actin rearrangement. *Molecular Therapy* **10**, 1011–1022 (2004).

195. Hong M. Moulton, *, Michelle H. Nelson, Susie A. Hatlevig, Muralimohan T. Reddy, and & Iversen, P. L. Cellular Uptake of Antisense Morpholino Oligomers Conjugated to Arginine-Rich Peptides. (2004) doi:10.1021/BC034221G.

196. Zorko, M. & Langel, Ü. Cell-penetrating peptides: Mechanism and kinetics of cargo delivery. *Advanced Drug Delivery Reviews* vol. 57 529–545 Preprint at https://doi.org/10.1016/j.addr.2004.10.010 (2005).

197. Nakase, I. *et al.* Arginine-rich cell-penetrating peptide-modified extracellular vesicles for active macropinocytosis induction and efficient intracellular delivery. *Sci Rep* **7**, 1–11 (2017).

198. Nakase, I. & Futaki, S. Combined treatment with a pH-sensitive fusogenic peptide and cationic lipids achieves enhanced cytosolic delivery of exosomes. *Sci Rep* **5**, (2015).

199. Nakase, I., Osaki, K., Tanaka, G., Utani, A. & Futaki, S. Molecular interplays involved in the cellular uptake of octaarginine on cell surfaces and the importance of syndecan-4 cytoplasmic v domain for the activation of protein kinase Cα. *Biochem Biophys Res Commun* **446**, 857–862 (2014).

200. Li, W., Nicol, F. & Szoka, F. C. GALA: A designed synthetic pH-responsive amphipathic peptide with applications in drug and gene delivery. *Adv Drug Deliv Rev* **56**, 967–985 (2004).

201. Yang, Y. *et al.* Virus-Mimetic Fusogenic Exosomes for Direct Delivery of Integral Membrane Proteins to Target Cell Membranes. *Advanced Materials* **29**, 1605604 (2017).

202. Meyer, C. *et al.* Pseudotyping exosomes for enhanced protein delivery in mammalian cells. *Int J Nanomedicine* **12**, 3153–3170 (2017).

203. Mangeot, P. E. *et al.* Protein transfer into human cells by vsv-g-induced nanovesicles. *Molecular Therapy* **19**, 1656–1666 (2011).

204. Breakefield, X. O., Frederickson, R. M. & Simpson, R. J. Gesicles: Microvesicle cookies for transient information transfer between cells. *Molecular Therapy* **19**, 1574–1576 (2011).

205. Finkelshtein, D., Werman, A., Novick, D., Barak, S. & Rubinstein, M. LDL receptor and its family members serve as the cellular receptors for vesicular stomatitis virus. *Proc Natl Acad Sci U S A* **110**, 7306–7311 (2013).

206. Ci, Y., Yang, Y., Xu, C. & Shi, L. Vesicular stomatitis virus G protein transmembrane region is crucial for the hemi-fusion to full fusion transition. *Scientific Reports 2018 8:1* **8**, 1–11 (2018).

207. Gee, P. *et al.* Extracellular nanovesicles for packaging of CRISPR-Cas9 protein and sgRNA to induce therapeutic exon skipping. *Nat Commun* 4–20 (2020) doi:10.1038/s41467-020-14957-y.

208. Gutierrez-Guerrero, A. *et al.* Baboon Envelope Pseudotyped "Nanoblades" Carrying Cas9/gRNA Complexes Allow Efficient Genome Editing in Human T, B, and CD34+ Cells and Knock-in of AAV6-Encoded Donor DNA in CD34+ Cells. *Front Genome Ed* **0**, 3 (2021).

209. Marin, M., Tailor, C. S., Nouri, A. & Kabat, D. Sodium-Dependent Neutral Amino Acid Transporter Type 1 Is an Auxiliary Receptor for Baboon Endogenous Retrovirus. *J Virol* **74**, 8085 (2000).

210. Segel, M. *et al.* Mammalian retrovirus-like protein PEG10 packages its own mRNA and can be pseudotyped for mRNA delivery. *Science* **373**, 882–889 (2021).

211. Piffoux, M. *et al.* Engineering and loading therapeutic extracellular vesicles for clinical translation: A data reporting frame for comparability. *Adv Drug Deliv Rev* **178**, 113972 (2021).

212. Pascucci, L. *et al.* Paclitaxel is incorporated by mesenchymal stromal cells and released in exosomes that inhibit in vitro tumor growth: a new approach for drug delivery. *J Control Release* **192**, 262–270 (2014).

213. Zhuang, X. *et al.* Treatment of brain inflammatory diseases by delivering exosome encapsulated anti-inflammatory drugs from the nasal region to the brain. *Mol Ther* **19**, 1769–1779 (2011).

214. Han, Y. *et al.* Overview and Update on Methods for Cargo Loading into Extracellular Vesicles. *Processes 2021, Vol. 9, Page 356* **9**, 356 (2021).

215. Loughlin, A. J. O., Woffindale, C. A. & Wood, M. J. A. Exosomes and the Emerging Field of Exosome-Based Gene Therapy. *Curr Gene Ther* 262–274 (2012).

216. Nizamudeen, Z. A. *et al.* Low-power sonication can alter extracellular vesicle size and properties. *Cells* **10**, (2021).

217. Lamichhane, T. N., Raiker, R. S. & Jay, S. M. Exogenous DNA loading into extracellular vesicles via electroporation is size-dependent and enables limited gene delivery. *Mol Pharm* **12**, 3650–3657 (2015).

218. Heiser, W. C. Optimizing electroporation conditions for the transformation of mammalian cells. *Methods Mol Biol* **130**, 117–134 (2000).

219. Rankin-Turner, S. *et al.* A call for the standardised reporting of factors affecting the exogenous loading of extracellular vesicles with therapeutic cargos. *Adv Drug Deliv Rev* **173**, 479–491 (2021).

220. Usman, W. M. *et al.* Efficient RNA drug delivery using red blood cell extracellular vesicles. *Nature Communications 2018 9:1* **9**, 1–15 (2018).

221. Kooijmans, S. A. A. *et al.* Electroporation-induced siRNA precipitation obscures the efficiency of siRNA loading into extracellular vesicles. *J Control Release* **172**, 229–238 (2013).

222. Johnsen, K. B. *et al.* Evaluation of electroporation-induced adverse effects on adipose-derived stem cell exosomes. *Cytotechnology* **68**, 2125–2138 (2016).

223. Jang, S. C. *et al.* Bioinspired exosome-mimetic nanovesicles for targeted delivery of chemotherapeutics to malignant tumors. *ACS Nano* **7**, 7698–7710 (2013).

224. Gangadaran, P. & Ahn, B. C. Extracellular Vesicle- and Extracellular Vesicle Mimetics-Based Drug Delivery Systems: New Perspectives, Challenges, and Clinical Developments. *Pharmaceutics* **12**, (2020).

225. Fu, S., Wang, Y., Xia, X. & Zheng, J. C. Exosome engineering: Current progress in cargo loading and targeted delivery. *NanoImpact* **20**, 100261 (2020).

226. Haney, M. J. *et al.* Exosomes as drug delivery vehicles for Parkinson's disease therapy. *Journal of Controlled Release* **207**, 18–30 (2015).

227. Seow, Y., Alvarez, L. & Wood, M. J. Targeted Delivery of Plasmid DNA and siRNA with Modified Dendritic Cell-Derived Exosomes. *Chemical And Molecular Conjugates* **17**, S7 (2009).

228. Shtam, T. A. *et al.* Exosomes are natural carriers of exogenous siRNA to human cells in vitro. *Cell Communication and Signaling* **11**, 1–10 (2013).

229. Zhupanyn, P. *et al.* Extracellular vesicle (ECV)-modified polyethylenimine (PEI) complexes for enhanced siRNA delivery in vitro and in vivo. *Journal of Controlled Release* **319**, 63–76 (2020).

230. Jeyaram, A. *et al.* Enhanced Loading of Functional miRNA Cargo via pH Gradient Modification of Extracellular Vesicles. *Molecular Therapy* **28**, 975–985 (2020).

231. Sato, Y. T. *et al.* Engineering hybrid exosomes by membrane fusion with liposomes. *Scientific Reports 2016 6:1* **6**, 1–11 (2016).

232. Piffoux, M., Silva, A. K. A., Wilhelm, C., Gazeau, F. & Tareste, D. Modification of Extracellular Vesicles by Fusion with Liposomes for the Design of Personalized Biogenic Drug Delivery Systems. *ACS Nano* **12**, 6830–6842 (2018).

233. Di, H. *et al.* General Approach to Engineering Extracellular Vesicles for Biomedical Analysis. *Anal Chem* **91**, 12752–12759 (2019).

234. Shi, J., Heegaard, C. W., Rasmussen, J. T. & Gilbert, G. E. Lactadherin binds selectively to membranes containing phosphatidyl-L-serine and increased curvature. *Biochim Biophys Acta Biomembr* **1667**, 82–90 (2004).

235. Gao, X. *et al.* Anchor peptide captures, targets, and loads exosomes of diverse origins for diagnostics and therapy. *Sci Transl Med* **10**, (2018).

236. van Lenten, B. J. *et al.* Apolipoprotein A-I mimetic peptides. *Current atherosclerosis reports* vol. 11 52–57 Preprint at https://doi.org/10.1007/s11883-009-0008-8 (2009).

237. Ye, Z. *et al.* Methotrexate-Loaded Extracellular Vesicles Functionalized with Therapeutic and Targeted Peptides for the Treatment of Glioblastoma Multiforme. *ACS Appl Mater Interfaces* **10**, 12341–12350 (2018).

238. Law, B., Quinti, L., Choi, Y., Weissleder, R. & Tung, C.-H. A mitochondrial targeted fusion peptide exhibits remarkable cytotoxicity. (2006) doi:10.1158/1535-7163.MCT-05-0509.

239. Masliah, E. & Spencer, B. Applications of ApoB LDLR-binding domain approach for the development of CNS-penetrating peptides for Alzheimer'Ss disease. *Methods in Molecular Biology* **1324**, 331–337 (2015).

240. Fike, J. R. *et al.* Low-density lipoprotein receptor expression in human glioblastoma. *International Journal of Radiation Oncology*Biology*Physics* **57**, S371–S372 (2003).

241. Wang, T. *et al.* Exosome-Mediated Delivery of the Neuroprotective Peptide PACAP38 Promotes Retinal Ganglion Cell Survival and Axon Regeneration in Rats With Traumatic Optic Neuropathy. *Front Cell Dev Biol* **9**, (2021).

242. Dong, X. *et al.* Exosome-mediated delivery of an anti-angiogenic peptide inhibits pathological retinal angiogenesis. *Theranostics* **11**, 5107–5126 (2021).

243. Guo, Y. *et al.* Ultrasound triggered topical delivery of Bmp7 mRNA for white fat browning induction via engineered smart exosomes. *J Nanobiotechnology* **19**, 1–13 (2021).

244. Wan, S. *et al.* Molecular Recognition-Based DNA Nanoassemblies on the Surfaces of Nanosized Exosomes. *J Am Chem Soc* **139**, 5289–5292 (2017).

245. Sutaria, D. S. *et al.* Low active loading of cargo into engineered extracellular vesicles results in inefficient miRNA mimic delivery. *J Extracell Vesicles* **6**, 1333882 (2017).

246. Dooley, K. *et al.* A versatile platform for generating engineered extracellular vesicles with defined therapeutic properties. *Molecular Therapy* **29**, 1729–1743 (2021).

247. Campbell, L. A. *et al.* Gesicle-Mediated Delivery of CRISPR / Cas9 Ribonucleoprotein Complex for Inactivating the HIV Provirus. *Molecular Therapy* **27**, 1–13 (2019).

248. Zhang, X. *et al.* Programmable Extracellular Vesicles for Macromolecule Delivery and Genome Modifications. *Dev Cell* **55**, 784-801.e9 (2020).

249. Yao, X. *et al.* Engineered extracellular vesicles as versatile ribonucleoprotein delivery vehicles for efficient and safe CRISPR genome editing. *J Extracell Vesicles* (2021) doi:10.1002/jev2.12076.

250. Ye, Y. *et al.* An engineered exosome for delivering sgRNA:Cas9 ribonucleoprotein complex and genome editing in recipient cells. *Biomater Sci* (2020) doi:10.1039/d0bm00427h.

251. Ye, Y. *et al.* In Vivo Visualized Tracking of Tumor-Derived Extracellular Vesicles Using CRISPR-Cas9 System. *Technology in Cancer Research and Treatment* vol. 21 Preprint at https://doi.org/10.1177/15330338221085370 (2022).

252. Somiya, M. & Kuroda, S. Engineering of extracellular vesicles for small molecule-regulated cargo loading and cytoplasmic delivery of bioactive proteins. *Mol Pharm* **xxx**, xxx–xxx (2022).

253. Yim, N. *et al.* Exosome engineering for efficient intracellular delivery of soluble proteins using optically reversible protein-protein interaction module. *Nat Commun* **7**, 1–9 (2016).

254. Li, Z. *et al.* In Vitro and in Vivo RNA Inhibition by CD9-HuR Functionalized Exosomes Encapsulated with miRNA or CRISPR/dCas9. *Nanoletters* **19**, 19–28 (2019).

255. Osteikoetxea, X. *et al.* Engineered Cas9 extracellular vesicles as a novel gene editing tool. *Journal of extracellular vesicles* vol. 11 e12225 Preprint at https://doi.org/10.1002/jev2.12225 (2022).

256. Heath, N., Osteikoetxea, X., Oliveria, T. M. de & Elisa, L. Endosomal escape enhancing compounds facilitate functional delivery of extracellular vesicle cargo. *Nanomedicine* **293**, 2799–2814 (2019).

257. Dreja, H. & Piechaczyk, M. The effects of N-terminal insertion into VSV-G of an scFv peptide. *Virol J* **3**, 1–8 (2006).

258. Dalton, K. P. & Rose, J. K. Vesicular stomatitis virus glycoprotein containing the entire green fluorescent protein on its cytoplasmic domain is incorporated efficiently into virus particles. *Virology* **279**, 414–421 (2001).

259. Corso, G. *et al.* Systematic characterization of extracellular vesicles sorting domains and quantification at the single molecule–single vesicle level by fluorescence correlation spectroscopy and single particle imaging. *J Extracell Vesicles* **8**, (2019).

260. Gupta, D. *et al.* Amelioration of systemic inflammation via the display of two different decoy protein receptors on extracellular vesicles. *Nat Biomed Eng* **5**, 1084–1098 (2021).

261. Silva, A. M. *et al.* Quantification of protein cargo loading into engineered extracellular vesicles at single-vesicle and single-molecule resolution. *J Extracell Vesicles* **10**, (2021).

262. Huang, L., Gu, N., Zhang, X. E. & Wang, D. B. Light-Inducible Exosome-Based Vehicle for Endogenous RNA Loading and Delivery to Leukemia Cells. *Adv Funct Mater* **29**, 1807189 (2019).

263. Lainšček, D., Lebar, T. & Jerala, R. Transcription activator-like effector-mediated regulation of gene expression based on the inducible packaging and delivery via designed extracellular vesicles. *Biochem Biophys Res Commun* **484**, 15–20 (2017).

264. Fan, J. *et al.* A peptide derived from the N-terminus of charged multivesicular body protein 6 (CHMP6) promotes the secretion of gene editing proteins via small extracellular vesicle production. *Bioengineered* **13**, 4702–4716 (2022).

265. Whitley, J. A. *et al.* Encapsulating Cas9 into extracellular vesicles by protein myristoylation. *J Extracell Vesicles* **11**, e12196 (2022).

266. Sette, P., Nagashima, K., Piper, R. C. & Bouamr, F. Ubiquitin conjugation to Gag is essential for ESCRT-mediated HIV-1 budding. *Retrovirology* **10**, 1–18 (2013).

267. Mangeot, P. E. *et al.* Genome editing in primary cells and in vivo using viral-derived Nanoblades loaded with Cas9-sgRNA ribonucleoproteins. *Nat Commun* 1–15 (2019) doi:10.1038/s41467-018-07845-z.

268. Hamilton, J. R. *et al.* Targeted delivery of CRISPR-Cas9 and transgenes enables complex immune cell engineering. *Cell Rep* **35**, 109207 (2021).

269. Sterzenbach, U. *et al.* Engineered Exosomes as Vehicles for Biologically Active Proteins. *Molecular Therapy* **25**, 1269 (2017).

270. Rauch, S. & Martin-Serrano, J. Multiple Interactions between the ESCRT Machinery and Arrestin-Related Proteins: Implications for PPXY-Dependent Budding. *J Virol* **85**, 3546–3556 (2011).

271. Lewis, N. D. *et al.* Exosome surface display of IL12 results in tumor-retained pharmacology with superior potency and limited systemic exposure compared with recombinant IL12. *Mol Cancer Ther* **20**, 523–534 (2021).

272. Hung, M. E. & Leonard, J. N. A platform for actively loading cargo RNA to elucidate limiting steps in EV-mediated delivery. *J Extracell Vesicles* **5**, (2016).

273. Yao, X. *et al.* Engineered extracellular vesicles as versatile ribonucleoprotein delivery vehicles for efficient and safe CRISPR genome editing. *J Extracell Vesicles* **10**, (2021).

274. Cheng, Y. & Schorey, J. S. Targeting soluble proteins to exosomes using a ubiquitin tag. *Biotechnol Bioeng* **113**, 1315–1324 (2016).

275. Théry, C. *et al.* Minimal information for studies of extracellular vesicles 2018 (MISEV2018): a position statement of the International Society for Extracellular Vesicles and update of the MISEV2014 guidelines. *J Extracell Vesicles* **7**, (2018).

276. Royo, F., Théry, C., Falcón-Pérez, J. M., Nieuwland, R. & Witwer, K. W. Methods for Separation and Characterization of Extracellular Vesicles: Results of a Worldwide Survey Performed by the ISEV Rigor and Standardization Subcommittee. *Cells 2020, Vol. 9, Page 1955* **9**, 1955 (2020).

277. Konoshenko, M. Y., Lekchnov, E. A., Vlassov, A. v. & Laktionov, P. P. Isolation of Extracellular Vesicles: General Methodologies and Latest Trends. *Biomed Res Int* **2018**, (2018).

278. Théry, C., Amigorena, S., Raposo, G. & Clayton, A. Isolation and Characterization of Exosomes from Cell Culture Supernatants and Biological Fluids. *Curr Protoc Cell Biol* **30**, (2006).

279. Bobrie, A., Colombo, M., Krumeich, S., Raposo, G. & Théry, C. Diverse subpopulations of vesicles secreted by different intracellular mechanisms are present in exosome preparations obtained by differential ultracentrifugation. *J Extracell Vesicles* **1**, (2012).

280. Jeppesen, D. K. *et al.* Comparative analysis of discrete exosome fractions obtained by differential centrifugation. *J Extracell Vesicles* **3**, (2014).

281. Linares, R., Tan, S., Gounou, C., Arraud, N. & Brisson, A. R. High-speed centrifugation induces aggregation of extracellular vesicles. *https://doi.org/10.3402/jev.v4.29509* **4**, (2015).

282. Auber, M., Fröhlich, D., Drechsel, O., Karaulanov, E. & Krämer-Albers, E. M. Serum-free media supplements carry miRNAs that co-purify with extracellular vesicles. *J Extracell Vesicles* **8**, 1656042 (2019).

283. Tauro, B. J. *et al.* Comparison of ultracentrifugation, density gradient separation, and immunoaffinity capture methods for isolating human colon cancer cell line LIM1863-derived exosomes. *Methods* **56**, 293–304 (2012).

284. Nordin, J. Z. *et al.* Ultrafiltration with size-exclusion liquid chromatography for high yield isolation of extracellular vesicles preserving intact biophysical and functional properties. *Nanomedicine* **11**, 879–883 (2015).

285. Benedikter, B. J. *et al.* Ultrafiltration combined with size exclusion chromatography efficiently isolates extracellular vesicles from cell culture media for compositional and functional studies. *Sci Rep* **7**, (2017).

286. Gupta, S. *et al.* An improvised one-step sucrose cushion ultracentrifugation method for exosome isolation from culture supernatants of mesenchymal stem cells. *Stem Cell Res Ther* **9**, 1–11 (2018).

287. Busatto, S. *et al.* Tangential Flow Filtration for Highly Efficient Concentration of Extracellular Vesicles from Large Volumes of Fluid. *Cells* **7**, (2018).

288. Carnino, J. M., Lee, H. & Jin, Y. Isolation and characterization of extracellular vesicles from Broncho-Alveolar lavage fluid: A review and comparison of different methods. *Respir Res* **20**, 1–11 (2019).

289. Deregibus, M. C. *et al.* Charge-based precipitation of extracellular vesicles. *Int J Mol Med* **38**, 1359–1366 (2016).

290. Brownlee, Z., Lynn, K. D., Thorpe, P. E. & Schroit, A. J. A novel 'salting-out' procedure for the isolation of tumor-derived exosomes. *J Immunol Methods* **407**, 120–126 (2014).

291. Liangsupree, T., Multia, E. & Riekkola, M. L. Modern isolation and separation techniques for extracellular vesicles. *J Chromatogr A* **1636**, (2021).

292. Ramirez, M. I. *et al.* Technical challenges of working with extracellular vesicles. *Nanoscale* **10**, 881–906 (2018).

293. Ying, W. *et al.* Adipose Tissue Macrophage-Derived Exosomal miRNAs Can Modulate In Vivo and In Vitro Insulin Sensitivity. *Cell* **171**, 372-384.e12 (2017).

294. Turchinovich, A., Tonevitsky, A. G. & Burwinkel, B. Extracellular miRNA: A Collision of Two Paradigms. *Trends Biochem Sci* **41**, 883–892 (2016).

295. Coenen-Stass, A. M. L. *et al.* Extracellular microRNAs exhibit sequence-dependent stability and cellular release kinetics. *RNA Biol* **16**, 696–706 (2019).

296. Modell, A. E., Lim, D., Nguyen, T. M., Sreekanth, V. & Choudhary, A. CRISPR-based therapeutics: current challenges and future applications. *Trends Pharmacol Sci* **43**, 151–161 (2022).

297. Min, S. *et al.* Cancer-derived exosomes as a delivery platform of CRISPR / Cas9 confer cancer cell tropism-dependent targeting. *Journal of Controlled Release* **266**, 8–16 (2017).

298. Lin, Y. *et al.* Exosome – Liposome Hybrid Nanoparticles Deliver CRISPR / Cas9 System in MSCs. *Advanced Science* **1700611**, 1–9 (2018).

299. Anand, S. *et al.* Arrestin-Domain Containing Protein 1 (Arrdc1) Regulates the Protein Cargo and Release of Extracellular Vesicles. *Proteomics* **18**, 1–16 (2018).

300. Chen, R. *et al.* Friend or Foe? Evidence Indicates Endogenous Exosomes Can Deliver Functional gRNA and Cas9 Protein. *Small* **1902686**, 1–13 (2019).

301. Clemmens, H. & Lambert, D. W. Extracellular vesicles: Translational challenges and opportunities. *Biochem Soc Trans* **46**, 1073–1082 (2018).

302. Chevillet, J. R. *et al.* Quantitative and stoichiometric analysis of the microRNA content of exosomes. *PNAS* **111**, (2014).

303. Meister, G. Argonaute proteins: functional insights and emerging roles. *Nature Reviews Genetics 2013 14:7* **14**, 447–459 (2013).

304. Zeelenberg, I. S. *et al.* Targeting Tumor Antigens to Secreted Membrane Vesicles In vivo Induces Efficient Antitumor Immune Responses. *Cancer Res* 1228–1236 (2008) doi:10.1158/0008-5472.CAN-07-3163.

305. Sork, H. *et al.* Heterogeneity and interplay of the extracellular vesicle small RNA transcriptome and proteome. *Sci Rep* **8**, (2018).

306. Wiegand, D. J., Ter-ovanesyan, D., Braff, J. L. & Davidsohn, N. Highly-efficient Cas9-mediated transcriptional programming Alejandro. *Nat Methods* **12**, 326–328 (2015).

307. Dowil, R. T., Lu, X., Saracco, S. A., Vierstra, R. D. & Downes, B. P. Arabidopsis Membrane-anchored Ubiquitin-fold (MUB) Proteins Localize a Specific Subset of Ubiquitin-conjugating (E2) Enzymes to the Plasma Membrane. *J Biol Chem* **286**, 14913–14921 (2011).

308. Doudna, J. A. & Charpentier, E. The new frontier of genome engineering with CRISPR-Cas9. *Science (1979)* **346**, 1258096–1258096 (2014).

309. Gao, G., Wei, Y., Li, L., He, Z. & Wei, X. Challenges in CRISPR / CAS9 Delivery: Potential Roles of Nonviral Vectors. *Hum Gene Ther* **26**, 452–462 (2015).

310. Resh, M. D. Covalent Lipid Modifications of Proteins. *Current Biology* **23**, (2014).

311. Montagna, C. *et al.* VSV-G-Enveloped Vesicles for Traceless Delivery of CRISPR-Cas9. *Mol Ther Nucleic Acids* **12**, 453–462 (2018).

312. Lainscek, D. *et al.* Delivery of an Artificial Transcription Regulator dCas9-VPR by Extracellular Vesicles for Therapeutic Gene Activation. *ACS Synth Biol* (2018) doi:10.1021/acssynbio.8b00192.

313. Villarroya-Beltri, C., Baixauli, F., Gutiérrez-Vázquez, C., Sánchez-Madrid, F. & Mittelbrunn, M. Sorting it out: Regulation of exosome loading. *Semin Cancer Biol* **28**, 3–13 (2014).

314. Ageta, H. & Tsuchida, K. Post -translational modification and protein sorting to small extracellular vesicles including exosomes by ubiquitin and UBLs. *Cellular and Molecular Life Sciences* (2019) doi:10.1007/s00018-019-03246-7.

315. Dilley, K. A., Gregory, D., Johnson, M. C. & Vogt, V. M. An LYPSL late domain in the gag protein contributes to the efficient release and replication of Rous sarcoma virus. *J Virol* **84**, 6276–6287 (2010).

316. VerPlank, L. *et al.* Tsg101, a homologue of ubiquitin-conjugating (E2) enzymes, binds the L domain in HIV type 1 Pr55(Gag). *Proc Natl Acad Sci U S A* **98**, 7724–7729 (2001).

317. Ka, F. L., Baron, R., Ali, B. R., Magee, A. I. & Seabra, M. C. Rab GTPases containing a CAAX motif are processed post-geranylgeranylation by proteolysis and methylation. *J Biol Chem* **282**, 1487–1497 (2007).

318. Ohtsubo, K. & Marth, J. D. Glycosylation in cellular mechanisms of health and disease. *Cell* **126**, 855–867 (2006).

319. Teng, F. & Fussenegger, M. Shedding Light on Extracellular Vesicle Biogenesis and Bioengineering. *Advanced Science* **8**, 2003505 (2021).

320. Moreno-Gonzalo, O., Fernandez-Delgado, I. & Sanchez-Madrid, F. Post-translational add-ons mark the path in exosomal protein sorting. *Cellular and Molecular Life Sciences* **75**, 1–19 (2018).

321. Moreno-Gonzalo, O., Villarroya-Beltri, C. & Sánchez-Madrid, F. Post-translational modifications of exosomal proteins. *Front Immunol* **5**, 383 (2014).

322. Apweiler, R., Hermjakob, H. & Sharon, N. On the frequency of protein glycosylation, as deduced from analysis of the SWISS-PROT database. *Biochimica et Biophysica Acta (BBA) - General Subjects* **1473**, 4–8 (1999).

323. Williams, C. *et al.* Glycosylation of extracellular vesicles: current knowledge, tools and clinical perspectives. *J Extracell Vesicles* **7**, (2018).

324. Ghazarian, H., Idoni, B. & Oppenheimer, S. B. A glycobiology review: carbohydrates, lectins, and implications in cancer therapeutics. *Acta Histochem* **113**, 236 (2011).

325. Bänfer, S. & Jacob, R. Galectins in Intra- and Extracellular Vesicles. *Biomolecules* **10**, 1–12 (2020).

326. Delacour, D., Koch, A., Jacob, R. & Jacob, R. The Role of Galectins in Protein Trafficking. *Traffic* **10**, 1405–1413 (2009).

327. Shen, B., Wu, N., Yang, M. & Gould, S. J. Protein targeting to exosomes/microvesicles by plasma membrane anchors. *Journal of Biological Chemistry* **286**, 14383–14395 (2011).

328. Bateman, A. *et al.* UniProt: the universal protein knowledgebase in 2021. *Nucleic Acids Res* **49**, D480–D489 (2021).

329. Lee, Y. X. F., Johansson, H., Wood, M. J. A. & el Andaloussi, S. Considerations and Implications in the Purification of Extracellular Vesicles – A Cautionary Tale. *Front Neurosci* **13**, 1067 (2019).

330. Pavani, K. C. *et al.* The Separation and Characterization of Extracellular Vesicles from Medium Conditioned by Bovine Embryos. *International Journal of Molecular Sciences 2020, Vol. 21, Page 2942* **21**, 2942 (2020).

331. Ruoslahti, E. RGD and other recognition sequences for integrins. *Annu Rev Cell Dev Biol* **12**, 697–715 (1996).

332. Pathak, E. Analysis of correlated mutations in Ras G-domain. *Bioinformation* **13**, 174 (2017).

333. Zhen, Y. & Stenmark, H. Cellular functions of Rab GTPases at a glance. *J Cell Sci* **128**, 3171–3176 (2015).

334. Hurley, J. H. & Yang, D. MIT Domainia. *Dev Cell* **14**, 6–8 (2008).

335. D'Cruz, A. A., Babon, J. J., Norton, R. S., Nicola, N. A. & Nicholson, S. E. Structure and function of the SPRY/B30.2 domain proteins involved in innate immunity. *Protein Science* **22**, 1–10 (2013).

336. Fehon, R. G., McClatchey, A. I. & Bretscher, A. Organizing the cell cortex: the role of ERM proteins. *Nature Reviews Molecular Cell Biology 2010 11:4* **11**, 276–287 (2010).

337. Claridge, B., Kastaniegaard, K., Stensballe, A. & Greening, D. W. Post-translational and transcriptional dynamics–regulating extracellular vesicle biology. *Expert Rev Proteomics* **16**, 17–31 (2019).

338. Jiang, H. *et al.* Protein Lipidation: Occurrence, Mechanisms, Biological Functions, and Enabling Technologies. *Chem Rev* **118**, 919–988 (2018).

339. Stenmark, H., Pe, D. & Pen, M. A. An Isoprenylation and Palmitoylation Motif Promotes Intraluminal Vesicle An Isoprenylation and Palmitoylation Motif Promotes Intraluminal Vesicle Delivery of Proteins in Cells from Distant Species. *PLoS One* (2014) doi:10.1371/journal.pone.0107190.

340. Xie, F. *et al.* Engineering Extracellular Vesicles Enriched with Palmitoylated ACE2 as COVID-19 Therapy. *Advanced Materials* **33**, 2103471 (2021).

341. Rudnik, S. & Damme, M. The lysosomal membrane—export of metabolites and beyond. *FEBS J* **288**, 4168–4182 (2021).

342. Liang, Y. *et al.* Complex N-linked glycans serve as a determinant for exosome/microvesicle cargo recruitment. *Journal of Biological Chemistry* **289**, 32526–32537 (2014).

343. Kamble, P. R., Patkar, S. R., Breed, A. A. & Pathak, B. R. N-glycosylation status of Trop2 impacts its surface density, interaction with claudin-7 and exosomal release. *Arch Biochem Biophys* **714**, 109084 (2021).

344. Meurer, S., Wimmer, A. E., Leur, E. van de & Weiskirchen, R. Endoglin Trafficking/Exosomal Targeting in Liver Cells Depends on N-Glycosylation. *Cells* **8**, (2019).

345. Li, Y. *et al.* Complex N-glycan promotes CD133 mono-ubiquitination and secretion. *FEBS Lett* **593**, 719–731 (2019).

346. Harada, Y. *et al.* Glycometabolic Regulation of the Biogenesis of Small Extracellular Vesicles. *Cell Rep* **33**, (2020).

347. Dennis, J. W., Lau, K. S. & Nabi, I. R. Adaptive Regulation at the Cell Surface by N -Glycosylation. *Traffic* **10**, 1569–1578 (2009).

348. Console, L., Scalise, M., Tarmakova, Z., Coe, I. R. & Indiveri, C. N-linked Glycosylation of human SLC1A5 (ASCT2) transporter is critical for traf fi cking to membrane. *BBA - Molecular Cell Research* **1853**, 1636–1645 (2015).

349. Chen, G. *et al.* Mature N -linked glycans facilitate UT-A1 urea transporter lipid raft compartmentalization. *The FASEB Journal* **25**, 4531–4539 (2011).

350. Quirk, P. L., Rao, S., Roth, B. L. & Siegel, R. E. Three Putative N-Glycosylation Sites Within The Murine 5-HT3 A Receptor Sequence Affect Plasma Membrane Targeting , Ligand Binding , and Calcium Influx in Heterologous Mammalian Cells. *J Neurosci Res* **506**, 498–506 (2004).

351. Torreno-pina, J. A., Castro, B. M., Manzo, C., Buschow, S. I. & Cambi, A. Enhanced receptor – clathrin interactions induced by N -glycan – mediated membrane micropatterning. *PNAS* **111**, 11037–11042 (2014).

352. Samavarchi-Tehrani, P., Samson, R. & Gingras, A. C. Proximity Dependent Biotinylation: Key Enzymes and Adaptation to Proteomics Approaches. *Molecular & Cellular Proteomics* **19**, 757–773 (2020).

353. Jong, O. G. de *et al.* A CRISPR-Cas9-based reporter system for single-cell detection of extracellular vesicle-mediated functional transfer of RNA Olivier. *Nat Commun* **11**, 1–13 (2020).

354. Kanuma, T. *et al.* CD63-Mediated Antigen Delivery into Extracellular Vesicles via DNA Vaccination Results in Robust CD8 + T Cell Responses. *J Immunol* **198**, 4707–4715 (2017).

355. Liang, G. *et al.* Engineered exosome-mediated delivery of functionally active miR-26a and its enhanced suppression effect in HepG2 cells. *Int J Nanomedicine* **Volume 13**, 585–599 (2018).

356. Read, M. L. *et al.* The PTTG1-binding factor (PBF/PTTG1IP) regulates p53 activity in thyroid cells. *Endocrinology* **155**, 1222–1234 (2014).

357. Wood, D. W., Wu, W., Belfort, G., Derbyshire, V. & Belfort, M. A genetic system yields self-cleaving inteins for bioseparations. *Nat Biotechnol* 889–892 (1994).

358. Osipiuk, J., Mulligan, R., Bargassa, M., Hamilton, J. E. & Cunningham, M. A. Characterization of Member of DUF1888 Protein Family ,. *J Biol Chem* **287**, 19452–19461 (2012).

359. Susa, F., Limongi, T., Dumontel, B., Vighetto, V. & Cauda, V. Engineered extracellular vesicles as a reliable tool in cancer nanomedicine. *Cancers* vol. 11 Preprint at https://doi.org/10.3390/cancers11121979 (2019).

360. Mishra, R., Grzybek, M., Niki, T., Hirashima, M. & Simons, K. Galectin-9 trafficking regulates apical-basal polarity in Madin-Darby canine kidney epithelial cells. *Proc Natl Acad Sci U S A* **107**, 17633–17638 (2010).

361. Endocytosis, L. & Johannes, L. Shiga Toxin—A Model for Glycolipid-Dependent and Lectin-Driven Endocytosis. *Toxins (Basel)* **9**, 1–11 (2017).

362. Hirabayashi, J., Hashidate, T., Arata, Y. & Nishi, N. Oligosaccharide specificity of galectins : a search by frontal affinity chromatography. *Biochim Biophys Acta* **1572**, 232–254 (2002).

363. Chien, W. & Pei, L. A novel binding factor facilitates nuclear translocation and transcriptional activation function of the pituitary tumor-transforming gene product. *Journal of Biological Chemistry* **275**, 19422–19427 (2000).

364. Smith, V. E., Franklyn, J. A. & McCabe, C. J. Pituitary tumor-transforming gene and its binding factor in endocrine cancer. *Expert Rev Mol Med* **12**, (2010).

365. Read, M. L. *et al.* The proto-oncogene PBF binds p53 and is associated with prognostic features in colorectal cancer. *Mol Carcinog* **55**, 15–26 (2016).

366. Imruetaicharoenchoke, W. *et al.* Functional consequences of the first reported mutations of the proto-oncogene PTTG1IP/PBF. *Endocr Relat Cancer* **24**, 459–474 (2017).

367. Read, M. L. *et al.* Elevated PTTG and PBF predicts poor patient outcome and modulates DNA damage response genes in thyroid cancer. *Oncogene* **36**, 5296–5308 (2017).

368. Lian, S., Song, J. & Huang, Y. PBF, a proto-oncogene in esophageal carcinoma. *DE GRUYTER* **14**, 748–756 (2019).

369. Read, M. L. *et al.* PTTG and PBF functionally interact with p53 and predict overall survival in head and neck cancer. *Cancer Research* vol. 78 5863–5876 Preprint at https://doi.org/10.1158/0008-5472.CAN-18-0855 (2018).

370. Tan, X. *et al.* Hypermethylation of the PTTG1IP promoter leads to low expression in early-stage non-small cell lung cancer. *Oncol Lett* **18**, 1278–1286 (2019).

371. Repo, H. *et al.* PTTG1-interacting protein (PTTG1IP/PBF) predicts breast cancer survival. *BMC Cancer* **17**, (2017).

372. Mathieu, M. *et al.* Specificities of exosome versus small ectosome secretion revealed by live intracellular tracking of CD63 and CD9. *Nat Commun* **12**, 1–18 (2021).

373. Duarte-Sanmiguel, S. *et al.* In Situ Deployment of Engineered Extracellular Vesicles into the Tumor Niche via Myeloid-Derived Suppressor Cells. *Adv Healthc Mater* **11**, (2022).

374. Dang, Y. *et al.* Optimizing sgRNA structure to improve CRISPR-Cas9 knockout efficiency. *Genome Biol* **16**, 1–10 (2015).

375. Kim, S., Kim, D., Cho, S. W., Kim, J. & Kim, J. S. Highly efficient RNA-guided genome editing in human cells via delivery of purified Cas9 ribonucleoproteins. *Genome Res* **24**, 1012–1019 (2014).

376. van Deun, J. *et al.* EV-TRACK: transparent reporting and centralizing knowledge in extracellular vesicle research. *Nature Methods 2017 14:3* **14**, 228–232 (2017).

377. Herrmann, I. K., Wood, M. J. A. & Fuhrmann, G. Extracellular vesicles as a next-generation drug delivery platform. *Nature Nanotechnology 2021 16:7* **16**, 748–759 (2021).

378. Cheng, L. & Hill, A. F. Therapeutically harnessing extracellular vesicles. *Nature Reviews Drug Discovery 2022 21:5* **21**, 379–399 (2022).

379. Yates, A. G. *et al.* In sickness and in health: The functional role of extracellular vesicles in physiology and pathology in vivo. *J Extracell Vesicles* **11**, e12151 (2022).

380. Tomás, H. A. *et al.* Improved GaLV-TR Glycoproteins to Pseudotype Lentiviral Vectors: Impact of Viral Protease Activity in the Production of LV Pseudotypes. *Mol Ther Methods Clin Dev* **15**, 1–8 (2019).

381. Lener, T. *et al.* Applying extracellular vesicles based therapeutics in clinical trials – an ISEV position paper. *https://doi.org/10.3402/jev.v4.30087* **4**, 30087 (2015).

382. Song, Y. *et al.* The emerging role of exosomes as novel therapeutics: Biology, technologies, clinical applications, and the next. *Am J Reprod Immunol* **85**, (2021).

383. Jang, S. C. *et al.* ExoSTING, an extracellular vesicle loaded with STING agonists, promotes tumor immune surveillance. *Communications Biology 2021 4:1* **4**, 1–17 (2021).

384. Kamerkar, S. *et al.* Exosome-mediated genetic reprogramming of tumor-associated macrophages by exoASO-STAT6 leads to potent monotherapy antitumor activity. *Sci Adv* **8**, 7002 (2022).

8. Appendix

8.1. Manuscripts accepted for publication

Coenen-Stass AML, Pauwels MJ, Hanson B, **Perez CM**, Conceição M, Wood MJA, Mäger I, Roberts TC. Extracellular microRNAs exhibit sequence-dependent stability and cellular release kinetics. RNA Biology 2019; 16:696–706. DOI: 10.1080/15476286.2019.1582956.

Martin Perez C, Conceição M, Raz R, Wood MJA, Roberts TC. Enhancing the Therapeutic Potential of Extracellular Vesicles Using Peptide Technology. Methods Mol Biol. 2022;2383:119-141. doi: 10.1007/978-1-0716-1752-6_8. PMID: 34766286.

8.2. Sequences of the constructs used in Chapter 4

mEGFP-cMyc

ATGGTGAGCAAGGGCGAGGAGCTGTTCACCGGGGTGGTGCCCATCCTGGTCGAGCT
GGACGGCGACGTAAACGGCCACAAGTTCAGCGTGTCCGGCGAGGGCGAGGGCGAT
GCCACCTACGGCAAGCTGACCCTGAAGTTCATCTGCACCACCGGCAAGCTGCCCGTG
CCCTGGCCCACCCTCGTGACCACCCTGACCTACGGCGTGCAGTGCTTCAGCCGCTAC
CCCGACCACATGAAGCAGCACGACTTCTTCAAGTCCGCCATGCCCGAAGGCTACGTC
CAGGAGCGCACCATCTTCTTCAAGGACGACGGCAACTACAAGACCCGCGCCGAGGT
GAAGTTCGAGGGCGACACCCTGGTGAACCGCATCGAGCTGAAGGGCATCGACTTCA
AGGAGGACGGCAACATCCTGGGGCACAAGCTGGAGTACAACTACAACAGCCACAA
CGTCTATATCATGGCCGACAAGCAGAAGAACGGCATCAAGGTGAACTTCAAGATCC
GCCACAACATCGAGGACGGCAGCGTGCAGCTCGCCGACCACTACCAGCAGAACACC
CCCATCGGCGACGGCCCCGTGCTGCTGCCCGACAACCACTACCTGAGCACCCAGTCC
AAGCTGAGCAAAGACCCCAACGAGAAGCGCGATCACATGGTCCTGCTGGAGTTCGT
GACCGCCGCCGGGATCACTCTCGGCATGGACGAGCTGTACAAGGAGCAGAAGCTGA
TCTCCGAAGAGGACCTG

Myc sequence

PTTG1IP

ATGGCGCCAGGAGTCGCCCGCGGACCAACGCCGTACTGGAGATTGAGACTCGGTGG
AGCCGCGCTGCTCCTGCTGCTCATCCCTGTCGCCGCCGCGCAGGAGCCTCCAGGAGC
TGCTTGTTCTCAGAACACAAACAAAACCTGTGAAGAGTGCCTGAAGAACGTCTCCTG
TCTTTGGTGCAACACTAACAAGGCTTGTCTGGACTACCCAGTTACAAGCGTCTTGCC
ACCGGCTTCCCTTTGTAAATTGAGCTCTGCACGCTGGGGAGTTTGTTGGGTGAACTTT
GAAGCGCTGATCATCACCATGTCGGTAGTCGGGGGAACCCTCCTCCTGGGCATTGCC
ATCTGCTGCTGCTGCTGCTGCAGGAGGAAGAGGAGCCGGAAGCCGGACAGGAGTGA
GGAGAAGGCCATGCGTGAGCGGGAGGAGAGGCGGATACGGCAGGAGGAACGGAGA
GCAGAGATGAAGACAAGACATGATGAAATCAGAAAAAAATATGGCCTGTTTAAAGA
AGAAAACCCGTATGCTAGATTTGAAAACAAC

SPRY7

ATGGCCACCTCGGTGTTGTGCTGCCTGCGGTGCTGCAGAGACGGGGGGACTGGCCA
CATCCCTCTGAAGGAGATGCCGGCCGTGCAGCTGGACACGCAGCACATGGGAACAG
ATGTTGTTATTGTAAAGAATGGAAGAAGAATATGTGGAACAGGAGGTTGTTTAGCC
AGCGCACCTTTACATCAAAACAAAAGCTATTTTGAATTCAAAATCCAGTCCACAGGA
ATCTGGGGTATTGGTGTTGCAACTCAGAAGGTTAACTTGAATCAGATTCCTCTTGGC
CGAGATATGCACAGTCTGGTGATGAGAAATGATGGAGCCCTTTACCACAACAATGA
AGAGAAAAATAGGCTGCCAGCAAACAGTCTTCCGCAGGAAGGAGATGTGGTGGGTA
TTACTTATGACCATGTCGAATTAAATGTATACTTGAATGGAAAAAACATGCATTGTC
CAGCATCAGGTATACGAGGGACAGTGTATCCAGTTGTTTATGTTGATGACAGTGCAA

TTTTGGATTGCCAGTTCAGTGAGTTTTATCATACGCCTCCACCTGGTTTTGAAAAAAT
ATTATTTGAACAGCAAATCTTC

MITD1

ATGGCGAAGTCCGGGCTGAGGCAGGACCCGCAGAGCACAGCTGCAGCCACTGTGCT
AAAGCGGGCAGTAGAACTAGATTCGGAGTCGCGGTATCCGCAGGCTCTGGTGTGTT
ACCAAGAGGGGATTGATCTGCTCCTGCAGGTTCTGAAAGGTACCAAAGATAATACT
AAGAGATGTAATCTCAGAGAAAAAATTTCCAAATACATGGACAGAGCGGAAAACAT
AAAGAAGTACTTGGACCAAGAAAAAGAAGATGGAAAATATCACAAGCAAATTAAA
ATAGAAGAGAATGCAACAGGTTTCAGTTATGAGTCACTTTTTCGCGAATACCTTAAT
GAGACAGTTACAGAAGTTTGGATAGAAGATCCTTATATTAGACATACTCATCAGCTG
TATAACTTTCTTCGATTTTGTGAGATGCTTATTAAGAGACCATGTAAAGTAAAAACT
ATTCACCTTCTCACCTCTCTGGATGAAGGCATTGAGCAAGTGCAGCAAAGTAGAGGC
CTGCAAGAAATAGAAGAGTCACTCAGGAGTCACGGAGTGCTGTTGGAAGTTCAATA
CTCTTCTTCAATACATGACCGAGAAATTAGGTTCAACAATGGATGGATGATTAAGAT
TGGAAGGGGACTTGATTATTTTAAGAAACCACAGAGTCGTTTTTCCCTTGGATATTG
TGATTTTGATTTAAGACCATGTCATGAAACAACAGTAGACATTTTTCATAAGAAGCA
TACAAAAAATATA

PTAP motif

CCCGGGCCAAGTGCTCCTGGTCCA

PTTG1IP-N45Q

ATGGCGCCAGGAGTCGCCCGCGGACCAACGCCGTACTGGAGATTGAGACTCGGTGG
AGCCGCGCTGCTCCTGCTGCTCATCCCTGTCGCCGCCGCGCAGGAGCCTCCAGGAGC
TGCTTGTTCTCAGAACACAcagAAAACCTGTGAAGAGTGCCTGAAGAACGTCTCCTGT
CTTTGGTGCAACACTAACAAGGCTTGTCTGGACTACCCAGTTACAAGCGTCTTGCCA
CCGGCTTCCCTTTGTAAATTGAGCTCTGCACGCTGGGGAGTTTGTTGGGTGAACTTTG
AAGCGCTGATCATCACCATGTCGGTAGTCGGGGGAACCCTCCTCCTGGGCATTGCCA
TCTGCTGCTGCTGCTGCTGCAGGAGGAAGAGGAGCCGGAAGCCGGACAGGAGTGAG
GAGAAGGCCATGCGTGAGCGGGAGGAGAGGCGGATACGGCAGGAGGAACGGAGAG
CAGAGATGAAGACAAGACATGATGAAATCAGAAAAAAATATGGCCTGTTTAAAGAA
GAAAACCCGTATGCTAGATTTGAAAACAAC

PTTG1IP-N54Q

ATGGCGCCAGGAGTCGCCCGCGGACCAACGCCGTACTGGAGATTGAGACTCGGTGG
AGCCGCGCTGCTCCTGCTGCTCATCCCTGTCGCCGCCGCGCAGGAGCCTCCAGGAGC
TGCTTGTTCTCAGAACACAAACAAAACCTGTGAAGAGTGCCTGAAGcagGTCTCCTGT
CTTTGGTGCAACACTAACAAGGCTTGTCTGGACTACCCAGTTACAAGCGTCTTGCCA
CCGGCTTCCCTTTGTAAATTGAGCTCTGCACGCTGGGGAGTTTGTTGGGTGAACTTTG
AAGCGCTGATCATCACCATGTCGGTAGTCGGGGGAACCCTCCTCCTGGGCATTGCCA
TCTGCTGCTGCTGCTGCTGCAGGAGGAAGAGGAGCCGGAAGCCGGACAGGAGTGAG
GAGAAGGCCATGCGTGAGCGGGAGGAGAGGCGGATACGGCAGGAGGAACGGAGAG

CAGAGATGAAGACAAGACATGATGAAATCAGAAAAAAATATGGCCTGTTTAAAGAA
GAAAACCCGTATGCTAGATTTGAAAACAAC

PTTG1IP-2NQ

ATGGCGCCAGGAGTCGCCCGCGGACCAACGCCGTACTGGAGATTGAGACTCGGTGG
AGCCGCGCTGCTCCTGCTGCTCATCCCTGTCGCCGCCGCGCAGGAGCCTCCAGGAGC
TGCTTGTTCTCAGAACACAcagAAAACCTGTGAAGAGTGCCTGAAGcagGTCTCCTGTC
TTTGGTGCAACACTAACAAGGCTTGTCTGGACTACCCAGTTACAAGCGTCTTGCCAC
CGGCTTCCCTTTGTAAATTGAGCTCTGCACGCTGGGGAGTTTGTTGGGTGAACTTTG
AAGCGCTGATCATCACCATGTCGGTAGTCGGGGGAACCCTCCTCCTGGGCATTGCCA
TCTGCTGCTGCTGCTGCTGCAGGAGGAAGAGGAGCCGGAAGCCGGACAGGAGTGAG
GAGAAGGCCATGCGTGAGCGGGAGGAGAGGCGGATACGGCAGGAGGAACGGAGAG
CAGAGATGAAGACAAGACATGATGAAATCAGAAAAAAATATGGCCTGTTTAAAGAA
GAAAACCCGTATGCTAGATTTGAAAACAAC

PTTG1IP-130-164Del

ATGGCGCCAGGAGTCGCCCGCGGACCAACGCCGTACTGGAGATTGAGACTCGGTGG
AGCCGCGCTGCTCCTGCTGCTCATCCCTGTCGCCGCCGCGCAGGAGCCTCCAGGAGC
TGCTTGTTCTCAGAACACAAACAAAACCTGTGAAGAGTGCCTGAAGAACGTCTCCTG
TCTTTGGTGCAACACTAACAAGGCTTGTCTGGACTACCCAGTTACAAGCGTCTTGCC
ACCGGCTTCCCTTTGTAAATTGAGCTCTGCACGCTGGGGAGTTTGTTGGGTGAACTTT
GAAGCGCTGATCATCACCATGTCGGTAGTCGGGGGAACCCTCCTCCTGGGCATTGCC
ATCTGCTGCTGCTGCTGCTGCAGGAGGAAGAGGAGCCGGAAGCCGTATGGCCTGTTT
AAAGAAGAAAACCCGTATGCTAGATTTGAAAACAAC

PTTG1IP-2YA (Y165A) (Y174A)

ATGGCGCCAGGAGTCGCCCGCGGACCAACGCCGTACTGGAGATTGAGACTCGGTGG
AGCCGCGCTGCTCCTGCTGCTCATCCCTGTCGCCGCCGCGCAGGAGCCTCCAGGAGC
TGCTTGTTCTCAGAACACAAACAAAACCTGTGAAGAGTGCCTGAAGAACGTCTCCTG
TCTTTGGTGCAACACTAACAAGGCTTGTCTGGACTACCCAGTTACAAGCGTCTTGCC
ACCGGCTTCCCTTTGTAAATTGAGCTCTGCACGCTGGGGAGTTTGTTGGGTGAACTTT
GAAGCGCTGATCATCACCATGTCGGTAGTCGGGGGAACCCTCCTCCTGGGCATTGCC
ATCTGCTGCTGCTGCTGCTGCAGGAGGAAGAGGAGCCGGAAGCCGGACAGGAGTGA
GGAGAAGGCCATGCGTGAGCGGGAGGAGAGGCGGATACGGCAGGAGGAACGGAGA
GCAGAGATGAAGACAAGACATGATGAAATCAGAAAAAAAgccGGCCTGTTTAAAGA
AGAAAACCCGgccGCTAGATTTGAAAACAAC

Cre-cMyc

ATGGTGCCCAAGAAGAAGAGGAAAGTCTCCAACCTGCTGACTGTGCACCAAAACCT
GCCTGCCCTCCCTGTGGATGCCACCTCTGATGAAGTCAGGAAGAACCTGATGGACAT
GTTCAGGGACAGGCAGGCCTTCTCTGAACACACCTGGAAGATGCTCCTGTCTGTGTG
CAGATCCTGGGCTGCCTGGTGCAAGCTGAACAACAGGAAATGGTTCCCTGCTGAAC
CTGAGGATGTGAGGGACTACCTCCTGTACCTGCAAGCCAGAGGCCTGGCTGTGAAA

ACCATCCAACAGCACCTGGGCCAGCTCAACATGCTGCACAGGAGATCTGGCCTGCC
TCGCCCTTCTGACTCCAATGCTGTGTCCCTGGTGATGAGGAGAATCAGAAAGGAGAA
TGTGGATGCTGGGGAGAGAGCCAAGCAGGCCCTGGCCTTTGAACGCACTGACTTTG
ACCAAGTCAGATCCCTGATGGAGAACTCTGACAGATGCCAGGACATCAGGAACCTG
GCCTTCCTGGGCATTGCCTACAACACCCTGCTGCGCATTGCCGAAATTGCCAGAATC
AGAGTGAAGGACATCTCCCGCACCGATGGTGGGAGAATGCTGATCCACATTGGCAG
GACCAAGACCCTGGTGTCCACAGCTGGTGTGGAGAAGGCCCTGTCCCTGGGGGTTA
CCAAGCTGGTGGAGAGATGGATCTCTGTGTCTGGTGTGGCTGATGACCCCAACAACT
ACCTGTTCTGCCGGGTCAGAAAGAATGGTGTGGCTGCCCCTTCTGCCACCTCCCAAC
TGTCCACCCGGGCCCTGGAAGGGATCTTTGAGGCCACCCACCGCCTGATCTATGGTG
CCAAGGATGACTCTGGGCAGAGATACCTGGCCTGGTCTGGCCACTCTGCCAGAGTG
GGTGCTGCCAGGGACATGGCCAGGGCTGGTGTGTCCATCCCTGAAATCATGCAGGCT
GGTGGCTGGACCAATGTGAACATTGTGATGAACTACATCAGAAACCTGGACTCTGA
GACTGGGGCCATGGTGAGGCTGCTCGAGGATGGGGACGAGCAGAAGCTGATCTCCG
AAGAGGACCTG

Myc sequence

PTTG1IP-Cre

ATGGCGCCAGGAGTCGCCCGCGGACCAACGCCGTACTGGAGATTGAGACTCGGTGG
AGCCGCGCTGCTCCTGCTGCTCATCCCTGTCGCCGCCGCGCAGGAGCCTCCAGGAGC
TGCTTGTTCTCAGAACACAAACAAAACCTGTGAAGAGTGCCTGAAGAACGTCTCCTG
TCTTTGGTGCAACACTAACAAGGCTTGTCTGGACTACCCAGTTACAAGCGTCTTGCC
ACCGGCTTCCCTTTGTAAATTGAGCTCTGCACGCTGGGGAGTTTGTTGGGTGAACTTT
GAAGCGCTGATCATCACCATGTCGGTAGTCGGGGGAACCCTCCTCCTGGGCATTGCC
ATCTGCTGCTGCTGCTGCTGCAGGAGGAAGAGGAGCCGGAAGCCGGACAGGAGTGA
GGAGAAGGCCATGCGTGAGCGGGAGGAGAGGCGGATACGGCAGGAGGAACGGAGA
GCAGAGATGAAGACAAGACATGATGAAATCAGAAAAAAATATGGCCTGTTTAAAGA
AGAAAACCCGTATGCTAGATTTGAAAACAACGATCCACCGGTCGCCACCGTGCCCA
AGAAGAAGAGGAAAGTC

PTTG1IP-intein-Cre

ATGGCGCCAGGAGTCGCCCGCGGACCAACGCCGTACTGGAGATTGAGACTCGGTGG
AGCCGCGCTGCTCCTGCTGCTCATCCCTGTCGCCGCCGCGCAGGAGCCTCCAGGAGC
TGCTTGTTCTCAGAACACAAACAAAACCTGTGAAGAGTGCCTGAAGAACGTCTCCTG
TCTTTGGTGCAACACTAACAAGGCTTGTCTGGACTACCCAGTTACAAGCGTCTTGCC
ACCGGCTTCCCTTTGTAAATTGAGCTCTGCACGCTGGGGAGTTTGTTGGGTGAACTTT
GAAGCGCTGATCATCACCATGTCGGTAGTCGGGGGAACCCTCCTCCTGGGCATTGCC
ATCTGCTGCTGCTGCTGCTGCAGGAGGAAGAGGAGCCGGAAGCCGGACAGGAGTGA
GGAGAAGGCCATGCGTGAGCGGGAGGAGAGGCGGATACGGCAGGAGGAACGGAGA
GCAGAGATGAAGACAAGACATGATGAAATCAGAAAAAAATATGGCCTGTTTAAAGA
AGAAAACCCGTATGCTAGATTTGAAAACAACGATCCACCGGTCGCCACCGCTCTTGC
TGAGGGCACCAGAATCTTCGATCCCGTGACCGGCACCACACACAGAATCGAGGATG
TCGTCGGCGGCAGAAAGCCCATTCATGTGGTGGCTGCCGCCAAGGATGGAACCCTG
CATGCCAGACCTGTGGTGTCTTGGTTTGACCAGGGCACAAGAGATGTGATCGGCCTG

AGAATTGCCGGCGGAGCCATTCTGTGGGCCACACCAGATCACAAGGTGCTGACAGA
GTACGGCTGGCGAGCTGCTGGGGAACTGAGAAAGGGCGATAGAGTGGCCCAGCCTA
GAAGATTCGACGGCTTCGGAGACAGCGCCCCTATTCCTGCTAGAGTGCAGGCTCTGG
CCGACGCTCTGGACGACAAGTTTCTGCACGATATGCTGGCCGAGGAACTGCGGTAC
AGCGTGATCAGAGAGGTGCTGCCTACCAGACGGGCCAGAACCTTTGGCCTGGAAGT
GGAAGAACTGCACACACTGGTGGCCGAAGGCGTGGTGGTTCACAAT

PTTG1IP-SC

ATGGCGCCAGGAGTCGCCCGCGGACCAACGCCGTACTGGAGATTGAGACTCGGTGG
AGCCGCGCTGCTCCTGCTGCTCATCCCTGTCGCCGCCGCGCAGGAGCCTCCAGGAGC
TGCTTGTTCTCAGAACACAAACAAAACCTGTGAAGAGTGCCTGAAGAACGTCTCCTG
TCTTTGGTGCAACACTAACAAGGCTTGTCTGGACTACCCAGTTACAAGCGTCTTGCC
ACCGGCTTCCCTTTGTAAATTGAGCTCTGCACGCTGGGGAGTTTGTTGGGTGAACTTT
GAAGCGCTGATCATCACCATGTCGGTAGTCGGGGGAACCCTCCTCCTGGGCATTGCC
ATCTGCTGCTGCTGCTGCTGCAGGAGGAAGAGGAGCCGGAAGCCGGACAGGAGTGA
GGAGAAGGCCATGCGTGAGCGGGAGGAGAGGCGGATACGGCAGGAGGAACGGAGA
GCAGAGATGAAGACAAGACATGATGAAATCAGAAAAAAATATGGCCTGTTTAAAGA
AGAAAACCCGTATGCTAGATTTGAAAACAACGATCCACCGGTCGCCACCTTCGCTCC
TCAGGGCCTGGCCCAGTTCATCAAGGTGAACGTGACCCTGGAGAACGGCGAGCCCG
TGTTCATCTACACCGACGCCAACGGCCAGGTGTGCCAGGGCGACATCACCGTGACC
CAGGCCGGCACCATCACCTACCTGCTGAACGACCAGACCCTGAAGGGCCTGAAGTT
CGTGGGCGTGGGCTTCGTGACCCCCTTCGACGGCATCATCGACGCCGTGACCATCAG
CAGCGACGGCATGCTGGTGCAGCTGGTGGACCTGGACAAGACCCCCGGCACCACCA
AGTTCCAGTTCGTGCTGAGCAACACCGCCAACACCCTGCTGGTGCTGAGCCCCGACC
CCCAGATCATCAACAGGCCCCAGAAC

PTTG1IP-130-180aa

ATGGCGCCAGGAGTCGCCCGCGGACCAACGCCGTACTGGAGATTGAGACTCGGTGG
AGCCGCGCTGCTCCTGCTGCTCATCCCTGTCGCCGCCGCGCAGGAGCCTCCAGGAGC
TGCTTGTTCTCAGAACACAAACAAAACCTGTGAAGAGTGCCTGAAGAACGTCTCCTG
TCTTTGGTGCAACACTAACAAGGCTTGTCTGGACTACCCAGTTACAAGCGTCTTGCC
ACCGGCTTCCCTTTGTAAATTGAGCTCTGCACGCTGGGGAGTTTGTTGGGTGAACTTT
GAAGCGCTGATCATCACCATGTCGGTAGTCGGGGGAACCCTCCTCCTGGGCATTGCC
ATCTGCTGCTGCTGCTGCTGCAGGAGGAAGAGGAGCCGGAAGCCGGACAGGAGTGA
GGAGAAGGCCATGCGTGAGCGGGAGGAGAGGCGGATACGGCAGGAGGAACGGAGA
GCAGAGATGAAGACAAGACATGATGAAATCAGAAAAAAATATGGCCTGTTTAAAGA
AGAAAACCCGTATGCTAGATTTGAAAACAACGATCCACCGGTCGCCACCGACAGGA
GTGAGGAGAAGGCCATGCGTGAGCGGGAGGAGAGGCGGATACGGCAGGAGGAACG
GAGAGCAGAGATGAAGACAAGACATGATGAAATCAGAAAAAAATATGGCCTGTTTA
AAGAAGAAAACCCGTATGCTAGATTTGAAAACAAC

PCR-amplified spCas9 from pSpCas9-2A-Puro (PX459)

Primer FW:
GTGGCCGAAGGCGTGGTGGTTCACAATGGCGGTTCTGGGGGGATCCGGGGGCAGCGC
CCCAAAGAAGAAGCGG

Primer RV:
CTCTACAAATGTGGTATGGCTGATTATGATCTAGAGTCGCCTACAGGTCCTCTTCGG
AGATCAGCTTCTGCTCCTTTTTCTTTTTTGCCTGGCC

sgRNA sequence

GGACAGTACTCCGCTCGAGTGTTTTAGAGCTAGAAATAGCAAGTTAAAATAAGGCT
AGTCCGTTATCAACTTGAAAAAGTGGCACCGAGTCGGTGCTTTTTT